Copyright

by

Hee Jeung Oh

2015

The Dissertation Committee for Hee Jeung Oh Certifies that this is the approved version of the following dissertation:

Sulfonated Polysulfone Desalination Membranes by Melt Extrusion

Committee:

Benny D. Freeman, Co-Supervisor

Donald R. Paul, Co-Supervisor

Christopher J. Ellison

Isaac C. Sanchez

Wei Li

Sulfonated Polysulfone Desalination Membranes by Melt Extrusion

by

Hee Jeung Oh, B.S.; M.S.E.

Dissertation

Presented to the Faculty of the Graduate School of

The University of Texas at Austin

in Partial Fulfillment

of the Requirements

for the Degree of

Doctor of Philosophy

The University of Texas at Austin

May 2015

Dedication

To my family

Acknowledgements

I would like to express my sincere gratitude to my advisers, Dr. Benny Freeman and Dr. Donald Paul for their support and guidance throughout my graduate studies. I also would like to thank my committee members, Dr. Isaac Sanchez, Dr. Christopher Ellison, and Dr. Wei Li for their help and guidance. I appreciate the financial support from the NSF Science and Technology Center for Layered Polymeric Systems (CLiPS, Grant 0423914), which allowed me to pursue this study.

I am also grateful to my collaborators: Dr. James E. McGrath, Dr. Sue Mecham, Dr. Chang Hyun Lee, Dr. Kwan-soo Lee from Virginia Tech, and Dr. Eric Baer, Dr. Anne Hiltner and their research group members in Case Western Reserve University, for their helpful discussions and advices.

I would like to thank all my colleagues in both Dr. Freeman's and Dr. Paul's research groups in the past, present and future. The CLiPS fellow colleagues Dr. Daniel Miller, Dr. Grant Offord, Dr. Tom Murphy, and Dr. Kevin Tung have given many advices and encouragements. Dr. Bryan McCloskey, Dr. Yuan-Hsuan Wu, Dr. Elizabeth van Wagner, Dr. Alyson Sagle, Dr. Brandon Rowe, Dr. Hao Ju, Dr. Hua Richard Li, Dr. Victor Kasuma, Dr. Lauren Greenlee, Dr. Norman Horn, Dr. Katrina Czenkusch, Dr. Claudio Ribeiro, Dr. Young-Jae Yoo, Dr. Lili Cui and Dr. Joseph Cook have been wonderful friends and mentors. My contemporaries, Dr. David Sanders and Dr. Zachery Smith have been great friends in every way. I would like to thank Sirirat Peach Kasemset, Albert Lee, Ben Chun, Qiang Liu, Kevin Stevens, Ni Yan, Zhenwang Lisa He, Jaesung Park, Euisung Jang, Amanda Paine, Lu Wang, Michelle Dose, Alon Kirschner and Josh Moon for their warm

companionship. Our postdoctoral researchers, Dr. Michele Galizia, Dr. Rajkiran Tiwari and Dr. Kris Gleason, have been wonderful mentors. I want to thank Ms. Carol A. Assadourian for her gracious help.

I would like to thank my undergraduate advisers from KAIST, Dr. Seung-Bin Park, Dr. Sun-won Park, Dr. Heun Lee, Dr. Hee-Tae Jung, Dr. Hyun-Kyu Park, Dr. Jung Ki Park, Dr. Kun Pyo Lee and others for their warm encouragement and inspiration. I want to thank Dr. Ho Bum Park from Han Yang University for his kind encouragement and help. I am also grateful to Dr. Gyeong Soon Hwang for his encouragement and advices.

I would like to thank my friends for their warm friendship. I thank my families for their support and encouragement.

Sulfonated Polysulfone Desalination Membranes by Melt Extrusion

Hee Jeung Oh, Ph.D.

The University of Texas at Austin, 2015

Co-Supervisors: Benny D. Freeman and Donald R. Paul

This dissertation discusses preparation and transport property characterization of sulfonated polysulfone desalination membranes by melt processing. One route to melt processing of high glass transition temperature polyelectrolytes, such as disulfonated poly(arylene ether sulfone) (BPS), involves mixing a plasticizer with the polymer. In this study, poly(ethylene glycol) (PEG) was used as a plasticizer for BPS. Currently, most ion containing membranes used for desalination, electrodialysis, etc. are prepared using solvent-based processing, which is costly and environmentally unfriendly. The goal of this study has been to conduct a fundamental exploration of processing conditions useful for preparing desalination membranes without the use of solvents. Long term, this research may has the foundation for melt processing to prepare desalination membranes having equivalent or better separation properties as those of conventional solution processed membranes.

Table of Contents

List of Tables

List of Figures

Chapter 1: Introduction[1]

1.1 Water scarcity and desalination using membranes

With the world's population growing rapidly, the need for clean water is greater than ever. The World Health Organization reported that one billion people live without clean and drinkable water. Nearly 41 % of the earth's population - 2.3 billion people – lives in water stressed regions and this number is expected to increase to 3.5 billion by 2025, considering the fast population growth and decreasing fresh water resources by climate change, etc., according to a World Resources Institute Analysis [1-3]. Therefore, there is a great need to supply clean water at low cost, and many water purification technologies have been investigated to fulfill this need.

Among these water purification methods, membrane processes with desalination draw attention because of their energy efficiency, small footprint and ability to eliminate virtually all water contaminants using appropriate membranes (see Figure 1.1) [4-6]. For example, in water containing total dissolved solids (TDS) up to 45,000 mg/L, mainly salt ions, commercial reverse osmosis (RO) membranes can eliminate contaminants to the level of human consumption guidelines [8, 9]. Indeed, desalination by RO membranes is a competitive method of obtaining fresh water over alternative technologies because of its efficiency and, thus, has been developed rapidly over the past 50 years [10-12]. As a result,

[1] Parts of this chapter have been adapted from the following articles with permission:
(1) H. J. Oh, B. D. Freeman, J. E. McGrath, C. H. Lee, and D. R. Paul, "Thermal analysis of disulfonated poly(arylene ether sulfone) plasticized with poly(ethylene glycol) for membrane formation," Polymer vol. 55, pp. 235-247, 2014.
(2) H. J. Oh, B. D. Freeman, J. E. McGrath, C. J. Ellison, S. Mecham, K.-S. Lee, and D. R. Paul, "Rheological studies of disulfonated poly(arylene ether sulfone) plasticized with poly(ethylene glycol) for membrane formation," Polymer, vol. 55, pp. 1574-1582, 2014.

out of nearly 14,000 desalination plant worldwide, 59 % of the production relies on RO membranes and this share is expected to increase [13].

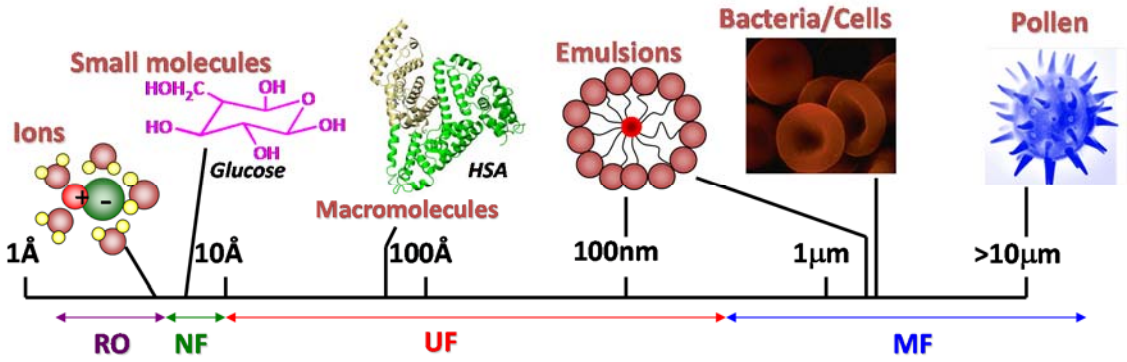

Figure 1.1 Classification of membranes used in water purification based on capabilities of size-sieving: reverse osmosis (RO), nanofiltration (NF), ultrafiltration (UF) and microfiltration (MF). Picture courtesy of Bryan McCloskey [14].

1.2 Current state-of-art membranes in reverse osmosis (RO)

Currently, polyamide (PA) thin film composite membranes are widely used in reverse osmosis (RO) because of their good transport properties and stability over a wide range of pH [10, 11]. However, these PA membranes have poor resistance to aqueous chlorine, which is often added as a disinfectant to prevent membrane fouling [4, 10, 15].

Susceptibility to chlorine

Membrane fouling, by suspended solids and microbial deposition on the membrane surface, or along the feed-channel spacer, is a major cause of membrane failure leading to reduced membrane lifetime. To prevent membrane fouling, chlorine is often added as a disinfectant and as an oxidizing agent. Since chlorine effectively prevents biofilm growth in the system and at low cost, it performs a crucial role in extending membrane lifetime [4, 10, 12].

Since PA membranes have poor resistance to chlorine, feed water must be de-chlorinated before contacting the membrane to avoid serious membrane degradation and then re-chlorinated after passing through the membrane as shown in Figure 1.2 [16, 17]. These additional steps increase operational costs. Therefore, there is a need to investigate chlorine-tolerant RO membranes for desalination to reduce these additional steps as illustrated in Figure 1.3 [4, 10, 15, 18].

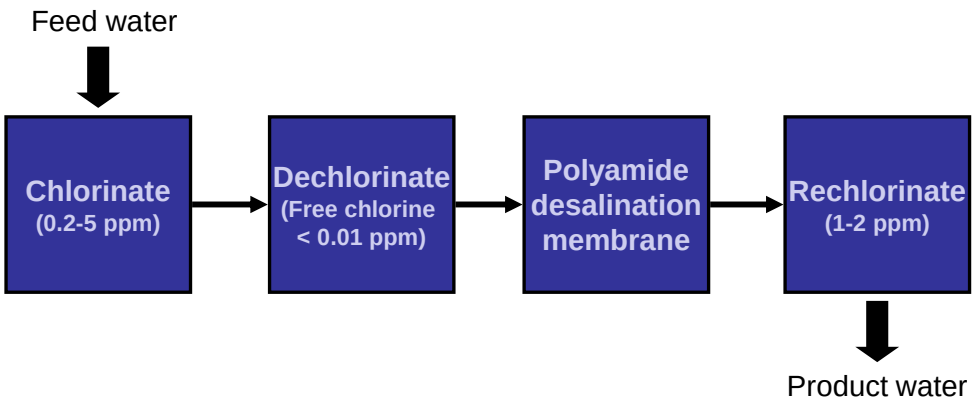

Figure 1.2 Current reverse osmosis desalination process using polyamide membranes. Feed water is chlorinated to prevent membrane fouling and bacterial infection and before contacting the polyamide membrane, feed water must be de-chlorinated to avoid serious membrane degradation and then re-chlorinated after passing through the membrane [4, 10, 12, 16, 17]. These additional steps increase operation costs. Picture courtesy of Benny Freeman.

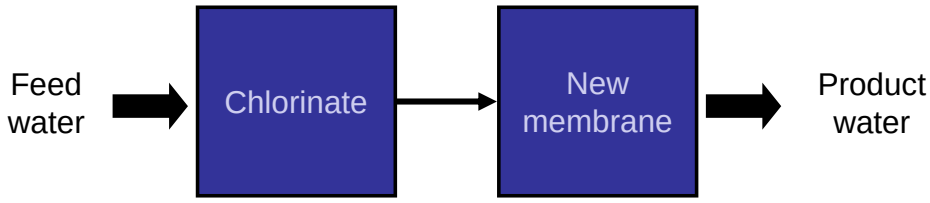

Figure 1.3 Potential reverse osmosis desalination process by introducing chlorine-tolerant membrane. De-, and re-chlorinate steps may be eliminated by using chlorine-tolerant membrane. Picture courtesy of Benny Freeman.

Environmentally unfriendly membrane preparation

Additionally, desalination membranes are produced via solution processing methods [11, 19]. The PA thin film composite membranes mentioned above are made by interfacial polymerization of monomers at an oil/water interface [11, 19]. Most ion containing membranes used for other applications such as electrodialysis [20, 21], etc. are prepared using solvent-based processing methods as well. Large volumes of volatile, flammable hydrocarbon solvents are used in this process. Solution processing has several disadvantages including environmental and health hazards and the high costs associated with solvent disposal. As a result, better methods of preparing membranes are of some interest.

1.3 Sulfonated polysulfone membrane as an alternative RO membrane

Strong tolerance to chlorine

Sulfonated polysulfone thin film composite membranes have good chlorine resistance as shown in Figure 1.4. Unlike a commercial polyamide membrane (e.g., SW 30HR Film Tec), sulfonated polysulfone thin film composite membranes (e.g., BPS-40N, BPS-40H) show nearly constant NaCl rejections at accelerated chlorine exposure experiments, making the de- and re-chlorination steps in Figure 1.2 unnecessary [10, 15, 18, 22]. These membranes exhibit selective ion transport properties as well as desirable mechanical properties, similar to those of PA membranes. Therefore, they are a feasible alternative to PA membranes for desalination [10, 15, 18, 22-24].

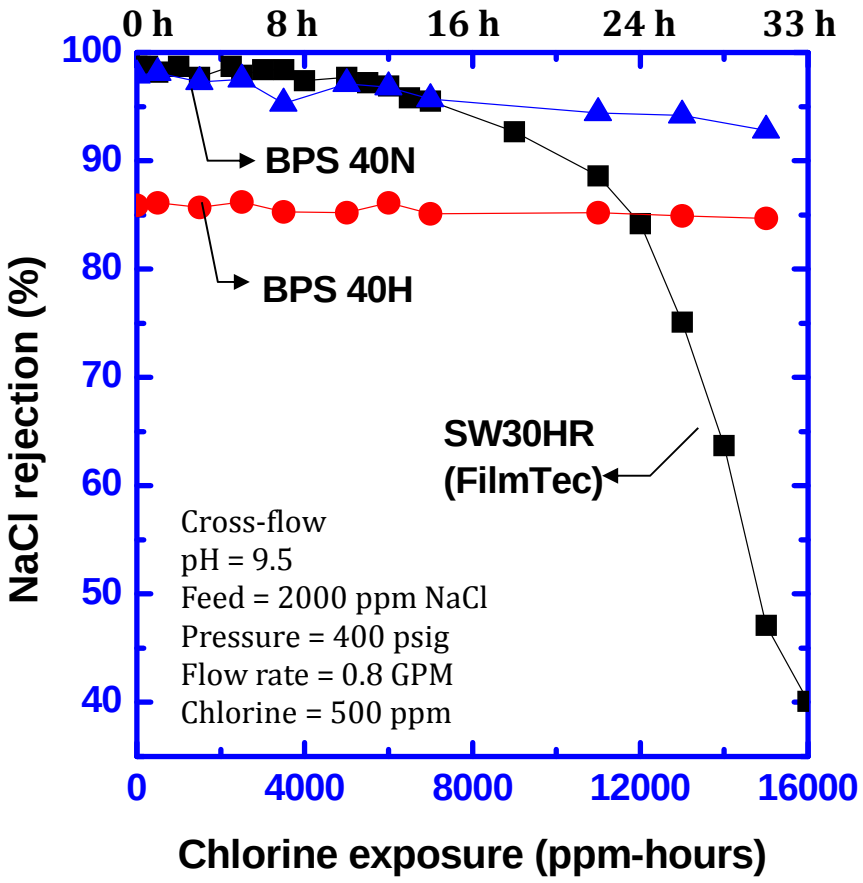

Figure 1.4 Influence of chlorine exposure (ppm-hours) on NaCl rejection (%) of sulfonated polysulfone (BPS-40N, BPS-40H) thin film composite membranes and commercial polyamide (SW 30HR Film Tec) membrane. Figure from Ref.[10].

Possibility of melt processing

Such membranes can be formed by typical solvent casting processes [10, 15, 18]. However, unlike most membranes, which can only be produced by solution processing, sulfonated polysulfone membranes may be prepared by a melt extrusion process, with appropriate plasticizers, avoiding the use of organic solvents in processing. Interestingly, sulfonated polysulfone can be plasticized using low molecular weight, water soluble

poly(ethylene glycol) (PEG) [25, 26]. This plasticizer can potentially be removed from the membrane by water extraction following melt processing.

Bebin et al. have reported on a similar approach for extruding single-layer, post-sulfonated (i.e., sulfonated after polymerization) polysulfone films for proton exchange membrane fuel cells (PEMFC). Proton conductivity and life span of the extruded films were compared with those of solvent cast films [27, 28]. Sanchez et al. also used post-sulfonated polysulfone for PEMFC. The influence of several plasticizers on the glass transition and rheological properties of post-sulfonated polysulfone was reported [29-33].

These previous studies focused on fuel cell applications, and the possibility of membrane formation for water purification applications has not been explored. Also previous studies prepared single layer membranes by extrusion, whereas, in this research, composite membranes may be obtained by coextrusion with a proper support material that can be made porous by stretching or by laminating the sulfonated polysulfone layer onto a porous support layer [34-36].

1.4 Vision: sulfonated polysulfone composite membranes by melt coextrusion

The vision for this study is to investigate the formation of sulfonated polysulfone desalination membranes without the use of solvents, by melt processing, particularly, coextrusion.

Coextrusion can be done in collaboration with Case Western Reserve University through the NSF CLiPS (Centered Layered Polymeric System) program. Figure 1.5 shows the multilayer coextrusion system for two component and the system consists of several extruders and multiplying dies, etc.[7, 34] By using this system, multilayered membranes with at least two layers, up to even thousands of layers, where the thickness of each layer can be as thin as 100 nm can be produced [7, 34, 37].

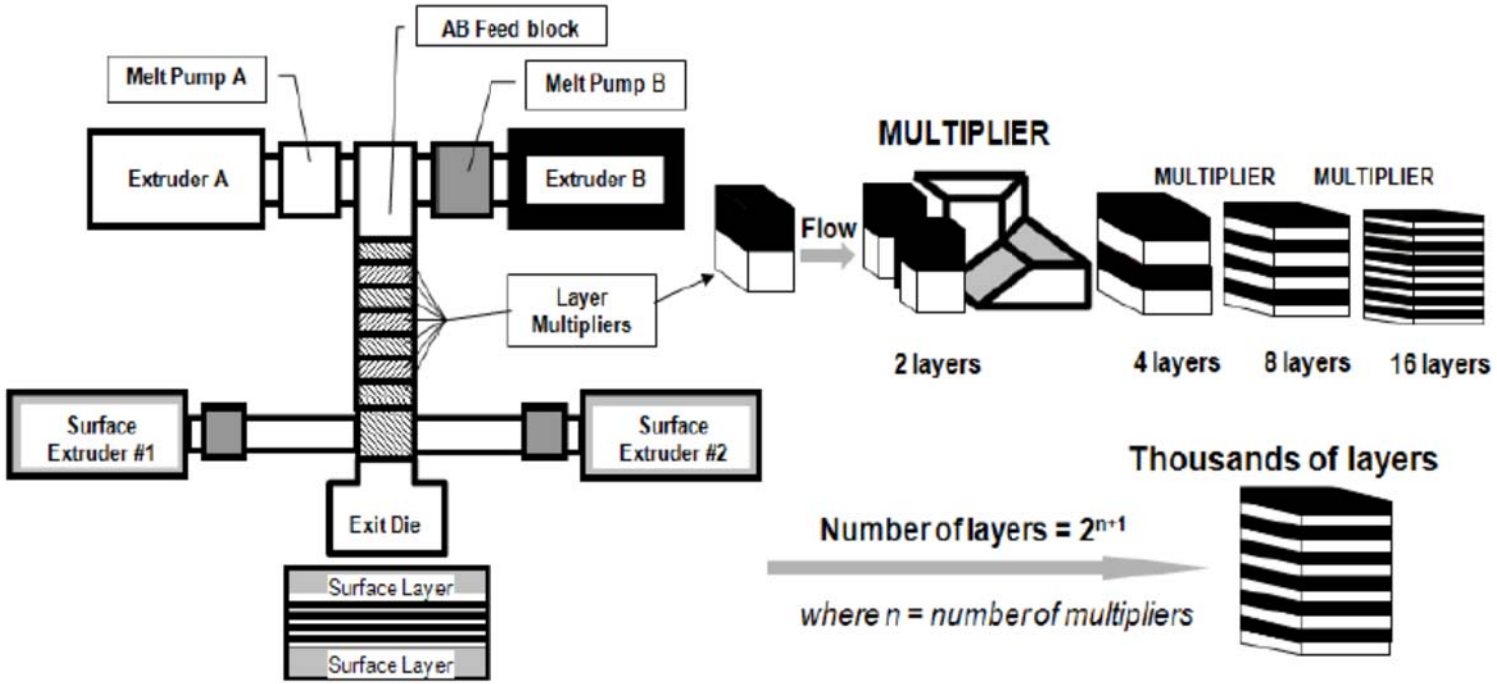

Figure 1.5 (Left) Multilayer coextrusion system for two components. The coextrusion system consists of extruders for two components, multiplying dies, feedblock, extruder for surface sacrificial layer, and exit die. (Right) Schematic description of layer multiplying process. Pictures courtesy of Michael Ponting (Figure 1.1 from Ref. [7]).

Thin film composite membranes are composed of an active selective layer supported by a porous layer. The active layer provides high water transport and salt rejection while the porous layer provides mechanical support with minimal obstruction of water flow [11, 38]. This study examines the feasibility of composite membranes that might be useful for desalination prepared via coextrusion of a sulfonated polysulfone with a suitable support layer material. Polypropylene (PP) is considered as a candidate support material for the proposed membranes since porous PP can be readily formed for various applications by a number of approaches involving post-extrusion stretching [35, 36]. For example, Offord and others coextruded PEBAX materials as the active layer and PP as the support layer for gas permeation applications [35, 36].

Two coextrusion strategies

Two coextrusion strategies are proposed to obtain thin composite membranes. The first method involves biaxial (or uniaxial) stretching to create porosity in the support layer after coextrusion as shown in Figure 1.6a. This stretching may generate some defects in the active layer. However, such defects are not likely to overlap in multilayer structures and could be removed by a subsequent annealing process, and thus selectivity would be retained. The lamination with a porous support layer after extrusion can also be an option as suggested in Figure 1.6b. The active layer is separated from a sacrificial skin layer and is pulled through a set of porous support layers that are already stretched to generate porosity before lamination.

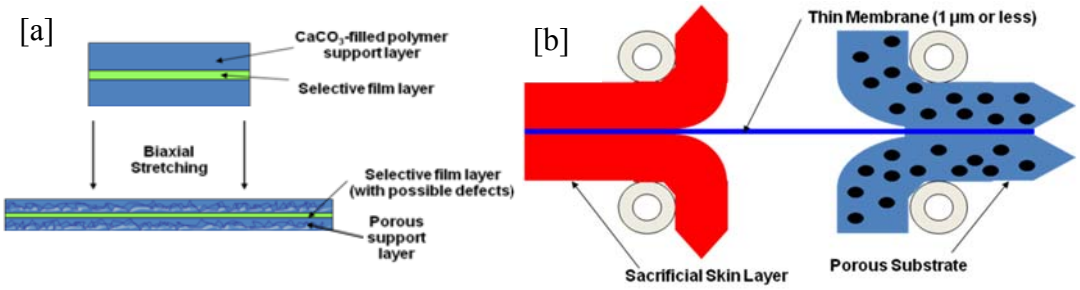

Figure 1.6 Proposed coextrusion strategies to obtain thin film composite membrane. [a] Biaxial stretching after coextrusion. [b] Lamination after extrusion. Pictures courtesy of Grant Offord.

1.5 Challenges and opportunities

To obtain uniform thickness and defect-free thin layers by coextrusion, viscosities of the coextruded materials need to be well matched at the potential processing temperature [7, 34, 37]. However, sulfonated polysulfone has a high glass transition temperature (T_g ~ 220-330 °C depending on sulfonation level), so it does not readily flow prior to reaching its decomposition temperature [24, 39], and, thus, it cannot be extruded in a neat form at the PP processing temperature range (180~250 °C). Therefore, a proper plasticizer is required, so poly(ethylene glycol) (PEG) is used here to modify the glass transition temperature and melt rheology of sulfonated polysulfone to enable coextrusion with PP [24, 40].

Moreover, membrane performance such as water/salt transport properties, etc. are strongly affected by chemical structure and morphology of polymers, and the polymer morphology is, especially, known to be sensitive to thermal processing history [22, 41-43]. Therefore, membranes prepared by melt processing may have interesting properties compared to those of solution cast membranes. This aspect can potentially be used to

manipulate transport properties by processing methods other than varying the polymer chemical structure.

1.6 Dissertation goals and organization

The goal of this dissertation is to explore the formation of sulfonated polysulfone desalination membranes by melt processing. Therefore, this dissertation is organized to address the following main topics:

1) Thermal analysis of plasticized sulfonated polysulfone (Chapters 4 and 5) to study the miscibility of sulfonated polysulfone and potential plasticizers (PEG), the influence of PEGs on the glass transition of sulfonated polysulfone, and the thermal stability of PEGs at the potential processing temperatures.
2) Rheological studies of plasticized sulfonated polysulfone (Chapter 6) to understand the fundamental flow behavior of sulfonated polysulfone plasticized with PEGs, and to identify coextrusion processing conditions with candidate polypropylene (PP).
3) Formation of extruded sulfonated polysulfone membranes (Chapter 7) to prepare defect-free, thin films of uniform thickness, similar to those of solution cast films.
4) Kinetics of PEG extraction from the extruded membranes (Chapter 8) to understand the PEG diffusion from these films and optimize extraction route for membrane preparation.
5) Characterization of extruded sulfonated polysulfone membranes (Chapter 9) to understand the effects of (a) PEG extraction method and (b) PEG composition on the water and salt transport properties of membrane. Properties of melt

processed membranes are compared to those of solution cast membranes to understand the influence of processing protocol on transport properties.

6) Identification of PEG extraction media other than water (Chapter 10) to understand the effect of PEG extraction media on transport properties

Chapter 2 presents background and theories about the rheology of ionomers, the fundamental water and salt transport properties across membranes and other related topics in the literature. Chapter 3 provides information about material selection, and experimental methodologies for characterization. Chapter 11 presents conclusions and future recommendations of this research.

1.7 References

[1] T. Oki, and S. Kanae, "Global hydrological cycles and world water resources," *Science,* vol. 313, no. 5790, pp. 1068-1072, 2006.

[2] UNEP, *Vital water graphics - An overview of the state of the world's fresh and marine waters, 2nd edition*, UNEP, Nairobi, Kenya, 2008.

[3] M. E. Webber, "Evergy versus water: solving both crises together," *Scientific American Special Edition Earth 3.0,* vol. 18, pp. 34-41, 2008.

[4] G. M. Geise, H.-S. Lee, D. J. Miller, B. D. Freeman, J. E. McGrath, and D. R. Paul, "Water purification by membranes: the role of polymer science," *Journal of Polymer Science Part B: Polymer Physics,* vol. 48, no. 15, pp. 1685-1718, 2010.

[5] R. F. Service, "Desalination freshens up," *Science,* vol. 313, pp. 1088-1090, 2006.

[6] R. W. Baker, "Overview of membrane science and technology," *Membrane technology and applications*, pp. 1-13: John Wiley & Sons, Ltd., 2004.

[7] M. T. Ponting, “Gradient multilayered films & confined crystallization of polymer nanolayers by forced assembly coextrusion,” Ph.D. Dissertation, Department of Macromolecular Science & Engineering, Case Western Reserve University, 2010.

[8] K. Scott, "Water desalination," *Handbook of industrial membranes*, pp. 489-517, Oxford: Elsevier, 2003.

[9] H. Ju, “Water transport study in crosslinked poly(ethylene oxide) hydrogels as fouling-resistant membrane coating materials,” Ph.D. Dissertation, Department of Chemical Engineering, the University of Texas at Austin, 2010.

[10] H. B. Park, B. D. Freeman, Z. B. Zhang, M. Sankir, and J. E. McGrath, “Highly chlorine-tolerant polymers for desalination,” *Angewandte Chemie International Edition,* vol. 47, no. 32, pp. 6019-6024, 2008.

[11] R. J. Petersen, “Composite reverse osmosis and nanofiltration membranes,” *Journal of Membrane Science,* vol. 83, no. 1, pp. 81-150, 1993.

[12] J. Kucera, “Understanding RO membrane performance,” *Chemical Engineering Progress,* vol. 104, no. 5, pp. 30-34, 2008.

[13] T. Pankratz, “Membrane desalination opportunities, technologies & costs,” in The Osmosis Membrane Summit, Amsterdam, 2008.

[14] B. D. McCloskey, “Novel surface modifications and materials for fouling resistant water purification membranes,” Ph.D. Dissertation, Department of Chemical Engineering, The University of Texas at Austin. 2009.

[15] W. Xie, J. Cook, H. B. Park, B. D. Freeman, C. H. Lee, and J. E. McGrath, “Fundamental salt and water transport properties in directly copolymerized disulfonated poly(arylene ether sulfone) random copolymer,” *Polymer,* vol. 52, no. 9, pp. 2244-2254, 2011.

[16] M. Abdel-Jawad, S. Ebrahim, M. Al-Tabtabaei, and S. Al-Shammari, "Advanced technologies for municipal wastewater purification: technical and economic assessment," *Desalination,* vol. 124, no. 1-3, pp. 251–261, 1999.

[17] W. G. Light, H. C. Chu, and C. N. Tran, "Reverse osmosis TFC magnum elements for chlorinated/dechlorinated feedwater processing," *Desalination,* vol. 64, pp. 411-421, 1987.

[18] W. Xie, J. Cook, H. B. Park, B. D. Freeman, C. H. Lee, and J. E. McGrath, "Advances in membrane materials: desalination membranes based on directly copolymerized disulfonated poly(arylene ether sulfone) random copolymers," *Water Science and Technology : a Journal of the International Association on Water Pollution Research,* vol. 61, no. 3, pp. 619-624, 2010.

[19] W. Xie, G. M. Geise, B. D. Freeman, H.-S. Lee, G. Byun, and J. E. McGrath, "Polyamide interfacial composite membranes prepared from m-phenylene diamine, trimesoyl chloride and a new disulfonated diamine," *Journal of Membrane Science,* vol. 403-404, no. 1-2, pp. 152-161, 2012.

[20] M. Y. Kariduraganavar, R. K. Nagarale, A. A. Kittur, and S. S. Kulkarni, "Ion-exchange membranes: preparative methods for electrodialysis and fuel cell applications," *Desalination,* vol. 197, no. 225-246, 2006.

[21] M. Heinzer, M. Lee, R. Van Houten, O. Lane, J. E. McGrath, and D. G. Baird, "Effects of solvent-casting conditions on the morphology and properties of highly fluorinated poly(arylene ethersulfone) copolymer films for polymer electrolyte membranes," *Annual Technical Conference - Society of Plastics Engineers,* vol. 67, pp. 606-610, 2009.

[22] W. Xie, G. M. Geise, B. D. Freeman, C. H. Lee, and J. E. McGrath, "Influence of processing history on water and salt transport properties of disulfonated polysulfone random copolymers," *Polymer,* vol. 53, no. 7, pp. 1581-1592, 2012.

[23] C. H. Lee, D. VanHouten, O. Lane, J. E. McGrath, J. Hou, L. A. Madsen, J. Spano, S. Wi, J. Cook, W. Xie, H. J. Oh, G. M. Geise, and B. D. Freeman, "Disulfonated poly(arylene ether sulfone) random copolymer blends tuned for rapid water

permeation via cation complexation with poly(ethylene glycol) oligomers," *Chemistry of Materials,* vol. 23, no. 4, pp. 1039-1049, 2011.

[24] H. J. Oh, B. D. Freeman, J. E. McGrath, C. H. Lee, and D. R. Paul, "Thermal analysis of disulfonated poly(arylene ether sulfone) plasticized with poly(ethylene glycol) for membrane formation," *Polymer* vol. 55, no. 1, pp. 235-247, 2014.

[25] F. E. Bailey Jr., and J. V. Koleske, "Properties of poly(ethylene oxide)," *Poly(ethylene oxide)*, pp. 29-31, 136-138, United Kingdom, London: Academic Press, INC. (London) LTD, 1976.

[26] L. Chen, C.-y. Sheng, Y.-x. Duan, and J.-m. Zhang, "Morphology, microstructure and properties of PEG-plasticized PVC," *Polymer-Plastic Technology and Engineering,* vol. 50, pp. 412-417, 2011.

[27] P. Bebin, and H. Galiano, "Processing of sulfonated polysulfone for PEMFC membrane applications: Part 2. polymer in salt form," *Advances in Polymer Technology,* vol. 25, no. 2, pp. 127-133, 2006.

[28] P. Bebin, and H. Galiano, "Processing of PEMFC membranes by extrusion: Part 1. sulfonated polysulfone in acid form," *Advances in Polymer Technology,* vol. 25, no. 2, pp. 121-126, 2006.

[29] J.-Y. Sanchez, C. Iojoiu, Y. Piffard, N. E. Kissi, and F. Chabert, *Extrusion of a thermoplastic polymer bearing acid ionic groupings*, United States Patent No. 7956095 B2, 2011.

[30] J.-Y. Sanchez, C. Iojoiu, R. Mercier, M. Marechal, N. E. Kissi, H. Galiano, and F. Chabert, *Membrane preparation method comprising the extrusion of a thermoplastic polymer bearing alkaline groupings*, United States Patent No. 7,973,089 B2, 2011.

[31] J.-Y. Sanchez, F. Chabert, C. Iojoiu, J. Salomon, N. E. Kissi, Y. Piffard, M. Marechal, H. Galiano, and R. Mercier, "Extrusion: an environmentally friendly process for PEMFC membrane elaboration," *Electrochimica Acta,* vol. 53, no. 4, pp. 1584-1594, 2007.

[32] Y. Molmeret, F. Chabert, N. E. Kissi, C. Iojoiu, R. Mercier, and J.-Y. Sanchez, "Toward extrusion of ionomers to process fuel cell membranes," *Polymers,* vol. 3, no. 3, pp. 1126-1150, 2011.

[33] Y. Molmeret, F. Chabert, C. Iojoiu, N. E. Kissi, and J.-Y. Sanchez, "Extruded proton exchange membranes based on sulfonated polyaromatic polymers for fuel cell application," in The XV International Congress on Rheology: The Society of Rheology 80th Annual Meeting, Monterey, CA, 2008.

[34] M. T. Ponting, A. Hiltner, and E. Baer, "Polymer nanostructures by forced assembly: process, structure, and properties," *Macromolecular Symposia,* vol. 294, no. 1, pp. 19-32, 2010.

[35] G. T. Offord, S. R. Armstrong, B. D. Freeman, E. Baer, A. Hiltner, J. S. Swinnea, and D. R. Paul, "Porosity enhancement in β nucleated isotactic polypropylene stretched films by thermal annealing," *Polymer,* vol. 54, no. 10, pp. 2577-2589, 2013.

[36] G. T. Offord, S. R. Armstrong, B. D. Freeman, E. Baer, A. Hiltner, and D. R. Paul, "Influence of processing strategies on porosity and permeability of β nucleated isotactic polypropylene stretched films," *Polymer,* vol. 54, no. 11, pp. 2796-2807, 2013.

[37] M. T. Ponting, Y. Lin, J. K. Keum, A. Hiltner, and E. Baer, "Effect of substrate on the isothermal crystallization kinetics of confined poly(ε–caprolactone) nanolayers," *Macromolecules,* vol. 43, no. 20, pp. 8619-8627, 2010.

[38] R. W. Baker, "Vapor and gas separation by membranes," *Advanced membrane technology and applications*, N. N. Li, A. G. Fane, W. S. Ho and T. Matsuura, eds., pp. 562-563: John Wiley & Sons, Inc., 2008.

[39] F. Wang, M. Hickner, Y. S. Kim, T. A. Zawodzinski, and J. E. McGrath, "Direct polymerization of sulfonated poly(arylene ether sulfone) random(statistical) copolymer: candidates for next proton exchange membranes," *Journal of Membrane Science,* vol. 197, no. 1-2, pp. 231-242, 2002.

[40] H. J. Oh, B. D. Freeman, J. E. McGrath, C. J. Ellison, S. Mecham, K.-S. Lee, and D. R. Paul, "Rheological studies of disulfonated poly(arylene ether sulfone) plasticized with poly(ethylene glycol) for membrane formation," *Polymer,* vol. 55, no. 6, pp. 1574-1582, 2014.

[41] Y. S. Kim, L. Dong, M. A. Hickner, B. S. Pivovar, and J. E. McGrath, "Processing induced morphological development in hydrated sulfonated poly(arylene ether sulfone) copolymer membranes," *Polymer,* vol. 44, no. 19, pp. 5729-5736, 2003.

[42] Y. S. Kim, M. A. Hickner, L. Dong, B. S. Pivovar, and J. E. McGrath, "Sulfonated poly(arylene ether sulfone) copolymer proton exchange membranes: composition and morphology effects on the methanol permeability," *Journal of Membrane Science,* vol. 243, no. 1-2, pp. 317-326, 2004.

[43] Y. S. Kim, F. Wang, M. A. Hickner, B. S. Pivovar, and J. E. McGrath, "Effect of acidification treatment and morphological stability of sulfonated poly(arylene ether sulfone) copolymer proton-exchange membranes for fuel-cell use above 100 °C," *Journal of Polymer Science Part B: Polymer Physics,* vol. 41, no. 22, pp. 2816-2828, 2003.

Chapter 2: Background and Theories[2]

2.1 RHEOLOGY OF IONOMERS

It is important to control the plasticized sulfonated polysulfone (BPS/PEG) rheology within a specific range for coextrusion with polypropylene (PP) to achieve uniform thickness and defect-free membranes [1-3].

Since the material of focus (i.e., sulfonated polysulfone, BPS) is an ionomer (or an associating polymer), it is important to understand the melt behavior of such ionomers. Many studies have reported that the melt behavior of ionomers is different from that of non-associating polymers, since the ionic groups act as physical cross-links, or may aggregate, leading to rheological complexity [4, 5]. Ionic associations are not permanent cross-links, however, because of their long lifetime, they perform like physical cross-links. Addition of ionic groups to the polymer matrix may increase viscosity and relaxation time by several orders of magnitude compared to those of uncharged polymers (i.e., non-associating polymers) [5]. However, ionic groups in the polymer can also be disrupted by several factors including heat, plasticizer, and stress, etc. [4-6].

In general, the rheology of ionomers may be affected by various factors [7, 8] such as counter-ion/bound-ion type, molecular weight, neutralization level, plasticizer, temperature and shear rate, etc. as summarized in Table 2.1, however no universal rules have been established to explain the effect of all of these factors on rheology [4-6].

---

2 Parts of this chapter have been adapted from the following articles with permission:
(1) H. J. Oh, B. D. Freeman, J. E. McGrath, C. H. Lee, and D. R. Paul, "Thermal analysis of disulfonated poly(arylene ether sulfone) plasticized with poly(ethylene glycol) for membrane formation," Polymer vol. 55, pp. 235-247, 2014.
(2) H. J. Oh, B. D. Freeman, J. E. McGrath, C. J. Ellison, S. Mecham, K.-S. Lee, and D. R. Paul, "Rheological studies of disulfonated poly(arylene ether sulfone) plasticized with poly(ethylene glycol) for membrane formation," Polymer, vol. 55, pp. 1574-1582, 2014.

Table 2.1 Various factors that influence the rheology of plasticized and non-plasticized ionomers [4-6]

Ionomer	Plasticizer	Condition
Counter-ion type	Type [polar, non-polar]	Temperature [°C]
Bound-ion type	Molecular weight [g/mol]	Time [s]
Neutralization level [mol%]	Concentration [wt%]	Shear rate [s^{-1}]
Molecular weight [g/mol]		

Table 2.2 shows various ionomer families that are extensively studied in the literature [6]. Styrene-based ionomers are investigated widely because they are not crystalline, and their parent polymers have been studied extensively as well. Therefore, any difference introduced by adding ionic groups to the polymer matrix can be directly correlated to the presence of such ionic groups [6].

Other ionomer families that hold much greater industrial importance than the styrene-based ionomers are, for example, the ethylene-based materials. However, the polyolefin crystallinity in these ionomers makes the interpretation more difficult, since the introduction of ionic groups brings changes in crystallinity [4, 6].

Table 2.2 Ionomer families that are extensively studied, Table 2 from Ref. [6]

Styrene-based ionomers	Ethylene-based ionomers	Others
Styrene-acrylates	Ethylene-methacrylates	Polyurethane-based ionomers
Styrene-methacrylates	Ethyl acrylate-methacrylates	Butadiene-methacrylates
Sulfonated polystyrenes	Sulfonated ethylene-propylene-diene terpolymers	Perflurosulfonates
Carboxylated polystyrenes		Sulfonated polyesters

2.1.1 Effect of counter ion/bound ion types, neutralization level, and molecular weight

Many ionomers exhibit ionic clusters (or ionic aggregates) in the polymer matrix when only a few mol% of ionic groups are added since the two kinds of chain segments show a significant thermodynamic difference [4-6].

2.1.1.1 Counter-ion type

Among various types of ionomers, the most available materials are anionomers, i.e., acidic polymers which are neutralized with a metallic cation such as Li^+, Na^+, Mg^{2+}, etc. (or often with an amine): a large literature regarding this subject is available [5]. Differences in rheological properties can be found depending on the cation type; however these differences do not seem to be related to ion valency [5]. For instance, ionomers neutralized with some divalent salts such as Zn^{2+} and Pb^{2+} show noticeably lower viscosities than those of ionomers with alkali-metal cations [5]. However, other divalent salts such as Ca^{2+} and Mg^{2+} yield relatively higher viscosities [5, 9, 10]. Note that the polymer backbone structure is different in many of these cases.

Makowki, et al. reported that in the study of metal sulfonate-containing ethylene-propylene-diene terpolymer (SEPDM, 31 meq sulfonate/100g), materials with Li^+, Na^+, Mg^{2+}, Ca^{2+}, Ba^{2+}, and Co^{2+} cations show very high viscosities (5.06~5.50 MPa) while these materials exhibited melt fracture under the test conditions ($\gamma < 0.88\ s^{-1}$). However, the material with Pb^{2+} which shows a viscosity of 3.28 MPa, does not show melt fracture until $\gamma = 88\ s^{-1}$ (γ is shear rate); also Zn^{2+} yields a viscosity of 1.20 MP and undergoes melt fracture at $\gamma = 147\ s^{-1}$ [5, 11]. These results imply the influence of cation type on rheological behavior, especially with Pb^{2+} and Zn^{2+}.

Many studies have consistently shown that neutralization with Zn^{2+} leads to a low viscosity compared to other cations [5]. Similar results could be found with Pb^{2+}; however, only a few examples for Pb^{2+} are available [5]. Bagrodia et al. explained the reason why materials neutralized with Zn^{2+} have lower viscosities using the 'hard-soft acid' concept [5, 12]. According to the 'hard-soft acid' concept, the 'soft' (or polarizable) cations construct ion pairs which tend to associate less. In contrast, 'hard' cations have a tendency to form stronger ionic aggregates, producing higher viscosity [5, 12]. Although most cations (e.g., alkali metal) in ionomers are assumed to be 'hard', Zn^{2+} and Pb^{2+} are likely to be at the borderline between 'soft' and 'hard' cations, according to Pearson, et al. [5, 13, 14].

2.1.1.2 Bound-ion type

Compared to the difference induced by changing counter-ion type in ionomers, a change of bound-ion type can affect the rheological properties to a greater extent. However, because of difficulties in such modifications for direct comparison, only a few examples are available [5]. As the most cited results, Lundberg, et al. compared sulfonated and carboxylated polystyrenes prepared by post-polymerization functionalization [5, 15]. The sodium sulfonated polystyrene (NaSPS) shows three orders higher viscosity than that of sodium carboxylated polystyrene (NaCPS) at 3% functionalization [15].

2.1.1.3 Neutralization level

Another way to control ionomer rheology is to modify the neutralization level below the stoichiometric point [5]. Ionomers that are partially neutralized are likely to have viscosities and relaxation times between those of the free acid and the 100% neutralized

materials. Since these differences can be in the range of several orders of magnitude, varying the neutralization level changes rheology dramatically.

Studies of anionomers neutralized with metal salts have been most widely reported. Bonotto, et al. reported the melt index of an ethylene-acrylic acid copolymer that is neutralized with several cations such as Na^+, K^+, Li^+, etc. The % neutralization level is varied between 0 and 70 % [5, 16]. As the neutralization level increases, melt index decreases (i.e., viscosity increases) by several orders of magnitude, but effects are different based on the counter-ion form. However, the effect of neutralization level on melt index is stronger compared to that of cations [5, 16]. Similar observations were reported with other ionomers such as carboxy-telechelic polybutadienes [10] and NaSPS [17]. Also, the viscosity curves from different cations intersect as neutralization level increases. The reasons are not apparent, but Register, et al. explained this with the observation reported by Iwakura, et al [5, 18]; some cations such as Zn^{2+} could more effectively increase viscosity than other cations such as Na^+ do, when the neutralization level is low, with styrene-methacrylic acid copolymers. This trend could be different at high neutralization levels and may explain the crossing of viscosity (or melt index) curves.

Adjusting the neutralization level is one method to control the rheology; however, it is not a general way to modify the rheological properties because a few free acid materials were reported not to be thermally stable, and thus can degrade at processing temperature [5, 19].

2.1.1.4 Molecular weight

Increasing the molecular weight of an associating polymer can enhance both molecular entanglements as well as ionic interactions, both of which could influence viscosity [5, 20-22]. It is difficult to distinguish the influences from entanglements and

ionic interactions, since the contribution of entanglements to the dynamic storage modulus is as significant as that of ionic associations, according to Weiss et al. in their studies with lightly sulfonated polystyrene (2.5 and 4.8 mol% sulfonation) [21-23].

Fouissac et al. reported for hyaluronate, a wormlike ionomer that, in the dilute region, where $M < M_c$ (M_c is the critical molecular weight for entanglements), the zero shear viscosity scales with molecular weight to the first power ($\eta_0 \propto M^1$), similar to that of non-associating polymers. However, M_c is observed at concentrations 10 times less than in entangled, non-associating flexible polymers in solution. Above the entanglement concentration, the zero shear viscosity scales with molecular weight to the fourth power ($\eta_0 \propto M^4$) in associating polymers rather than the 3.4 power ($\eta_0 \propto M^{3.4}$) typically observed in non-associating polymers [20]. This may be explained by the stronger molecular entanglement induced by the interchain ionic interactions in ionomers.

2.1.2 Effect of plasticizer

Since ionomers exhibit high viscosities and long relaxation times, a plasticizer can be used to modify rheological properties to enable melt processing for industrial applications [4, 5]. Addition of a plasticizer to ionomers can reduce the glass transition temperature (T_g) and viscosity of ionomers for two reasons: (1) a plasticizer adds more free volume to the polymer matrix, which would reduce interchain restrictions on polymer segmental mobility, and (2) the interaction between a plasticizer and the ionic groups may reduce the ionic interactions in ionomers [5, 17, 24-26]. For example, Lundberg, et al. reported the plasticization effect of several nonvolatile diluents such as glycerol, dioctyl phthalate (DOP), and dibutyl phthalate (DBP) on lightly Na-sulfonated polystyrene ionomers (NaSPS, 1~5 mol% sulfonation level) [5, 17, 27]. The viscosity of 1.78 mol% NaSPS plasticized with 3.5 wt% glycerol decreases by three orders of magnitude and is

within an order of magnitude of the viscosity of unfunctionalized polystyrene [5, 17, 27]. In their studies, glycerol was seen to interact effectively with the ionic groups, so it was effective in lowering the viscosity (more details in Section 2.1.2.1).

However, although ionic interactions need to be interrupted by a plasticizer at the potential melt processing temperature, ionic interactions are often necessary to maintain good ionomer properties (e.g., mechanical strength, etc.) at use temperature. For this reason, a plasticizer should be extracted after melt processing to preserve the ionomer properties, since plasticizers can lessen the ionic associations of ionomers at all temperature [5].

On the other hand, some crystalline plasticizers can be preserved in the final product after melt processing, since these plasticizers are immobilized at use temperature, as proposed by Canter et al. [5, 28]. For instance, Makowski and others reported that when zinc stearate (ZnSt) was used as a plasticizer for Zn sulfonated SEPDM (ZnSEPDM), ZnSt improved the melt flow at high temperature and maintained good mechanical properties of ZnSEPDM [5, 28-30]. Indeed, adding ZnSt increases tensile strength and elongation of ZnSEPDM and the high concentration of ZnSt does not affect the modulus of ZnSEPDM. When cooled after melt processing, small crystallites formed from crystallization of ZnSt function as a 'filler' and may have interactions with the ionic groups (i.e., good adhesion). As a result, ZnSt as a plasticizer can improve the ionomer properties while promoting melt processability [5, 31].

2.1.2.1 Viscosity changes by polar and non-polar plasticizers

The plasticization of ionomers by low-molecular weight diluents is not entirely explained by simple free-volume effects. For non-associating polymers, diluents add more free volume, promote polymer segmental mobility and, therefore, decrease the glass

transition temperature (T_g) [4, 6, 17, 32, 33]. However, for ionomers, the interactions between a plasticizer and the ionic groups are likely to reduce the ionic interactions [5, 17, 24-26]. These interactions need to be considered when selecting proper plasticizers, since plasticizers of different polarity may exhibit different degrees of effects when plasticizing the polymer backbone and/or the ionic groups [4, 6, 17, 33].

For example, Lundberg et al., reported in their studies of lightly Na-sulfonated polystyrene ionomers (NaSPS, 1~5 mol% sulfonation level) that were plasticized by several nonvolatile diluents, that the plasticization effect of glycerol is different from that of dioctyl phthalate (DOP) [4, 17]. DOP, a representative of low polarity (i.e., low dielectric constant) plasticizers, mainly solvates the polymer backbone (or matrix), and, thus, it depresses the polymer matrix T_g significantly but reduces viscosity modestly, since the ionic groups are not fully disrupted. In contrast, glycerol, a representative of high polarity (i.e., high dielectric constant) plasticizers, is likely to incorporate with the ionic groups so that it effectively lowers the viscosity; however, it does not decrease the polymer matrix T_g significantly [4, 27].

There are an extensive number of issues discussed in the literature explaining the changes in mechanical properties and morphology of ionomers by addition of plasticizers [4, 17, 21, 27, 34]. Fitzgerald and Weiss reported studies of the lightly sulfonated polystyrene salt of manganese, Mn, (2.65 mol% MnSPS); the SAXS peak position was not changed with the addition of 1~10 wt% DOP (low polarity plasticizer), although the intensity decreased with increasing DOP concentration, indicating DOP is mainly located in the hydrocarbon-rich phase (i.e., matrix) [4, 34]. On the other hand, for glycerol (high polarity plasticizer), the peak moved to lower angles and the intensity was increased significantly at 1~10 wt% glycerol [4, 34]. The authors related this change induced by

glycerol to the swelling of the ionic clusters; as the ionic clusters absorb a larger amount of plasticizer, the volume fraction of ionic clusters increases, and the strength of ionic interactions is lowered [34]. The varying effectiveness of different plasticizers is likely to correspond to the different interactions between the diluents and the ionic groups, although more investigations regarding the detailed mechanism are required [4].

Another example can be found in the studies of sulfonated poly(aryl ether) sulfone, similar to our material of focus, by Drzewinski, et al. [33]. Higher alcohols (i.e., more lipophilic or less polar), have a tendency to lower the polymer matrix T_g; however, alcohols (e.g., methanol or ethanol) increase the polymer matrix T_g, but not as much as water does. Alcohols of medium molecular weight are likely to be the most effective plasticizers because they may incorporate with the polymer backbone and the ionic groups at the same time [4, 27, 33]. Plasticization effects on ionomers by low or high polarity diluents have been explored for various ionomer types [4, 17, 21, 22, 27, 33, 34].

2.1.2.2 Viscosity changes by the addition of salts

The rheology of ionomer solutions is complicated when counter-ions are added to the solution (i.e., ionizable salt molecules) [35, 36]. Most theories focus on the dilute and semidilute polymer solutions but there has been little attention paid to entangled and concentrated ionomer solutions [36], which is the focus in this research.

Wyatt and others reported changes in viscosity of ionomer solutions by salt addition for all concentration regimes [36]. In the case of the Xanthan solution at low concentration (i.e., the unentangled concentration region), the zero shear viscosity was lowered around 100-fold when monovalent salt (i.e., NaCl) was added. In contrast, beyond a certain critical concentration (C_D = 2,000 ppm) of Xanthan, the zero shear viscosity was increased around

fourfold with salt addition. Similar observations were made with other ionomers such as cationic and anionic polysaccharides.

Waytt, et al. explained these rheological changes by the competing effects of: (1) collapse of chain configuration and (2) hydrogen bonds induced by salt addition [36]. In the pure polymer solutions without any salt and at a suitable pH, ionomers show a reasonably extended chain configuration due to the electrostatic repulsions between polymer segments. As a monovalent salt is added, the salt ions shade the electrostatic interactions between the ionic groups of ionomers, and this leads to the collapse of chain configuration. Subsequently, hydrogen bonds are likely to form among polymer chains; however, because of long enough distance among polymer chains (due to the low concentration of polymer), the number of hydrogen bond is not significant. As a result, the viscosity decreases, and this is widely known for dilute and semidilute polymer solutions.

On the other hand, at higher polymer concentrations (e.g. entangled and concentrated regime), the number of hydrogen bonds among polymer segments increases, since the distance between polymer chains decreases. This greater number of hydrogen bonds surpasses the influence of polymer configuration, and therefore the viscosity increases significantly when salt is added [36].

2.1.3 Effect of temperature and shear rate

2.1.3.1 Temperature dependence on viscosity

Generally, the viscosities of polymer melts decrease as temperature increases, since thermal expansion promotes chain mobility by adding extra free volume to local segment [37]. For melts of glassy polymers at $T_g < T < T_g + 100$ °C, the Williams-Landel-Ferry

(WLF) equation is usually followed, but a simple Arrhenius type like the Andrade-Eyring equation is obeyed at higher temperatures [20, 38].

For ionomers, the temperature dependence of viscosity is more complex due to 'ion-hopping' as mentioned by Cooper and others [4, 5, 39, 40]. The ionic associations are in dynamic equilibrium [5]; these ionic associations remain intact to elevated temperature, although little migration of ion pairs could exist. Slow ion hopping at low temperatures corresponds to the well-defined rubbery plateau modulus in the dynamic storage modulus (E') versus temperature curves (and reduces creep at use temperature). At high temperatures, the migration or intechange of ion pairs becomes fast enough to be within the time scale of measurments, resulting in a noticeable decrease of modulus. Rapid rates of ion hopping at high temperatures enable melt flow and stress relaxation [4, 5, 39-41].

Hird and Eisenberg quantitatively reported the activation energy, E_a, for ion hopping in their studies of sulfonated polystyrene ionomer, by analyzing the modulus versus temperature curves; the temperature where the plateau modulus starts to decrease dramatically is regarded as the onset of ion hopping [4, 40]. Also, by comparing the well-defined plateau modulus of Na-sulfonated polystyrene ionomers (PSS-Na) to the non-existing plateau of Na-carboxylated polystyrne ionomers (PSC-Na), they concluded that Na-sulfonated groups are likely to have stronger electrostatic attractions among themselves than those of Na-carboxylate groups [40]. Similar analyses were conducted with other ionomers [4, 42].

These temperature dependences are the foundation for the principle of time-temperature superposition (TTS) [38]. Although TTS is an essential tool to investigate ionomer behavior [5, 8], ionomers generally do not follow TTS since the various phases present in ionomers are likely to have different temperature dependences. Sometimes, the

deviation from TTS is apparent when the concentration of ionic groups increases. However, one may apply TTS to ionomers for restricted time and temperature ranges if the concentration of ionic groups is significantly low (WLF type of dependence) or if the ionomers have fairly short polymer segments. (Arrhenius type of dependence) [5].

2.1.3.2 Shear rate dependence on viscosity

For the shear rate dependence of the viscosity, most polymers are pseudoplastic in the non-Newtonian region at high shear rate, whereas some associating polymer solutions (for example, Na and Li substituted sulfonated polystyrene) exhibit shear thickening where, after the Newtonian regime, the viscosity increases by a factor of 2-3, and then shear thinning follows at higher shear rates [5, 43-48]. Witten, et al. explained that the ionic intrachain pairs separated and interchain connections increase as shear flow elongated the polymer chains, forming larger ionic networks, which contributed to higher viscosity. As the shear rate increased to levels exceeding the chain relaxation time, a shear thinning region appeared [43, 49]. Therefore, ionic interactions as well as polymer entanglements should be considered in interpreting the rheology of associating polymers [5, 21, 22, 50].

2.1.4 Verification of the Cox-Merz Rule

The Cox-Merz rule is used to connect the complex viscosity, $|\eta^*|$, versus frequency measured in oscillatory shear flow to the steady shear viscosity, η, versus shear rate. For some polymer fluids, the sample may be expelled from the plates at high shear rates, leading to flow instability and incorrect results. Data collection using the oscillatory shear mode is generally more reliable in such cases and is used to predict the steady shear viscosity at high shear rates using the Cox-Merz rule [51] that considers the steady state

shear viscosity, η, at shear rate, $\dot{\gamma}$, to be identical to the magnitude of the complex viscosity, $|\eta^*|$, at angular frequency, ω[38, 52] :

$$\eta(\dot{\gamma}) = |\eta^*(\omega)| \quad when \ \dot{\gamma} = \omega \tag{2.1}$$

The Cox-Merz rule is valid in many cases. However, for more complex polymers including ion-associating ones, the Cox-Merz rule is not followed because of their rheological complexity. The extent of departure from the Cox-Merz rule is dependent on ion content, counter-ion type, etc. [5, 53].

2.2 MORPHOLOGY OF SULFONATE POLYSULFONE

Several morphological models for ionomers have been developed to interpret the ionic peaks in SAXS studies [4, 6]. Examples include the Hard-Sphere model, the Core-Shell model and the Eisenberg-Hird-Moore (EHM) model. The Hard-Sphere model assumes the SAXS peak as the inter-particle distance (i.e., the distance between ionic clusters), whereas the Core-Shell model assigned the peak as the intra-particle distance, although both models are based on the presence of ionic clusters (i.e., aggregates). The EHM model is the latest model and suggests that the ionic aggregates reduce the polymer segmental motion, leading to phase separation (although the aggregation level may depends on various factors such as cation counter-ion type, etc.) and two glass transitions (matrix T_g and cluster phase T_g). Many ionomers exhibit two T_gs by adding only 5~10 mol% ionic group into the polymer matrix [4, 6].

However, Drzewinski, et al. concluded from DSC and SAXS studies that phase separation does not occur in sulfonated polysulfone (SPSF) ionomers [33]. The SAXS profiles confirmed that there was no apparent scattering existing and even though some scattering was found, the scattering intensities were much smaller (i.e., by several orders of magnitude) than those of other ionomers which were known to have ionic clusters. The

addition of ionic groups in SPSF does not appear to lead to separate phases (instead most of them are located in multiplets); however, as the concentration of ionic groups increases, the glass transition temperature (T_g) increases since the ionic groups hinder the polymer chain movements [4, 33, 40, 54]. The T_g was found to increase at a rate of 1.5 °C/mol% sulfonation [33].

On the other hand, Feng et al. reported that disulfonated poly(arylene ether sulfone)s or BPS, the material used in this study, might have ionic clusters on the order of 10~25nm diameter, by using tapping mode AFM [55]. As shown in Figure 2.1, the unfunctionalized control polysulfone, BPS-00, has undistinguished morphology (part [a] in Figure 2.1). As sulfonation level increases from 0 to 60 mol%, black-colored and aggregate-like domains are found and the size of domain becomes larger; they assigned this dark domain to hydrophilic sulfonate groups. When the degree of sulfonation reaches 60 mol% (i.e., BPS-60, part [e] in Figure 2.1), the dark domain forms a large and continuous network of ionic group rich phases. They concluded from AFM phase images that the percolation limit was obtained with 50 mol% sulfonation (i.e., BPS-50); the water uptake also shows a rapid increase over the similar range (see Figure 2.1 (Right)), and two T_g are observed from 50 mol% sulfonation [55].

Considering that many ionomers exhibit two T_gs by adding only 5~10 mol% ionic group [4], BPS exhibits a single T_g up to 50 mol% sulfonation level [55]. Feng et al., explained this as being due to the presence of small and isolated ionic domains below 50 mol% sulfonation level. Indeed, the DMA thermograms of BPS-20K (20 mol% K-sulfonated BPS) material show a broad tan δ response at the glass transition, implying that these ionic domains might have different sizes and/or be randomly distributed [24, 32]. More characterization such as SAXS, need to be performed to confirm the details.

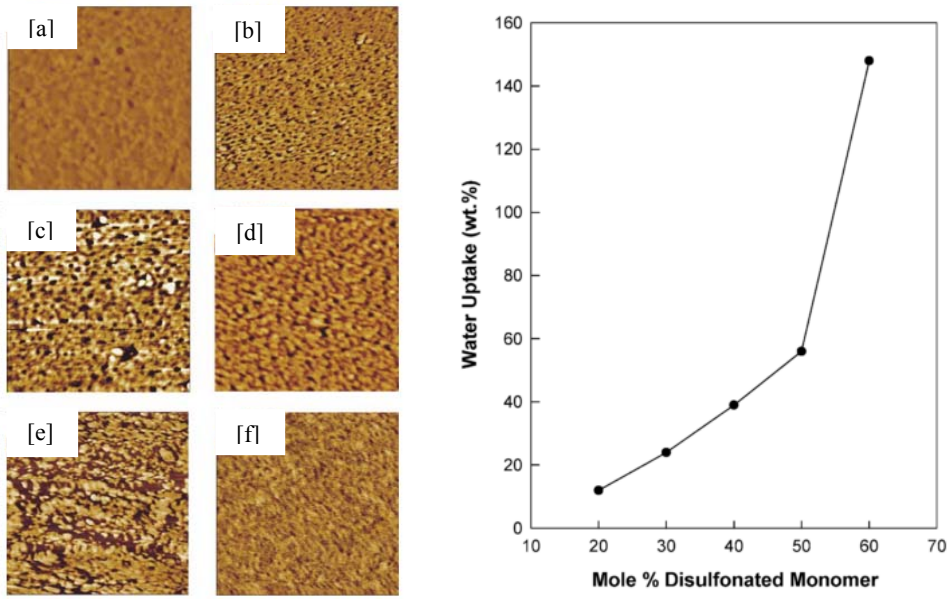

Figure 2.1 (Left) AFM images of disulfonated poly(arylene ether sulfone) (BPS) polymers and Nafion 117. Tapping mode was used: (a) BPS-00, unsulfonated polysulfone; (b) BPS-20H; (c) BPS-40H; (d) BPS-50H; (e) BPS-60H; (f) Nafion 117 (acid form). (Right) Effect of the sulfonation level (i.e., mol% disulfonated monomer) on the water uptake of BPS polymers. Figures from Ref. [55].

2.3 WATER AND SALT TRANSPORT PHENOMENA IN POLYMER MEMBRANES

2.3.1 Fundamental transport of water molecules in polymer membrane

The transport of solvent (e.g., water) and solute (e.g., salt) across reverse osmosis (RO) membranes is generally explained by the solution-diffusion model [56, 57]. Figure 2.2 illustrates the water concentration and pressure profiles across a polymer membrane.

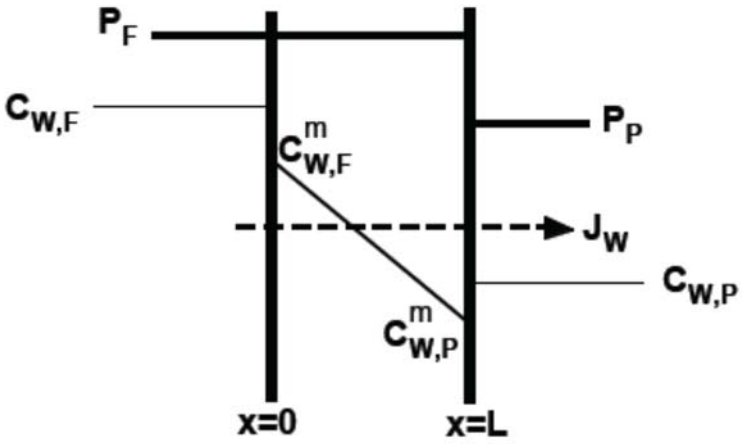

Figure 2.2 Schematic description of water concentration and pressure profiles in a polymer membrane [56-58]. L is the membrane thickness (x = 0 means the feed side of the membrane, whereas x = L denotes the permeate side of the membrane). P_F and P_P are the pressures of feed and permeate, respectively. $C^m_{W,F}$ and $C^m_{W,P}$ are the water concentrations on feed and permeate sides of the membrane. $C^m_{W,F}$ and $C^m_{W,P}$ are in equilibrium with the feed water ($C_{W,F}$) and permeate water ($C_{W,P}$), respectively [56-60].

The water concentration gradient induced by the pressure difference in the dense membrane leads to water diffusion [56, 57]. Thus, the water flux, J_W, can be written in simplified form based on Fick's law as follows [56, 57]:

$$J_W = -D_w \frac{dC^m_W}{dx} = \frac{D_W}{L}(C^m_{W,F} - C^m_{W,P}) \quad (2.2)$$

where L is the thickness of the membrane, D_w is the average water diffusivity (i.e., water diffusion coefficient) in the membrane, and, $C_{W,F}^m$ and $C_{W,P}^m$ are the water concentrations on feed and permeate sides of the membrane. $C_{W,F}^m$ and $C_{W,P}^m$ are in equilibrium with the feed water ($C_{W,F}$) and permeate water ($C_{W,P}$), respectively. Note that the convective term for water transport is ignored in equation (2.2) assuming the water weight fraction (i.e., water uptake) of the polymer membrane is small (<15 vol%) [56-60]. When the convective term is considered, the concentration profile in Figure 2.2 (i.e., C_W^m versus x) is not linear, and a more complete analysis for this case can be found in the literature [56-60] .

The water flux, J_W, can also be expressed in terms of the chemical potential gradient (i.e., $\Delta\mu_W^m$) according to thermodynamics. Standard thermodynamics suggest the chemical potential difference can be described with regards to the net pressure difference applied across the membrane. The net pressure difference, $\Delta p - \Delta\pi$, can be related to the water concentration term in equation (2.2), and equation (2.2) can be rewritten as follows [56, 57]:

$$J_W = \frac{D_W C_{W,F}^m \overline{V_W}}{L R T} (\Delta p - \Delta\pi) \tag{2.3}$$

where R is the gas constant, T is the absolute temperature, $\overline{V_W}$ is the partial molar volume of water (e.g., molar volume of pure water, or 18 cm^3/mol), Δp is the pressure difference across the membrane (i.e., $\Delta p = P_F - P_P$, where P_F and P_P are the pressures of feed and permeate, respectively) and $\Delta\pi$ is the osmotic pressure difference in the membrane (i.e., $\Delta\pi = \pi_F - \pi_P$, where π_F and π_P are the osmotic pressures of feed and permeate, respectively).

The dissolved solutes (i.e., salt) in solution generate osmotic pressure, π, as defined as below [56]:

$$\pi \equiv -\frac{RT}{\overline{V_W}} \ln a_w \tag{2.4}$$

where a_w is the solvent activity (i.e., water activity). For dilute solutions, as shown in Figure 2.2, π_F and π_P can be approximated by the van't Hoff equation and, thus, expressed in terms of salt concentration in the feed and permeate solutions, respectively, as follows [56, 57, 61]:

$$\pi_F = \mathrm{R\ T}\ C_{S,F} \tag{2.5}$$

and

$$\pi_P = \mathrm{R\ T}\ C_{S,P} \tag{2.6}$$

2.3.1.1 Water partition coefficient (K_w)

The water partition coefficient (i.e., water solubility or water sorption coefficient), K_W, is the ratio of water concentration in the polymer membrane (i.e., C_W^m) to the water concentration of solution (i.e., C_W) [56, 62, 63]. Typically the C_W^m and C_W values are taken as the water concentration at the feed side of membrane, $C_{W,F}^m$, and that of feed solution, $C_{W,F}$, respectively. The K_W value determined by the feed side of membrane and that by the permeate side are assumed to be identical in reverse osmosis membranes [57].

$$K_W = \frac{C_{W,F}^m}{C_{W,F}} \left[\equiv \frac{g\ water/cm^3 swollen\ polymer}{g\ water/cm^3 solution}\right] \tag{2.7}$$

The $C_{W,F}^m$ value can be related to the volume fraction of water in the polymer membrane, ϕ_W, as follows [62, 63]:

$$C_{W,F}^m = \phi_W \frac{M_W}{\bar{V}_W} \tag{2.8}$$

where M_W is the water molecular weight (i.e., 18 g/mol). Therefore, equation (2.7) can be rewritten as:

$$K_W = \frac{\phi_W M_W}{C_{W,F}\bar{V}_W} \tag{2.9}$$

For sufficiently dilute solutions such as pure water, $C_{W,F}$ can be approximated as the density of pure water, ρ_W. The partial molar volume of water in the polymer membrane,

$\bar{V}_W$ is assumed to be identical to the molar volume of water in solution (i.e., 18 cm^3/mol) and also the contiguous water contacting the polymer membrane is presumed to have the density of pure water, ρ_W. With these reasonable assumptions, equation (2.9) can be rewritten as follows [62, 63]:

$$K_W = \phi_W \tag{2.10}$$

Thus, K_W is equal to the volume fraction of water in the polymer membrane, and this approximation is used to estimate K_W value based on water uptake measurements. Details of experiments to measure K_W are explained in Chapter 3.

Using the definition of K_W (equation (2.9)):

$$C^m_{W,F} = K_W \cdot C_{W,F} = K_W \cdot \rho_W \tag{2.11}$$

Equation (2.3) can be rewritten as:

$$J_W = \frac{D_W K_W \rho_W \bar{V}_W}{L\,R\,T}\,(\Delta p - \Delta\pi) = \frac{P_W \rho_W \bar{V}_W}{L\,R\,T}\,(\Delta p - \Delta\pi) \tag{2.12}$$

since $P_W = D_W \cdot K_W$ according to the solution-diffusion model [56, 57, 59, 60, 62, 63]. In the practice, water flux, J_w, can be written by the simplified equation [56, 61]:

$$J_w = A \cdot (\Delta p - \Delta\pi) \tag{2.13}$$

where A is the water permeance. Combining equations (2.12) and (2.13) yields:

$$A = \frac{P_w \rho_W \bar{V}_W}{LRT} \tag{2.14}$$

2.3.1.2 Water permeability (P_w)

Hydraulic water permeability (P_W^H)

Hydraulic water permeability, P_W^H, is defined from water flux, J_w, membrane thickness, L, and pressure difference, Δp, as follows [58, 62-64]:

$$P_W^H = \frac{J_w}{\Delta p} \cdot L \tag{2.15}$$

The steady-state water flux, J_w, can be calculated from the following equation:

$$J_w = \frac{\Delta V}{A \cdot \Delta t} \tag{2.16}$$

where ΔV is the permeate volume passing through a membrane (membrane area is A) during a given period of time Δt. Combining equations (2.15) and (2.16) provides:

$$P_W^H = \frac{\Delta V}{A \cdot \Delta t} \cdot \frac{L}{\Delta p} \tag{2.17}$$

The units of P_W^H are $[L \cdot \mu m/(m^2 \cdot h \cdot bar)]$.

Diffusive water permeability (P_W^D)

In the previous section 2.3.1, the water flux, J_w, was simplified in equation (2.2) by assuming the water weight fraction (i.e., water uptake) of the polymer membrane is small (<15 vol%) and the convective term is negligible [56-60]. However, for charged polymer membranes used in this study (i.e., sulfonated polysulfone), the water uptake of the polymer membrane is somewhat high (>15 vol%) [58] and the convective term should be considered for analysis [57, 58, 62, 63]. To describe these effects on water diffusion induced by concentration gradient (this concentration gradient is generated by the pressure difference across the polymer membrane as mentioned earlier.), the Flory-Huggins model is employed to investigate the influence of water activity on water uptake of the polymer membrane [58, 62, 63].

Therefore, the diffusive water permeability, P_W^D (unit is cm^2/s), can be expressed in terms of hydraulic water permeability, P_W^H, as follows [60, 62, 63, 65, 66]:

$$P_W^H = D_W \cdot K_W = P_W^H \cdot \frac{RT}{\overline{V_W}}[(1 - K_W)^2(1 - 2\chi K_W)] \tag{2.18}$$

where D_W is the average effective water diffusivity of the polymer membrane, and χ is the Flory-Huggins interaction parameter. Based on the Flory-Huggins theory, χ can be used to relate the chemical potential of water, a_W, in a swollen polymer to the water concentration in polymer as follows [58, 62, 63, 67, 68]:

$$ln\, a_W = ln\, K_W + (1 - K_W) + \chi(1 - K_W)^2 \quad (2.19)$$

Since, for each membrane sample, the water concentration in an equilibrated polymer membrane can be experimentally measured, and the pure water has a_W value of 1, χ values can be estimated. Using this information, P_W^{D} can be indirectly calculated from P_W^H, which can be easily measured using equation (2.17) and experiments described in Chapter 3.5.

2.3.1.3 Water diffusivity (D_w)

Based on $P_W = D_W \cdot K_W$, the average, effective water diffusivity, D_W, can be estimated from P_W^{D} and K_W values as follows [58, 62, 63]:

$$D_W = \frac{P_W^D}{K_W} \quad (2.20)$$

The units of D_W are [cm^2/s].

2.3.2 Transport of salt molecules in polymer membranes

Figure 2.3 illustrates the salt concentration and pressure profiles in a polymer membrane. Similar to the water diffusion process across the membrane as described in Figure 2.2, salt molecules are transported by diffusion. However, the salt transport in a membrane induced by a hydrostatic pressure difference is typically negligible [56]. In other words, the salt flux, J_s, is mainly caused by the salt concentration difference (i.e., ΔC_S) and is largely independent of the pressure difference across the membrane. Therefore, the salt flux, J_s, can be expressed by Fick's law as follows:

$$J_S = -D_S \frac{dC_S^m}{dx} = \frac{D_S}{L}(C_{S,F}^m - C_{S,P}^m) \quad (2.21)$$

The salt permeability, P_s, can be expressed as a function of salt diffusivity, D_s, and salt partition coefficient, K_s, according to the solution-diffusion model [56-60] :

$$P_s = D_s \cdot K_s \quad (2.22)$$

$$K_s = \frac{C_{S,F}^m}{C_{S,F}} \tag{2.23}$$

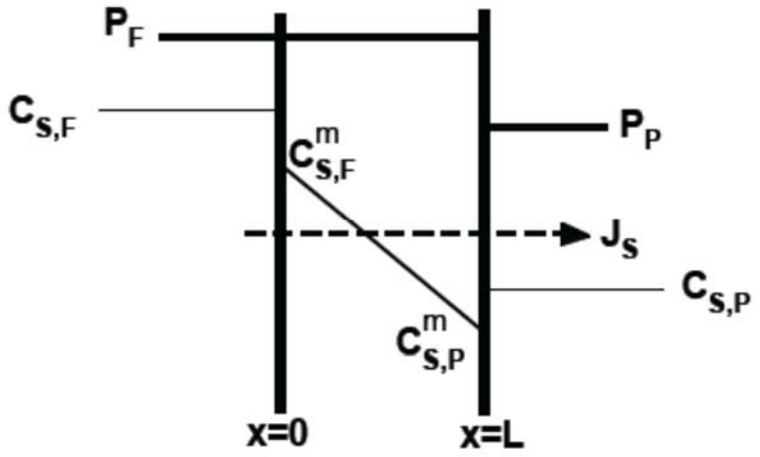

Figure 2.3 Schematic description of salt concentration and pressure profiles in a polymer membrane [56, 57]. L is the thickness of membrane (x = 0 is the feed side of the membrane, whereas x = L denotes the permeate side of the membrane). P_F and P_P are the pressures of feed and permeate, respectively. $C_{S,F}^m$ and $C_{S,P}^m$ are the salt concentrations on feed and permeate sides of the membrane. $C_{S,F}^m$ and $C_{S,P}^m$ are in equilibrium with the feed solution ($C_{S,F}$) and permeate solution ($C_{S,P}$), respectively [56-60].

Equation (2.21) can be rewritten in terms of salt permeability, P_s, as follows:

$$J_S = \frac{P_S}{L}\left(C_{S,F} - C_{S,P}\right) = \frac{P_S}{L} \cdot \Delta C_S \tag{2.24}$$

In practice, the salt flux, J_s, is often expressed as follows [56]:

$$J_s = B \cdot \Delta C_s \tag{2.25}$$

where B is salt permeance [56, 61], and is written as:

$$B = \frac{P_S}{L} \tag{2.26}$$

Note that the A (mentioned previously) and B parameters are not material properties since they depend on membrane thickness [56].

2.3.2.1 Salt permeability (P_s), diffusivity (D_s) and partition coefficient (K_s)

Salt permeability, P_s, salt diffusivity, D_s, and salt partition coefficient, K_s, have similar fundamental background as those of water permeability, P_W, water diffusivity, D_W, and water partition coefficient, K_W. Experimental details to measure the parameters are described in the following Chapter 3.

2.3.2.2 Salt rejection (R)

In practice, salt rejection, R (%), is used to describe the capability of desalination membranes to produce a permeate solution with low salt content, as follows:

$$R = \frac{C_{S,F} - C_{S,P}}{C_{S,F}} \times 100 \tag{2.27}$$

Often salt passage, S, is used to characterize the membrane performance as well:

$$S = 100 - R \tag{2.28}$$

Using the transport parameters described in previous sections, R can be rewritten as:

$$R = \frac{\frac{P_W}{P_s} \cdot \frac{\bar{V}_W}{RT}(\Delta p - \Delta\pi)}{1 + \frac{P_W}{P_s}\frac{\bar{V}_W}{RT}(\Delta p - \Delta\pi)} \times 100 \tag{2.29}$$

or R can be also rewritten in terms of A and B as follows:

$$R = \frac{\frac{A}{B}(\Delta p - \Delta\pi)}{1 + \frac{A}{B}(\Delta p - \Delta\pi)} \times 100 \tag{2.30}$$

R is not an intrinsic property of the polymer membrane since it depends on operation conditions such as applied pressure difference and osmotic pressure difference.

2.3.3 Water/salt selectivity

Water permeability, P_W, can be expressed as a function of water diffusivity, D_W, and water partition coefficient, K_W, according to the solution-diffusion model [56-60]:

$$P_W = D_W \cdot K_W \tag{2.31}$$

Also, salt permeability, P_S can be expressed as a function of salt diffusivity, D_s, and salt partition coefficient, K_s, as follows [56-60] :

$$P_s = D_s \cdot K_s \tag{2.22}$$

The ideal water/salt permeability selectivity, $\alpha_{W/S}$, is the ratio of water permeability, P_W, to salt permeability, P_S, as follows:

$$\alpha_{W/S} = \frac{P_W}{P_S} = \frac{D_W}{D_S} \cdot \frac{K_W}{K_S} \tag{2.32}$$

where D_W/D_S is the water/salt diffusivity selectivity, and K_W/K_S is the water/salt solubility selectivity. Compared to salt rejection, *R,* which is dependent on operating conditions, the selectivity, $\alpha_{W/S}$, is less dependent on operating conditions and thus can be used to characterize the intrinsic ability of a polymer membrane to separate salt from water [62].

2.3.4 Permeability-selectivity trade-off relationship

When the water permeability, P_W, is plotted against the water/salt permeability selectivity, $\alpha_{W/S}$, this correlation is similar to the permeability-selectivity trade-off relationship often used for gas separation membranes [56, 62, 69]. Intuitively a polymer membrane which has higher permeability has a tendency to sacrifice selectivity. For the last several decades, many researchers have aimed to overcome the so-called upper-bound by introducing new polymeric materials [61].

Therefore, to characterize the membrane performance, transport property parameters such as water permeability, P_w, water partition coefficient, K_W, water diffusivity, D_W, salt permeability, P_s, salt partition coefficient, K_s, and salt diffusivity, D_S are measured in this work and compared to those of various polymer membranes.

2.4 EFFECT OF PROCESSING HISTORY ON TRANSPORT

Transport properties of materials are strongly affected by the chemical structure and the morphology of polymers. The polymer morphology is, especially, known to be sensitive to thermal processing history [63, 70-72].

For the materials of interest here, i.e., sulfonated polysulfone (BPS), previous literature reported that their properties are likely to depend on a nano-phase hydrophilic (i.e., ionic) domain structure to some extent under hydrated conditions [70-72]; however, this is not yet firmly established. The morphology is affected by several factors such as sulfonation level, membrane preparation methods, solution casting solvent, and thermal history, etc. [63, 70, 71]. For example, Xie et al. reported that, by soaking BPS-32K (32 mol% K sulfonated BPS) films in boiling deionized water for 4 hours, water permeability of BPS-32K membrane is 2.3 times higher and salt permeability is around 8 times higher than those of an untreated control membrane; they attributed these difference to morphological change induced by this hydrothermal treatment.

Transport properties of melt processed membranes may also have interesting properties compared to those of solution cast membranes. For example, Bebin, et al. reported that the membrane preparation method has a significant effect on the properties of the sulfonated polysulfone (sPSU) films for Proton Exchange Membrane Fuel Cell (PEMFC) membrane applications [73, 74]. Solution processed membranes show two times higher proton conductivity than that of melt processed membranes, whereas, melt processed membranes have longer lifetime than solution cast membranes. Therefore, it is of interest to study the effect of melt processing on transport properties of such desalination membranes, and correlate these properties with the morphological changes induced by different processing methods.

2.5 REFERENCES

[1] M. T. Ponting, A. Hiltner, and E. Baer, “Polymer nanostructures by forced assembly: process, structure, and properties,” *Macromolecular Symposia,* vol. 294, no. 1, pp. 19-32, 2010.

[2] M. T. Ponting, Y. Lin, J. K. Keum, A. Hiltner, and E. Baer, “Effect of substrate on the isothermal crystallization kinetics of confined poly(ε–caprolactone) nanolayers,” *Macromolecules,* vol. 43, no. 20, pp. 8619-8627, 2010.

[3] M. T. Ponting, “Gradient multilayered films & confined crystallization of polymer nanolayers by forced assembly coextrusion,” Ph.D. Dissertation, Department of Macromolecular Science & Engineering, Case Western Reserve University, 2010.

[4] A. Eisenberg, and J. S. Kim, "Introduction to ionomers," pp. 1-16, 30-31, 38-85, 114-117, 244-266: John Wiley & Sons, Inc., 1998.

[5] R. A. Register, and R. K. Prud'homme, "Melt rheology," *Ionomers*, M. R. Tant, K. A. Mauritz and G. L. Wilkes, eds., pp. 208-260: Blackie Academic & Professional, 1997.

[6] J. S. Kim, and A. Eisenberg, "Ion aggregation and its effect on ionomer properties," *Ionomers: characterization, theory and applications*, S. Schlick, ed., pp. 7-34: CRC Press, Inc., 1996.

[7] M. Tirrell, "Rheology of polymeric liquids," *Rheology principles, measurements, and applications*, C. W. Macosko, ed., pp. 475-514: VCH Publishers, Inc., 1994.

[8] J. D. Ferry, "Viscoelastic properties of polymers," New York: Wiley, 1980.

[9] G. Broze, R. Jerome, and P. Teyssie, “Halato-telechelic polymers. VII. Viscoelastic behavior of α,ω-divalent cation dicarboxylato polybutadiene,” *Journal of Polymer Science: Polymer Physics Edition,* vol. 21, pp. 2205-2217, 1983.

[10] E. P. Otocka, M. Y. Hellman, and L. L. Blyler, “Terminal-group association in carboxy-and carboxylate-terminated polybutadiene,” *Journal of Applied Physics,* vol. 40, pp. 4421-4428, 1969.

[11] H. S. Makowski, and R. D. Lundberg, "Synthesis and properties of sulfonated EPDM," *Ions in polymers*, A. Eisenberg, ed., pp. 3-19, Washington DC, USA: Americal Chemical Socienty 1980.

[12] S. Bagrodia, and G. L. Wilkes, “Comments on the effect of cation, type on ionomer properties,” *Polymer Bulletin,* vol. 12, no. 5, pp. 389-392, 1984.

[13] R. G. Pearson, “Hard and soft acids and bases, HSAB, Part 1: Fundamental principles,” *Journal of Chemical Education,* vol. 45, no. 9, pp. 581-587, 1968.

[14] R. G. Pearson, “Hard and soft acids and bases, HSAB. Part 2. Underlying theories,” *Journal of Chemical Education,* vol. 45, pp. 643-648, 1968.

[15] R. D. Rundberg, and H. S. Makowski, "A comparison of sulfonate and carboxylate ionomers," *Ions in polymers*, A. Eisenberg, ed., pp. 21-36, Washington DC, USA: American Chemical Society.

[16] S. Bonotto, and E. F. Bonner, “Effect of ion valency on the bulk physical properties of salt of ethylene-acylyic acid copolymers,” *Macromolecules,* vol. 1, pp. 510-515, 1968.

[17] R. D. Lundberg, and H. S. Makowski, "The dual plasticization of sulfonated polystyrene ionomer," *Ions in Polymers*, A. Eisenberg, ed., pp. 67-76, Washington DC, USA: American Chemical Society, 1980.

[18] K. Iwakura, and T. Fujimura, “Rheogoniometry of molten blends of polystyrene and styrenic ionomers,” *Journal of Applied Physics,* vol. 19, pp. 1427-1437, 1975.

[19] D. Brenner, and A. A. Osward, "Effect of counterion structure on ionomer properties: quaternary phosphonium counterions in sulfonated EPDM," *Ions in*

Polymers, A. Eisenberg, ed., pp. 53-66, Washington DC, USA: American Chemical Society, 1980.

[20] E. Fouissac, M. Milas, and M. Rinauldo, "Shear-rate, concentration, molecular weight and temperature viscosity dependences of hyaluronate, a wormlike polyelectrolyte," *Macromolecules,* vol. 26, no. 25, pp. 6945-6951, 1993.

[21] R. A. Weiss, J. J. Fitzgerald, and D. Kim, "Viscoelastic behavior of lightly sulfonated polystyrene ionomers," *Macromolecules,* vol. 24, no. 5, pp. 1071-1076, 1991.

[22] R. A. Weiss, and H. Zhao, "Rheological behavior of oligomeric ionomers," *Journal of Rheology,* vol. 53, no. 1, pp. 191-213, 2009.

[23] K. B. Wiles, F. Wang, and J. E. McGrath, "Directly copolymerized poly(arylene sulfide sulfone) disulfonated copolymers for PEM-based fuel cell systems. I. Synthesis and characterization," *Journal of Polymer Science Part A: Polymer Chemistry,* vol. 43, no. 14, pp. 2964-2976, 2005.

[24] C. H. Lee, D. VanHouten, O. Lane, J. E. McGrath, J. Hou, L. A. Madsen, J. Spano, S. Wi, J. Cook, W. Xie, H. J. Oh, G. M. Geise, and B. D. Freeman, "Disulfonated poly(arylene ether sulfone) random copolymer blends tuned for rapid water permeation via cation complexation with poly(ethylene glycol) oligomers," *Chemistry of Materials,* vol. 23, no. 4, pp. 1039-1049, 2011.

[25] N. Ghious, and M. T. Benaniba, "The effect of epoxidized sunflower oil on the miscibility of plasticizer PVC/NBR blends," *International Journal of Polymeric Materials,* vol. 59, no. 7, pp. 463-474, 2010.

[26] A. Eisenberg, and J. S. Kim, "Plasticization," *Introduction to ionomers*, pp. 244-256, Canada: John Wiley & Sons, Inc., 1998.

[27] R. D. Lundberg, H. S. Makowski, and L. Westerman, *Ionic polymer plasticized with preferential plasticizers*, United States Patent No. 4 014 847, 1977.

[28] N. H. Canter, and D. J. Beckley, *Preferential plasticization of ionometric compounds* United States Patent No. 3 847 854, 1974.

[29] H. S. Makowski, P. K. Agarwal, R. A. Weistt, and R. D. Lundberg, "Ionic domain plasticizers. Tensile enhancement of zinc sulfonate EPDM with zinc stearate," *Polymer Preprints (American Chemical Society, Division of Polymer Chemistry),* vol. 20, no. 2, pp. 281-286, 1979.

[30] H. S. Makowski, D. Brenner, and J. Bock, *Zinc neutralized sulfonated elastomeric polymer*, United States Patent No. 4 137 203, 1979.

[31] I. Duvdevani, R. D. Lundberg, C. Wood-Cordova, and G. L. Wilkes, "Modification of ionic associations by crystalline polar additives," *Coulombic Interactions in Macromolecular System*, A. Eisenberg and F. E. Bailey, eds., pp. 184-200, Washington DC, USA: American Chemical Society, 1986.

[32] H. J. Oh, B. D. Freeman, J. E. McGrath, C. H. Lee, and D. R. Paul, "Thermal analysis of disulfonated poly(arylene ether sulfone) plasticized with poly(ethylene glycol) for membrane formation," *Polymer* vol. 55, no. 1, pp. 235-247, 2014.

[33] M. Drzewinski, and W. J. MacKnight, "Structure and properties of sulfonated polysulfone ionomers," *Journal of Applied Polymer Science,* vol. 30, no. 12, pp. 4753-4770, 1985.

[34] J. J. Fitzgerald, and R. A. Weiss, "The effects of low molar mass diluents on the microstructure of ionomers," *Journal of Polymer Science Part B: Polymer Physics,* vol. 28, no. 10, pp. 1719-1736, 1990

[35] D. C. Boris, and R. H. Bolby, "Rheology of sulfonated polystyrene solutions," *Macromolecules,* vol. 31, pp. 5746-5755, 1998.

[36] N. B. Wyatt, C. M. Gunther, and M. W. Liberatore, "Increasing viscosity in entangled polyelectrolyte solutions by the addition of salt," *Polymer,* vol. 52, pp. 2437-2444, 2011.

[37] F. Bueche, "Physical properties of polymer," pp. 88-107, New York: Interscience Publishers, 1962.

[38] C. W. Macosko, "Rheology: priciples, measurement and application," pp. 123-124, 141, 510-512: VCH Publishers. Inc., 1993.

[39] W. Cooper, "Copolymers of butadiene and unsaturated acids: crosslinking by metal oxides," *Journal of Polymer Science,* vol. 28, pp. 195-206, 1958.

[40] B. Hird, and A. Eisenberg, "Copolymers of butadiene and unsaturated acids: crosslinking by metal oxides," *Macromolecules,* vol. 25, pp. 6466-6474, 1992.

[41] W. Cooper, "Ionic interchange reactions with metal salts of copolymers from butadiene and unsaturated acids," *Journal of Polymer Science,* vol. 28, no. 195, pp. 628-629, 1958.

[42] J. S. Kim, R. J. Jackman, and A. Eisenberg, "Filler and percolation behavior of ionic aggregates in styrene-sodium methacrylate ionomers," *Macromolecules,* vol. 25, pp. 6466-6474, 1994.

[43] T. A. Witten, "Associating polymers and shear thickening," *Journal de Physique,* vol. 49, no. 6, pp. 1055-1063, 1988.

[44] S. Bhargava, and S. L. Cooper, "Effect of water on viscosity and shear-thickening behavior of telechelic ionomers in nonpolar solvents," *Macromolecules,* vol. 31, no. 2, pp. 508–514, 1998.

[45] L. Li, G. Guo, and R. K. Prud'homme, "Shear thickening ionomers prepared by conjugate addition reaction," *ACS Polymer. Preprints,* vol. 47, no. 1, pp. 271, 2006.

[46] C. Maus, R. Fayt, R. Jerome, and P. Teyssie, "Shear thickening of halato-telechelic polymers in apolar solvents," *Polymer,* vol. 36, no. 10, pp. 2083–2088, 1995.

[47] D. G. Pieffer, R. D. Lundberg, and I. Duvdevani, “Synthesis and rheological properties of low charge density polyampholytes in nonaqueous solvents,” *Polymer,* vol. 27, no. 9, pp. 1453-1362, 1986.

[48] L. Saho, R. A. Weiss, and R. D. Lundberg, “Solution behavior of lightly sulfonated polystyrene ionomer/poly-benzyl-l-glutamate complexes,” *Journal of Polymer Science Part B: Polymer Physics,* vol. 33, no. 14, pp. 2083-2092, 1995.

[49] T. A. Witten, and M. H. Cohen, “Crosslinking in shear-thickening ionomers,” *Macromolecules,* vol. 18, no. 10, pp. 1915-1918, 1985.

[50] X. Lu, W. P. Steckle, and R. A. Weiss, “Ionic aggregation in a block copolymer ionomer,” *Macromolecules,* vol. 26, no. 22, pp. 5876-5884, 1993.

[51] H. A. Barnes, and J. F. Hutton, "An introduction to rheology," pp. 11-35: Wlsevier, 1989.

[52] W. P. Cox, and E. H. Merz, “Correlation of dynamic and steady flow viscosities,” *Journal of Polymer Scinece,* vol. 28, no. 119, pp. 619-622, 1958.

[53] P. E. Erhadrdt, J. M. O'Reilly, W. E. Richards, and M. W. Williams, “Viscoelastic behavior of styrene/n-butylmethacrylate/potassium metharcylate polymers,” *Journal of Polymer Science Symposium,* vol. 45, no. 1, pp. 139-151, 1974.

[54] A. Noshay, and L. M. Robeson, “Sulfonated polysulfone,” *Journal of Applied Polymer Science,* vol. 20, pp. 1885-1903, 1976.

[55] F. Wang, M. Hickner, Y. S. Kim, T. A. Zawodzinski, and J. E. McGrath, “Direct polymerization of sulfonated poly(arylene ether sulfone) random(statistical) copolymer: candidates for next proton exchange membranes,” *Journal of Membrane Science,* vol. 197, no. 1-2, pp. 231-242, 2002.

[56] G. M. Geise, H.-S. Lee, D. J. Miller, B. D. Freeman, J. E. McGrath, and D. R. Paul, “Water purification by membranes: the role of polymer science,” *Journal of Polymer Science Part B: Polymer Physics,* vol. 48, no. 15, pp. 1685-1718, 2010.

[57] D. R. Paul, "Reformulation of the solution-diffusion theory of reverse osmosis " *Journal of Membrane Science,* vol. 241, pp. 371-386, 2004.

[58] W. Xie, "Preparation and characterization of disulfonated polysulfone films and polyamide thin film composite membranes for desalination," Ph.D. Dissertation, Department of Chemical Engineering, The University of Texas at Austin. 2011

[59] D. R. Paul, "The role of membrane pressure in reverse osmosis," *Journal of Applied Polymer Science,* vol. 16, pp. 771-782, 1972.

[60] D. R. Paul, "Relation between hydraulic permeability and diffusion in homogeneous swollen membranes," *Journal of Polymer Science: Polymer Physics Edition,* vol. 11, pp. 289-296, 1973.

[61] R. W. Baker, *Membrane technology and applications*, 3rd ed., West Sussex, United Kingdom: John Wiley and Sons Ltd, 2012.

[62] W. Xie, J. Cook, H. B. Park, B. D. Freeman, C. H. Lee, and J. E. McGrath, "Fundamental salt and water transport properties in directly copolymerized disulfonated poly(arylene ether sulfone) random copolymer," *Polymer,* vol. 52, no. 9, pp. 2244-2254, 2011.

[63] W. Xie, G. M. Geise, B. D. Freeman, C. H. Lee, and J. E. McGrath, "Influence of processing history on water and salt transport properties of disulfonated polysulfone random copolymers," *Polymer,* vol. 53, no. 7, pp. 1581-1592, 2012.

[64] A. C. Sagle, E. M. Van Wagner, H. Ju, B. D. McCloskey, B. D. Freeman, and M. M. Sharma, "PEG-coated reverse osmosis membranes: desalination properties and fouling resistance," *Journal of Membrane Science,* vol. 340, no. 1-2, pp. 92-108, 2009.

[65] J. G. Wijmans, and R. W. Baker, "The solution-diffusion model: a review," *Journal of Membrane Science,* vol. 107, pp. 1-21, 1995.

[66] H. Yasuda, C. E. Lamaze, and A. Peterlin, "Diffusive and hydraulic permeabilities of water in water-swollen polymer membranes," *Journal of Polymer Science Part A-2: Polymer Physics,* vol. 9, no. 6, pp. 1117-1131, 1971.

[67] P. J. Flory, "Thermodynamics of high polymer solutions," *Journal of Chemical Physics,* vol. 10, pp. 51-61, 1942.

[68] M. L. Huggins, "Solutions of long chain compounds," *Journal of Chemical Physics,* vol. 9, no. 5, pp. 440, 1941.

[69] G. M. Geise, H. B. Park, A. C. Sagle, B. D. Freeman, and J. E. McGrath, "Water permeability and water/salt selectivity tradeoff in polymers for desalination," *Journal of Membrane Science,* vol. 369, pp. 130-138, 2011.

[70] Y. S. Kim, L. Dong, M. A. Hickner, B. S. Pivovar, and J. E. McGrath, "Processing induced morphological development in hydrated sulfonated poly(arylene ether sulfone) copolymer membranes," *Polymer,* vol. 44, no. 19, pp. 5729-5736, 2003.

[71] Y. S. Kim, M. A. Hickner, L. Dong, B. S. Pivovar, and J. E. McGrath, "Sulfonated poly(arylene ether sulfone) copolymer proton exchange membranes: composition and morphology effects on the methanol permeability," *Journal of Membrane Science,* vol. 243, no. 1-2, pp. 317-326, 2004.

[72] Y. S. Kim, F. Wang, M. A. Hickner, B. S. Pivovar, and J. E. McGrath, "Effect of acidification treatment and morphological stability of sulfonated poly(arylene ether sulfone) copolymer proton-exchange membranes for fuel-cell use above 100 °C," *Journal of Polymer Science Part B: Polymer Physics,* vol. 41, no. 22, pp. 2816-2828, 2003.

[73] P. Bebin, and H. Galiano, "Processing of PEMFC membranes by extrusion: Part 1. sulfonated polysulfone in acid form," *Advances in Polymer Technology,* vol. 25, no. 2, pp. 121-126, 2006.

[74] P. Bebin, and H. Galiano, "Processing of sulfonated polysulfone for PEMFC membrane applications: Part 2. polymer in salt form," *Advances in Polymer Technology,* vol. 25, no. 2, pp. 127-133, 2006.

Chapter 3: Material and Experimental Methods[3]

3.1 MATERIALS

3.1.1 Polymer: Disulfonated poly(arylene ether sulfone) (BPS)

The disulfonated poly(arylene ether sulfone) random copolymers (BPS-XY) used in this study were synthesized by direct aromatic nucleophilic substitution step polymerization, as established by McGrath, et al. (See Figure 3.1) [1-5]. The nomenclature for these polymers is BPS-XY, where X is the mole percent (mol%) of sulfone groups in the polymer (i.e., disulfonated monomer), and Y is the cation, such as H (acid form) or K (potassium form). For instance, BPS-20K consists of 20 mol% of disulfonated monomer in the potassium form.

The BPS polymer was synthesized in the potassium form by Akron Polymer Systems (Akron, OH) following the synthetic procedure established by McGrath, et al. [3, 4, 6, 7] and was used as received. The acid or H form can be obtained by boiling BPS-K in sulfuric acid solution and then in de-ionized (DI water) [6].

---

3 Parts of this chapter have been adapted from the following articles with permission:
(1) H. J. Oh, B. D. Freeman, J. E. McGrath, C. H. Lee, and D. R. Paul, "Thermal analysis of disulfonated poly(arylene ether sulfone) plasticized with poly(ethylene glycol) for membrane formation," *Polymer* vol. 55, pp. 235-247, 2014.
(2) H. J. Oh, B. D. Freeman, J. E. McGrath, C. J. Ellison, S. Mecham, K.-S. Lee, and D. R. Paul, "Rheological studies of disulfonated poly(arylene ether sulfone) plasticized with poly(ethylene glycol) for membrane formation," *Polymer,* vol. 55, pp. 1574-1582, 2014.

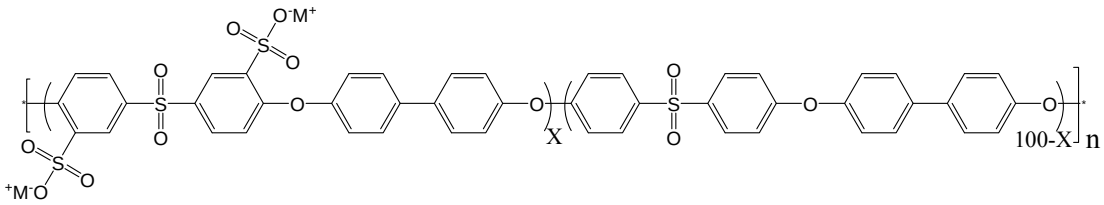

Figure 3.1 Chemical structure of disulfonated poly(arylene ether sulfone) random copolymer: for BPS-XY series, X = mol% of disulfonated monomer (0<X<100), Y = H (acid form) or K (potassium salt form).

3.1.1.1 Selection of BPS form

The potassium form of the sulfonated polysulfone, or BPS-K, was selected for use in this study. While the BPS-H form has a somewhat lower T_g than BPS-K [3], the acid form has a much lower degradation temperature than BPS-K. The better thermal stability of the K form in the potential melt processing temperature range (180~230 °C) is evident from the TGA scan presented in Figure 3.2. Substantial weight loss in the BPS-H sample, presumably related to the onset of thermal degradation, begins at approximately 230 °C, which is much lower than the onset of significant weight loss in the BPS-K sample, which occurs above 400 °C.

BPS-20K (ion exchange capacity = IEC = 0.92 meq/g) was selected for this initial study since it has a good balance of thermal stability and membrane performance [1-4]; selected properties are listed in Table 3.1.

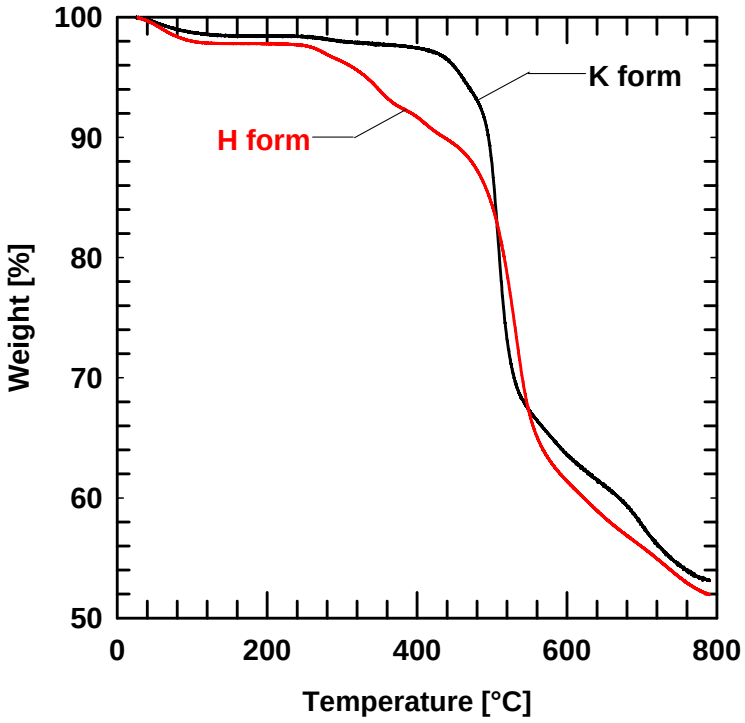

Figure 3.2 Weight change of BPS-20K and BPS-20H as a function of temperature. The TGA scan was run in a nitrogen atmosphere with a ramp rate of 5 C°/min.

Table 3.1 Characteristics of BPS polymer

Material	$\bar{M}_w$[a] [g/mol]	IV[a] [mL/g]	T_g[b]* [°C]	Density[c]* [g/cm^3]	Water Permeability[d] [L µm m^{-2} h^{-1} bar^{-1}]	NaCl rejection[d] [%]
BPS-20K	33,900	48.2	273	1.30	0.03	99.2

[a] Determined by SEC using NMP with 0.05 M LiBr at 50 °C. Note that specific refractive index increment (dn/dc) values were measured using an assumption of 100 % mass recovery. dn/dc values for BPS-20K polymers of this study are 0.17 [mL/g]

[b] Measured by DSC at 20 °C/min

[c] Measured using a Mettler Toledo density determination kit (Part# 238490, Switzerland) with *n*-heptane (Cat# 32287, Sigma-Aldrich, St. Louis, MO) at ambient temperature (20~22°C)

[d] Table 1 from Reference [4]

* Measurements were conducted using solution cast films. Transparent and uniform thickness films (30~40 μm) were formed by the solution casting method reported previously [8]

3.1.2 Plasticizer: Poly(ethylene glycol)

The ideal characteristics of a plasticizer for disulfonated polysulfone or BPS polymer in this study are as follows:

- good miscibility with BPS polymer
- decrease the T_g of BPS to 100-150 ºC or lower
- good water solubility and high diffusivity for water extraction
- low volatility at the potential processing temperature range (180-230 ºC)
- environmentally friendly and economical

Poly(ethylene glycol), PEG, materials (H-(-OCH_2CH_2-)$_n$-OH) were used as plasticizers in this study since PEG oligomers have been reported to be miscible with BPS [9]. Additionally, such oligomers are water soluble, which could permit water extraction of the PEG after melt extrusion [10, 11]. The following chapters (Chapter 4 and Chapter 5) confirm the miscibility of PEG oligomers and BPS and explore a number of other questions (e.g., thermal stability, volatility of low molar mass PEG oligomers, etc.) related to extrusion of such blends.

PEGs are available with number average molecular weights spanning a very large range. However, low molecular weight PEGs, with $\bar{M}_n$ between 200 and 600 g/mol, are of particular interest for this study because they can depress the T_g of BPS-20K to the 100~150 °C range with relatively small amounts (< 30 wt%) of plasticizer, and, being relatively small, they should be more rapidly removed, via leaching into water following melt processing, than higher molecular weight PEG materials. Furthermore, higher molecular weight PEGs are less effective for T_g depression, may be far more difficult to

extract from the extruded blend with water owing to their large molecular size, and would contribute significantly to the blend viscosity.

The physical properties of PEGs used in this study are summarized in Table 3.2 [8]. These PEGs were purchased from Sigma Aldrich (St. Louis, MO) and were used as received. Product details are PEG 200 Cat# P3015, PEG 300 Cat# 202371, PEG 400 Cat# 202398, and PEG 600 Cat# 87333.

Table 3.2 Properties of PEG oligomers

Material	Average $\bar{M}_n$ [g/mol]	PDI[a]	T_g[b] [°C]	T_m[b] [°C]	Density at 20°C[c] [g/cm^3]
PEG 200	200	1.04	-83	-	1.124
PEG 300	300	1.01	-76	-15	1.125
PEG 400	400	1.02	-72	2	1.126
PEG 600	600	1.02	-69	17	1.130

[a] Determined by ESI, details are mentioned in Reference [8]

[b] Measured by DSC at 20 °C/min, Table 2 from Reference [8]

[c] Number reported in Sigma-Aldrich product documentation [12-15]

Note that PDIs are in the range of 1.01~1.04 (see Table 3.2). This value implies a narrow molecular weight distribution and is characteristic of polymers prepared using a living polymerization method [8, 16].

3.2 SAMPLE PREPARATION

3.2.1 Solution casting method

For some of the studies reported here, solution casting was used as a convenient way to form films. A desired amount of BPS-20K/PEG was dissolved in N,N-dimethylacetamide (DMAc, Sigma Aldrich, Cat# 39940) to prepare a solution with 10 wt% solids. This solution was poured onto a glass plate and kept in an oven for 24 hours at 60

°C and then in a vacuum oven for another 48 hours to evaporate most of the DMAc [2, 4, 6]. Residual solvent was extracted by soaking this film in deionized (DI) water for 24 hours and vacuum drying at 120 °C for 24 hours [6]. Transparent films of uniform thickness (30-50 μm) were obtained and used for further characterization.

3.2.2. Melt extrusion

Extruded membrane samples of BPS-20K/PEG blends were prepared using a 5 mL twin screw micro-compounder (DSM Xplore, the Netherlands) and attached film die (heated film die, width of 65 mm, DSM Xplore, the Netherlands) as shown in Figure 3.3. The processing temperature was set to be at least 50~100 °C higher than the T_g of the blend and lower than the degradation temperature, T_d, and it was in the range of 170~245 °C. The desired quantities of BPS-20K and PEG were well mixed prior to feeding to the compounder and were extruded under an extra dry nitrogen atmosphere (99.9 %, Matheson Tri-Gas, Austin, TX) to minimize degradation. The thin films (as thin as 5 μm) were made using a film die and two rollers, where the speed and torque of the take-up unit can be adjusted to obtain the thin films of desired thickness [17].

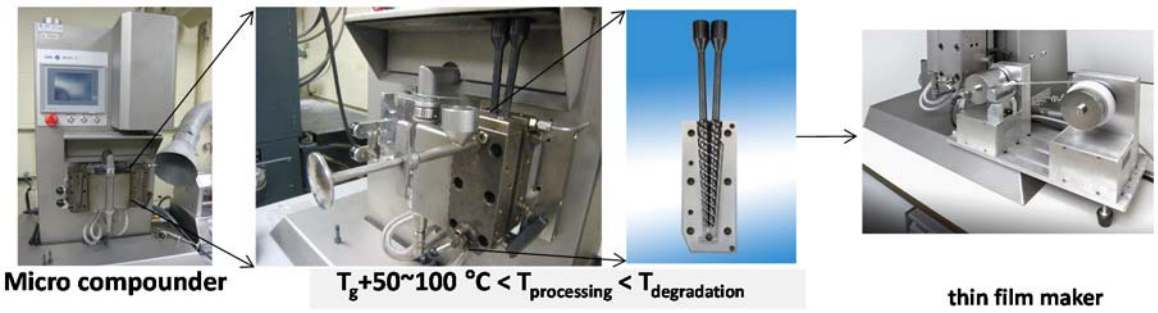

Figure 3.3 Single layer film preparation set up using a DSM micro compounder, a film die and rollers. The processing temperature was set to be at least 50-100 °C higher than the T_g of the blend and lower than the degradation temperature, T_d. The thin films (as thin as 5 µm) were made using a film die and two rollers, where the speed and torque of the winding unit can be adjusted to obtain the thin films of desired thickness. Twin screws and thin film die photos are from DSM Xplore brochures [17].

3.3 THERMAL ANALYSIS

3.3.1 Differential scanning calorimetry (DSC)

DSC (Q100, TA Instruments, New Castle, DE) was used to measure the glass transition, T_g, and melting, T_m, temperatures of the various mixtures and components. For a typical experiment, a 5 mg sample of polymer was sealed in an aluminum pan, and a DSC thermogram was recorded under ultra high purity nitrogen (UHP 99.999 %, Air Gas, Austin, TX) purge using a heating rate of 20 °C/min over the temperature range from -150 °C to 400 °C. The T_g was recorded as the midpoint of the heat capacity step change (Chapters 4, 5 and 9).

3.3.2 Dynamic mechanical analysis (DMA)

DMA (Q800, TA Instruments, New Castle, DE) was used to determine the T_g and the secondary transitions of the polymer systems. A film tension clamp was used with rectangular films of uniform thickness. The storage and loss moduli (G', G'') and damping

factor ($\tan\delta$) were recorded over the temperature range from -150 °C to 400 °C at a heating rate of 2 °C/min and a frequency of 1 Hz under an ultra high purity nitrogen atmosphere. The T_g (°C) was determined as the temperature of the maximum loss tangent ($\tan\delta_{max}$) (Chapter 4).

3.3.3 Thermogravimetric analysis (TGA)

TGA (Q500, TA Instruments, New Castle, DE) was used to investigate sample weight changes as a function of time and temperature under an ultra high purity nitrogen atmosphere at a flow rate of 40 mL/min. A heating rate of 5 °C/min was used for the temperature ramp over the range from 25 °C to 600 °C. Isothermal scans were made by ramping the temperature to 230 °C at a heating rate of 20 °C/min and holding at this temperature for up to an hour (Chapters 3 and 5).

3.4 RHEOLOGICAL MEASUREMENT

3.4.1 Sample preparation for rheological measurement

Extruded samples of BPS-20K/PEG blends were prepared using a 5 mL twin screw micro-compounder (DSM Xplore, the Netherlands) and molded in a compression press (Wabash Metal Products Inc., Wabash, IN) to form samples (circular coupon of 25 mm diameter and 1 mm thickness) for rheological measurements. The processing temperature was set to be at least 50-100 °C higher than the T_g of the blend and lower than the degradation temperature, T_d, and it was in the range of 170~210 °C. The desired quantities of BPS-20K and PEG were well mixed prior to feeding to the compounder and were extruded under an extra dry nitrogen atmosphere (99.9 %, Matheson Tri-Gas, Austin, TX) to minimize degradation.

3.4.2 Rheological measurement

The rheological properties were measured using a rotational rheometer, AR2000EX (TA Instruments, New Castle, DE) with the Electrically Heated Plates (EHP) fixture. All measurements were conducted at a temperature range of 170~250 °C under an extra dry nitrogen atmosphere.

Rheological properties were measured using oscillatory shear flow with 25 mm diameter parallel plates (gap distance of 1 mm). Strain sweep tests were performed to confirm that the % strain was in the linear viscoelastic range. Frequency sweep tests were conducted over the angular frequency range of 0.1~400 rad/s within the linear % strain region depending on the blend compositions. Time sweep tests were also done at the frequency of 1 Hz (i.e., $\omega = 6.283$ rad/s) for 10~30 minutes to check the thermal stability of BPS/PEG blends (Chapter 6).

3.5 WATER AND SALT TRANSPORT PROPERTIES MEASUREMENT

3.5.1 Water permeability (P_w)

3.5.1.1 Hydraulic water permeability

Pure water flux, J_w, was measured by a constant transmembrane pressure difference cross flow filtration system at ambient temperature [1, 2, 6, 18, 19]. Six cross flow cells were connected in series, and the effective mass transfer area of each cell was 18 cm^2. The feed solution was ultra pure deionized water (5-10 ppb TOC [18], from a Millipore Milli-Q system, Darmstadt, Germany), and feed flow rate was 1 gallon/min (i.e., 3.8 L/min). The applied feed (i.e., upstream) pressure was 400 psig (i.e., 27.6 bar) and the permeate (i.e., downstream) pressure was atmospheric pressure (i.e., 1.0 bar). A refrigerated water bath (Neslab RTE 17, Thermo Scientific, Waltham, MA) was used to maintain a constant feed temperature of 25 °C.

The volume of permeate (i.e., water) passing through a membrane (area is A), ΔV, was recorded as a function of time, t (or Δt), and the steady-state water flux, J_w, can be calculated using the equation (2.16) (details in Section 2.3.1.2). Hydraulic water permeability, P_W^H, can be calculated from water flux, J_w, membrane thickness, L, and pressure difference, Δp, using the equation (2.17). The units of P_W^H are [$L \cdot \mu m/(m^2 \cdot h \cdot bar)$].

3.5.1.2 Diffusive water permeability

The diffusive water permeability, P_W^{D}, was calculated from the hydraulic water permeability, P_W^H, using equation (2.18) (details in Section 2.3.1.2). The units of P_W^{D} are [cm^2/s].

3.5.2 Water partition coefficient (K_w)

The water partition coefficient (i.e., water solubility or water sorption coefficient), K_W, is identical to the volume fraction of water in the polymer membrane using equation (2.10) (details in Section 2.3.1.1), and this approximation is used to estimate K_W based on water uptake.

The water uptake (or water weight fraction) of polymer membrane, ω_W, is determined from the mass of dried sample (m_d) and the mass of hydrated sample (m_h) as follows [2, 6]:

$$\omega_W = \frac{m_h - m_d}{m_d} \times 100\ [\%] \tag{3.1}$$

Membrane samples of similar size were dried in a vacuum oven at 110 °C for at least 48 hours before measuring their dry mass, m_d. The sample mass was measured occasionally

to ensure a constant dry mass was reached [2, 6]. After measuring the dry mass, the samples were soaked in ultrapure deionized water (using Millipore Milli-Q system) at ambient temperature for 48 hours. Before weighting the sample mass, the excessive water on the sample surface was carefully removed using tissue paper. The hydrated sample mass, m_h, was measured periodically to ensure a constant hydrated mass was reached.

The equilibrium volume fraction of water of the hydrated polymer membrane, ϕ_W, was calculated by assuming ideal mixing of water with the polymer membrane:

$$\phi_W = \frac{(m_h - m_d)/\rho_W}{(m_h - m_d)/\rho_W + {m_d}/{\rho_P}} \tag{3.2}$$

where ρ_W is the water density (1.0 g/cm^3 is used) and ρ_P is the density of polymer membrane. Therefore, water partition coefficient, K_W, was obtained using ϕ_W value. The units of K_W are [g water/cm^3 hydrated polymer]/[g water/cm^3 solution].

3.5.3 Water diffusivity (D_w)

Based on $P_W = D_W \cdot K_W$ relationship, the water diffusivity, D_W, can be estimated from P_W^D and K_W values using the equation (2.20) [2, 6, 20].The units of D_W are [cm^2/s].

3.5.4 Salt permeability (P_s)

Salt permeability, P_s, was measured using a dual chamber direct permeation cells (Side-Bi-Side Cells, PermeGear, Hellertown, PA) at atmospheric pressure and ambient temperature [1, 2, 6]. The donor and the receiver chamber glass cells have volumes of 35 mL each, and a polymer membrane coupon was located between two chamber cells. The effective area of mass transfer (A) is 1.77 cm^2. At the start, the Donor cell was filled with 1.0 M NaCl solution, and the receiver cell was filled with ultra pure deionized water (from

the Millipore Milli-Q system). The donor/receiver cells were sealed with Parafilms, and stir bars were used with a magnetic drive in each cell to ensure homogeneity of the solutions. As this salt diffuses through the membrane from the donor cell to the receiver cell filled with deionized water, the diffused salt gradually changes the conductivity in the receiver cell. The conductivity in the receiver cell was recorded as a function of time, *t*, using the conductivity probe (LR325/01, WTW, Oberbayem, Germany) and meter (InoLab Cond 730, WTW, Oberbayem, Germany). The diffused salt concentration in the receiver cell was calculated from the recorded conductivity, using the calibration curve which correlates conductivity to salt concentration.

By measuring the salt concentration change over the time in the receiver cell, the salt permeability, P_s, can be calculated using following equation:

$$-\frac{V_R L}{2A}\ln\left[1-\frac{2C_R[t]}{C_D[0]}\right]=P_s t \tag{3.3}$$

where $C_R[\mathrm{t}]$ is the salt concentration in the receiver cell at time t, $C_D[0]$ is the initial concentration of salt in the donor cell (i.e., 1 M NaCl), V_R is the volume of donor/receiver cell (i.e., 35 mL), L is the membrane thickness, and A is the membrane area (1.77 cm^2).

3.5.5 Salt diffusivity (D_s) and partition coefficient (K_s)

The salt diffusivity, D_S, and the salt partition coefficient, K_s, were measured using desorption experiments at atmospheric pressure and ambient temperature [2, 21]

The membrane samples of known dimensions (diameter was 2.2 cm) were soaked in 60 mL of 1.0 M NaCl solution for between 12 and 72 hours [21]. Soaking time was estimated based on L^2/P_s value, where L is the thickness of film, P_s is salt permeability of the membrane determined at the particular NaCl solution (i.e., 1.0 M in this study), and the

time was at least 3 times of L^2/P_s value. The value of L^2/P_s depends on several factors including sample dimensions (thickness and diameter), salt concentration of external salt solution, polymer and temperature. During this period of time, the membrane samples were expected to absorb an equilibrium amount of ions from the solution.

After soaking in the salt solution, the excessive salt on the sample surface was removed using tissue paper. The sample was immersed in a clean tube (disposable centrifuge tube, Cat# 06-443-18, Fisher Scientific Waltham, MA), containing 50 mL of deionized water for at least 3 times of L^2/P_s value, as mentioned above. The samples desorbed the equilibrium amount of ions (chloride ion, Cl^-) to the external deionized water during this period of time, and ion chromatography (ICS-2100, Dionex Corp. Sunnyvale, VA) was used to analyze the concentration of chloride ion in the desorption solution [21]. The amount of NaCl in cm^3 swollen membrane was calculated using the chloride ion concentration, the volume of desorption solution (i.e., 50 mL), and sample dimension.

The salt partition coefficient, K_s, is defined as the ratio of the salt (i.e., NaCl) concentration in the polymer membrane, to the salt concentration (i.e., 1.0 M) in the contiguous solution as follows:

$$K_s = \frac{C_{S,F}^m}{C_{S,F}} \left[\equiv \frac{g\ NaCl/cm^3\ swollen\ membrane}{g\ NaCl/cm^3\ solution}\right] \tag{3.4}$$

Since the total mass of desorbed NaCl into the membrane sample was measured as above, K_s was directly calculated.

The salt diffusivity, D_S, can be determined from P_s and K_s, based on the solution-diffusion model (i.e., $P_s = D_s \cdot K_s$),

3.6 OTHER CHARACTERIZATION METHODS

3.6.1 Fourier transform infrared spectroscopy (FT-IR)

Attenuated Total Refection (ATR) FT-IR (Nicolet 6700 FT-IR Spectrometer, Thermo Scientific, Waltham, MA) was employed to probe for chemical structural changes after thermal treatment of PEG 200. For each measurement, 256 spectra were collected at a resolution of 4 cm^{-1}.

3.6.2 Proton nuclear magnetic resonance (^{1}H NMR)

^{1}H NMR spectra were recorded using a Varian DirectDrive spectrometer (Agilent Technologies, Santa Clara, CA) operating at 400 MHz to characterize chemical structure, number average molecular weights ($\overline{M}_n$) of the PEGs, degree of sulfonation of the BPS-20K, and concentration (wt%) of the PEGs in the BPS-20K/PEG blends. NMR samples were prepared by dissolving 20 mg of material in 2 cm^3 of $(CD_3)_2SO$, dimethyl sulfoxide-D6 (99.9 %, Cat# DLM-10, Cambridge Isotope Laboratories, Andover, MA). ^{1}H NMR data were recorded under the following conditions: numbers of scans = 8, relaxation delay = 2 seconds, spin rate = 20 Hz.

3.6.3 Electrospray ionization (ESI)

ESI (Agilent 6530 Accurate-Mass QTOF LCMS, Agilent Technologies, Santa Clara, CA) in the positive mode was used to determine number ($\overline{M}_n$), and weight ($\overline{M}_w$) average molecular weight, as well as polydispersity (PDI) of the PEG materials (Chapter 5). The carrier solvent was methanol, and the ion source temperature was 250 °C.

3.6.4 Sulfur elemental analysis

Sulfur elemental analysis was conducted at Galbraith Laboratories, Inc. (Knoxville, TN) to determine the polysulfone content in extruded blends with PEG. ASTM D4239-12 was used to measure the sulfur content in these samples (Chapter 5).

3.6.5 Size-exclusion chromatography (SEC)

The SEC system was used to determine weight ($\bar{M}_w$) average molecular weight and intrinsic viscosity of the BPS materials. These measurements were performed by Dr. Sue Mecham at the Virginia Tech.

The SEC system consisted of an isocratic pump (Agilent 1260 infinity, Agilent Technologies, Santa Clara, CA) with an online degasser (Agilent 1260, Agilent Technologies, Santa Clara, CA), autosampler and column oven used for mobile phase delivery and sample injection, and three Agilent PLgel 10µm Mixed B-LS columns 300×7.5mm connected in series with a guard column as the stationary phase. A system of multiple detectors connected in series was used for the analysis. A multi-angle laser light scattering (MALS) detector (DAWN-HELEOS II, Wyatt Technology Corporation, Goleta, CA), operating at a wavelength of 658 nm, a viscometer detector (Viscostar, Wyatt Technology Corporation, Goleta, CA), and a refractive index detector operating at a wavelength of 658 nm (Optilab T-rEX, Wyatt Technology Corporation, Goleta, CA) provided online results. The system was corrected for interdetector delay, band broadening, and the MALS signals were normalized using a 21,720 g/mol polystyrene standard obtained from Agilent Technologies or Varian. Data acquisition and analysis was conducted using Astra 6 software (Wyatt Technology Corporation, Goleta, CA). The mobile phase was 1-methyl-2-pyrrolidinone (NMP, Cat# BS770, Spectrum Chemicals & Laboratory Products, Gardena, CA), which was vacuum distilled over phosphorus

pentoxide (P_2O_5) (99%, Cat# 214701, Sigma Aldrich) before use. The salt, 0.05M dried lithium bromide (LiBr) (99+%, Cat# 213225, Sigma Aldrich), was added and dissolved in the NMP before the solvent was degassed and filtered. The sample solutions were prepared in a concentration range of 2~3 mg/mL and were filtered to remove any dust or insoluble particles using 0.22 μm PTFE filters. Molecular weight values were measured using light scattering and the intrinsic viscosity values were measured online. Note that specific refractive index increment (dn/dc) values were calculated for each backbone type based on 100 % mass recovery using Astra 6 software. If multiple samples of one backbone were available, the values were averaged and applied to all samples of that backbone. All measurements were conducted with both the solvent system and detectors maintained at 50 ℃.

3.6.6 Density measurement

A density determination kit (Part# 238490, Mettler Toledo, Switzerland) was used to measure polymer density at ambient temperature (20-22°C) based on Archimedes' principle [22]. The samples were dried in the vacuum oven at 110 °C for 24 hours prior to the measurement. The dry polymer density, ρ, can be determined as follows [2]:

$$\rho = \frac{m_A}{m_A - m_L} \times \rho_0 \tag{3.5}$$

where m_A is the sample weight measured in air, m_L is the sample weight measured in a non-solvent, and ρ_0 is the density of an auxiliary liquid (i.e., non-solvent). N-heptane (Cat# 32287, Sigma-Aldrich, St. Louis, MO) or mineral oil (Cat# O121-4, Fisher Scientific, Waltham, MA) were used as the auxiliary liquids since these alkanes have low affinity to the sulfonated polysulfone [23, 24], so that they do not swell these polymer samples [2].

3.6.7 Film thickness determination

A Mitutoyo micrometer (Model#: MDH-25M, Mitutoyo, Aurora, IL) was used to measure the thickness of membrane samples. Before and after the water/salt transport properties measurements, thickness was measured at 5~10 equally spaced points. The thickness of membranes was not changed during the experiments and similar observations were reported previously [2, 20].

3.7 REFERENCES

[1] W. Xie, J. Cook, H. B. Park, B. D. Freeman, C. H. Lee, and J. E. McGrath, "Advances in membrane materials: desalination membranes based on directly copolymerized disulfonated poly(arylene ether sulfone) random copolymers," *Water Science and Technology : a Journal of the International Association on Water Pollution Research,* vol. 61, no. 3, pp. 619-624, 2010.

[2] W. Xie, J. Cook, H. B. Park, B. D. Freeman, C. H. Lee, and J. E. McGrath, "Fundamental salt and water transport properties in directly copolymerized disulfonated poly(arylene ether sulfone) random copolymer," *Polymer,* vol. 52, no. 9, pp. 2244-2254, 2011.

[3] F. Wang, M. Hickner, Y. S. Kim, T. A. Zawodzinski, and J. E. McGrath, "Direct polymerization of sulfonated poly(arylene ether sulfone) random(statistical) copolymer: candidates for next proton exchange membranes," *Journal of Membrane Science,* vol. 197, no. 1-2, pp. 231-242, 2002.

[4] H. B. Park, B. D. Freeman, Z.-B. Zhang, M. Sankir, and J. E. McGrath, "Highly chlorine-tolerant polymers for desalination," *Angewandte Chemie International Edition* vol. 47, no. 32, pp. 6019-6024, 2008.

[5] L. Yang, F. Heatley, T. G. Blease, and R. I. G. Thompson, "A study of the mechanism of the oxidative thermal degradation of poly(ethylene oxide) and poly(propylene oxide) using ^{1}H and ^{13}C-NMR," *European Polymer Journal,* vol. 32, no. 5, pp. 535-547, 1996.

[6] W. Xie, G. M. Geise, B. D. Freeman, C. H. Lee, and J. E. McGrath, "Influence of processing history on water and salt transport properties of disulfonated polysulfone random copolymers," *Polymer,* vol. 53, no. 7, pp. 1581-1592, 2012.

[7] Y. Li, F. Wang, J. Yang, D. Liu, A. Roy, S. Case, J. Lesko, and J. E. McGrath, "Synthesis and characterization of controlled molecular weight disulfonated poly(arylene ether sulfone) copolymers and their applications to proton exchange membranes," *Polymer,* vol. 47, no. 11, pp. 4210-4217, 2006.

[8] H. J. Oh, B. D. Freeman, J. E. McGrath, C. H. Lee, and D. R. Paul, "Thermal analysis of disulfonated poly(arylene ether sulfone) plasticized with poly(ethylene glycol) for membrane formation," *Polymer* vol. 55, no. 1, pp. 235-247, 2014.

[9] C. H. Lee, D. VanHouten, O. Lane, J. E. McGrath, J. Hou, L. A. Madsen, J. Spano, S. Wi, J. Cook, W. Xie, H. J. Oh, G. M. Geise, and B. D. Freeman, "Disulfonated poly(arylene ether sulfone) random copolymer blends tuned for rapid water permeation via cation complexation with poly(ethylene glycol) oligomers," *Chemistry of Materials,* vol. 23, no. 4, pp. 1039-1049, 2011.

[10] J.-Y. Sanchez, F. Chabert, C. Iojoiu, J. Salomon, N. E. Kissi, Y. Piffard, M. Marechal, H. Galiano, and R. Mercier, "Extrusion: an environmentally friendly process for PEMFC membrane elaboration," *Electrochimica Acta,* vol. 53, no. 4, pp. 1584-1594, 2007.

[11] Y. Molmeret, F. Chabert, N. E. Kissi, C. Iojoiu, R. Mercier, and J.-Y. Sanchez, "Toward extrusion of ionomers to process fuel cell membranes," *Polymers,* vol. 3, no. 3, pp. 1126-1150, 2011.

[12] Sigma-Aldrich. "Poly(ethylene glycol) average Mn 300 (cat# 202371), http://www.sigmaaldrich.com/catalog/product/aldrich/202371?lang=en&region=US."

[13] Sigma-Aldrich. "Poly(ethylene glycol) average Mn 400 (cat# 202398), http://www.sigmaaldrich.com/catalog/product/aldrich/202398?lang=en&region=US."

[14] Sigma-Aldrich. "Poly(ethylene glycol) 600 (cat# 87333), http://www.sigmaaldrich.com/catalog/product/sigma/87333?lang=en&region=US. "

[15] Sigma-Aldrich. "Poly(ethylene glycol) average mol wt 200 (cat# P3015), http://www.sigmaaldrich.com/catalog/product/sial/p3015?lang=en&region=US."

[16] H. Lin, T. Kai, B. D. Freeman, S. kalakkunnath, and D. Kalika, "The effect of cross-linking on gas permeability in cross-linked poly(ethylene glycol diacrylate)," *Macromolecules,* vol. 38, no. 20, pp. 8381-8393, 2005.

[17] "DSM Xplore micro film device, http://www.xplore-together.com/microfilm-device.html."

[18] A. C. Sagle, E. M. Van Wagner, H. Ju, B. D. McCloskey, B. D. Freeman, and M. M. Sharma, "PEG-coated reverse osmosis membranes: desalination properties and fouling resistance," *Journal of Membrane Science,* vol. 340, no. 1-2, pp. 92-108, 2009.

[19] W. Xie, G. M. Geise, B. D. Freeman, H.-S. Lee, G. Byun, and J. E. McGrath, "Polyamide interfacial composite membranes prepared from m-phenylene diamine, trimesoyl chloride and a new disulfonated diamine," *Journal of Membrane Science,* vol. 403-404, no. 1-2, pp. 152-161, 2012.

[20] W. Xie, "Preparation and characterization of disulfonated polysulfone films and polyamide thin film composite membranes for desalination," Ph.D. Dissertation, Department of Chemical Engineering, The University of Texas at Austin. 2011

[21] G. M. Geise, "Water and salt transport structure/property relationship in polymer membranes for desalination and power generation applications," Ph.D. Dissertation, Department of Chemical Engineering, University of Texas at Austin 2012.

[22] "Archimedes' principle, http://www.britannica.com/EBchecked/topic/32827/Archimedes-principle."

[23] C. Wohlfarth, "CRC handbook of enthalpy data of polymer-solvent systems," Boca Raton, FL: Taylor & Francis Group, 2006.

[24] S. S. Madaeni, and A. Rahimpour, “Effect of type of solvent and non-solvents on morphology and performance of polysulfone and polyethersulfone ultrafiltration membranes for milk concentration,” *Polymers for Advanced Technologies,* vol. 16, no. 10, 2005.

Chapter 4: Glass Transition of Disulfonated Polysulfone Plasticized with Poly(ethylene Glycol)[4]

4.1 INTRODUCTION

The melt processing temperature of a glassy polymer is typically at least 50~100 °C higher than its T_g and lower than temperatures that would result in significant polymer degradation during the time that the material is being processed. Based on this rule of thumb, since the T_gs of BPS polymers are in the range of 220~320 °C, depending on the sulfonation level and ionic form [1], the minimum extrusion temperature range would be around 270~420 °C. However, because the sulfonated groups are susceptible to thermal degradation and the degradation temperature decreases with increasing sulfonation level [1], BPS polymers cannot be melt extruded. Therefore, extrusion of BPS requires a suitable plasticizer to lower the processing temperature range to well below the decomposition point.

Since PEG oligomers have been reported to be miscible with BPS [2], these materials are potentially attractive as plasticizers [2-6]. Additionally, such oligomers are water soluble, which could permit water extraction of the PEG after melt extrusion [7, 8]. The following results confirm the miscibility of PEG oligomers and the effect of PEG molecular weight and concentration on the glass transition of BPS/PEG blends.

---

4 Parts of this chapter have been adapted from the following article with permission:
(1) H. J. Oh, B. D. Freeman, J. E. McGrath, C. H. Lee, and D. R. Paul, "Thermal analysis of disulfonated poly(arylene ether sulfone) plasticized with poly(ethylene glycol) for membrane formation," Polymer vol. 55, pp. 235-247, 2014.

4.2 RESULTS AND DISCUSSION

4.2.1 Thermal analysis of PEG

4.2.1.1 Plasticizer selection

PEGs are available with number average molecular weights spanning a very large range. However, low molecular weight PEGs, with $\bar{M}_n$ values between 200 and 600 g/mol, are of particular interest for this study because they can depress the T_g of BPS-20K to the 100~150 °C range with relatively small amounts (< 30 wt%) of plasticizer, and, being relatively small, they should be more rapidly removed, via leaching into water following melt processing, than higher molecular weight PEG materials. Furthermore, higher molecular weight PEGs are less effective for T_g depression, may be far more difficult to extract from the extruded blend with water owing to their large molecular size, and would contribute significantly to the blend viscosity.

4.2.2.2 PEG glass transition behavior

Estimation of the glass transitions of BPS/PEG blends requires accurate values of the T_g of each PEG considered. There is some literature on the T_g of PEG materials; however, the available data do not include all of the materials of interest to this study. Some papers report T_g values for PEG 200, 300 and 400 [7-12]. However, different methods to obtain T_g data were used in each report, so a consistent database cannot be assembled from the available literature sources for all of the materials considered in this study. Thus, we characterized the T_gs of the PEG 200~600 materials using DSC.

Figure 4.1 presents first scan DSC thermograms of the PEG 200~600 materials. The sample preparation methods to obtain these data varied somewhat depending on the material. With no special sample preparation, PEG 200 and PEG 300 samples exhibit distinct glass transitions, and PEG 300 has a crystallization peak on heating above its T_g.

However, with no special sample preparation, the PEG 400 and PEG 600 (or higher molecular weight PEG) samples do not show a distinct glass transition by DSC owing to their high level of crystallinity [9].

Therefore, the following procedure was used to obtain clear T_g values from DSC for the PEG 400 and 600 materials. Samples of PEG 400 and 600 were sealed in aluminum DSC pans at room temperature (i.e., above their melting points) and rapidly quenched in liquid nitrogen to prevent crystallization to the largest extent possible. Nevertheless, due to the extremely high crystallization rate of these materials, samples with some crystallinity were produced by this procedure; similar observations have been reported for torsion pendulum and NMR studies [9, 13]. However, this technique does reduce the crystallinity enough to make a glass transition observable by DSC. After 1 hour in liquid nitrogen, the samples were quickly moved to the DSC cell where the temperature had already been equilibrated at -150 °C, and a scan was run between -150 °C to 30~50 °C at a heating rate of 20 °C/min. The T_g was reported as the midpoint of the heat capacity step change during the first heat cycle. In the case of PEG 400 and 600 second and third cycles do not reveal any detectable glass transitions since all samples become highly crystalline after the first cycle; whereas, for PEG 200 and 300, the subsequent cycles overlap with the first cycle. Strong recrystallization exotherms are observed for PEG 400 and 600 in Figure 4.1 at about -61 °C and -57 °C, respectively, and the beginning of a recrystallization exotherm is also observed in the PEG 300 sample.

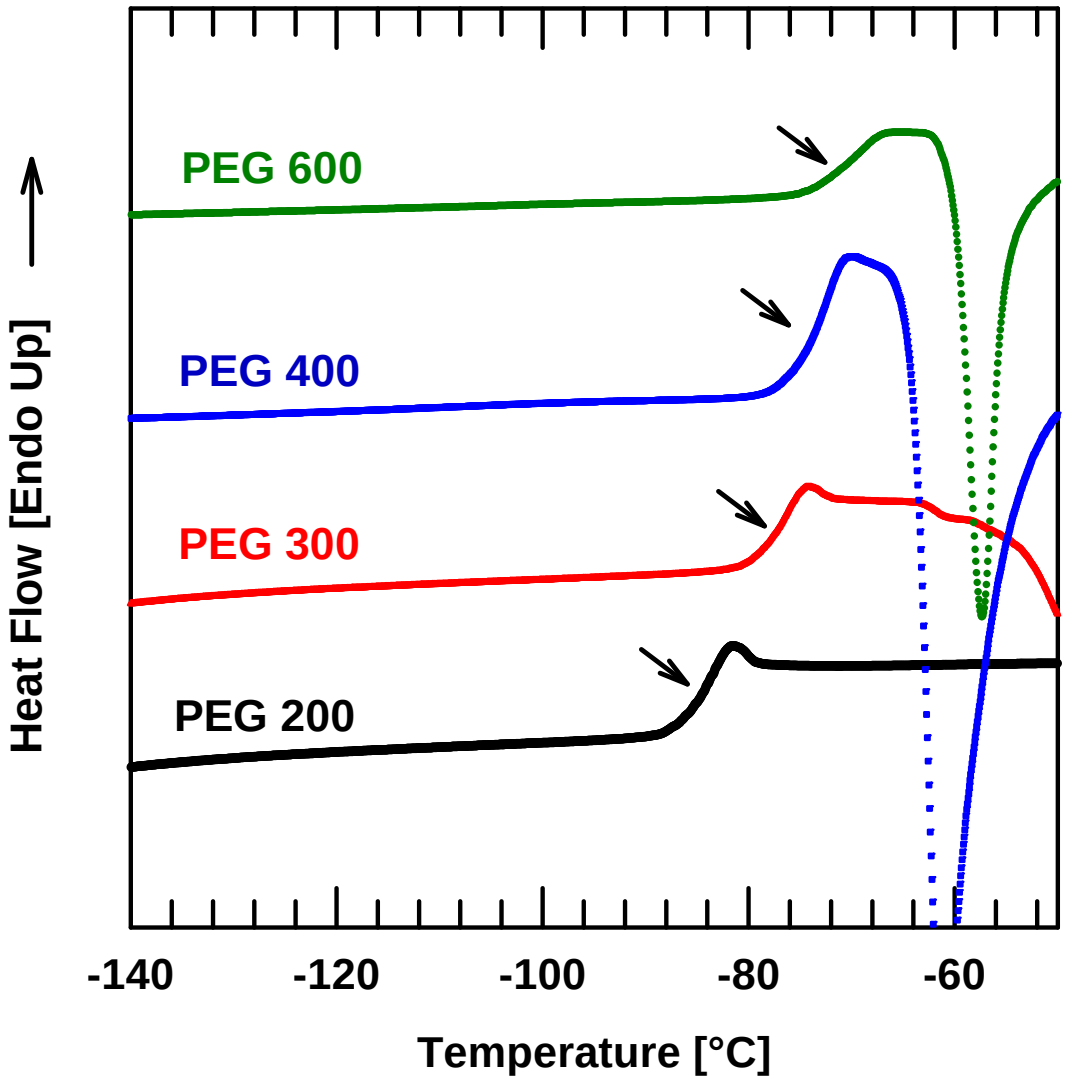

Figure 4.1 First scan DSC thermograms of PEGs. The thermograms have been displaced vertically for clarity. The arrows denote the location of the glass transition temperatures.

The T_g and peak crystalline melting temperature, T_m, values from the first scan DSC thermograms are summarized in Table 4.1. The T_gs reported here are in a good agreement with the previous literature [7, 8, 10] and are used to predict the T_gs of BPS/PEG blends using the Fox equation [14]. After the glass transition (shown by the arrows in Figure 4.1),

crystallization occurred for PEG 300~600, followed by melting. The melting peaks are not shown in Figure 4.1; however the T_m values detected here are similar to those given in the product literature, as shown in Table 4.1 [15-18].

Table 4.1 Properties of PEG oligomers

Material	Average M_n [g/mol]	Data obtained in this study		Literature data		
		T_g [a] [°C]	T_m [a] [°C]	T_g [b] [°C]	T_m [c] [°C]	Density [c] at 20 °C [g/cm^3]
PEG 200	200	-83	-	-86	-65	1.124
PEG 300	300	-76	-15	-78	-15~-8	1.125
PEG 400	400	-72	2	-78	4~8	1.126
PEG 600	600	-69	17	-60	17~22	1.130

[a] Measured by DSC, 20 °C/min

[b] PEG 200 from ref. [10], PEG 300 from ref. [11], PEG 400 from ref. [7, 8], PEG 600 from ref. [2]

[c] Data reported in Sigma-Aldrich product documentation [15-18]

In general, glassy polymers show a monotonic increase in T_g with increasing molecular weight up to a plateau value at high molecular weights [19, 20]. As shown in Figure 4.1, the PEG 200~600 samples exhibit this trend at least qualitatively. Faucher and others reported that higher molecular weight PEGs (greater than 4,000 g/mol) do not follow this relation and have a maximum T_g at around 6,000 g/mol [9, 13]. This behavior is attributed to high crystallinity in these PEG materials, which restricts chain mobility in the amorphous phase, thereby influencing T_g. PEG crystallinity reaches a maximum in the range of 4,000~30,000 g/mol [21], and above this range, the crystallinity drops significantly [9].

4.2.2 Glass transition of BPS-20K/PEG blends

The glass transition temperatures of BPS-20K/PEG blends were measured using both DSC and DMA. Before each DSC run, extruded BPS-20K/PEG blend samples were placed in aluminum DSC pans and kept under a nitrogen atmosphere at T_g+10~20 °C for 10 minutes to remove any previous thermal history. Following this, the sample was cooled to -90 °C and scanned to 75~185 °C, depending on the blend composition, at a rate of 20 °C/min. This thermal cycle was repeated 3 times. The T_g (°C) was taken as the midpoint of the heat capacity step change during the third (and final) thermal cycle. In the case of DMA, the T_g (°C) was determined as the temperature of the maximum loss tangent ($\tan \delta_{max}$). DMA was used in addition to DSC because it is a sensitive method to verify T_g, as well as the secondary transitions of polymer segments, that might not be easily observable in DSC scans [13, 22].

Thermograms of a mixture where one component is an amorphous polymer and the other is a semi-crystalline oligomer can reveal useful information about the physical state of the mixture such as the state of mixing in the amorphous phase and any crystallinity. Here the traditional criteria of a single T_g located between the T_gs of the individual components is adequate evidence for miscibility [23-25]. On the other hand, Lodge et al. claimed that some miscible blends such as PEO/PMMA containing low molecular weight PEG show two T_gs using DSC [11, 12]. Other secondary transitions due to the water (-35 °C), etc. [13, 26] can be seen as well and will be mentioned later.

Figure 4.2 shows exemplary DMA and DSC scans for a series of BPS-20K/PEG 600 blends; similar data were observed for blends containing PEG samples with different molecular weights. The tan δ peak with the greatest intensity in the DMA scans, or the step change in heat capacity in the DSC scans, is associated with the T_g or α transition of the

polymer mixtures. Both DSC and DMA scans exhibit a single composition-dependent T_g for the PEG concentrations considered (i.e., up to 40 wt%). The T_gs detected by DSC and DMA agree with each other within differences expected from these techniques and their characteristic time scales [22].

The pure BPS-20K (i.e., BPS-20K/PEG 600 0 wt%) has a T_g of about 273 °C by DSC and 299 °C by DMA (see Table 4.2), and these values are somewhat higher than the previously reported values [1, 2]. This difference can be explained by the different sample preparation procedures, and a similar observation has been reported by Xie, et al. [27]. In our measurement, residual solvent was removed by soaking in DI water and vacuum drying; however, in the previously reported measurements, this solvent extraction process was not employed so some residual solvent may have remained in the sample, which would have lowered the T_g. Moreover, processing history (i.e., thermal treatment, filtering, etc.) as well as measurement method (i.e., ramp rate, sample size, etc.) can affect properties such as T_g [27-29].

Figure 4.2a shows the storage moduli for all BPS-20K/PEG 600 0~40 wt% blends, with values in the range of 3,000~5,000 MPa at low temperatures, followed by a sharp decrease, characteristic of a glass-to-rubber transition, while a corresponding maximum in tan δ occurs in the same range. As the PEG concentration (wt%) increases, the characteristic decrease in storage modulus and the peak in tan δ progressively shift to lower temperature, indicating T_g depression as expected for a plasticizer [2, 30-32].

Interestingly, the tan δ peak for the mixture containing 20 wt% PEG 600 is quite sharp. However, as more PEG is added to the blend, the peak decreases in height and becomes broader in width. This flattening and broadening effect has been reported for a number of polymer blends and plasticized polymers including poly(vinyl chloride) (PVC)

and polystyrene (PS), etc. [23, 33, 34]. This broadening has been attributed to local concentration fluctuations [23, 24, 30, 33-38]. Since the time scale of these fluctuations is longer than the time needed for chain segmental motion, the relaxing segments are likely to encounter varying local environments and, thus, relax at different rates. As a result, the DMA profile reflects a broad range of local relaxation processes [23, 24].

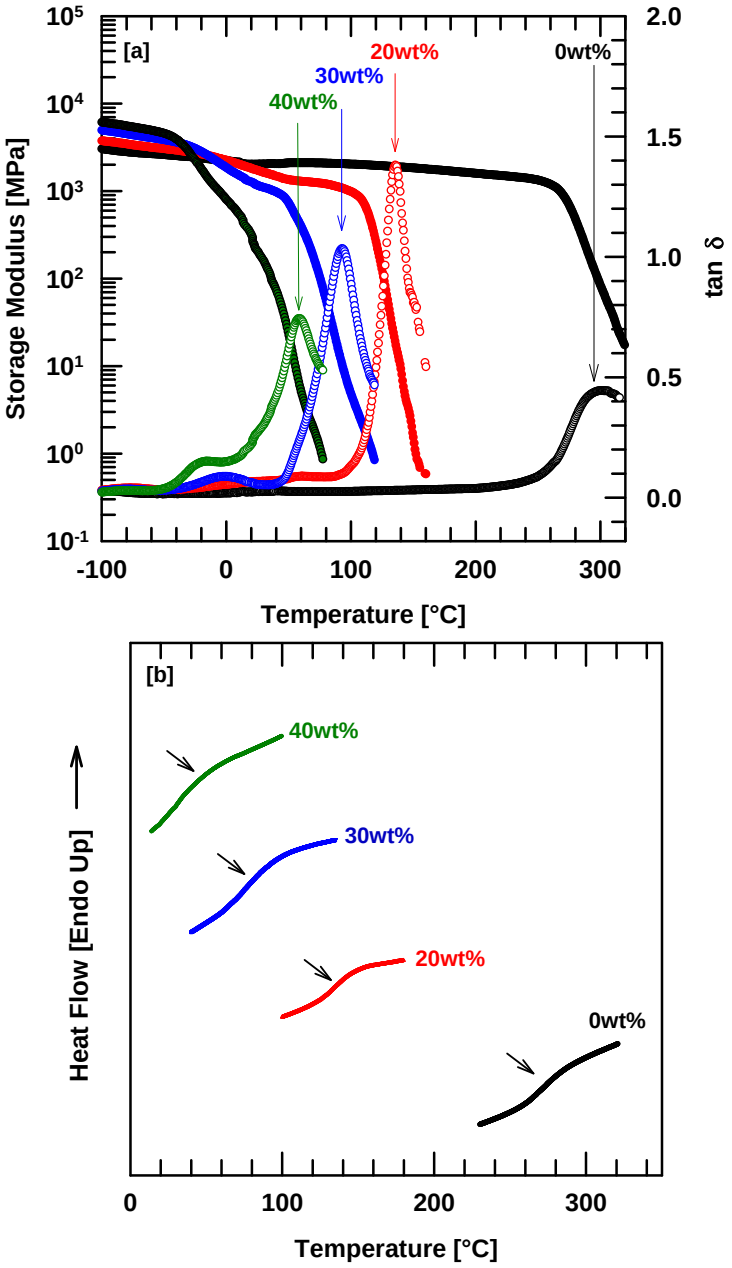

Figure 4.2 [a] Dynamic mechanical analyses scans for BPS-20K/PEG 600 mixtures. (Frequency = 1 Hz, ramping rate = 2 °C/min) [b] Differential scanning calorimetric thermograms (final scan) of BPS-20K/PEG 600 blends. The DSC thermograms have been magnified vertically (magnification is different for each thermogram for easier viewing) and displaced along the vertical axis for clarity. The arrows identify the transitions selected as the glass-rubber transition in each blend.

Some secondary or sub-T_g relaxation processes are evident in the range between -50 °C and -25 °C. These transitions are not seen in pure BPS-20K but appears in all mixtures with PEG 600. At 20 wt% PEG, this relaxation is very small. However, as more PEG is added to the blend, the intensity of this tan δ peak increases and seems to shift to the lower temperatures. This peak may be related to moisture absorbed by the hygroscopic PEG and/or to some relaxation associated with PEG [13, 26, 38-42].

Table 4.2 presents the onset, mid- and end- temperatures of the heat capacity step change (DSC) and the temperatures where the tan δ reaches its maximum (DMA) at the glass transition of BPS-20K/PEG 600 blends as described in Figure 4.2.

Table 4.2 The onset, mid- and end- temperatures of heat capacity step change (DSC) and the temperatures where loss modulus (G'') and tan δ reach their maximum (DMA) at the glass transition of BPS-20K/PEG 600 blends. The mid temperature is used to report the T_gs of the blends for DSC. In the case of DMA, the T_g was determined as the temperature of the maximum loss tangent ($\tan \delta_{max}$)

PEG 600 [wt%]	DSC				DMA	
	Onset temp [°C]	Mid Temp [°C]	End Temp [°C]	ΔT_g [a] [°C]	Temp at G''_{max} [°C]	Temp at $tan\ \delta_{max}$ [°C]
0	256	273	288	32	273	299
20	122	132	147	25	112	131
30	64	75	94	30	58	93
40	38	43	54	16	-*	58

[a] ΔT_g [°C] = $T_{end\ temp} - T_{onset\ temp}$

*not distinguishable

Figure 4.3 summarizes the effect of PEG concentration and molecular weight on the T_gs of BPS-20K/PEG blends. The T_gs determined by DSC were used for this analysis since the PEG T_gs were detected with DSC because of difficulties when measuring liquid

samples using DMA, [13] so it was consistent to employ DSC T_gs for further analysis. As the PEG concentration increases, the blend T_g is depressed (see Figure 4.3a). Two potential reasons for this decrease are: (1) the PEG adds more free volume to the polymer matrix, which would reduce interchain restrictions on polymer segmental mobility, and (2) PEG interactions with the ionic groups in BPS could reduce ionic interactions of the sulfonated groups in BPS-20K [2, 30, 32]. The dashed lines, shown in Figure 4.3a, represent the prediction of the Fox equation [23]:

$$\frac{1}{T_g} = \frac{w_1}{T_{g1}} + \frac{w_2}{T_{g2}} \tag{4.1}$$

where w_1, T_{g1}, w_2 and T_{g2} are the weight fractions and glass transition temperatures of BPS-20K and PEG, respectively [14]. As shown in Figure 4.3b, at a fixed PEG concentration, the blend T_g is slightly lower at lower PEG molecular weight. This result is reasonable given the influence of PEG molecular weight on the T_g of PEG (see Table 4.2) [37]. The dashed lines in Figure 4.3b are also predictions of the Fox equation, calculated using the known T_g values of the BPS-20K and PEG as well as their concentrations in the blend.

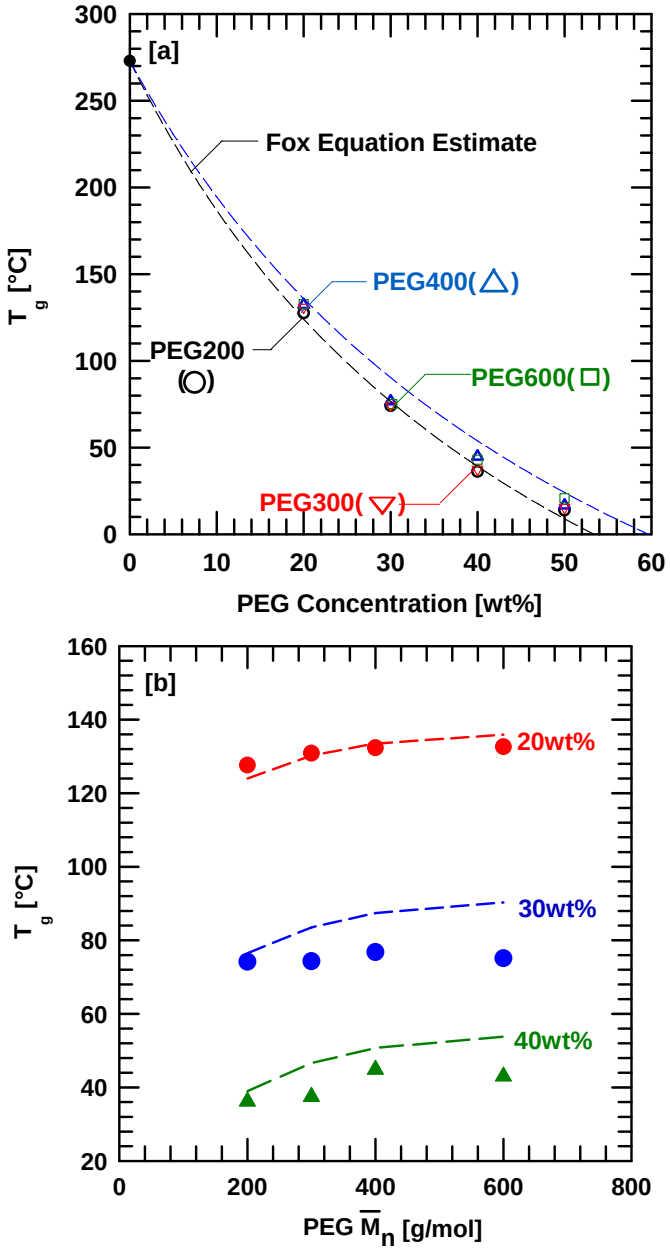

Figure 4.3 Effect of PEG $\bar{M}_n$ and concentration on T_g of BPS-20K/PEG blends. T_gs were measured using DSC: [a] effect of PEG concentration (wt%) and [b] effect of the PEG $\bar{M}_n$ (g/mol) on T_g of BPS-20K/PEG blends. Dashed lines are the Fox equation estimates. In [a], dashed lined are the Fox equation estimates of BPS-20K/PEG 200 (lower) and BPS-20K/PEG 600 (upper). The Fox equation estimates for PEG 300 and PEG 400 lie between those of PEG 200 and PEG 600 and are not shown for easier viewing.

4.3 CONCLUSIONS

In this work, a disulfonated poly(arylene ether sulfone) (BPS) synthesized from the sulfonated monomer combined with a plasticizer, poly(ethylene glycol) (PEG) was used to melt extrude films. PEGs with molecular weights ranging from 200 to 600 g/mol were chosen since they can be conveniently removed by water extraction after membrane extrusion.

BPS and PEG are miscible, and the effect of PEG molecular weight and concentration on the T_g of BPS/PEG blends were investigated. As PEG molecular weight decreases and concentration increases, the blend T_g was depressed significantly.

4.4 REFERENCES

[1] F. Wang, M. Hickner, Y. S. Kim, T. A. Zawodzinski, and J. E. McGrath, "Direct polymerization of sulfonated poly(arylene ether sulfone) random(statistical) copolymer: candidates for next proton exchange membranes," *Journal of Membrane Science,* vol. 197, no. 1-2, pp. 231-242, 2002.

[2] C. H. Lee, D. VanHouten, O. Lane, J. E. McGrath, J. Hou, L. A. Madsen, J. Spano, S. Wi, J. Cook, W. Xie, H. J. Oh, G. M. Geise, and B. D. Freeman, "Disulfonated poly(arylene ether sulfone) random copolymer blends tuned for rapid water permeation via cation complexation with poly(ethylene glycol) oligomers," *Chemistry of Materials,* vol. 23, no. 4, pp. 1039-1049, 2011.

[3] B. Cabane, "Structure of some polymer-detergent aggregates in water," *The Journal of Physical Chemistry,* vol. 81, no. 17, pp. 1639-1645, 1977.

[4] P. Dutta, S. Sen, S. Mukherjee, and K. Bhattacharyya, "Solvation dynamics of TNS in polymer (PEG)-surfactant (SDS) aggregate " *Chemical Physics Letters,* vol. 359, pp. 15-21, 2002.

[5] M. Han, and B. Han, "The solubilization of n-pentane gas in sodium dodecyl sulfate-polyethylene glycol solutions with and without electrolyte," *Journal of Colloid and Interface Science,* vol. 267, pp. 173-177, 2003.

[6] M. N. Jones, “The interaction of sodium dodecyl sulfate with polyethylene oxide,” *Journal of Colloid and Interface Science,* vol. 23, pp. 36-42, 1967.

[7] J.-Y. Sanchez, F. Chabert, C. Iojoiu, J. Salomon, N. E. Kissi, Y. Piffard, M. Marechal, H. Galiano, and R. Mercier, “Extrusion: an environmentally friendly process for PEMFC membrane elaboration,” *Electrochimica Acta,* vol. 53, no. 4, pp. 1584-1594, 2007.

[8] Y. Molmeret, F. Chabert, N. E. Kissi, C. Iojoiu, R. Mercier, and J.-Y. Sanchez, “Toward extrusion of ionomers to process fuel cell membranes,” *Polymers,* vol. 3, no. 3, pp. 1126-1150, 2011.

[9] J. A. Faucher, J. V. Koleske, E. R. Santee, J. J. Stratta, and C. W. Wilson, “Glass transitions of ethylene oxide polymers,” *Journal of Applied Physics,* vol. 37, no. 11, pp. 3962-3964, 1966.

[10] P. Bebin, and H. Galiano, “Processing of PEMFC membranes by extrusion: Part 1. sulfonated polysulfone in acid form,” *Advances in Polymer Technology,* vol. 25, no. 2, pp. 121-126, 2006.

[11] T. P. Lodge, E. R. Wood, and J. C. Haley, “Two calorimetric glass transitions do not necessarily indicate immiscibility: the case of PEO/PMMA,” *Journal of Polymer Science Part B: Polymer Physics,* vol. 44, no. 4, pp. 756-763, 2005.

[12] A. N. Gaikwad, E. R. Wood, T. Ngai, and T. P. Lodge, “Two calorimetric glass transitions in miscible blends containing poly(ethylene oxide),” *Macromolecules,* vol. 41, no. 7, pp. 2502-2508, 2008.

[13] S. W. Bigger, J. S. Delatycki, and N. C. Billingham, “Effect of frequency, molecular weight and thermal oxidation on the dynamic mechanical response of poly(ethylene oxide),” *Polymer International,* vol. 26, no. 3, pp. 181-186, 1991.

[14] P. C. Hiemenz, and T. P. Lodge, "Glass transition," *Polymer chemistry*, p. 494: CPC Press, 2007.

[15] Sigma-Aldrich. "Poly(ethylene glycol) average mol wt 200 (cat# P3015), http://www.sigmaaldrich.com/catalog/product/sial/p3015?lang=en&region=US."

[16] Sigma-Aldrich. "Poly(ethylene glycol) 600 (cat# 87333), http://www.sigmaaldrich.com/catalog/product/sigma/87333?lang=en&region=US. "

[17] Sigma-Aldrich. "Poly(ethylene glycol) average Mn 400 (cat# 202398), http://www.sigmaaldrich.com/catalog/product/aldrich/202398?lang=en&region=US."

[18] Sigma-Aldrich. "Poly(ethylene glycol) average Mn 300 (cat# 202371), http://www.sigmaaldrich.com/catalog/product/aldrich/202371?lang=en&region=US."

[19] T. G. Fox, and S. Loshaek, "Influence of molecular weight and degree of crosslinking on the specific volume and glass temperature of polymers," *Journal of Polymer Science,* vol. 15, no. 80, pp. 371-390, 1955.

[20] T. G. Fox, and P. J. Flory, "Second-order transition temperatures and related properties of polystyrene. I. Influence of molecular weight," *Journal of Applied Physics,* vol. 21, pp. 581-591, 1950.

[21] T. M. Connor, B. E. Read, and G. Williams, "The dielectric, dynamic mechanical, and nuclear resonance properties of poly(ethylene oxide) as a function of molecular weight," *Journal of Applied Chemistry,* vol. 14, no. 2, pp. 74-80, 1964.

[22] J. Foreman, S. R. Sauerbrunn, and C. L. Marcozzi, *Exploring the sensitivity of thermal analysis techniques to the glass transition*, TA Instruments Inc.

[23] D. S. Kalika, "Viscoelastic characterization of polymer blends," *Polymer blends: volume 1: formulation*, D. R. Paul and C. B. Bucknall, eds., pp. 291-317, Canada: John Wiley & Sons, Inc., 2000.

[24] J. M. G. Cowie, and V. Arrighi, "Miscibility and relaxation processes in blends," *Polymer blends and alloys*, G. O. Shonaike and G. P. Simon, eds., pp. 81-124, New York, USA: Marcel Dekker, Inc., 1999.

[25] G. H. Hofmann, "Polymer blend modification of PVC," *Polymer blends and mixtures*, D. J. Walsh and J. S. Higgins, eds., pp. 117-148, the Netherlands: Martinus Nijhoff Publishers, 1985.

[26] M. Dionisio, A. C. Fernandes, J. F. Mano, N. T. Correia, and R. C. Sousa, "Relaxation studies in PEO/PMMA blends," *Macromolecules,* vol. 33, no. 3, pp. 1002-1011, 2000.

[27] W. Xie, G. M. Geise, B. D. Freeman, C. H. Lee, and J. E. McGrath, "Influence of processing history on water and salt transport properties of disulfonated polysulfone random copolymers," *Polymer,* vol. 53, no. 7, pp. 1581-1592, 2012.

[28] Y. S. Kim, L. Dong, M. A. Hickner, B. S. Pivovar, and J. E. McGrath, "Processing induced morphological development in hydrated sulfonated poly(arylene ether sulfone) copolymer membranes," *Polymer,* vol. 44, no. 19, pp. 5729-5736, 2003.

[29] K. Pielichowski, and K. Flejtuch, "Differential scanning calorimetry studies on poly(ethylene glycol) with different molecular weights for thermal energy storage materials," *Polymers for Advanced Technologies,* vol. 13, pp. 690-696, 2002.

[30] N. Ghious, and M. T. Benaniba, "The effect of epoxidized sunflower oil on the miscibility of plasticizer PVC/NBR blends," *International Journal of Polymeric Materials,* vol. 59, no. 7, pp. 463-474, 2010.

[31] A. S. Wilson, "Plasticizers: principles and practice," pp. 9-18, Cambridge, UK: The Institute of Materials, 1995.

[32] A. Eisenberg, and J. S. Kim, "Plasticization," *Introduction to ionomers*, pp. 244-256, Canada: John Wiley & Sons, Inc., 1998.

[33] L. E. Nielsen, R. Buchdahl, and R. Levreault, “Mechanical and electrical properties of plasticized vinyl chloride compositions,” *Journal of Applied Physics,* vol. 21, no. 6, pp. 607-615, 1950.

[34] K. Schmeieder, and K. Wolf, “The temperature and frequency dependence of the mechanical properties of some high polymers,” *Kolloid-Zeitschrift,* vol. 127, pp. 65-78, 1952.

[35] K. Nakamura, “Dynamic mechanical properties of plasticized poly(vinyl chloride),” *Journal of Polymer Science: Polymer Physics Edition,* vol. 13, pp. 137-149, 1975.

[36] H.-H. Huang, and E. M. Yorkgitis, “A morphological study on the plasticization of poly(vinyl chloride) by diethylhexyl succinate and dibutyl phthalate,” *Journal of Macromolecular Science, Physics,* vol. B32, no. 2, pp. 163-181, 1993.

[37] A. J. Curtis, "Dielectric properties of polymeric systems," *Progress in dielectrics*, J. B. Birks and J. H. Schulman, eds., pp. 31-76, Hertfordshire, UK: Heywood & Company Ltd., 1960.

[38] N. G. McGrum, B. E. Read, and G. Williams, "Anelastic and dielectric effects in polymeric solids," pp. 308-312, 327-331,431-434,551-561, UK: John Wiley & Sons Ltd., 1947.

[39] B. E. Read, “Mechanical relaxation in some oxide polymers,” *Polymer,* vol. 3, pp. 529-542, 1962.

[40] D. Q. M. Craig, “A review of thermal methods used for the analysis of the crystal form, solution thermodynamics and glass transition behavior of polyethylene glycols,” *Thermochimica Acta,* vol. 248, pp. 189-203, 1995.

[41] G. Ceccorulli, M. Pizzoli, M. Scandola, G. C. Alfonso, and A. Turturro, “Dynamic mechanical relaxations of poly(vinylidene fluoride)-poly(vinylpyrrolidone) blends,” *Polymer,* vol. 30, no. 7, pp. 1251-1256, 1989.

[42] G. Allen, J. McAinsh, and G. M. Jeffs, “Relaxation phenomena in some aromatic polymers: effect of water content on the low temperature relaxation,” *Polymer,* vol. 12, no. 2, pp. 85-100, 1971.

Chapter 5: Thermal Stability of Disulfonated Polysulfone Plasticized with Poly(ethylene glycol) during Melt Processing and Identification of Melt Processing Temperature[5]

5.1 INTRODUCTION

Based on the T_g values obtained in the blends (see Chapter 4) and the rule of thumb that melt processing is performed 50~100 °C above the T_g, the highest melt processing temperature needed would be in the range of 230 °C, based upon the T_g of BPS-20K plasticized with 20 wt% of PEG 600 (see Figure 4.2). Of course, the melt processing temperature could be lower, if more plasticizer or lower molecular weight plasticizer were used. Consequently, it was of interest to explore the thermal stability of these BPS-20K/PEG blends. The following results confirm thermal stability and volatility of low molar mass PEG oligomers, which are related to extrusion of such blends.

5.2 RESULTS AND DISCUSSION

Before studying the thermal stability of PEG oligomers, thermal stability of BPS-20K material was first examined.

5.2.1 Thermal stability of BPS-20K during extrusion conditions

BPS-20K exhibits good thermal stability at the temperature of interest. For example, Figure 5.1 presents the mass loss of a sample of BPS-20K as a function of time in a TGA experiment. In this particular experiment, the temperature of the sample was increased at 20 °C/min to 230 °C and then held at 230 °C for 60 minutes under nitrogen atmosphere. There is a slight mass loss initially, which may well be due to traces of water

---

5 Parts of this chapter have been adapted from the following article with permission:
(1) H. J. Oh, B. D. Freeman, J. E. McGrath, C. H. Lee, and D. R. Paul, "Thermal analysis of disulfonated poly(arylene ether sulfone) plasticized with poly(ethylene glycol) for membrane formation," Polymer vol. 55, pp. 235-247, 2014.

remaining in this hydrophilic material. However, the mass is very nearly constant during the isothermal hold at 230 °C.

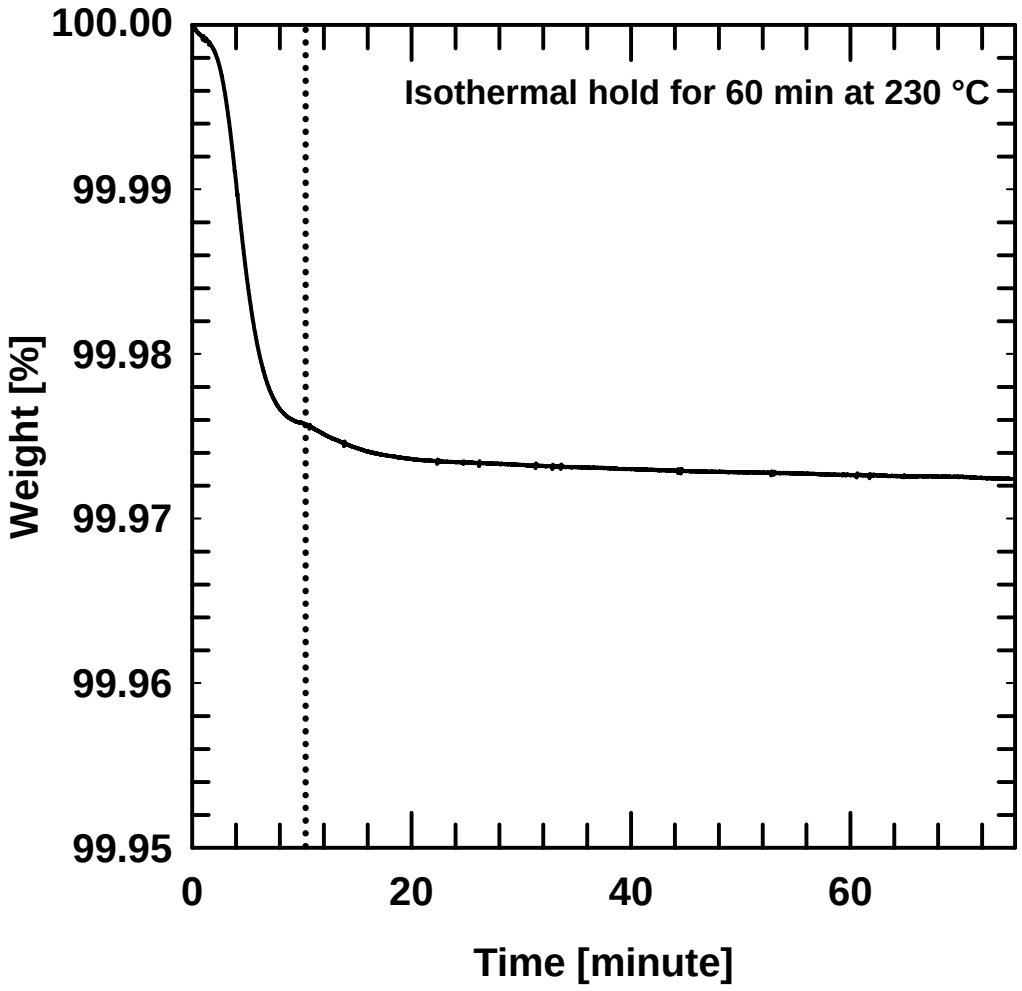

Figure 5.1 Weight change of BPS-20K as a function of time under nitrogen atmosphere. The sample was heated from ambient to 230 °C at a heating rate of 20 °C/min and was then held isothermally at 230 °C for 60 minutes. The dashed line represents the time with the temperature reached 230 °C.

5.2.2 Thermal stability of PEGs: TGA

There is a significant literature on the thermal and chemical stability of PEGs for applications in various fields, including energy storage materials, biomedical engineering, and archeology [1-4]. The time scale of thermal stability in these applications is much longer (a week to several years) relative to extrusion, which takes only a few minutes. Thus, the temperature range, PEG molecular weight, and environmental conditions considered in previous studies of thermal and chemical stability were quite different from the relevant conditions in this study [4-10]. Therefore, the thermal stability of low molecular weight PEGs of interest for this study was investigated.

At high temperatures in air, the hydroxyl groups in PEG are readily attacked by oxygen to form hydroperoxide radicals. Random chain scission then proceeds, producing many oxygenated products [1, 2, 5, 6, 8, 9]. For this reason, lower molecular weight PEG materials degrade faster since more hydroxyl groups exist per unit mass, and, thus, peroxides are formed faster. For the non-oxidative thermal degradation, depolymerization or decomposition takes place when the main chain backbone is broken by ether cleavage, leading to radical or non-radical scission [4]. In either case, the hydroxyl groups are susceptible to degradation.

One way to probe the thermal stability at elevated temperatures is via TGA experiments. The weight change of PEG materials as a function of temperature is shown in Figure 5.2a. As molecular weight increases, the temperature where the mass loss becomes significant increases. However, this mass loss could result from either degradation or evaporation. Similar observations apply when the PEG materials are held isothermally at 230 °C for 30 minutes in the TGA, as shown in Figure 5.2b. PEG 200 mass decreases to 50 % of the initial value during the temperature ramp to reach 230 °C mainly

because of evaporation, as will be discussed further below. Consequently, it is difficult to determine the mass loss due to degradation during the hold at 230 °C. As a result, methods other than TGA are needed to assess the thermal stability of PEGs at various temperatures and times.

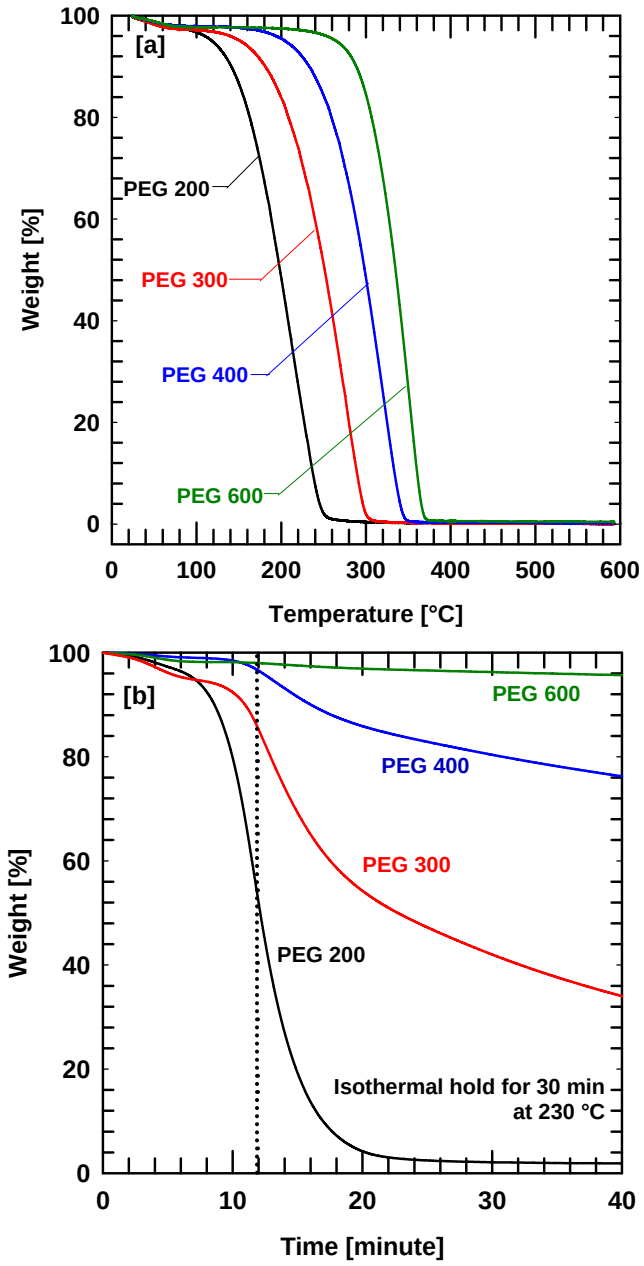

Figure 5.2 Mass loss of PEGs of various molecular weights in a nitrogen atmosphere. [a] The weight change as a function of temperature at a ramp rate of 5 C°/min. [b] The weight change as a function of time. The temperature was ramped from ambient to 230 °C at 20 °C/min and then held at 230 °C. The vertical dashed lines shows the time when the temperature first reached 230 °C.

5.2.3 Thermal stability of PEG 200

PEG degradation, with or without oxygen, may cause random chain scission and result in low molecular weight products. As a result, the chemical structure is changed, the molecular weight is decreased, polydispersity (PDI) is increased, and the T_g, T_m and heat of fusion are reduced [1, 2, 4, 5, 11]. A major difference between oxidative and non-oxidative degradation of PEG lies in the products formed [4, 5, 11]. These aspects were tested by different characterization techniques to understand the thermal stability of PEG 200 at extrusion conditions.

PEG samples were held at high temperatures, in the range of 170~250 °C, for times ranging from 10 to 30 minutes, in a rheometer (AR2000EX from TA Instruments, 25mm EHP parallel plate, gap distance of 1 mm) in both nitrogen and air atmospheres. A rheometer was used since it offered accurate control of isothermal hold and environmental conditions. A minimum time of 10 minutes was chosen since the approximate sample residence time at high temperature in the compounder and compression press used to prepare the blend samples was less than 10 minutes. PEG 200 is the least stable of the PEGs of interest, so it was selected for study. If PEG 200 is stable under the most aggressive thermal conditions of interest for this study, other higher molecular weight PEG materials should be stable as well. Characteristics such as number average molecular weight ($\bar{M}_n$), molecular structure, polydispersity (PDI), etc. after the isothermal hold were investigated to ascertain thermal stability.

5.2.3.1 Thermal stability under nitrogen

5.2.3.1.1 FT-IR: Chemical structure

FT-IR was used to detect chemical structural changes by tracking characteristic absorption bands. Figure 5.3 shows the FT-IR spectra (4000~500 cm^{-1}) of PEG 200 after

holding isothermally for 10~30 minutes at temperatures ranging from 220 to 250 °C under nitrogen.

No significant changes were observed in the PEG 200 spectra after holding at 230 °C for 30 minutes or at 250 °C for 10 minutes. However, after holding for 30 minutes at 250 °C, a stretching vibration for carbonyl groups at 1710~1750 cm^{-1} appears (shown by the arrows in Figure 5.3), which is likely due to aldehyde formation. Similar observations were reported by Pielichowski et al. using TG/FT-IR and TG/MS; in the early stages of non-oxidative thermal degradation (350~410 °C), the main absorption bands are from C=O stretching (from aldehyde, 1750 cm^{-1}) along with other volatile products such as C=O (from CO_2, 2320 cm^{-1}), C=C (from alkenes, 1600 cm^{-1}), and OH groups (from alcohols and ethers, 1140 cm^{-1}) [4]. However, here the absorbance associated with the carbonyl stretching is small, so no characteristic band other than this stretching was seen. This result is reasonable because the isothermal hold temperature was only 250 °C, which is 100~150 °C lower than the degradation temperature mentioned in the literature. In subsequent ^{1}H NMR studies, this sample does not exhibit any characteristic peaks from aldehydes, and the molecular weight is in a similar range to that of as-received PEG 200. (Details will be explained in the subsequent section.)

Based on the FT-IR analysis, PEG 200 seems stable up to 230 °C for 30 minutes or 250 °C for 10 minutes in a nitrogen atmosphere.

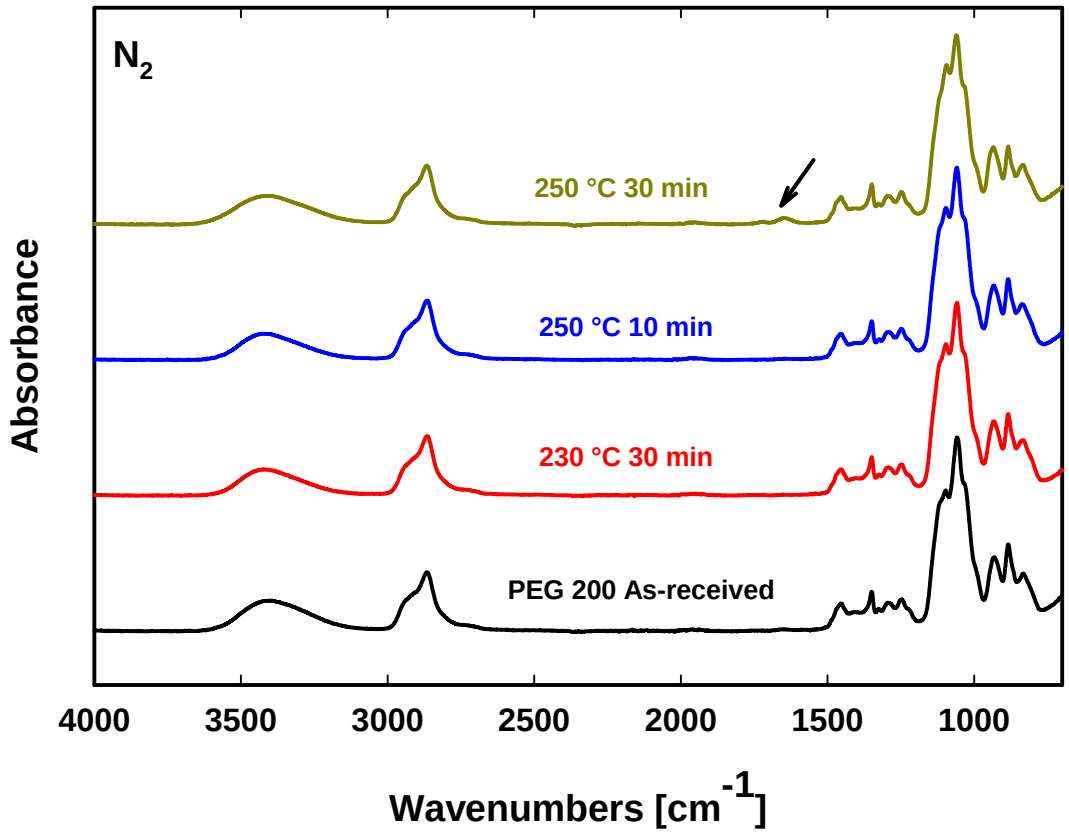

Figure 5.3 FT-IR (ATR mode) spectra of PEG 200 exposed to various temperatures and times under nitrogen. FT-IR spectra were placed vertically for easier viewing. The arrows denote a stretching vibration for carbonyl groups at 1710~1750 cm^{-1}.

5.2.3.1.2 ^{1}H NMR: Molecular structure and $\bar{M}_n$

^{1}H NMR was employed to verify the molecular structure of PEG 200 and to calculate the $\bar{M}_n$ before and after holding isothermally at various temperatures for various times. The peak assignments of PEGs in $(CD_3)_2SO$ are presented in Figure 5.4 and numbers next to each peak are the integrated ratios of the proton peaks. For PEG 200, the $\bar{M}_n$ was determined by the ratios of proton peaks at: (a) δ = 4.56 ppm (2H,–OH groups), (b) δ = 3.39 ppm and (c) δ = 3.46 ppm (4H, external CH_2-CH_2-O), (d) δ = 3.49 ppm (4(n-2)H, internal –(CH_2-CH_2-O)$_{n-2}$-). Therefore, the integral H_b (δ = 3.39 ppm) should be identical

to the integral H_c (δ = 3.46 ppm), and it should be twice the integral H_a (δ = 4.56 ppm). Based on this relationship, the number of repeat units, n, in the polymer chain was calculated as follows:

$$n = \left\{\frac{(\int H_d + \int H_c) - \int H_b}{4}\right\} + 2 \quad (5.1)$$

$\bar{M}_n$ was calculated as follows:

$$\bar{M}_n = (n \times 44) + 18 \text{ [g/mol]} \quad (5.2)$$

Based on this analysis, as-received PEG 200 has a $\bar{M}_n$ value of 210 g/mol.

Table 5.1 presents the $\bar{M}_n$s determined by ^{1}H NMR for an as-received PEG 200 sample and for samples exposed, under nitrogen, for two times (i.e., 10 and 30 minutes) at two different temperatures, 230 °C and 250°C. After holding under nitrogen, the $\bar{M}_n$ is slightly increased with longer time and higher temperature exposure. This change is likely due to the selective evaporation of small molecular weight components, and details will be explained with ESI and DSC results in the following section. The ^{1}H NMR spectra of these samples, which are not shown for the sake of brevity, were quite similar to that of the as-received sample.

After holding PEG 200 at 250 °C for 30 minutes under nitrogen, a stretching vibration for carbonyl groups is observed in FTIR at 1710~1750 cm^{-1} (see Figure 5.3). However, there is no evidence of aldehyde or other oxygenated products by ^{1}H NMR. The amount of by-product may be very small so it could not be detected by ^{1}H NMR, considering the sensitivity of two different techniques [12]. Even though the amount of by-product is very small, extrusion conditions involving holding a sample at 250 °C for 30 minutes will not be included in future studies to prevent any possible degradation.

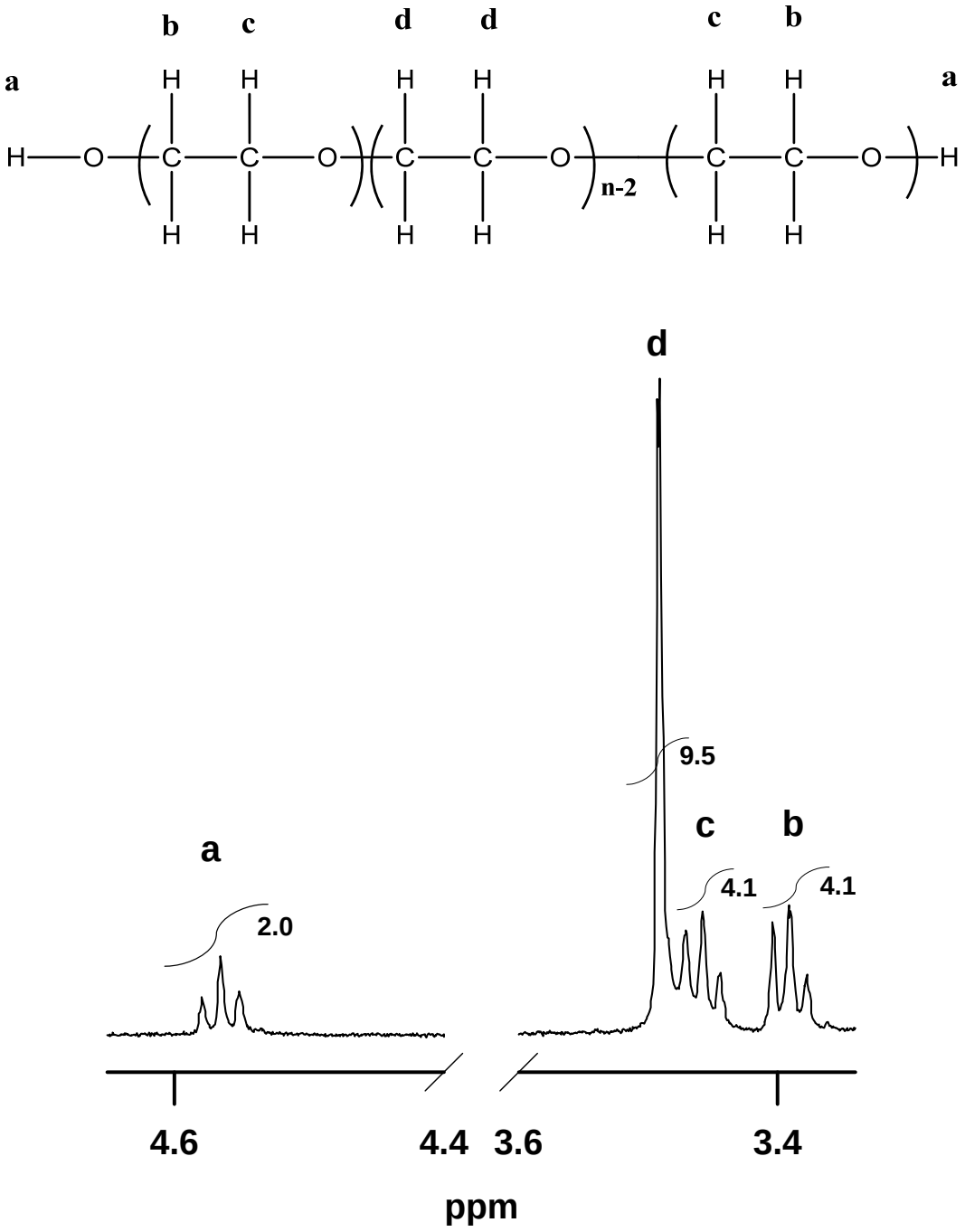

Figure 5.4 ^{1}H NMR spectra of as-received PEG 200. The numbers next to each peak are the integrated ratios of proton peaks.

5.2.3.1.3 ESI and DSC: $\bar{M}_n$, PDI and T_g

When PEG degrades, random chain scission reduces the polymer chain length and produces low molecular weight products. Therefore, $\bar{M}_n$ is decreased, and the polydispersity (PDI) is broadened. The low molecular weight products also lower T_m and the heat of fusion, as much as 13 °C and 32 J/g, respectively [1, 4]. The T_g is also reduced by thermal degradation since the polymer chain length is shortened, and low molecular weight products act as plasticizers. For example, in HDPE, after 3 days of ageing at 120 °C in air, the T_g is depressed from -106 °C to -116 °C [11].

However, Bigger et al. reported that by DMA, PEG ($\bar{M}_n$ = 100,000 g/mol) exhibits little change in T_g after holding in air for 26 hours at 120 °C. A noticeable increase in the area under the tan δ curve appears as oxidization proceeds because this area indicates the amorphous portion of the polymer, but T_g was only slightly changed. They explained these observations in terms of the competing effects of chain scission and crosslinking, which shift the T_g in opposite directions. Still, large scale crosslinking, i.e., forming a microgel, was not observed, so they suspected a loose crosslinked network might form due to oxidation [11]. In contrast, PEG aged at 60 °C (below its T_m) changes from a free-flowing powder to a waxy solid, suggesting a decrease in T_g owing to random chain scission [11, 13]. Although many previous studies agree that thermal degradation leads to chain scission and produces low molecular weight products, it is also important to confirm whether crosslinking occurs under the extrusion conditions of interest for this study.

Since PEG 200 does not exhibit a T_m, its glass transition after thermal exposure was measured using DSC, and $\bar{M}_n$ was calculated from ^{1}H NMR and ESI data. The $\bar{M}_n$s measured using both approaches are usually in good agreement. Since ESI also gives the relative intensities of different molecular weight species in a sample, the PDI can be

estimated. If crosslinking occurs during thermal treatment, high molecular weight products should be observed, so ESI analysis provides a tool for assessing crosslinking.

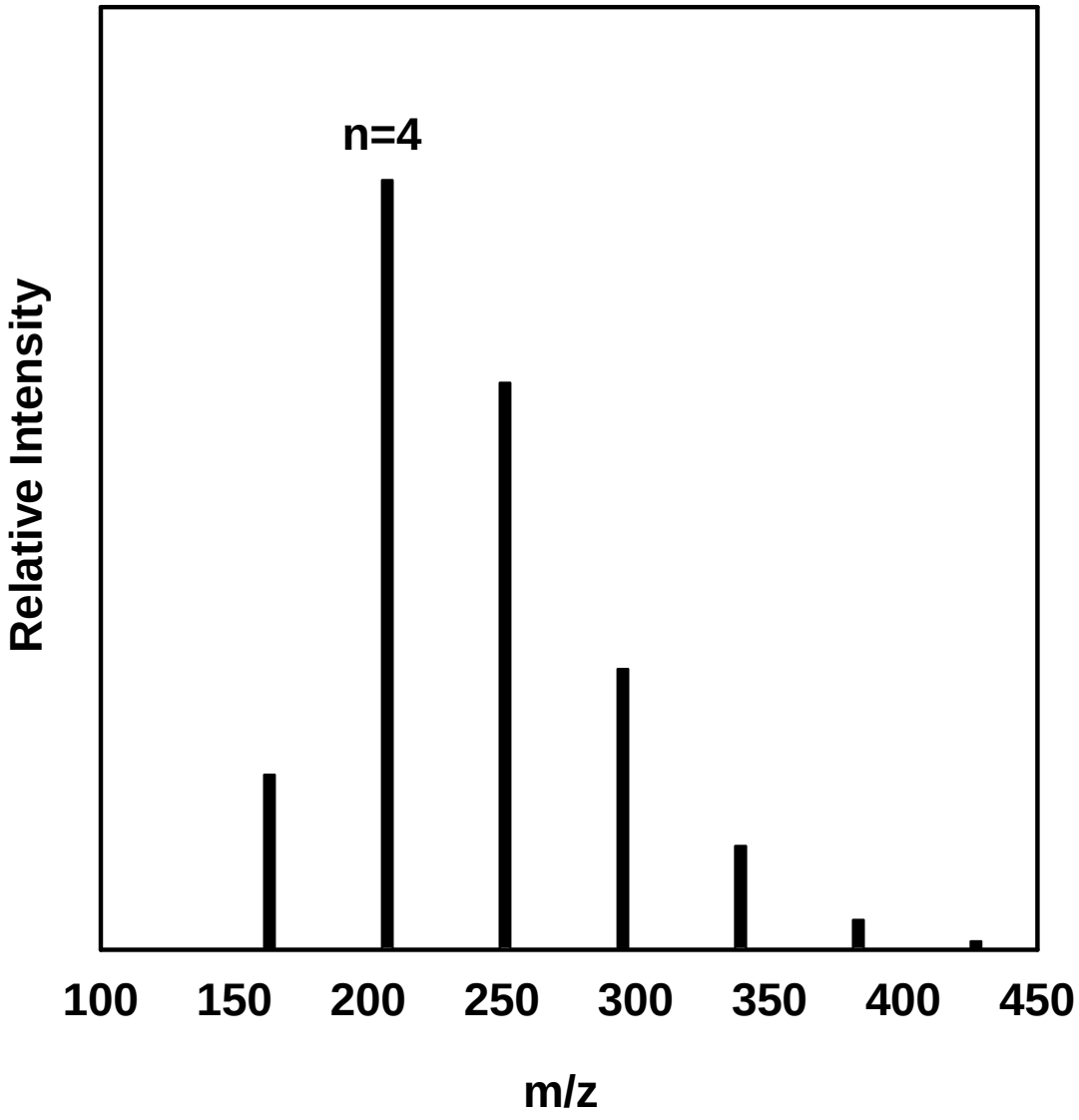

Figure 5.5 Electrospray ionization (ESI) spectrum of as-received PEG 200. The peak at m/z = 217 corresponds to 4 repeat units, (i.e., n = 4), which corresponds to a molecular weight of 194 g/mol. For clarity, signals from noise were not included in this plot.

Figure 5.5 shows the ESI spectrum of as-received PEG 200. A standard ESI result provides the relative intensity (area) versus mass-to-charge (m/z) as shown in Figure 5.5. From this data, $\bar{M}_n$, $\bar{M}_w$ and PDI are calculated as follows:

$$\bar{M}_n = \frac{\sum M_i \cdot N_i}{\sum N_i} \tag{5.3}$$

$$\bar{M}_w = \frac{\sum {M_i}^2 \cdot N_i}{\sum M_i \cdot N_i} \tag{5.4}$$

$$PDI = \frac{\bar{M}_w}{\bar{M}_n} \tag{5.5}$$

where M_i is calculated as m/z - 23, since z is usually 1 and the mass of Na^+, an adduct ion, should be subtracted, and N_i corresponds to the relative intensity. From this equation, $\bar{M}_n$ and $\bar{M}_w$ were determined to be 230 g/mol and 240 g/mol, respectively, so the PDI is 1.04.

PEG 200 has a nominal molecular weight of 200 (the average number of repeating unit is 4~5; if n = 4, $\bar{M}_n$ = 194 g/mol, if n = 5, $\bar{M}_n$ = 238 g/mol) based on the manufacturer's specification. The $\bar{M}_n$ values determined by ^{1}H NMR (210 g/mol) and ESI (230 g/mol) are consistent with this specification within the uncertainty of the measurements. The PDI is around 1.04, meaning a narrow molecular weight distribution typical of a living polymerization method [14].

Figure 5.6 presents DSC thermograms of PEG 200 after isothermal holds in nitrogen, and Table 5.1 summarizes $\bar{M}_n$, PDI and T_g, measured by ^{1}H NMR, ESI and DSC, respectively. After isothermal holds, the $\bar{M}_n$ and T_g are observed to increase slightly with longer time or higher temperature exposure, while the PDI remains low (1.03~1.04). This is due to the evaporation of low molar mass constituents and is confirmed by comparing ESI spectra after isothermal holds.

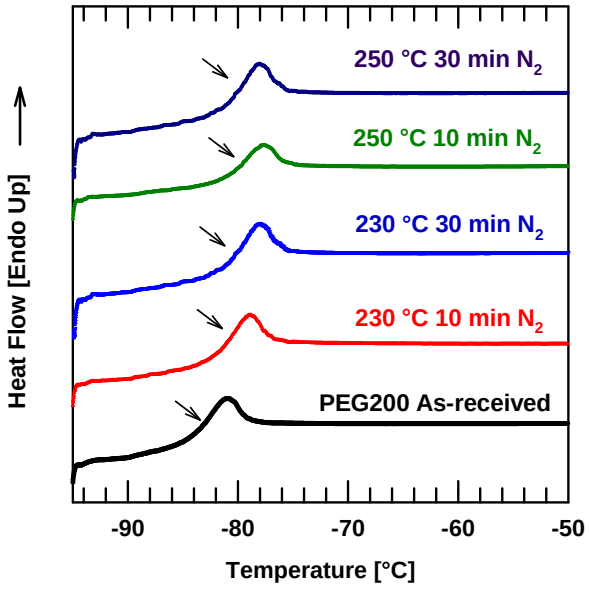

Figure 5.6 DSC thermograms of PEG 200 after the isothermal holds at various temperatures and times in a nitrogen atmosphere. The thermograms have been displaced vertically for clarity. The arrows denote the location of the glass transition temperatures.

Table 5.1 $\bar{M}_n$, PDI and T_g of as-received PEG 200 and PEG 200 following isothermal holds at various temperatures and times in a nitrogen atmosphere

PEG 200	$\bar{M}_n$ [a] [g/mol]	Highest Intensity M_n[b] [g/mol]	$\bar{M}_n$ [b] [g/mol]	PDI [b]	T_g [c] [°C]
As-received	210	190	230	1.04	-83
230 °C, 10 min, N_2	210	240	260	1.04	-81
230 °C, 30 min, N_2	230	240	260	1.04	-80
250 °C, 10 min, N_2	230	240	250	1.04	-79
250 °C, 30 min, N_2	260	280	270	1.03	-79

[a] Determined by ^{1}H NMR

[b] Determined by ESI

[c] Determined by DSC, 20 °C/min

Figure 5.7 shows ESI spectra for PEG 200 after isothermal holds under a nitrogen atmosphere. The intensities of different molecular weights are normalized by the highest

molecular weight (238 g/mol) to compare the relative ratio of each molecular weight constituent between samples. As shown in Figure 5.7a, when PEG 200 was held at 230 °C, the molecular weight distribution shifts somewhat to higher molecular weights, most likely because the low molecular weight oligomers evaporate during the isothermal hold. Figure 5.7b shows an enlargement of the molecular weight range between 100 to 200 g/mol. The amount of low molecular weight material is sharply reduced after the isothermal holds compared to that of as-received PEG 200.

The results are consistent with selective evaporation of low molar mass constituents. NMR and FT-IR do not show any strong changes in chemical structure upon exposure to these temperature/time combinations under nitrogen. $\bar{M}_n$ increases somewhat with longer time or higher temperature exposure, which is consistent with the loss of low molecular weight species during the isothermal hold. The T_g increases slightly, which would also be consistent with loss of low molecular weight molecules via evaporation. The PDIs remain similar (1.03~1.04) or perhaps become slightly smaller at the highest temperature and longest exposure time, which would also be consistent with the selective evaporation of low molecular weight species. While some longer chain species may also evaporate, it is presumed that the smaller species would evaporate more rapidly, and the results are consistent with this hypothesis.

Therefore, chain scission is not significant for PEG 200 during isothermal holds in a nitrogen atmosphere. Also crosslinking is not likely to occur since no higher molecular weight species were found in the ESI spectra, PDI values were changed little, and the $\bar{M}_n$ was in a similar range of 230~270 g/mol (although there was a slight increase due to selective evaporation as mentioned earlier). All of these results suggest little, if any,

degradation for the PEG 200 at these conditions. (Still, the extrusion condition of 250 °C for 30 minutes will not be included for future studies due to the FT-IR results.)

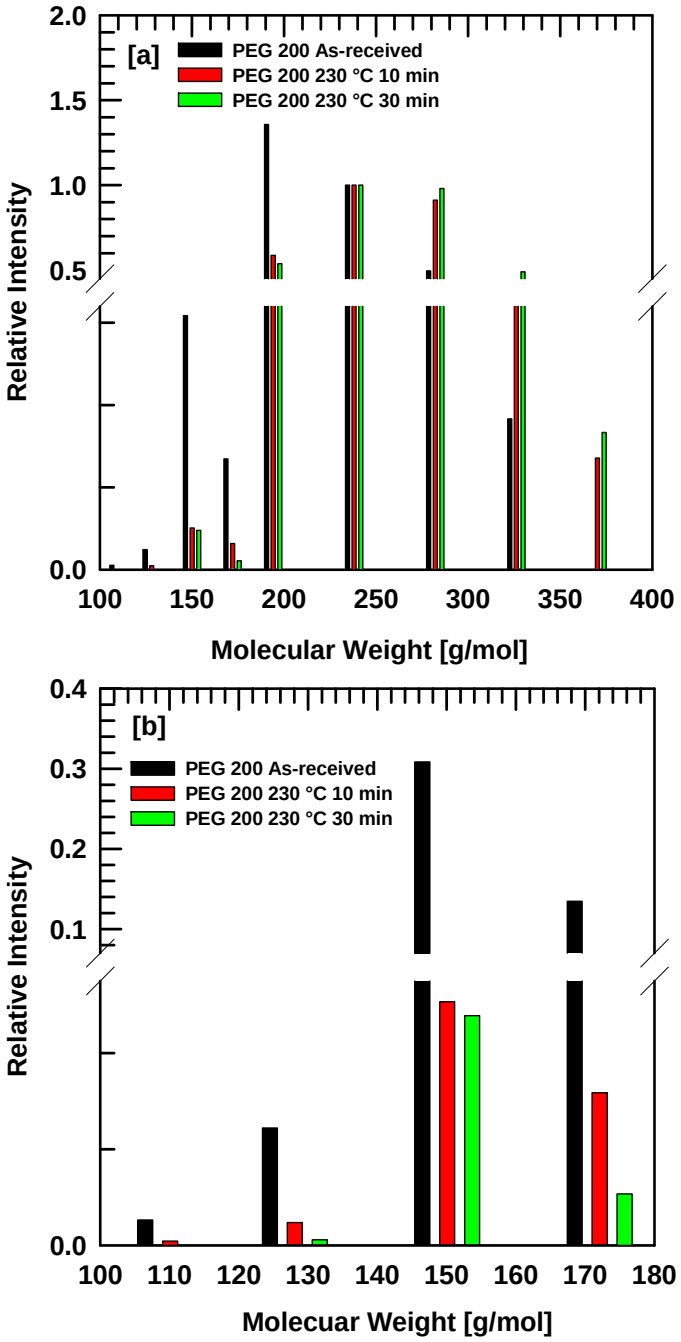

Figure 5.7 ESI spectra of PEG 200 after isothermal holds at various temperatures and times under nitrogen. [a] The molecular weight range between 100~400 g/mol and [b] between 100~200 g/mol.

5.2.3.2 Thermal stability in air

5.2.3.2.1 FT-IR: Chemical structure

Following thermal exposure in air, shown in Figure 5.8, the change in the spectrum is more obvious because of oxidation. Because PEG 200 was held at higher temperatures and for longer times, the intensity of the C=O stretching peak (1710~1750 cm^{-1}) becomes greater, which may originate from degradation-induced formation of aldehyde or other oxygenated products containing ketone [1, 4, 5]. Based on the FT-IR analysis, PEG 200 seems stable up to 220 °C for 10 minutes in air.

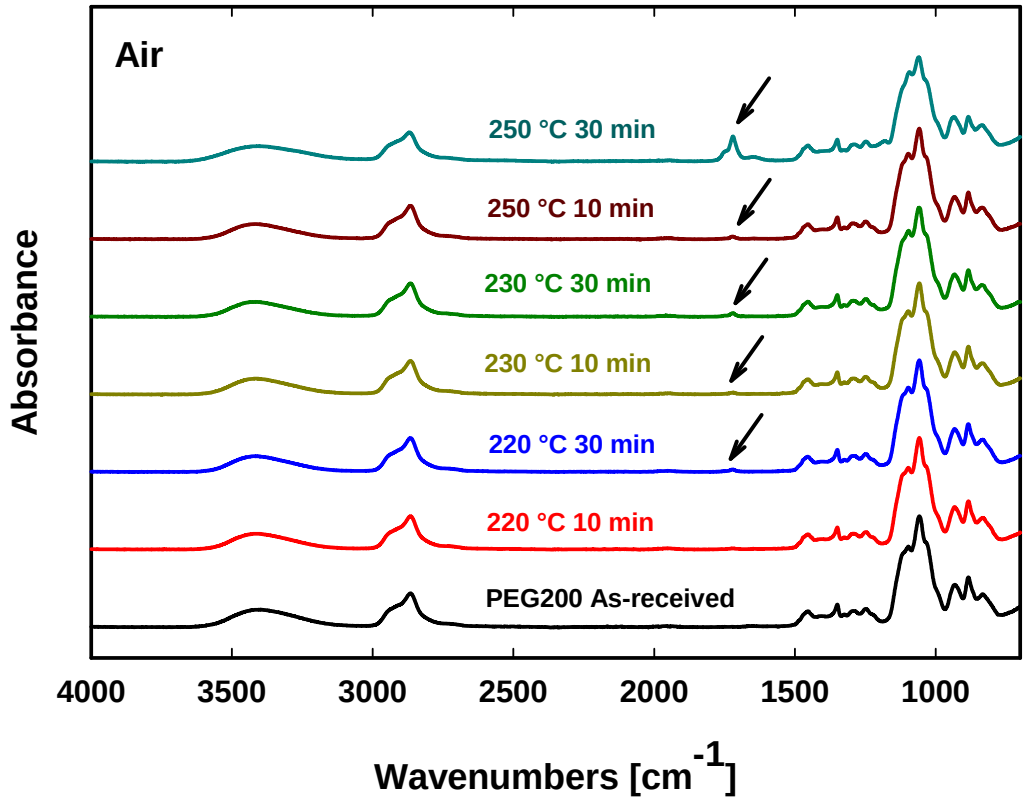

Figure 5.8 FT-IR (ATR mode) spectra of PEG 200 exposed to various temperatures and times in air. FT-IR spectra were placed vertically for easier viewing. The arrows denote a stretching vibration for carbonyl groups at 1710~1750 cm^{-1}.

5.2.3.2.2 ^1H NMR: Molecular structure and $\bar{M}_n$

The ^{1}H NMR spectrum after holding a sample in air at 220 °C for 10 minutes is also identical to the spectrum of as-received PEG 200 (see Figure 5.4). However, as shown in Figure 5.9, after holding at 250 °C for 30 minutes in air, many additional peaks can be seen in the spectrum. In the FT-IR of the sample held at these conditions, a distinct C=O stretching peak appeared. The chemical structure was no longer identical to that of as-received PEG 200 and, thus, $\bar{M}_n$ cannot be calculated from the NMR results. Oxygenated by-products may have been generated [4, 5, 11]; further investigation would be required to identify these by-products and this is not an objective of this study.

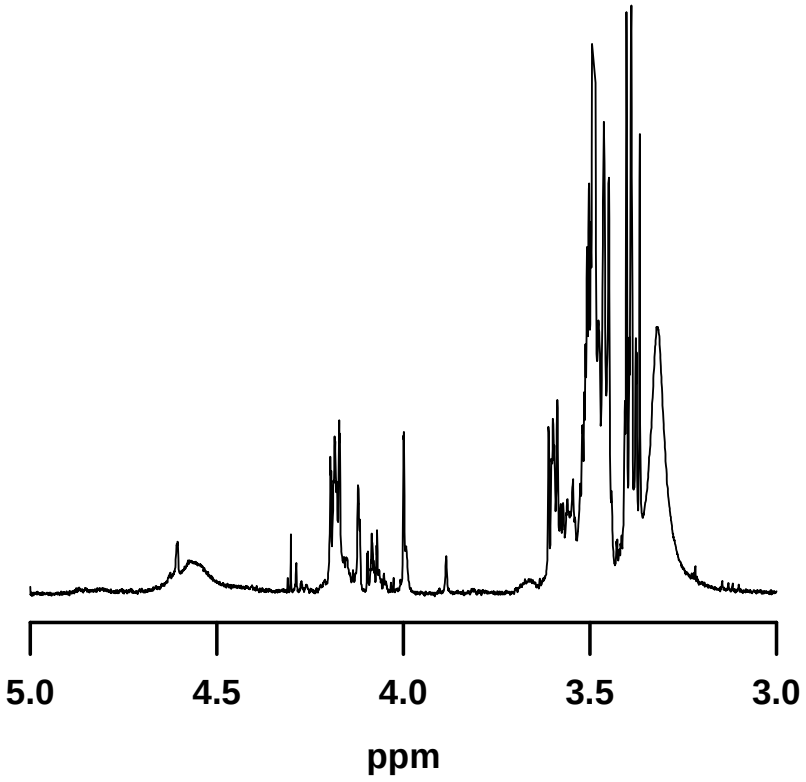

Figure 5.9 ^{1}H NMR spectra of PEG 200 after isothermal holding at 250 °C for 30 minutes in air.

5.2.3.2.3 ESI and DSC: $\bar{M}_n$, PDI, and T_g

Figure 5.10 presents DSC thermograms of PEG 200 after isothermal holds in air and in nitrogen, and Table 5.2 summarizes $\bar{M}_n$, PDI and T_g, measured by ^{1}H NMR, ESI and DSC, respectively. Similar to the results under nitrogen, the $\bar{M}_n$ and T_g values increase slightly while PDI exhibited little change, indicating the selective evaporation of low molar mass constituents.

For the temperature range of 220~230 °C, there is no difference in terms of the molecular structure, $\bar{M}_n$, T_g and PDI between PEG 200 that was isothermally held for 10 minutes in air and in nitrogen. This implies good potential thermal stability during melt processing of PEG 200 at temperatures up to 220 °C for at least 10 minutes without a nitrogen blanket.

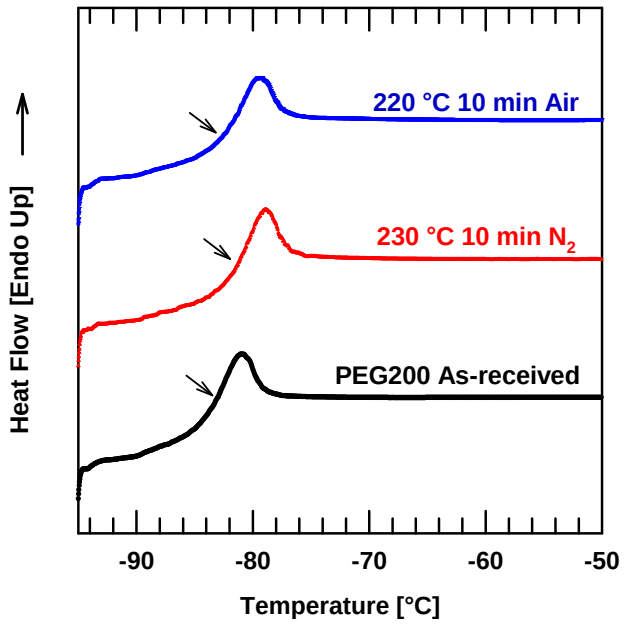

Figure 5.10 DSC thermograms of PEG 200 after isothermal holds at various temperatures and times under nitrogen atmosphere and in air. The thermograms have been displaced vertically for clarity. The arrows denote the location of the glass transition temperatures.

Table 5.2 $\bar{M}_n$, PDI and T_g of PEG 200 after isothermal holds at various temperatures and times under nitrogen atmosphere and in air

PEG 200	$\bar{M}_n$ [a] [g/mol]	Highest Intensity M_n [b] [g/mol]	$\bar{M}_n$ [b] [g/mol]	PDI [b]	T_g [c] [°C]
As-received	210	190	230	1.04	-83
230 °C, 10 min, N_2	210	240	260	1.04	-81
220 °C, 10 min, Air	210	240	260	1.03	-81

[a] Determined by ^{1}H NMR

[b] Determined by ESI

[c] Determined by DSC, 20 °C/min

Based on results from these studies, PEG 200 is stable up to 250 °C for 10 minutes or 230 °C for 30 minutes under a nitrogen atmosphere and up to 220 °C for 10 minutes in

air. Accordingly, higher molecular weight PEGs, such as PEG 300~600, should be stable within this temperature/time ranges as well.

5.2.4 Thermal stability of PEG 200 following compounding and film pressing

BPS-20K/PEG 200 blends were prepared using a DSM micro-compounder and a compression press using the processing temperature range identified. To confirm whether blending or melt processing induced any thermal degradation, the molecular structure, the PEG $\bar{M}_n$, and the PEG content of the extruded samples were analyzed using ^{1}H NMR and sulfur elemental analysis.

^{1}H NMR was used to determine the molecular structure of PEG and BPS-20K (especially the degree of sulfonation), the PEG $\bar{M}_n$ and the PEG concentration (wt%) in the extruded samples. All extruded samples were analyzed by ^{1}H NMR. However, in Figure 5.11, only the BPS-20K/PEG 200 60 wt% sample is shown since the sample containing 60 wt% PEG is expected to be the least stable among the extruded samples in terms of the evaporation and thermal degradation during melt processing.

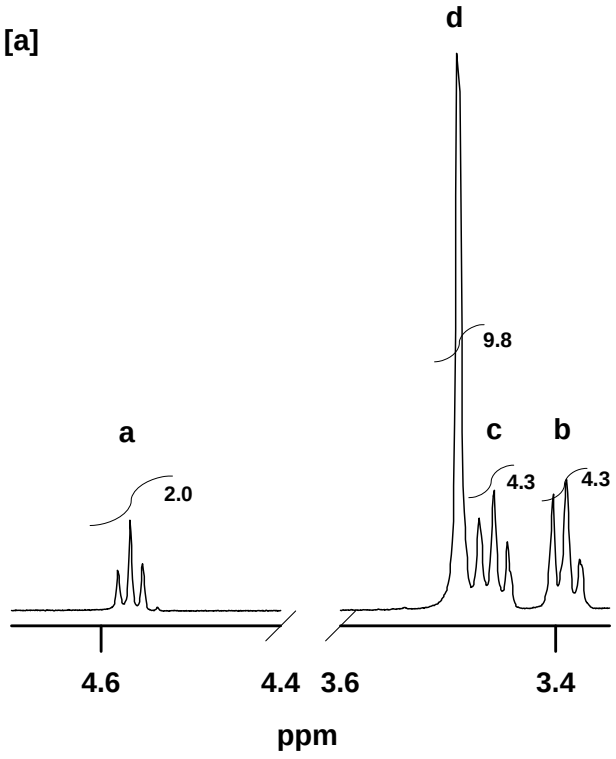
[a]
d
9.8
a
2.0
c
4.3
b
4.3
4.6
4.4
3.6
3.4
ppm

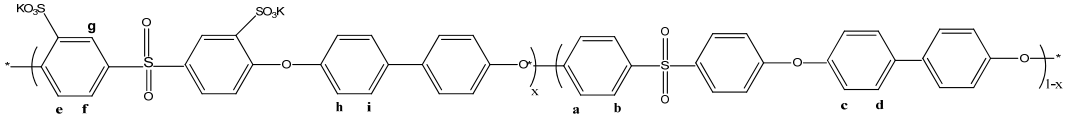
KO3S
g
SO3K
e f
h i
a b
c d
1-x

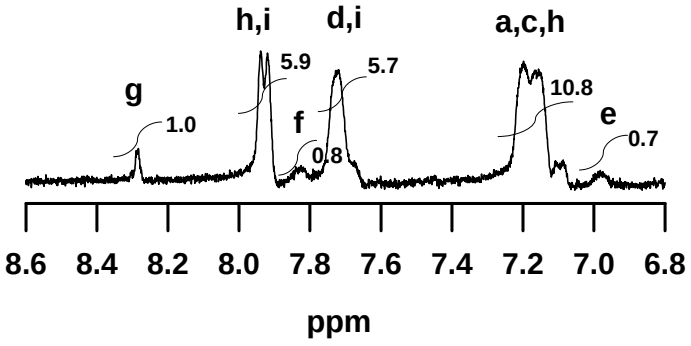
[b]
h,i
d,i
a,c,h
5.9
5.7
10.8
g
1.0
f
0.8
e
0.7
8.6
8.4
8.2
8.0
7.8
7.6
7.4
7.2
7.0
6.8
ppm

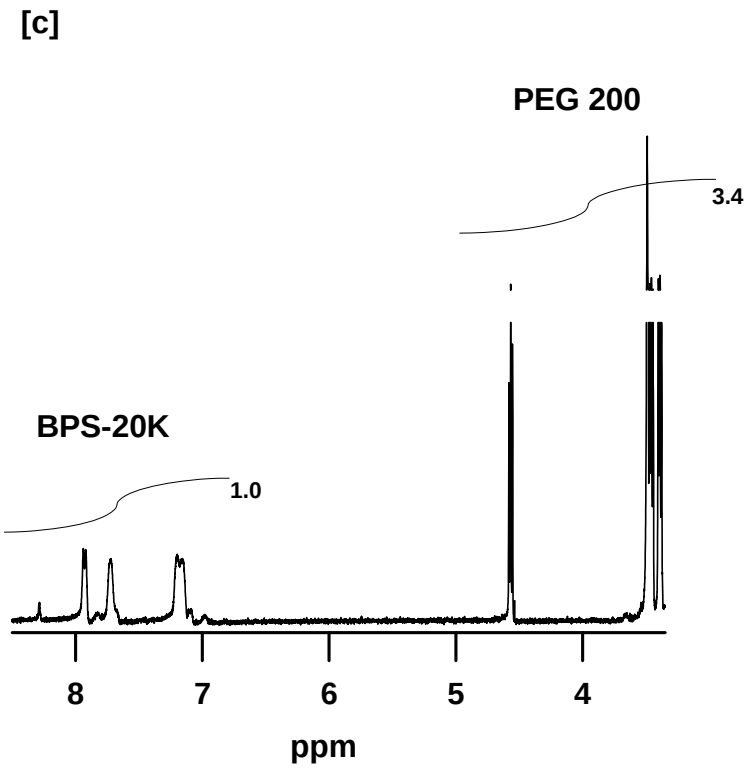

Figure 5.11 [1]H NMR spectrum of the extruded film: BPS-20K/PEG 200 60 wt%. [a] PEG 200, $\bar{M}_n$ = 210 g/mol. [b] BPS-20K, DS = 22 mol%. [c] wt % PEG = 59.5 wt%. The numbers next to each peak are the integrated ratios of proton peaks.

The molecular structure of PEG 200 is not changed, as shown in Figure 5.11a, and no peaks for oxygenated products are observed. The PEG $\bar{M}_n$ was determined using the method previously discussed and was found to be 210 g/mol. The PEG concentration (wt%) was calculated using the ratio of the aromatic proton integral, $\int H_{BPS-20K}$ to the PEG proton integral, $\int H_{PEG\ 200}$, and it was found to be 59.5 wt% based on the spectrum in Figure 5.11c.

Any molecular structural changes for BPS-20K during extrusion were carefully checked by verifying the sulfonation level (mol%) of BPS, since sulfonated groups are susceptible to thermal degradation. According to Wang et al., $T_{5\%}$ (°C), the temperature for 5 % weight loss (by TGA), decreases with increasing sulfonation level [15]. Lee et al. reported thermal desulfonation of BPS polymers at temperatures of 375~420 °C [16]. Although the desulfonation temperature is higher than the potential extrusion temperature, BPS polymer could show a weaker thermal stability in the presence of PEG. To eliminate this possibility, the BPS thermal stability at potential processing temperatures needed to be confirmed. To determine the degree of sulfonation, we used the method reported in the literature with peak assignment as shown in Figure 5.11b [17]. The calculated sulfonation level is 22 mol%, which is similar to the target of 20 mol%, meaning BPS-20K polymer is thermally stable during the extrusion process. Note that as-received BPS-20K polymer shows a sulfonation level of 20~22 mol% by ^{1}H NMR. Based on the ^{1}H NMR analysis, all extruded BPS-20K/PEG 200 blends are thermally stable during extrusion.

To complement the ^{1}H NMR analysis, elemental analysis was also performed. The elemental analysis was used to determine the PEG concentration in the extruded samples, and sulfur (S) was chosen as a reference element because it is only found in the BPS polymer. The S content in the BPS/PEG blends compared to that of the neat BPS polymer is proportional to the BPS concentration in the blends, and, thus, the PEG concentration can be estimated. As shown in Table 5.3, the calculated PEG concentrations correspond to the target amount of PEG and the results of ^{1}H NMR analysis.

Table 5.3 summarizes comparisons between the target amount of PEG 200 and the actual amount of PEG 200 in extruded films after compounding and pressing into films. In all cases, the actual amount of PEG 200 corresponds to the target amount of PEG 200, and,

thus, PEG 200 loss by evaporation or thermal degradation was insignificant during extrusion. The molecular structure of PEG 200 remains unchanged, and the $\bar{M}_n$ remains near 200 g/mol. The calculated PEG concentrations by the different techniques agree well with each other and confirm that melt processing, within this temperature range, does not lead to thermal degradation or evaporation of the plasticizer.

Table 5.3 PEG 200 concentration in the extruded BPS-20K/PEG 200 blends after micro-compounding and compression pressing. PEG 200 concentrations were determined by ^{1}H NMR and S (sulfur) elemental analysis

Intended amount of PEG 200 [wt%]	Processing temperature [°C]	Actual amount of PEG 200 [wt%]		
		^{1}H NMR	S (Sulfur) Elemental Analysis	Average
0	-	0	0	0
20	210	23.3	19.3	21.3
30	200	31.2	33.1	32.2
40	200	42.3	43.0	42.7
50	180	53.8	50.1	52.0
60	160	59.5	62.9	61.2

5.3 CONCLUSIONS

Based on the PEG 200 characterization after isothermal holds at various temperatures and times, these PEGs were found to be thermally stable up to 220 °C for at least 10 minutes in air or 250 °C for at least 10 minutes in nitrogen.

5.4 REFERENCES

[1] S. Han, C. Kim, and D. Kwon, "Thermal/oxidative degradation and stabilization of polyethylene glycol," *Polymer,* vol. 38, no. 2, pp. 317-323, 1997.

[2] M. N. Mortensen, H. Egssaard, S. Hvilsted, Y. Shashoua, and J. Glastrup, "Tetraethylene glycol thermoxidation and the influence of certain compounds relevant to conserved archaeological wood," *Journal of Archaeological Science* vol. 39, pp. 3341-3348, 2012.

[3] K. Knop, R. Hoogenboom, D. Fischer, and U. Schuber, "Poly(ethylene glycol) in drug delivery: pros and cons as well as potential alternatives," *Angewandte Chemie International Edition,* vol. 49, no. 36, pp. 6288-6308, 2010.

[4] K. Pielichowski, and K. Flejtuch, "Non-oxidative thermal degradation of poly(ethylene oxide): kinetic and thermoanalytical study," *Journal of Analytical and Applied Pyrolysis,* vol. 73, no. 1, pp. 131-138, 2005.

[5] J. Glastrup, "Degradation of polyethylene glycol. A study of the reaction mechanism in a model molecule: tetraethylene glycol," *Polymer Degradation and Stability,* vol. 52, no. 3, pp. 217-222, 1996.

[6] P. Malik, M. Castro, and C. Carrot, "Thermal degradation during melt processing of poly(ethylene oxide), poly(vinylidenefluoride-*co*-hexafluoropropylene) and theri blends in the presence of additives, for conducting applications," *Polymer Degradation and Stability,* vol. 91, no. 4, pp. 634-640, 2006.

[7] Y. Kitahara, S. Takahashi, and T. Fujii, "Thermal analysis of polyethylene glycol: evolved gas analysis with ion attachment mass spectrometry," *Chemosphere,* vol. 88, no. 5, pp. 663-669, 2012.

[8] O. A. Mkhatresh, and F. Heatley, "A study of the products and mechanism of the thermal oxidative degradation of poly(ethylene oxide) using ^{1}H and ^{13}C 1-D and 2-D NMR," *Polymer International,* vol. 53, no. 9, pp. 1336-1342, 2004.

[9] O. A. Mkhatresh, and F. Heatley, "A 13C NMR study of the products and mechanism of the thermal oxidative degradation of poly(ethylene glycol)," *Macromolecular Chemistry and Physics,* vol. 203, no. 16, pp. 2273-2280, 2002.

[10] L. Yang, F. Heatley, T. G. Blease, and R. I. G. Thompson, "A study of the mechanism of the oxidative thermal degradation of poly(ethylene oxide) and poly(propylene oxide) using ^{1}H and ^{13}C-NMR," *European Polymer Journal,* vol. 32, no. 5, pp. 535-547, 1996.

[11] S. W. Bigger, J. S. Delatycki, and N. C. Billingham, “Effect of frequency, molecular weight and thermal oxidation on the dynamic mechanical response of poly(ethylene oxide),” *Polymer International,* vol. 26, no. 3, pp. 181-186, 1991.

[12] R. M. Silverstein, F. X. Webster, and D. Kiemle, "Spectrometric identification of organic compounds," pp. 72-75: John Wiley & Sons Inc., 2005.

[13] J. Scheris, S. W. Bigger, and O. Delatycki, “Characterizing the solid-state thermal oxidation of poly(ethylene oxide) powder,” *Polymer,* vol. 32, no. 11, pp. 2014-2019, 1991.

[14] H. Lin, T. Kai, B. D. Freeman, S. kalakkunnath, and D. Kalika, “The effect of cross-linking on gas permeability in cross-linked poly(ethylene glycol diacrylate),” *Macromolecules,* vol. 38, no. 20, pp. 8381-8393, 2005.

[15] F. Wang, M. Hickner, Y. S. Kim, T. A. Zawodzinski, and J. E. McGrath, “Direct polymerization of sulfonated poly(arylene ether sulfone) random(statistical) copolymer: candidates for next proton exchange membranes,” *Journal of Membrane Science,* vol. 197, no. 1-2, pp. 231-242, 2002.

[16] C. H. Lee, D. VanHouten, O. Lane, J. E. McGrath, J. Hou, L. A. Madsen, J. Spano, S. Wi, J. Cook, W. Xie, H. J. Oh, G. M. Geise, and B. D. Freeman, “Disulfonated poly(arylene ether sulfone) random copolymer blends tuned for rapid water permeation via cation complexation with poly(ethylene glycol) oligomers,” *Chemistry of Materials,* vol. 23, no. 4, pp. 1039-1049, 2011.

[17] Y. Li, F. Wang, J. Yang, D. Liu, A. Roy, S. Case, J. Lesko, and J. E. McGrath, “Synthesis and characterization of controlled molecular weight disulfonated poly(arylene ether sulfone) copolymers and their applications to proton exchange membranes,” *Polymer,* vol. 47, no. 11, pp. 4210-4217, 2006.

Chapter 6: Rheological Studies of Disulfonated Poly(arylene ether sulfone) Plasticized with Poly(ethylene glycol) for Membrane Formation[6]

6.1 INTRODUCTION

PEG was used to modify the glass transition temperature and melt rheology of BPS to enable coextrusion with polypropylene (PP). This chapter reports rheological properties of the plasticized sulfonated polysulfone to identify formulations that are rheologically compatible for coextrusion with PP. The effects of various factors including PEG molecular weight, concentration, temperature and BPS molecular weight on the complex viscosity of blends are investigated. An approach by Bueche and Harding was employed to generalize the rheological behavior of the blends and to compare it with that of non-associating polymers [1, 2].

6.2 RESULTS AND DISCUSSION

It is important to control the BPS/PEG rheology within a specific range for coextrusion with PP to achieve uniform thickness and defect-free membranes [3]. Since the rheology is sensitive to small changes in the blend [4, 5], various factors that influence the rheology, such as PEG molecular weight, PEG concentration, temperature, and BPS molecular weight, etc. should be considered [6].

A sulfonation level of 20 mol% BPS-K form ($\bar{M}_w$ = 33,900 g/mol) was chosen for this study because it offers good membrane properties and thermal stability as mentioned previously (see Chapter 3.1.1) [7-11]. PEGs, with $\bar{M}_n$ values between 200 and 600 g/mol,

---

6 Parts of this chapter have been adapted from the following article with permission:
[1] H. J. Oh, B. D. Freeman, J. E. McGrath, C. J. Ellison, S. Mecham, K.-S. Lee, and D. R. Paul, "Rheological studies of disulfonated poly(arylene ether sulfone) plasticized with poly(ethylene glycol) for membrane formation," Polymer, vol. 55, pp. 1574-1582, 2014.

were used (see Chapter 3.1.2) [11]. BPS-20K/PEG blends composed of 20~45 wt% PEG were prepared for rheological property measurements.

6.2.1 PEG viscosity

Before studying the blend viscosities, the viscosities of individual materials (i.e., BPS-20K and PEGs) were investigated. However, since BPS-20K has a T_g of 273 °C and does not readily flow prior to reaching its decomposition temperature [9, 11], its viscosity could not be measured.

For the various PEG materials, the viscosity was recorded by steady shear flow using a Peltier plate geometry (40 mm diameter cone and plate, a gap distance of 55 μm, TA Instruments, New Castle, DE) over the temperature range of 25~200 °C. Due to the characteristics of the Peltier plate, the maximum temperature that this geometry offers is 200 °C, and all measurements were conducted in an ambient atmosphere. Note that PEG materials with $\bar{M}_n$ in the 200~600 g/mol range are thermally stable at 25~220 °C in air according to our previous studies [11]. Under nitrogen atmosphere, PEG materials with $\bar{M}_n$ in the range of 200~600 g/mol are stable up to 250 °C for 10 minutes [11].

PEG is a Newtonian fluid as shown in Figure 6.1. The viscosities of PEG 200~600 are essentially independent of shear rate (see Figure 6.1a) and decrease with increasing temperature because of chain relaxation at high temperature (see Figure 6.1b). At a fixed temperature, the viscosity is proportional to $\bar{M}_n$ as shown in Figure 6.1b, since these materials are below the critical entanglement molecular weight of 4,400 g/mol reported for PEG [12, 13]. PEG viscosities measured here were used to generate a master curve in the later section.

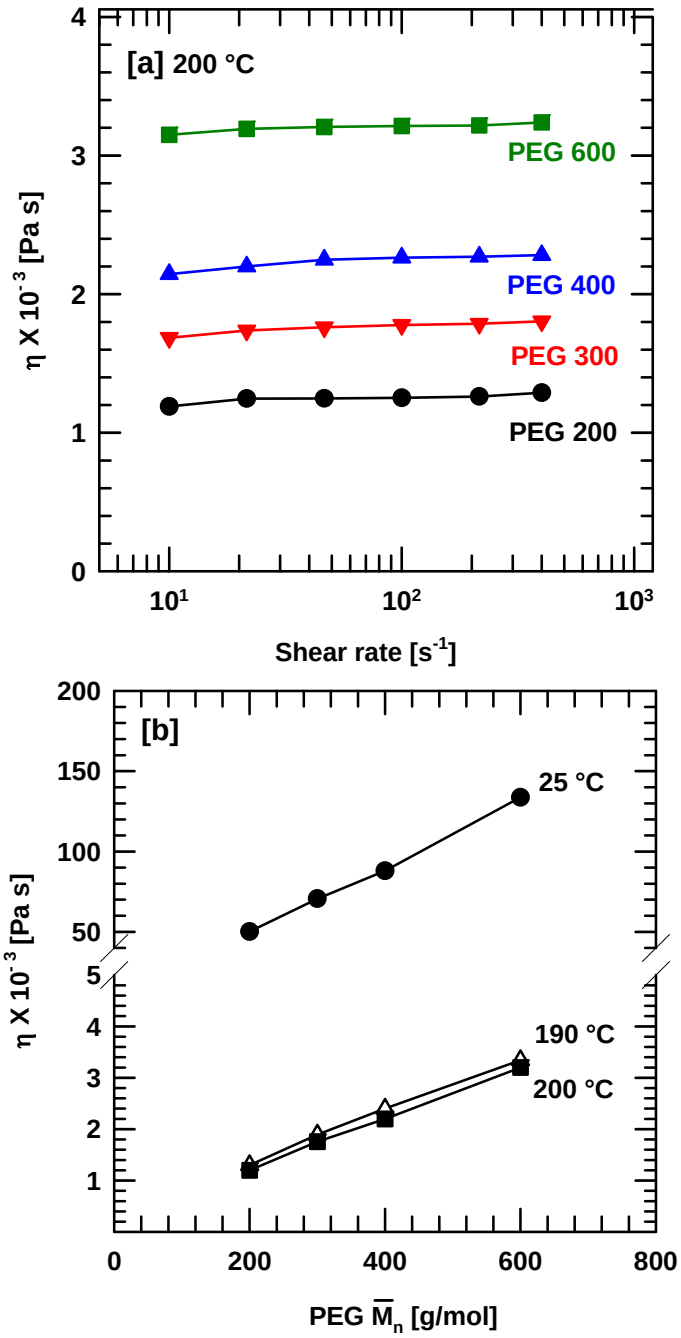

Figure 6.1 Viscosities of PEGs. [a] viscosity versus shear rate curves of PEG 200~600 g/mol at 200 °C and [b] viscosity versus PEG molecular weight ($\bar{M}_n$) (g/mol) at various temperatures. All measurements were conducted under an ambient atmosphere.

6.2.2 Thermal stability of BPS/PEG blends

As previously reported, most BPS-20K/PEG blends show adequate thermal stability at 170~210 °C for rheological measurements [11]. However, for some BPS-20K/PEG blends with lower molecular weight PEGs, evaporation can occur when the measurements are performed at high temperatures for long times [11, 14, 15]. Thermal stability of BPS-20K/PEG blends depends on the combination of PEG molecular weight ($\bar{M}_n$), PEG concentration, measurement temperature and the measurement duration. For example, BPS-20K/PEG 200 30 wt% blend is thermally stable up to 200 °C during the frequency sweep (around 10 minutes), but it is only stable for a few minutes at 210 °C, so its viscosity at this temperature cannot be readily obtained over a broad range of frequency.

All rheological data shown here represent thermally stable mixtures. Three methods were used to confirm stability and reproducibility of the data: continuous frequency sweeps to check whether a second scan agrees with the first scan; time sweeps for 10~30 minutes; and ^{1}H NMR to verify the lack of change in molecular structure, PEG molecular weight ($\bar{M}_n$), and PEG concentration after each measurement [11].

6.2.3 Effect of PEG concentration on viscosity

Figure 6.2 presents the effect of PEG concentration (wt%) on the complex viscosity of BPS-20K/PEG blends at 200 °C in the range of 20~45 wt% PEG 600. With one exception, all viscosity versus frequency curves exhibit a Newtonian plateau followed by shear thinning; the BPS-20K/PEG 600 20 wt% blend does not exhibit a clear Newtonian plateau. As the PEG (i.e., plasticizer) concentration increases, the complex viscosity decreases as expected when a polymer is diluted with a low molecular weight solvent or plasticizer [16]. Figure 6.3 summarizes the effect of PEG 600 weight fraction on the zero shear viscosity, η_0, of BPS-20K/PEG 600 blends; the trend is consistent with a log-mean

mixing rule as often found for miscible mixtures [17, 18]. For cases where the Newtonian plateau is not clearly observed at the lowest frequency, i.e., ω = 0.1 rad/s, a value of η_0 was estimated with the help of the Bueche-Harding model as will be explained in section 6.2.7. As PEG concentration increases from 20 to 45 wt%, η_0 decreases by three orders of magnitude, following a linear logarithmic relation.

As shown in the 20 wt% PEG blend (see Figure 6.2), the viscosity measured from low to high frequency (filled symbols) agrees well with the viscosity measured from high to low frequency (unfilled symbols), so the shear history or the time at temperature does not affect the rheological properties. Similar data were found for all of the other compositions but are not shown for brevity.

For all compositions in Figure 6.2, the frequency sweep was run twice to verify reproducibility. Data from the BPS-20K/PEG 600 45 wt% blend, which is the least stable composition among the blends considered, is shown as an example in Figure 6.2. The viscosity measured from the first frequency sweep (filled symbols) overlaps with that from the second (unfilled symbols). A time sweep at the same temperature (200 °C) was conducted for 10 minutes to ascertain any changes in rheological properties ($G', G'', |\eta^*|$), but no significant differences were found as shown in Figure 6.4. Moreover, ^{1}H NMR analyses confirm that the PEG molecular structure, PEG $\bar{M}_n$, or PEG concentration in the blends were not significantly changed during the rheological measurements.

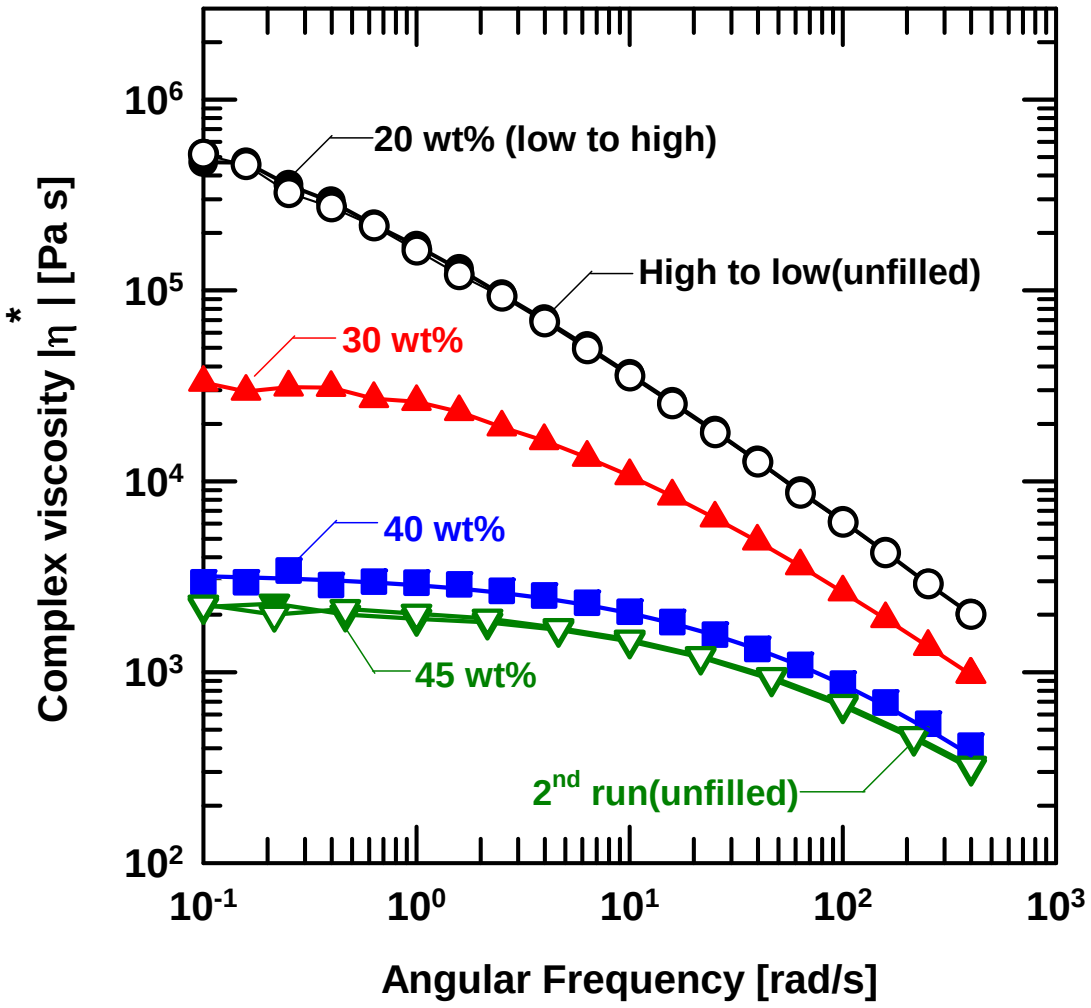

Figure 6.2 Effect of PEG concentration (wt%) on blend viscosity. BPS-20K/PEG 600 blends were used at 200 °C. For 20 wt% PEG curves, the filled symbols (●) are from frequency sweep done from low to high frequency; whereas the unfilled symbols (○) are from high to low frequency sweep. For the 45 wt% PEG curves, the filled symbols (▼) are from the 1st frequency sweep and the unfilled symbols (▽) are from the 2nd frequency sweep. Unless otherwise indicated, a low to high frequency sweep was conducted.

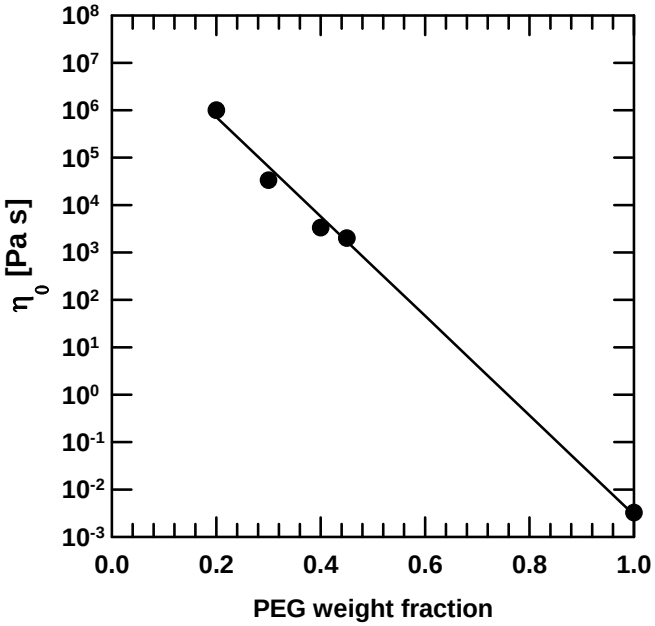

Figure 6.3 Effect of PEG 600 weight fraction on zero shear viscosity, η_0, of BPS-20K/PEG 600 blends at 200 °C.

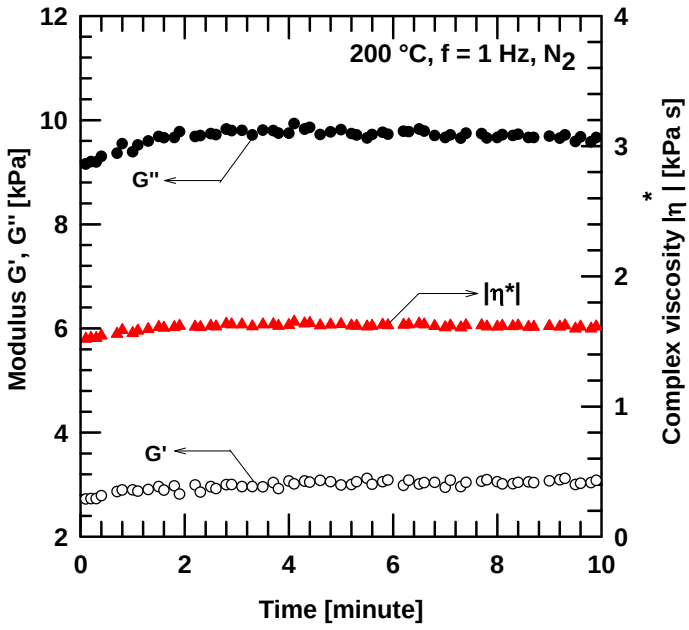

Figure 6.4 Storage modulus, G'(○), loss modulus, G''(●) and complex viscosity, $|\eta^*|$(▲) of BPS-20K/PEG 600 45 wt% blend as a function of time (minute). f = 1 Hz, T = 200 °C under a nitrogen atmosphere.

6.2.4 Effect of PEG $\bar{M}_n$ on viscosity

Figure 6.5 shows the effect of PEG molecular weight ($\bar{M}_n$) on the complex viscosity of BPS-20K/PEG blends at a fixed PEG concentration of 30 wt%. At a fixed PEG concentration, the blend viscosity decreases with decreasing PEG $\bar{M}_n$ since shorter chain PEG molecules themselves have a lower viscosity are more effective plasticizers than higher molecular weight PEG [11, 16, 19]. The hydroxyl groups are likely to interact much more strongly with sulfonated groups than do the ether oxygen [20]. Thus, lower molecular weight PEG molecules may more effectively plasticize the BPS polymer owing to this high content of hydroxyl groups. Figure 6.6 summarizes the effect of PEG $\bar{M}_n$ on the zero shear viscosity, η_0, of BPS-20K/PEG 30 wt% blends at 200 °C. As the PEG $\bar{M}_n$ decreases from 600 g/mol to 200 g/mol, η_0 decreases by about a factor of three.

However, compared to the three orders of magnitude decrease in the blend viscosity as PEG concentration increases between 20 wt% to 45 wt% (see Figure 6.2), this η_0 decrease induced by decreasing PEG $\bar{M}_n$ is relatively small (i.e., less than an order of magnitude decrease). Indeed, the viscosity difference between the BPS-20K/PEG 30 wt% blends with PEG 300 g/mol, 400 g/mol and 600 g/mol is very small as shown in Figure 6.5, so that their viscosities almost overlap each other at the higher frequency range (i.e., > 50 rad/s).

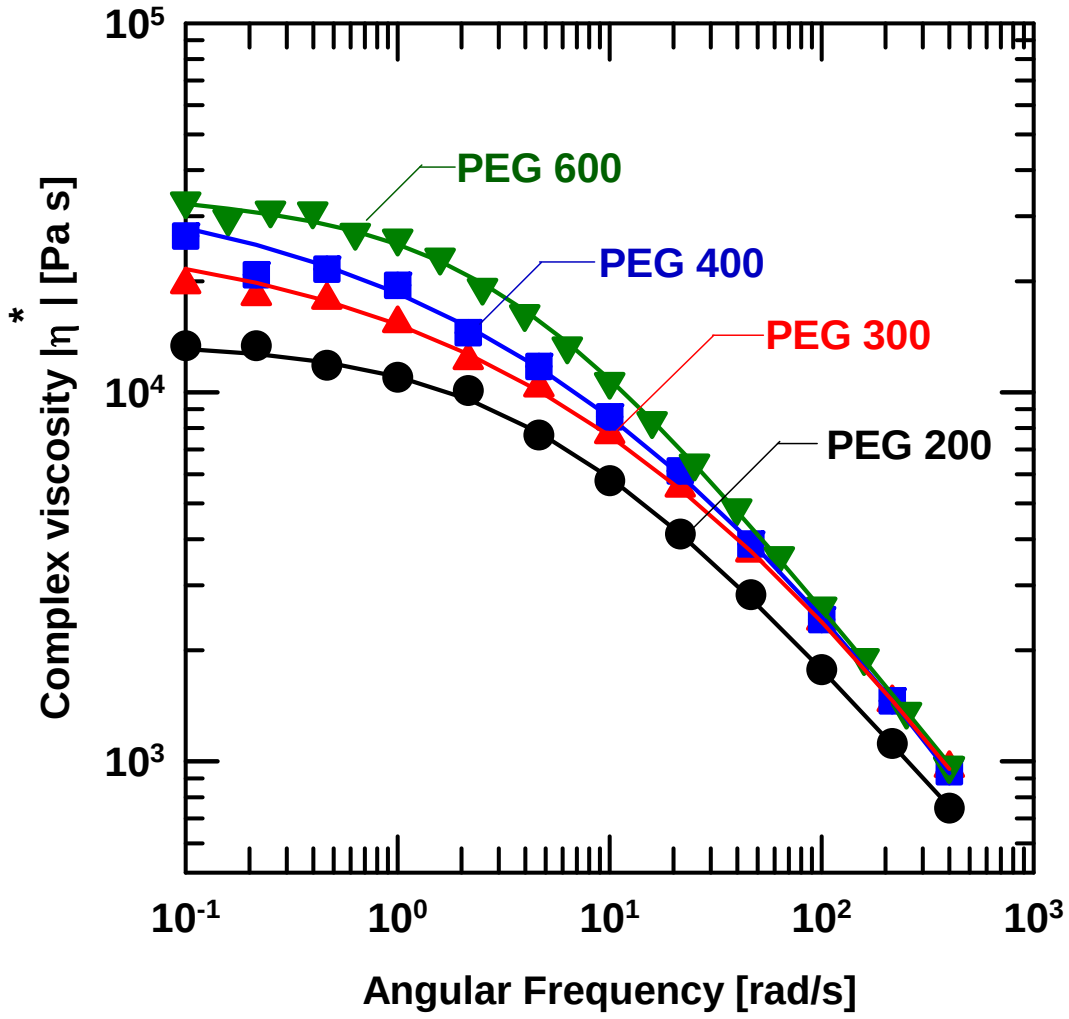

Figure 6.5 Effect of PEG molecular weight ($\bar{M}_n$) (g/mol), on the complex viscosity, $|\eta^*|$, of BPS-20K/PEG 30 wt% blends at 200 °C.

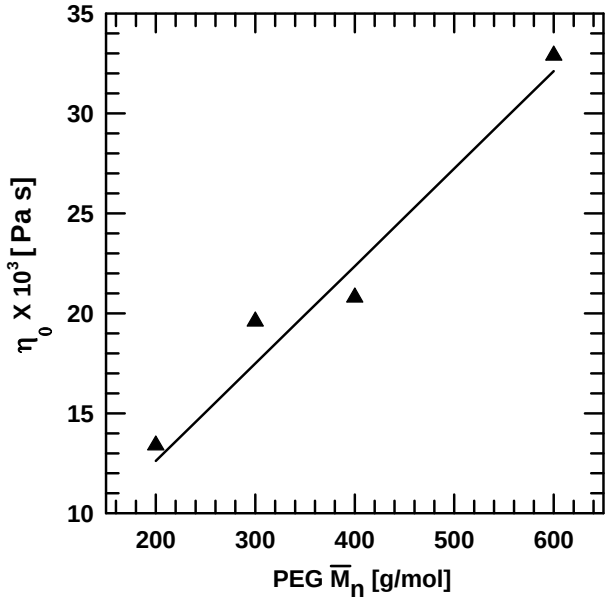

Figure 6.6 Effect of PEG molecular weight ($\bar{M}_n$) (g/mol), on zero shear viscosity, η_0, of BPS-20K/PEG 30 wt% blends at 200 °C

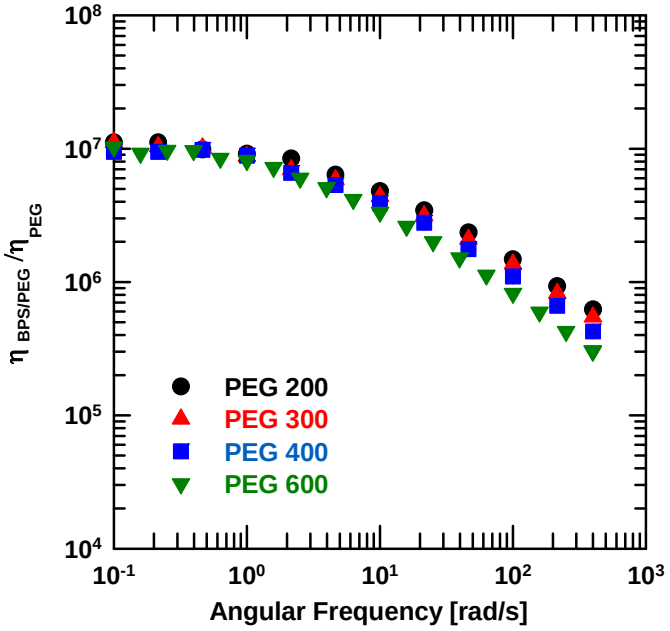

Figure 6.7 Normalized viscosity, $\eta_{BPS/PEG}/\eta_{PEG}$, versus frequency of BPS-20K/PEG 30 wt% blends at 200 °C. PEGs with $\bar{M}_n$ ranging between 200~600 g/mol were used.

When the complex viscosity is normalized by the PEG viscosity (i.e., $\eta_{BPS/PEG}/\eta_{PEG}$), the data approach a single master curve as shown in Figure 6.7. At a PEG concentration of 30 wt% and 200 °C, the BPS-20K/PEG blends, with PEG $\bar{M}_n$ ranging from 200 g/mol to 600 g/mol, lead to a similar shear thinning behavior.

6.2.5 Effect of temperature on viscosity

The effect of temperature on the complex viscosity of BPS/PEG blends is shown in Figure 6.8. For a blend of BPS-20K containing 30 wt% of PEG 600, the viscosity decreases as temperature increases from 170 to 210 °C [21].

At temperatures well above T_g (i.e., T_g+100 °C or above), viscosity is typically expressed by an Arrhenius equation [22]:

$$\eta_0 = A \cdot \exp(\frac{\Delta E_\eta}{RT}) \tag{6.1}$$

where η_0 is the zero shear viscosity, A is a pre-exponential factor, ΔE_η is the activation energy for flow, R is a gas constant, and T is temperature. Plots of $\log \eta_0$ versus 1/T are presented in Figure 6.9 for BPS-20K/PEG 600 30~40 wt% blends. Some values of η_0 were estimated with the help of the Bueche-Harding model as will be explained in section 6.2.7. The Arrhenius model provides a reasonable fit for the data, and model parameters are recorded in Table 6.1. As PEG concentration increases from 30 to 40 wt%, ΔE_η decreases by almost a factor of two, presumably due to increased plasticization in the blend containing more PEG. Typical values for ΔE_η for non-associating polymer fluids are of the order of 20~65 kJ/mol [21]. For associating polymers, the ΔE_η values can vary depending on various factors including cation, bound ion type, and ion content, et al. [6, 23, 24]. Weiss et al. reported the ΔE_η values around 230 ~ 270 kJ/mol with Na and Zn substituted sulfonated polystyrene (sulfonation level = 1.82 ~ 5.81 mol%) [24].

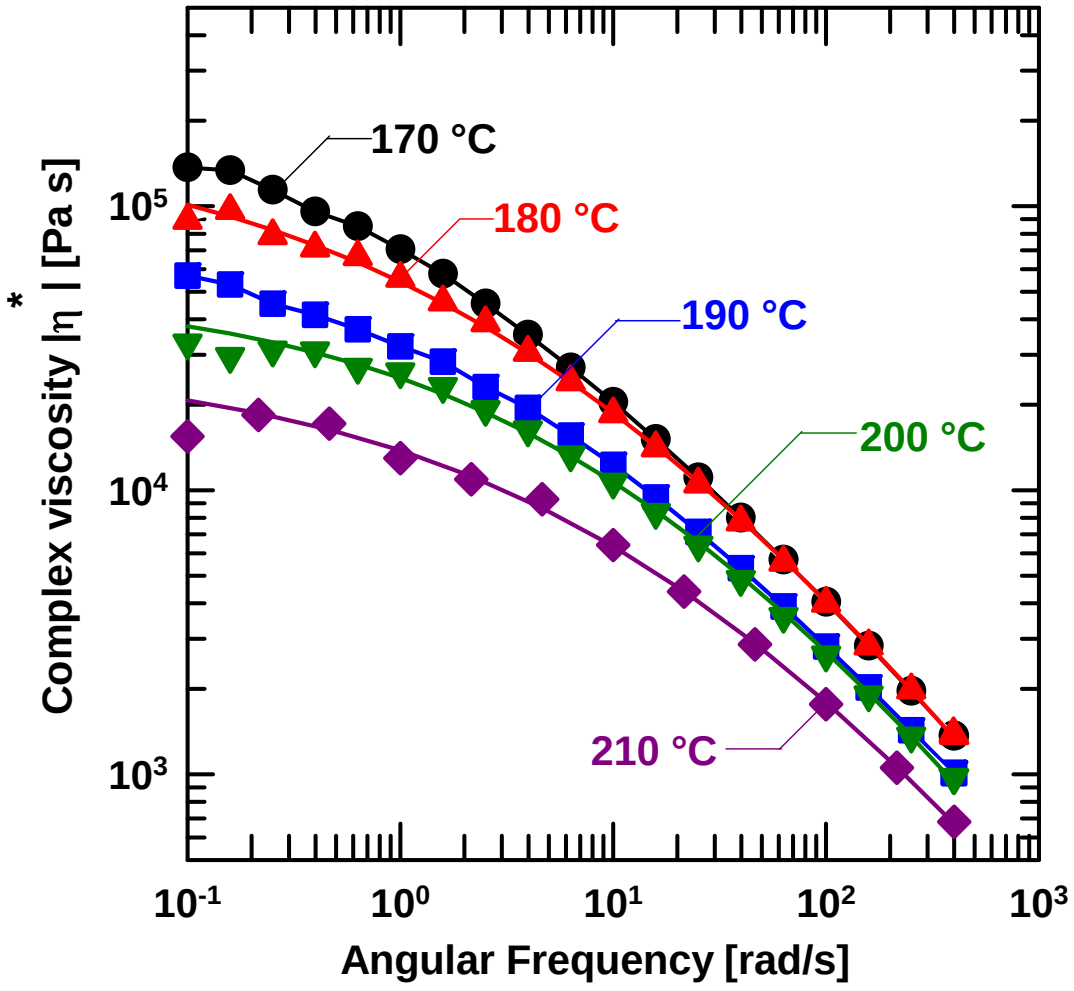

Figure 6.8 Effect of temperature (°C) on the complex viscosity, $|\eta^*|$, of BPS-20K/PEG 600 30 wt% blends.

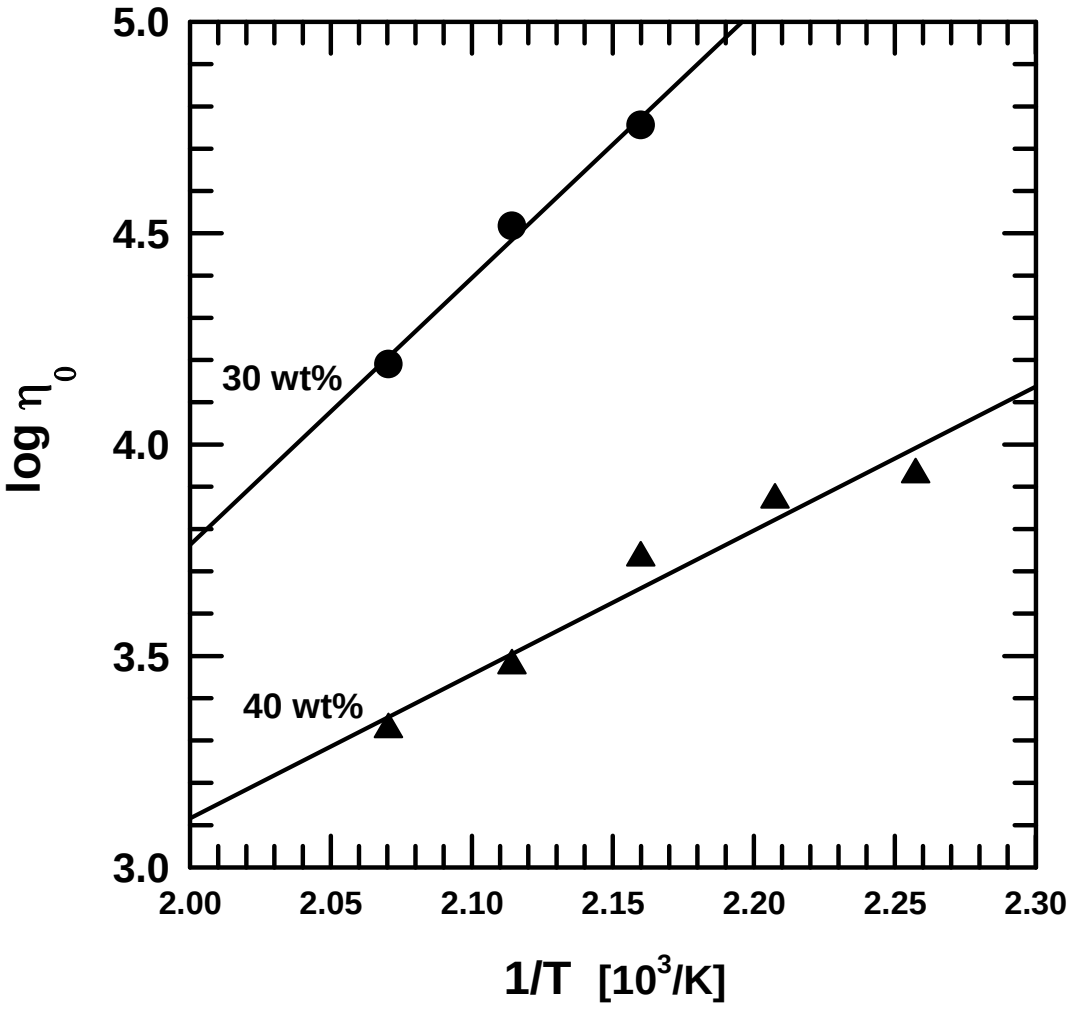

Figure 6.9 Influence of temperature on zero shear viscosity, η_0, in blends of BPS-20K with 30 wt% and 40 wt% PEG 600.

Table 6.1 Parameters calculated from the Arrhenius type equation (6.1)

PEG 600 concentration [wt%]	ΔE_η [kJ/mol]	A [Pa-s]
30	52.5	1.41
40	28.3	2.49

6.2.6 Effect of BPS $\bar{M}_w$ and DS on viscosity

In the discussion so far, results have been presented using only one sulfonated polysulfone (BPS-20K, $\bar{M}_w$ = 33,900 g/mol). More limited sets of measurements were made for other sulfonated polysulfones with higher molecular weight and higher sulfonation levels (i.e., higher degree of sulfonation (DS)). Polymers with various molecular weights (BPS-20K, $\bar{M}_w$ = 33,900~70,200 g/mol), and higher sulfonation level (BPS-32K, $\bar{M}_w$ = 70,200 g/mol) were used to investigate the effect of molecular weight and sulfonation level on viscosity. Selected properties are summarized in Table 6.2. Using these additional sulfonated polymers, blends were prepared using 30 wt% PEG 600, and rheological properties were measured at 200 °C.

Table 6.2 Characteristics of the polymers of this study

Material	$\bar{M}_w$[a] [g/mol]	IV[a] [ml/g]	T_g[b]* [°C]	Density[c]* [g/cm^3]	Water Permeability[d] [L μm m^{-2} h^{-1} bar^{-1}]	NaCl rejection[d] [%]
BPS-20K	33,900	48.2	273	1.30	0.03	99.2
BPS-20K	45,500	61.8	273	1.31	0.03	99.2
BPS-20K	56,700	72.3	273	1.35	0.03	99.2
BPS-32K	70,200	81.7	320	1.39	0.18	96.2

[a] Determined by SEC using NMP with 0.05 M LiBr at 50 °C. Note that specific refractive index increment (dn/dc) values were measured using an assumption of 100 % mass recovery. dn/dc values for BPS-20K polymers of this study are 0.17 [ml/g].

[b] Measured by DSC at 20 °C/min

[c] Measured using a Mettler Toledo density determination kit (Part# 238490, Switzerland) with *n*-heptane (Cat# 32287, Sigma-Aldrich, St. Louis, MO) at ambient temperature (20~22°C)

[d] Table 1 from Reference [10]

* Measurements were conducted using solution cast films. Transparent and uniform thickness films (30~40 μm) were formed by the solution casting method reported previously [11]

Note that the polydispersity (PDI) of sulfonated polysulfone from step growth polymerization is around 2 [25], although the ratio of $\bar{M}_w/\bar{M}_n$ determined by Size Exclusion Chromatography (SEC) is around 1.4~1.5. This is related to the characteristics of light scattering measurements employed for SEC, which have a tendency to overestimate number average molecular weight ($\bar{M}_n$) since the light scattering measurements are not sensitive to the lower molecular weight portion of the molecular weight distribution, as reported previously [26]. The molar mass determined by the light scattering measurements is the weight average molecular weight ($\bar{M}_w$), so we report $\bar{M}_w$s of BPS-20K materials in Table 6.2.

6.2.6.1 Effect of BPS $\bar{M}_w$ on viscosity

The effect of the polymer molecular weight on the complex viscosity of BPS-20K/PEG blends is presented in Figure 6.10. The BPS-20K weight average molecular weights range from 33,900 g/mol to 56,700 g/mol. At a fixed sulfonation level (DS = 20 mol%), the complex viscosity increases with increasing molecular weight.

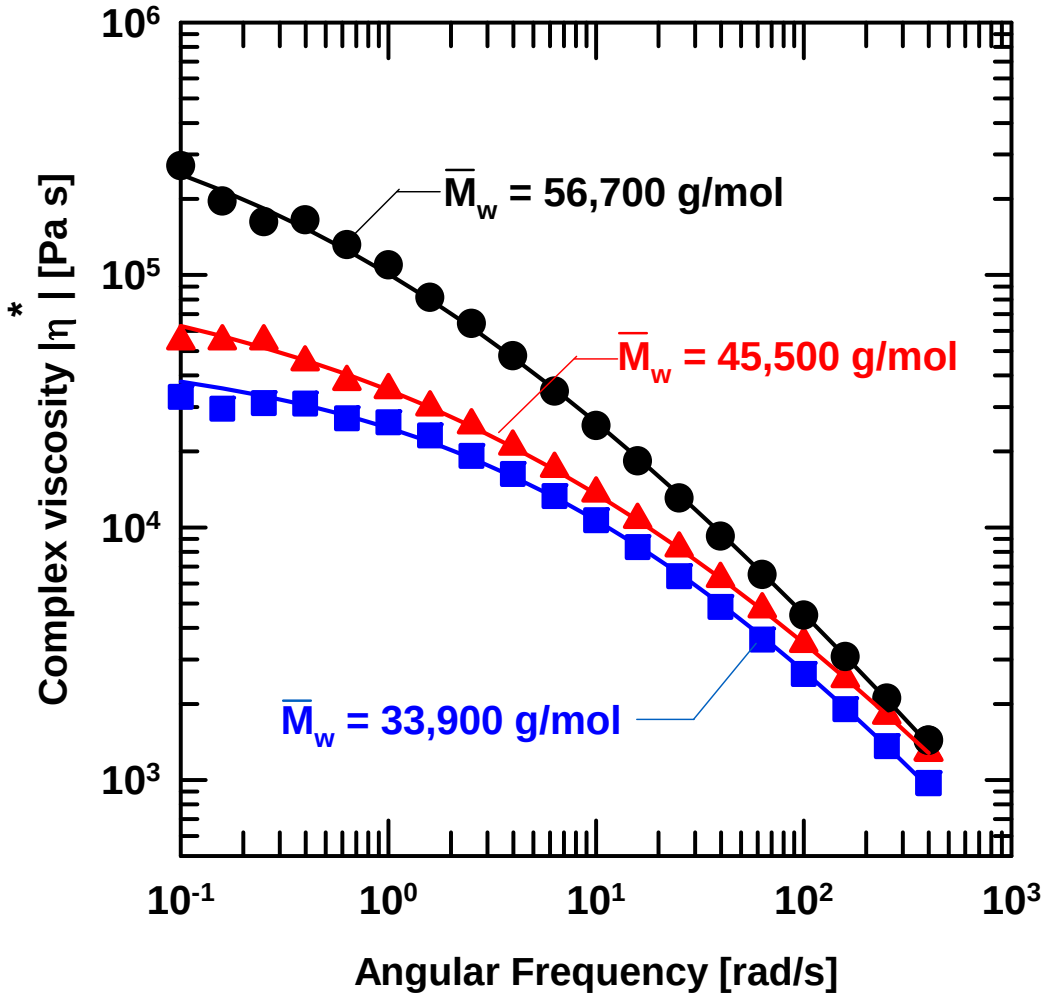

Figure 6.10 Effect of BPS-20K molecular weight (g/mol) on the complex viscosity, $|\eta^*|$, of BPS-20K/PEG 600 30 wt% blends at 200 °C.

Increasing the molecular weight of an associating polymer can enhance both molecular entanglements as well as ionic interactions, both of which could influence viscosity [6, 23, 24, 27]. It is difficult to distinguish the influences from entanglements and ionic interactions, since the contribution of the entanglements to the dynamic storage modulus is as significant as that of ionic associations, according to Weiss et al. in their studies with lightly sulfonated polystyrene (2.5 and 4.8 mol% sulfonation) [23, 24, 28].

Fouissac et al. also reported for hyaluronate, a wormlike ionomer, that, in the dilute region, where $M < M_c$ (M_c is the critical molecular weight for entanglements), the zero shear viscosity scales with molecular weight to the first power ($\eta_0 \propto M^1$), similar to that of non-associating polymers. However, M_c is observed at concentrations 10 times less than in entangled, non-associating flexible polymers in solution. It has been suggested that above the entanglement concentration, the zero shear viscosity scales with molecular weight to the fourth power ($\eta_0 \propto M^4$) in associating polymers rather than the 3.4 power ($\eta_0 \propto M^{3.4}$) typically observed in non-associating polymers [27].

A plot of zero shear viscosity as a function of molecular weight in BPS-20K materials is presented in Figure 6.11. Since the Newtonian plateau is not fully developed for some curves in Figure 6.10, the Bueche-Harding model was used to estimate the η_0 values as mentioned earlier. In RADEL® polysulfones, which are not sulfonated, the zero shear viscosity scales with molecular weight raised to the 3.4 power above the critical molecular weight, which is 10,000 g/mol [29]. Similarly, in the BPS-20K materials, the exponent is more or less consistent, based on these limited data, with the expected value of 3.4 for non-associating polymers.

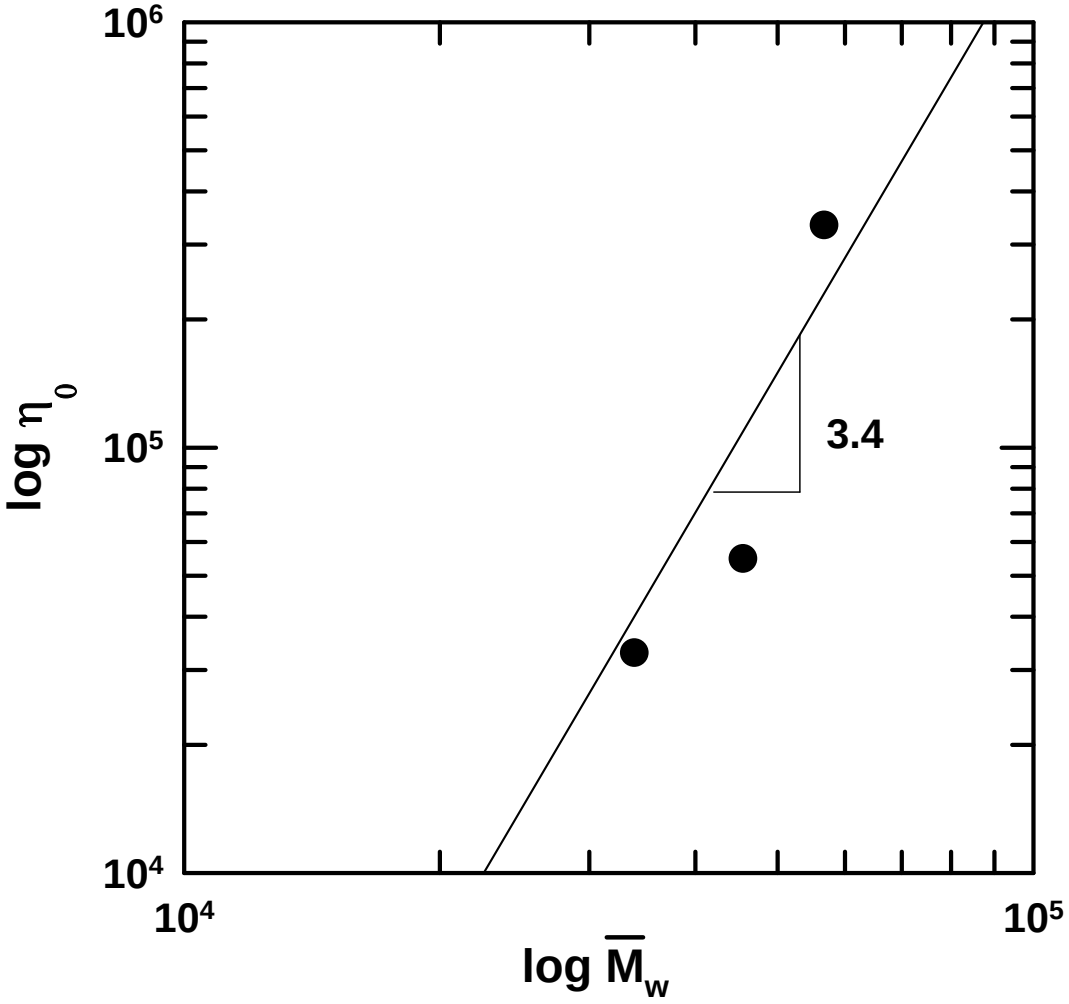

Figure 6.11 Influence of molecular weight on zero shear viscosity, η_0, in blends of BPS-20K containing 30 wt% of PEG 600. These measurements were performed at 200 °C. The solid line has a slope of 3.4.

6.2.6.2 Effect of BPS sulfonation level on viscosity

Figure 6.12 presents the effect of BPS-K sulfonation level (mol%) on the complex viscosity of BPS/PEG blends. Comparing BPS-K polymers of similar molecular weight ranges (exactly identical molecular weight materials did not exist due to the difficulties in molecular weight control), the viscosity is higher at the higher sulfonation level, consistent

with ionic interactions acting as physical cross-links due to their long lifetime [6, 30]. Sulfonation affects the viscosity but does not affect the shape of the viscosity versus frequency curve.

Since the molecular weights of the samples used to prepare the data in Figure 6.12 are different, the scaling of zero shear viscosity with the 3.4 power of the molecular weight can be used to estimate the zero shear viscosity of BPS-20K at 70,200 g/mol and compare this estimated value to the experimentally determined zero shear viscosity in BPS-32K, which has an average molecular weight of 70,200 g/mol. Based on this calculation, the complex viscosity is expected to increase by 220×10^3 [Pa s] for each mole % increase in degree of sulfonation in BPS-K samples having a molecular weight of 70,200 g/mol. Therefore, for BPS-32K, approximately 88 % of the viscosity increase, relative to BPS-20K, is due to the sulfonation, and the rest (12 %) is due to the molecular weight increase. Although more data are required for clear estimation, this might imply the stronger effect of ionic group association on the viscosity increase, although the influence of ionic interactions (by adding more ionic groups) and entanglement (by the molecular weight increase) are closely related as mentioned earlier [6, 23, 24, 27].

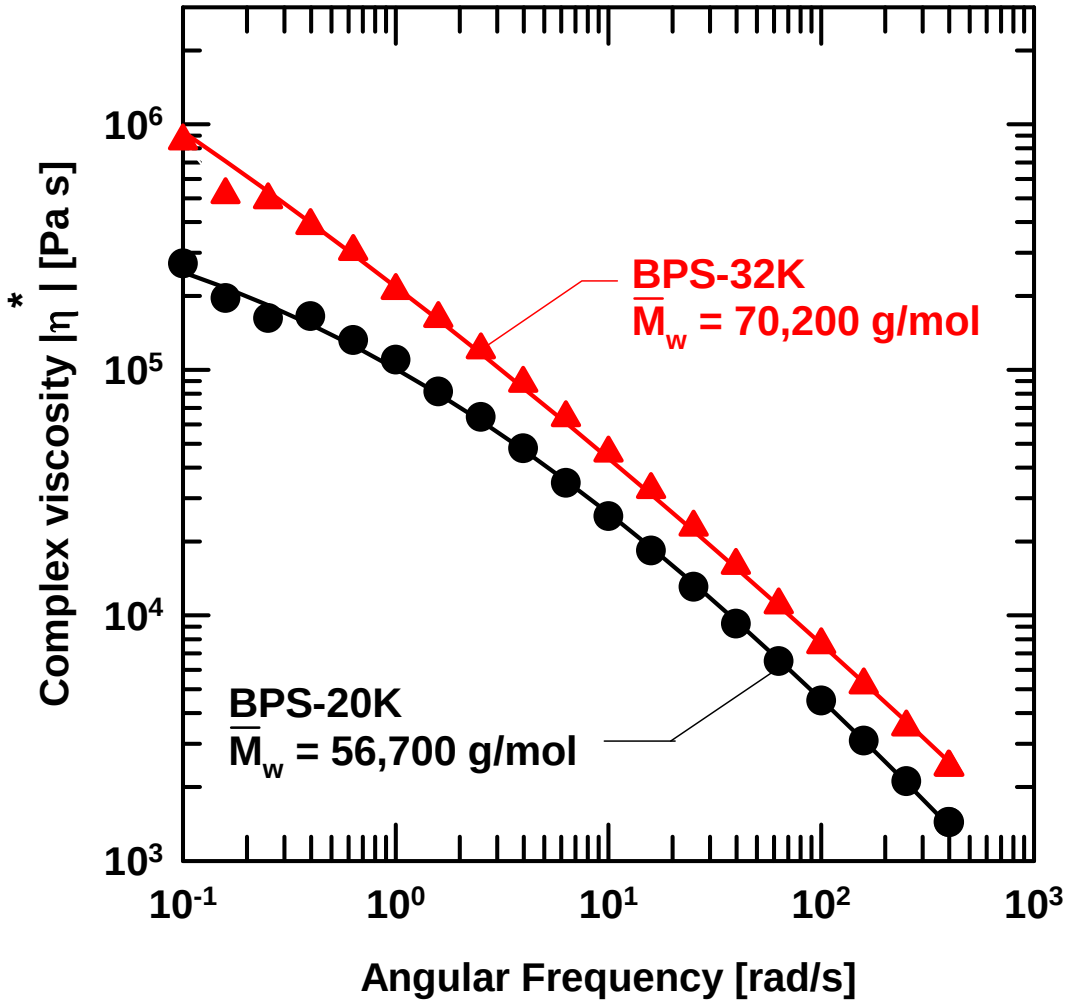

Figure 6.12 Effect of BPS-K sulfonation level (mol%) on the complex viscosity of BPS-K/PEG 600 30 wt% blends at 200°C.

6.2.7 Master curve using Bueche-Harding Model

Many studies reported that the melt behavior of associating polymers (or ionomers) is different from that of non-associating polymers since the ionic groups act as physical cross-links, or may aggregate, leading to rheological complexity. In general, the rheology of ionomers may be affected by various factors such as counter ion/bound ion type, molecular weight, neutralization level, plasticizer, temperature and shear rate, etc., but no

universal rule has been established to explain the effect of all of these factors on rheology [6, 30].

For the shear rate dependence of the viscosity, most polymers are pseudoplastic in the non-Newtonian region at high shear rate, whereas some associating polymer solutions (for example, Na and Li substituted sulfonated polystyrene) exhibit shear thickening where, after the Newtonian regime, the viscosity increases by a factor of 2-3 times, and then shear thinning follows at higher shear rates [6, 31-36]. Witten, et al. explained that the ionic intrachain pairs separated and interchain connections increase as shear flow elongated the polymer chains, forming larger ionic networks, which contributed to higher viscosity. As the shear rate increased to levels exceeding the chain relaxation time, a shear thinning region appeared [31, 37]. Therefore, ionic interactions as well as polymer entanglement should be considered in interpreting the rheology of associating polymers [6, 23, 24, 38].

For a variety of non-associating polymers with similar molecular weight distributions like polystyrene, poly(methyl methacrylate), and mixtures of such polymers with diluents, Bueche and Harding [2] showed that plots of η/η_0 versus $\tau\dot{\gamma}$, lead to a single master curve, where $\dot{\gamma}$ is the shear rate, and τ is the longest relaxation time [2, 39-42]:

$$\tau = \frac{12}{\pi^2}\frac{\bar{M}_w\,\eta_0}{CRT} \tag{6.2}$$

where $\bar{M}_w$ is the weight average molecular weight of the polymer, and C is the polymer concentration per unit volume (g polymer/cm^3) [1, 2].

It was of interest to learn whether the data for the current mixtures of the ion containing polymer BPS-K could be described by the master curve established by Bueche and Harding [1, 2]. The viscosity versus frequency curves shown earlier can be converted to the viscosity versus shear rate curves using the Cox-Merz rule [43-46] since it was found to be applicable for these materials within acceptable error ranges (see Figure 6.16 in the

supplemental material section 6.4). The plots of η/η_0 versus $\dot{\gamma}$ were shifted horizontally for superposition for cases where η_0 was well defined experimentally. When plotted in this manner, all of the rheological data collapse onto a single master curve as shown in Figure 6.13. The solid line in Figure 6.13 is the master curve developed by Bueche and Harding in the form of the following analytical equation [2, 39]:

$$\frac{\eta}{\eta_0} = [1 + 0.6(\tau\dot{\gamma})^{0.75}]^{-1} \tag{6.3}$$

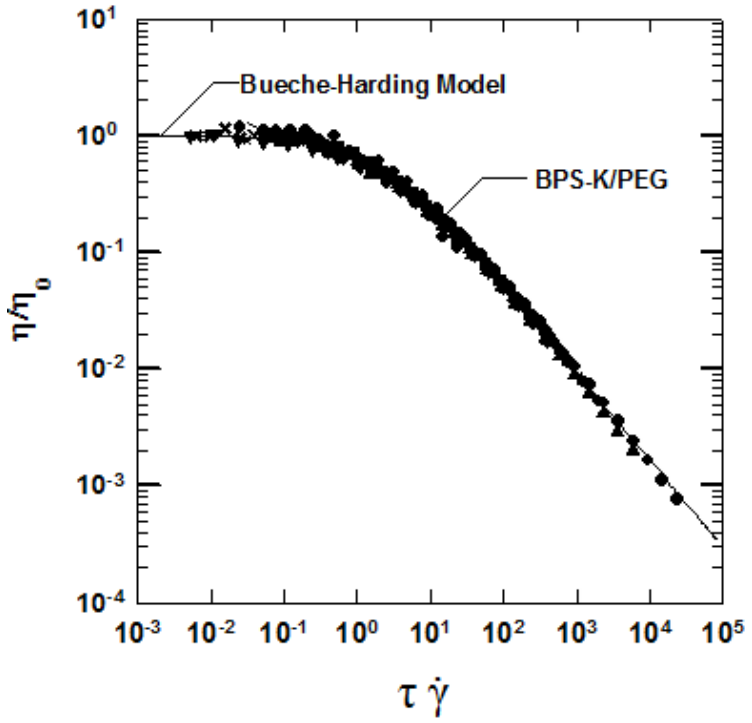

Figure 6.13 Master curve of BPS-K/PEG blends using the Bueche-Harding Model. All dots (BPS-K/PEG blends) are the rheological data in Figures 6.2, 6.5, 6.8, 6.10, and 6.121. The solid line is the master curve that Bueche and Harding found with many linear polymer systems including the concentrated solutions of poly(methyl methacrylate) (PMMA) and polystyrene (PS) [2, 39].

For the cases where the Newtonian plateau is not developed in the measured angular frequency range, η_0 was estimated as follows. Equation (6.3) can be rearranged to:

$$\frac{1}{\eta} = \frac{1}{\eta_0} + \frac{0.6\tau^{0.75}}{\eta_0}(\dot{\gamma})^{0.75} \tag{6.4}$$

When 1/η is plotted versus $\dot{\gamma}^{0.75}$, the data align linearly as illustrated in Figure 6.14. From the reciprocal of the intercept on the ordinate of such plots, a value for η_0 was estimated. Figure 6.14 shows an example of BPS-20K/PEG 600 20 wt% blend; similar data were found for all of the other compositions but are not shown for brevity (see Table 6.3).

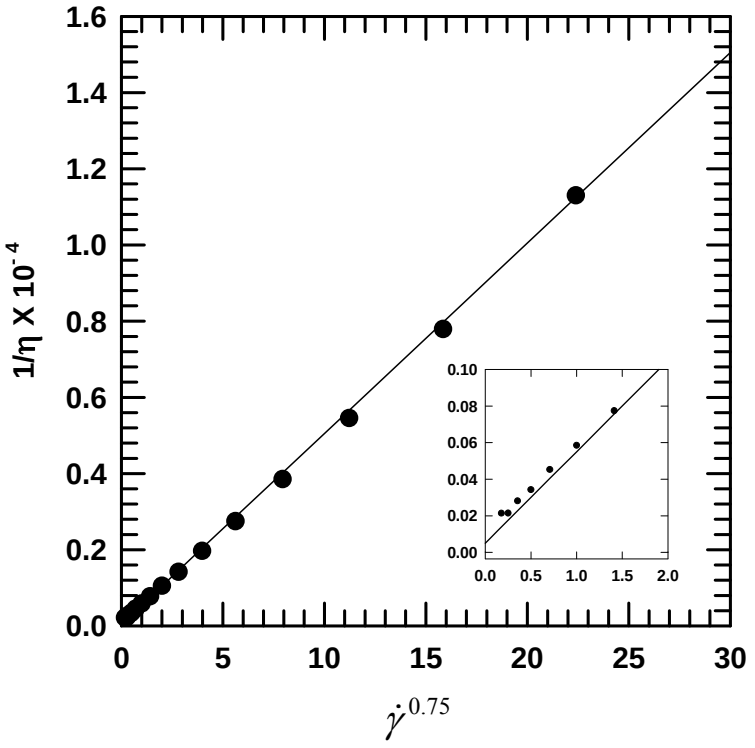

Figure 6.14 A plot of 1/η versus $\dot{\gamma}^{0.75}$ for BPS-20K/PEG 600 20 wt% blend at 200 °C from Figure 6.2. Viscosity values in the angular frequency range of 0.1 ~ 63.1 rad/s are shown for easier viewing. Solid line is a linear trend line to determine η_0 value. The inset graph shows the magnified view near the origin ($0.0 < \dot{\gamma}^{0.75} < 2.0$).

The parameters ($\overline{M}_w$, η_0, and τ) calculated from this analysis are presented in Table 6.3. When plots of η/η_0 versus $\dot{\gamma}$ were shifted horizontally for superposition with the equation (6.3), the shift factor yields a value of τ, therefore, $\overline{M}_w$ can be determined based on equation (6.2). For the BPS-20K ($\overline{M}_w$ = 33,900 g/mol)/PEG blends, regardless of blend composition and test temperature, the calculated $\overline{M}_w$s are in the consistent range of 42,200~49,500 g/mol. The η_0 and τ parameters are proportional to each other at a given composition and temperature, as shown by equation (6.2).

Table 6.3 η_0, $\bar{M}_w$, and τ of BPS-K/PEG blends using Bueche-Harding (B-H) model. The data are from Figure 6.2, 6.5, 6.8, 6.10, and 6.12

BPS-K	BPS-K $\bar{M}_w$ [g/mol] by SEC	PEG $\bar{M}_n$ [g/mol]	PEG wt%	Temp [°C]	η_0 [Pa s]	$\bar{M}_w$ [g/mol] by B-H	τ [s]
BPS-20K	33,900	200	30	200	12,500	49,500	0.23
BPS-20K	33,900	300	30	200	16,700	43,100	0.25
BPS-20K	33,900	400	30	200	20,000	44,600	0.32
*BPS-20K	33,900	600	30	200	33,300	47,500	0.56
BPS-20K	33,900	600	20	200	1,000,000**	49,300	14.71
*BPS-20K	33,900	600	30	200	33,300	47,500	0.56
BPS-20K	33,900	600	40	200	3,300	45,500	0.06
BPS-20K	33,900	600	45	200	2,000	48,900	0.05
BPS-20K	33,900	600	30	170	167,000**	45,200	2.86
BPS-20K	33,900	600	30	180	100,000**	42,200	1.56
BPS-20K	33,900	600	30	190	50,000	48,400	1.00
*BPS-20K	33,900	600	30	200	33,300	47,500	0.56
BPS-20K	33,900	600	30	210	16,700	53,800	0.31
*BPS-20K	33,900	600	30	200	33,300	47,500	0.56
BPS-20K	45,500	600	30	200	50,000	44,900	0.80
BPS-20K	56,700	600	30	200	333,300**	53,100	5.00
BPS-32K	70,200	600	30	200	3,333,300	70,500	80.00

*Duplicated for easier comparison, **η_0 is determined via the procedure in Figure 6.14

Table 6.4 compares the weight average molecular weights calculated using the Bueche-Harding model with these measured by SEC. There is a good agreement between three of the four points. Therefore, reasonably accurate $\bar{M}_w$ values were estimated using this rheological analysis.

Table 6.4 Comparison between weight average molecular weight ($\bar{M}_w$) determined experimentally from SEC and estimated from the Bueche-Harding (B-H) model

Polymer	$\bar{M}_w$ [g/mol] by SEC	$\bar{M}_w$ [g/mol] by B-H
BPS-20K	33,900	47,500
BPS-20K	45,500	44,900
BPS-20K	56,700	53,100
BPS-32K	70,500	70,200

The experimental data for the BPS-K/PEG blends matches well with the Bueche-Harding master curve, implying that the rheological behavior of plasticized sulfonated polysulfone is similar to that of the non-associating linear polymers used to establish this curve. Thus the relaxation of polymer entanglements with shear determines the nature of the flow curve rather than ionic interactions. Two possible reasons explaining this observation are: (1) PEG is likely to interact with ionic groups (i.e., sulfonated group) in BPS, leading to less ionic association [6, 11, 16, 20], and (2) due to the plasticization effect of PEG, at the elevated temperatures for rheological measurements, elastic force (increasing with temperature) surpasses the dipole-dipole interactions (somewhat unaffected by temperature increase) of ionic clusters, so that ionic aggregation may be less associated [38].

6.2.8 Coextrusion with polypropylene

One goal of this research has been to identify experimental conditions that enable coextrusion of BPS/PEG blends with polypropylene (PP) for membrane applications. Table 6.5 shows some candidate isotactic PPs that might be considered for coextrusion [47, 48]. For multilayer coextrusion to be effective, the viscosity of the BPS/PEG blend must match that of the PP at the conditions of extrusion (temperature, shear rate, etc.). To identify the viscosity matching points, the viscosities of PPs and BPS/PEG blends at ω = 10 rad/s are plotted against temperature (190~250 °C) in Figure 6.15. The angular frequency of 10 rad/s is selected because this corresponds to a typical low shear rate in the layer multiplication dies used for coextrusion [3, 49]. For example, a good viscosity match would be obtained at 200 °C for PP 2252 with BPS-20K/PEG 600 40 wt% blend. In this way, several processing conditions with various BPS/PEG blends can be identified, and this information will be used for future coextrusion studies.

Table 6.5 Properties of candidate PPs

Grade	Company	MFI [a] [g/10min]
PP 5341E1	Exxon	-
PP 1572	Exxon	2.1
PP 2252	Exxon	3.5
PP H700-12	Dow	12

[a] at 230 °C and 2.16 kg

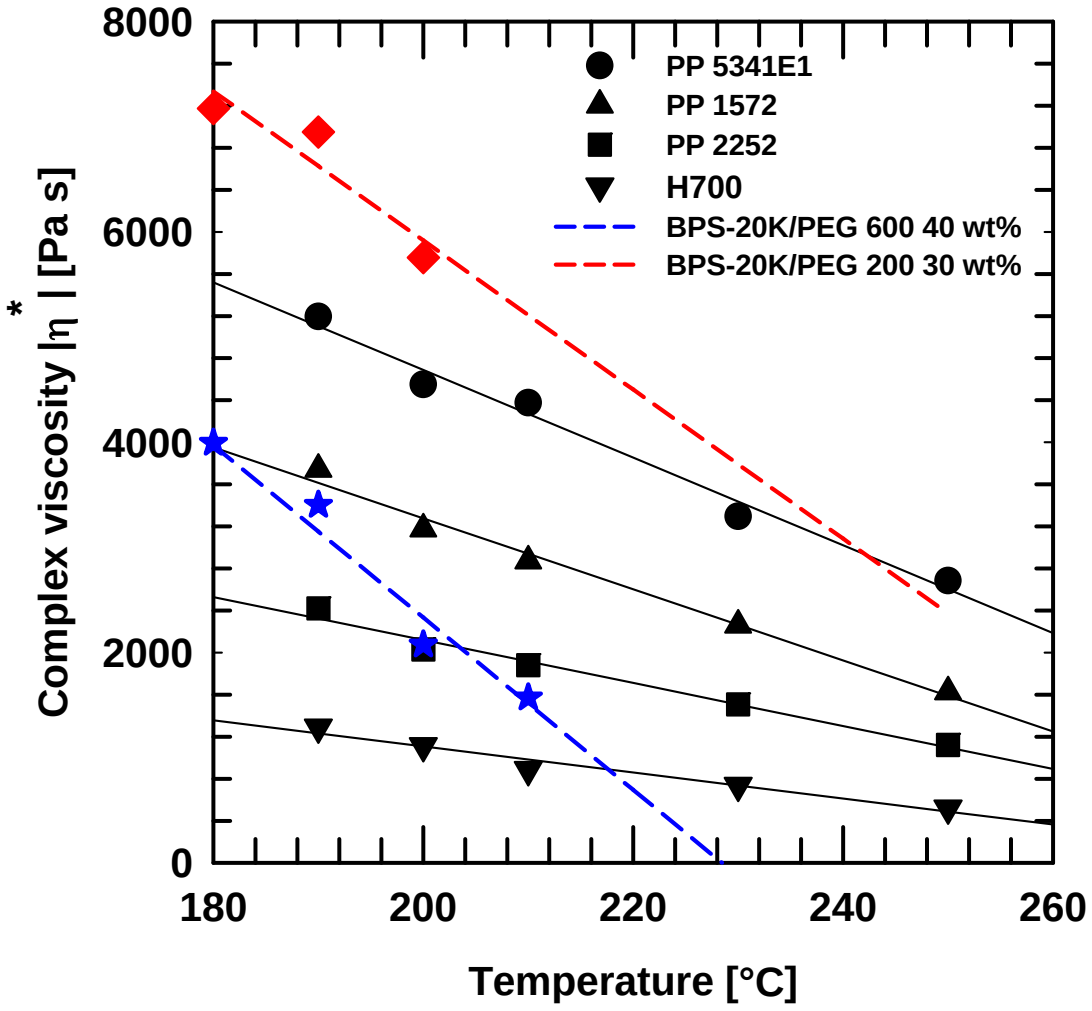

Figure 6.15 Complex viscosities versus temperature (190~250°C) of various PPs used in this study. Dashed lines are BPS-20K/PEG blends. All measurements were conducted at the angular frequency of 10 rad/s.

6.3 CONCLUSIONS

The rheological properties of disulfonated poly(arylene ether sulfone)s plasticized with poly(ethylene glycol) (PEG) were investigated to identify the coextrusion processing conditions with candidate PPs for potential membrane applications such as desalination, fuel cells, etc. The effects of PEG molecular weight, PEG concentration, temperature and BPS molecular weight on blend viscosity were determined. All of the viscosity data are

consistent with a single master curve, and this master curve was established by Bueche and Harding for non-associating polymers such as PMMA and PS. Although sulfonated polysulfone contains ionic groups, this plasticized sulfonated polysulfone follows the same shear thinning behavior as non-associating polymers, suggesting that its flow is dominated by the relaxation of polymer entanglements rather than by ionic interactions. The weight average molecular weights obtained from analysis of the rheological data are comparable to the values measured by SEC. Using the rheological data, conditions were identified for coextrusion of BPS/PEG blends with polypropylene.

6.4 SUPPLEMENTAL MATERIAL

The Cox-Merz rule is valid in many cases. However, for some polymer systems, the Cox-Merz rule is not followed because of their rheological complexity [6, 50].

Since there is no universal guideline for use of the Cox-Merz rule, it is necessary to check whether the Cox-Merz rule works well for the BPS-20K/PEG blends in this work. Steady shear viscosity was obtained (25 mm diameter cone and plate geometry, a gap distance of 156 μm, TA Instruments, New Castle, DE) and compared to the complex viscosity to check whether they were within acceptable error ranges. Figure 6.16 exhibits one example for a BPS-20K mixture containing 30 wt% PEG 600 at 200 °C. Similar data were observed for BPS-20K/PEG blends but were not shown for brevity. The two viscosity curves overlay within the shear rate range of 0.1-1 s^{-1} where data could be obtained in steady shear, implying that the Cox-Merz rule can be used for the BPS-20K/PEG blends.

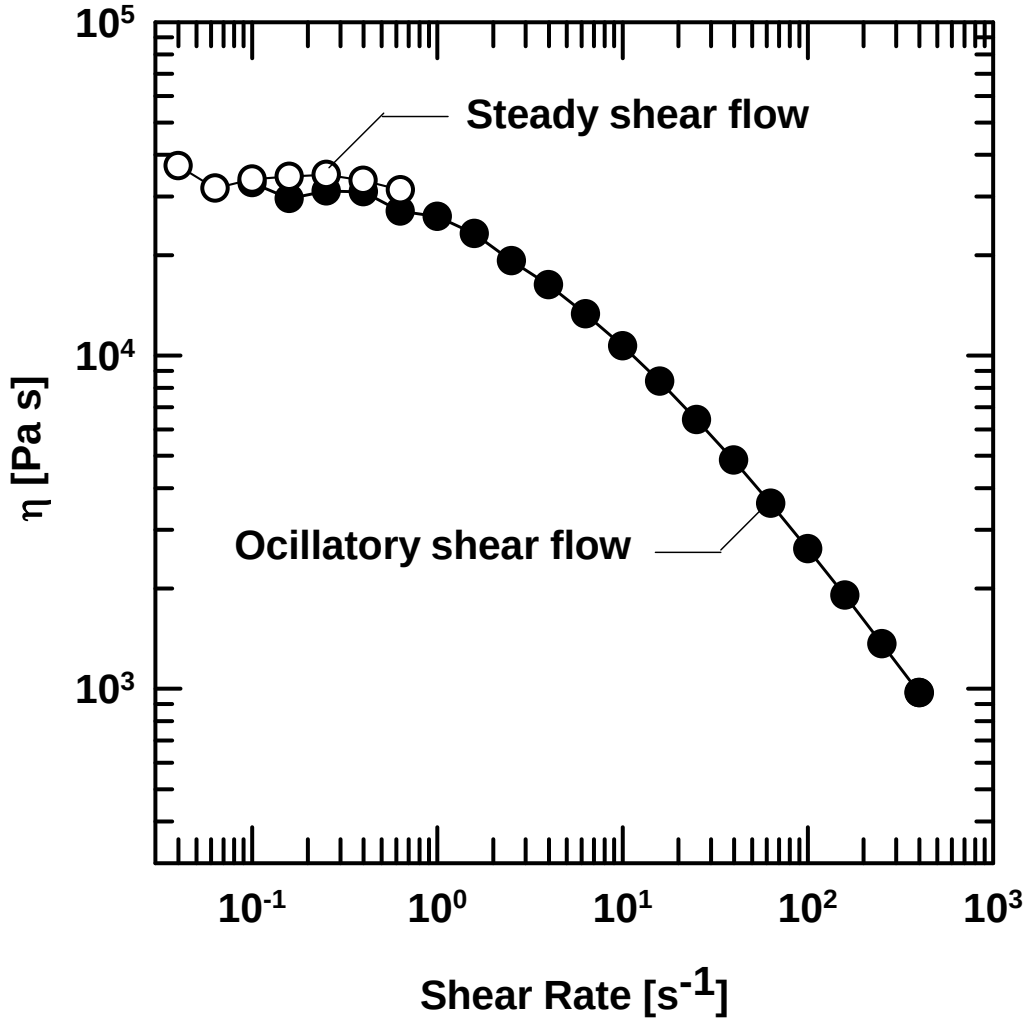

Figure 6.16 Cox-Merz rule verification of BPS/PEG blends at 200°C. BPS-20K/PEG 600 30 wt% blend were used. The unfilled symbols (○) are from a steady shear flow, while the filled symbols (●) are from an oscillatory shear flow.

6.5 REFERENCES

[1] D. R. Paul, “A study of spinnability in the wet-spinning of acrylic fibers,” *Journal of Applied Polymer Science,* vol. 12, pp. 2273-2298, 1968.

[2] F. Bueche, and S. W. Harding, “A new absolute molecular weight method for linear polymers,” *Journal of Polymer Science,* vol. 32, pp. 177-186, 1958.

[3] M. T. Ponting, A. Hiltner, and E. Baer, “Polymer nanostructures by forced assembly: process, structure, and properties,” *Macromolecular Symposia,* vol. 294, no. 1, pp. 19-32, 2010.

[4] M. Tirrell, "Rheology of polymeric liquids," *Rheology principles, measurements, and applications*, C. W. Macosko, ed., pp. 475-514: VCH Publishers, Inc., 1994.

[5] J. D. Ferry, "Viscoelastic properties of polymers," New York: Wiley, 1980.

[6] R. A. Register, and R. K. Prud'homme, "Melt rheology," *Ionomers*, M. R. Tant, K. A. Mauritz and G. L. Wilkes, eds., pp. 208-260: Blackie Academic & Professional, 1997.

[7] W. Xie, J. Cook, H. B. Park, B. D. Freeman, C. H. Lee, and J. E. McGrath, “Advances in membrane materials: desalination membranes based on directly copolymerized disulfonated poly(arylene ether sulfone) random copolymers,” *Water Science and Technology : a Journal of the International Association on Water Pollution Research,* vol. 61, no. 3, pp. 619-624, 2010.

[8] W. Xie, J. Cook, H. B. Park, B. D. Freeman, C. H. Lee, and J. E. McGrath, “Fundamental salt and water transport properties in directly copolymerized disulfonated poly(arylene ether sulfone) random copolymer,” *Polymer,* vol. 52, no. 9, pp. 2244-2254, 2011.

[9] F. Wang, M. Hickner, Y. S. Kim, T. A. Zawodzinski, and J. E. McGrath, “Direct polymerization of sulfonated poly(arylene ether sulfone) random(statistical) copolymer: candidates for next proton exchange membranes,” *Journal of Membrane Science,* vol. 197, no. 1-2, pp. 231-242, 2002.

[10] H. B. Park, B. D. Freeman, Z.-B. Zhang, M. Sankir, and J. E. McGrath, "Highly chlorine-tolerant polymers for desalination," *Angewandte Chemie International Edition* vol. 47, no. 32, pp. 6019-6024, 2008.

[11] H. J. Oh, B. D. Freeman, J. E. McGrath, C. H. Lee, and D. R. Paul, "Thermal analysis of disulfonated poly(arylene ether sulfone) plasticized with poly(ethylene glycol) for membrane formation," *Polymer* vol. 55, no. 1, pp. 235-247, 2014.

[12] B. Zdyrko, S. K. Varshney, and I. Luzinov, "Effect of molecular weight on synthesis and surface morphology of high-density poly(ethylene glycol) grafted layers," *Langmuir,* vol. 20, pp. 6727-6735, 2004.

[13] R. P. Wool, "Polymer interfaces: structure and strength," p. 102, Munich: Carl Hanser Verlag, 1995.

[14] K. Pielichowski, and K. Flejtuch, "Non-oxidative thermal degradation of poly(ethylene oxide): kinetic and thermoanalytical study," *Journal of Analytical and Applied Pyrolysis,* vol. 73, no. 1, pp. 131-138, 2005.

[15] S. Han, C. Kim, and D. Kwon, "Thermal/oxidative degradation and stabilization of polyethylene glycol," *Polymer,* vol. 38, no. 2, pp. 317-323, 1997.

[16] A. Eisenberg, and J. S. Kim, "Plasticization," *Introduction to ionomers*, pp. 244-256, Canada: John Wiley & Sons, Inc., 1998.

[17] L. A. Utracki, "Polymer alloys and blends: thermodynamics and rheology," Hanser Publishers, 1989.

[18] J. R. Wagner Jr., "Polymer blend for packaging applications " *Multilayer flexible packaging*, pp. 158-159: Technology & Engineering, 2009.

[19] A. J. Curtis, "Dielectric properties of polymeric systems," *Progress in dielectrics*, J. B. Birks and J. H. Schulman, eds., pp. 31-76, Hertfordshire, UK: Heywood & Company Ltd., 1960.

[20] C. H. Lee, D. VanHouten, O. Lane, J. E. McGrath, J. Hou, L. A. Madsen, J. Spano, S. Wi, J. Cook, W. Xie, H. J. Oh, G. M. Geise, and B. D. Freeman, "Disulfonated poly(arylene ether sulfone) random copolymer blends tuned for rapid water permeation via cation complexation with poly(ethylene glycol) oligomers," *Chemistry of Materials,* vol. 23, no. 4, pp. 1039-1049, 2011.

[21] F. Bueche, "Physical properties of polymer," pp. 88-107, New York: Interscience Publishers, 1962.

[22] T. P. Lodge, and P. C. Hiemenz, "Polymer chemistry," pp. 58-60, 481-485: CRC Press Taylor & Francis Group, 2007.

[23] R. A. Weiss, and H. Zhao, "Rheological behavior of oligomeric ionomers," *Journal of Rheology,* vol. 53, no. 1, pp. 191-213, 2009.

[24] R. A. Weiss, J. J. Fitzgerald, and D. Kim, "Viscoelastic behavior of lightly sulfonated polystyrene ionomers," *Macromolecules,* vol. 24, no. 5, pp. 1071-1076, 1991.

[25] G. Ordian, "Principles of polymerization," p. 82: John Wiley and Sons, 2004.

[26] S. Podzimek, "Light scattering," *Light scattering, size exclusion chromatography and asymmetric flow field flow fractionation: powerful tools for the characterization of polymers, proteins and nanoparticles*, S. Podzimek, ed., pp. 37-98: Wiley, 2011.

[27] E. Fouissac, M. Milas, and M. Rinauldo, "Shear-rate, concentration, molecular weight and temperature viscosity dependences of hyaluronate, a wormlike polyelectrolyte," *Macromolecules,* vol. 26, no. 25, pp. 6945-6951, 1993.

[28] K. B. Wiles, F. Wang, and J. E. McGrath, "Directly copolymerized poly(arylene sulfide sulfone) disulfonated copolymers for PEM-based fuel cell systems. I. Synthesis and characterization," *Journal of Polymer Science Part A: Polymer Chemistry,* vol. 43, no. 14, pp. 2964-2976, 2005.

[29] J. Roovers, P. M. Toporowski, and R. Ethier, “Viscoelastic properties of melts of 'RADEL R' polysulfone fractions,” *High Performance Polymers,* vol. 2, no. 3, pp. 165-179, 1990.

[30] J. S. Kim, and A. Eisenberg, "Ion aggregation and its effect on ionomer properties," *Ionomers: characterization, theory and applications*, S. Schlick, ed., pp. 7-34: CRC Press, Inc., 1996.

[31] T. A. Witten, “Associating polymers and shear thickening,” *Journal de Physique,* vol. 49, no. 6, pp. 1055-1063, 1988.

[32] S. Bhargava, and S. L. Cooper, “Effect of water on viscosity and shear-thickening behavior of telechelic ionomers in nonpolar solvents,” *Macromolecules,* vol. 31, no. 2, pp. 508–514, 1998.

[33] L. Li, G. Guo, and R. K. Prud'homme, “Shear thickening ionomers prepared by conjugate addition reaction,” *ACS Polymer. Preprints,* vol. 47, no. 1, pp. 271, 2006.

[34] C. Maus, R. Fayt, R. Jerome, and P. Teyssie, “Shear thickening of halato-telechelic polymers in apolar solvents,” *Polymer,* vol. 36, no. 10, pp. 2083–2088, 1995.

[35] D. G. Pieffer, R. D. Lundberg, and I. Duvdevani, “Synthesis and rheological properties of low charge density polyampholytes in nonaqueous solvents,” *Polymer,* vol. 27, no. 9, pp. 1453-1362, 1986.

[36] L. Saho, R. A. Weiss, and R. D. Lundberg, “Solution behavior of lightly sulfonated polystyrene ionomer/poly-benzyl-l-glutamate complexes,” *Journal of Polymer Science Part B: Polymer Physics,* vol. 33, no. 14, pp. 2083-2092, 1995.

[37] T. A. Witten, and M. H. Cohen, “Crosslinking in shear-thickening ionomers,” *Macromolecules,* vol. 18, no. 10, pp. 1915-1918, 1985.

[38] X. Lu, W. P. Steckle, and R. A. Weiss, “Ionic aggregation in a block copolymer ionomer,” *Macromolecules,* vol. 26, no. 22, pp. 5876-5884, 1993.

[39] J. H. Dealy, and K. F. Wissbrun, "Melt rheology and its role in plastic processing: theory and applications," pp. 74-80, 159-170: Van Nostrand Reinhold, 1990.

[40] F. Bueche, "Non-Newtonian viscosity of synthetic rubber and its solutions," *Journal of Applied Physics,* vol. 30, no. 7, pp. 1114, 1959.

[41] W. W. Graessley, "Viscosity of entangling polydisperse polymers," *The Journal of Chemical Physics,* vol. 47, no. 6, pp. 1942, 1967.

[42] D. R. Paul, J. E. S. Lawrence, and J. H. Troell, "Flow behavior of concentrated solutions of an SBS block copolymer," *Polymer Engineering & Science,* vol. 10, no. 2, pp. 70-78, 1970.

[43] W. P. Cox, and E. H. Merz, "Correlation of dynamic and steady flow viscosities," *Journal of Polymer Science,* vol. 28, no. 119, pp. 619-622, 1958.

[44] T. S. R. Al-Hadithi, H. A. Barnes, and K. Walters, "The relationship between the linear (oscillatory) and nonlinear (steady-state) flow properties of a series of polymer and colloidal systems," *Colloid and Polymer Science,* vol. 270, no. 1, pp. 40-46, 1992.

[45] S. T. Milner, "Relating the shear-thinning curve to the molecular weight distribution in linear polymer melts," *Journal of Rheology,* vol. 40, no. 2, pp. 303-315, 1996.

[46] H. M. Laun, "Prediction of elastic strains of polymer melts in shear and elongation," *Journal of Rheology,* vol. 30, no. 3, pp. 459-501, 1986.

[47] G. T. Offord, S. R. Armstrong, B. D. Freeman, E. Baer, A. Hiltner, J. S. Swinnea, and D. R. Paul, "Porosity enhancement in β nucleated isotactic polypropylene stretched films by thermal annealing," *Polymer,* vol. 54, no. 10, pp. 2577-2589, 2013.

[48] G. T. Offord, S. R. Armstrong, B. D. Freeman, E. Baer, A. Hiltner, and D. R. Paul, "Influence of processing strategies on porosity and permeability of β nucleated

isotactic polypropylene stretched films," *Polymer,* vol. 54, no. 11, pp. 2796-2807, 2013.

[49] M. T. Ponting, "Gradient multilayered films & confined crystallization of polymer nanolayers by forced assembly coextrusion," Ph.D. Dissertation, Department of Macromolecular Science & Engineering, Case Western Reserve University, 2010.

[50] P. E. Erhadrdt, J. M. O'Reilly, W. E. Richards, and M. W. Williams, "Viscoelastic behavior of styrene/n-butylmethacrylate/potassium metharcylate polymers," *Journal of Polymer Science Symposium,* vol. 45, no. 1, pp. 139-151, 1974.

Chapter 7: Preparation of Single Layer, BPS/PEG Thin Film Membranes by Extrusion

7.1 INTRODUCTION

Single layer, extruded membrane samples of BPS-20K/PEG blends were prepared using a twin screw micro-compounder (DSM Xplore, the Netherlands) with an attached film die (heated film die, width of 65 mm) and film take-up system. The objective was to produce defect-free, thin films of uniform thickness in the range of 30~50 μm, similar to those of solution cast BPS-20K films.

In this chapter, various factors that influence the film characteristics were identified and carefully adjusted to obtain reproducible films. These factors include using various BPS-20K molecular weights, PEG molecular weights, PEG concentrations, processing temperatures, residence time in extruder, film drawing speed and the winding torque of drums, etc. Conditions were identified to produce defect-free films of uniform thickness; these films were used for further studies.

7.2 RESULTS AND DISCUSSION

7.2.1 Identification of various factors influencing the film characteristics by extrusion

Since BPS-20K polymers have a high glass transition temperature (T_g) and viscosity, PEG was used to modify the T_g and viscosity of BPS-20K to enable melt processing [1, 2]. For a given composition of BPS-20K/PEG blends, different processing conditions (for example, processing temperature, film drawing speed, drawing torque, etc.) produce films of different quality. Therefore, it was of interest to identify the optimal processing conditions as well as blend compositions to prepare reproducible defect-free films. Table 7.1 summarizes the range of factors used in the film extrusion.

Table 7.1 Range of factors used in film extrusion

Factors	Range
[a] BPS-20K molecular weight, $\bar{M}_w$ [g/mol]	22,000 ~ 33,900
[b] PEG molecular weight, $\bar{M}_n$ [g/mol]	200 ~ 600
[c] PEG concentration [wt%]	20 ~ 30
[d] Processing temperature [°C]	220 ~ 250
[e] Residence time in extruder [min]	2 ~ 5
[f] Twin screw speed* [rpm]	100 ~ 200
[g] Polymer/plasticizer drying before extrusion	None
[h-1] Film drawing speed** [mm/min]	100 ~ 275
[h-2] Winding torque of roller*** [N·mm]	60 ~ 250

* Twin screw speed controls the shear rate. The speed range in the DSM micro-compounder is between 1 ~ 400 rpm

** The film drawing speed is between 100 ~ 5,000 mm/min with increments of 1 mm/min [3]

*** The torque of the winding drum is between 0 ~ 300 N·mm with increments of 1 N·mm [3]

7.2.1.1 BPS-20K molecular weight, $\bar{M}_w$

Generally, as the molecular weight ($\bar{M}_w$) of a polymer decreases, viscosity decreases (typically $\eta \propto \bar{M}_w^{3.4}$ for entangled polymers, when $\bar{M}_w > M_c$. However, as molecular weight decreases, the polymer mechanical properties are likely to be sacrificed. Because of this trade-off relationship, a proper molecular weight range of BPS-20K polymers that enables effective melt processing while maintaining mechanical strength must be identified.

Table 7.2 summarizes the characteristics of BPS-20K polymers used for thin film extrusion. The BPS-20K polymer with $\bar{M}_w$ = 31,300 g/mol has the minimum molecular weight that can maintain good mechanical properties of extruded membranes. It was

mainly used to prepare thin films of different compositions because of its good processability. Other BPS-20K polymers of higher molecular weights ($\bar{M}_w$ = 31,300 ~ 39,000 g/mol) were also used to prepare thin films; however, because of their higher viscosities, extruded films of some compositions could not be obtained.

As the molecular weight of BPS-20K decreases, the T_g decreases, indicating easier processability, but the salt permeability values are in a similar range. The typical molecular weights of BPS polymers used to prepare solution cast membranes for desalination in the previous literature [4-6] were higher than 40,000 g/mol to maintain good mechanical strength. The salt permeability values reported in Table 7.2 are similar to previously reported values [5-7].

Table 7.2 Characteristics of the BPS-20K polymers used for extrusion

Material	$\bar{M}_w$[a] [g/mol]	IV[a] [mL/g]	T_g[b]* [°C]	Salt Permeability[c]* [cm^2/s]
BPS-20K	31,300	41.1	256	0.054 ± 0.002
BPS-20K	33,200	46.7	257	0.097 ± 0.013
BPS-20K	39,000	47.0	273	0.076 ± 0.003

[a] Determined by SEC using NMP with 0.05 M LiBr at 50 °C. Note that specific refractive index increment (dn/dc) values were measured using an assumption of 100 % mass recovery. dn/dc values for BPS-20K polymers in this study are 0.17 [mL/g].

[b] Measured by DSC at 20 °C/min

[c] Measured by direct permeation cells in Chapter 3 (details in Chapter 3.5.4)

* Measurements were conducted using solution cast films. Transparent and uniform thickness films (30~40 μm) were formed by the solution casting method reported previously [5]

7.2.1.2 PEG concentration (wt%)

PEG concentrations in the range of 20 ~ 30 wt% were used for BPS-20K/PEG film extrusion. PEG concentration of 20 wt% in the blend is the minimum PEG concentration

to prepare a uniform thickness and defect-free membranes by extrusion. Also, PEG concentrations above 30 wt% in the blend produced sticky films of weak mechanical properties and were, thus, excluded from further studies.

7.2.1.3 PEG molecular weight, $\bar{M}_n$

At a fixed PEG concentration of 20 wt%, thin films prepared with PEG having a molecular weight ($\bar{M}_n$) of 600 g/mol exhibited many defects and voids as shown in Figure 7.2e, so this composition (BPS-20K/PEG 600 20 wt%) was excluded from further studies.

7.2.1.4 Processing temperatures

The processing temperature is one of the most important factors influencing the viscosity. The processing temperature was set to be at least 50~100 °C higher than the T_g of the blend, but always lower than the degradation temperature (T_d), so it was in the range of 220~250 °C. The T_gs of the BPS-20K/PEG blends and degradation temperature studies were reported previously [1] (details in Chapter 4 and Chapter 5).

7.2.1.5 Drying polymer/plasticizer before extrusion

During the extrusion process, any volatile components (for example, water) from the polymer (i.e., BPS-20K) and/or plasticizer (i.e., PEG) can evaporate at high temperatures and escape from the polymer melt to the atmosphere. However, if the viscosity of the polymer melt is too high so that the rate of loss of these volatile components is relatively slow, then these trapped gases remain in the extruded films as defects [8-10]. Note that no volatile components are generated by depolymerization and/or degradation of polymers, since the processing temperatures were carefully adjusted to avoid such issues, as previously reported [1, 2].

One method to verify if the bubbles in the extruded films are trapped gases is to increase the temperature until the films soften: for trapped gases, the bubble size will

increase [8]. If the bubbles collapse with increasing temperature, there are vacuum voids instead of trapped gases, since the bubble walls are pushed inward by the atmosphere pressure. In this study, the bubbles found in some of the extruded films are mostly trapped gases based on this test (see Figure 7.1).

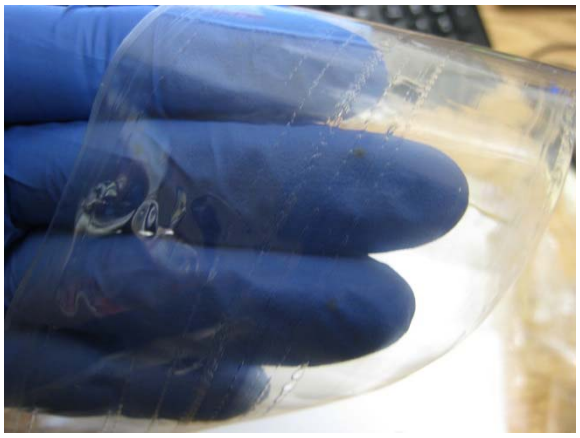

Figure 7.1 An example of a film with trapped gas defects.

To eliminate trapped gases in the films, the gas generation during extrusion should be reduced, and the escape of generated gases should be facilitated as follows:

$$[\text{Total amount of trapped gas in film}] = [\text{Gas generated }] - [\text{Gas escaped}]$$

First, any volatile components from the polymer and/or plasticizer should be removed by pre-drying before extrusion. Second, the processing temperature should be decreased to prevent evaporation of any volatile components. To facilitate the gas escaping from the melt, the viscosity of polymer melt should be lowered to promote the faster diffusion of small molecules, and thus the processing temperature should be increased and/or more plasticizers used [8-10]. Vacuum systems may be used to remove any trapped gases during extrusion in industrial processes [9, 11].

However, the strategies mentioned above are intervention with each other. For example, the processing temperature should be higher to facilitate gas escape; however, it should to be lower so as not to generate any gases during extrusion. Therefore, each strategy was tested individually to verify which step (i.e., gas generation vs. gas escaping) was more important to reduce the trapped gases in BPS-20K/PEG films. As a result, it was found that the pre-drying process of BPS-20K and/or PEG materials did not help limit trapped gases. Instead, the pre-drying process eliminates low molar mass of PEG, resulting in less plasticization and, thus, failure during extrusion. Therefore, the pre-drying process was not employed for extrusion in this study.

Instead of controlling gas generation, the viscosity of the polymer melt was lowered by increasing the processing temperature, and the residence time of the polymer melt in the extruder was prolonged to facilitate the escape of gas. This way, most of defects from the trapped gases were removed during the extrusion.

7.2.1.6 Film drawing speed and winding torque of take-up system

The film thickness was mainly determined by the film drawing speed and the torque of the winding drums. The specific values can be varied depending on the blend compositions and other processing conditions. However, both values were maintained as low as possible to eliminate any void formation due to rapid stretching. The film drawing speed was kept in the range of 100 ~ 270 mm/min, and the winding torque was maintained between 60 ~ 250 N·mm for all compositions.

7.2.2 Single layer, thin BPS-20K/PEG films by extrusion

Based on the preliminary tests as mentioned in the previous section, films with different compositions were prepared by extrusion and defect-free, uniform thickness films were selected for further studies. Table 7.3 summarizes the film composition and

processing temperatures of BPS-20K/PEG films. Figures 7.2, 7.3, and 7.4 show pictures of these extruded films for easier comparison.

For other BPS-20K polymers with higher $\bar{M}_w$ values (33,200 ~ 39,000 g/mol), the thickness control of extruded films is somewhat difficult because of their high viscosities. This is one of the reasons why BPS-20K polymer with lower molecular weight ($\bar{M}_w$ = 31,300 g/mol) was mainly used for further characterization, as mentioned earlier in this chapter.

Table 7.3 Film compositions and processing temperatures of BPS-20K/PEG films prepared by extrusion in Figures 7.2, 7.3, and 7.4

Polymer	$\bar{M}_w$[a] [g/mol]	PEG $\bar{M}_n$ [g/mol]	PEG wt%	Processing temperature [°C]
BPS-20K	31,300	PEG 200	20	230~240
BPS-20K	31,300	PEG 300	20	230~240
BPS-20K	31,300	PEG 400	20	230~240
BPS-20K	31,300	PEG 600	20	230~240
BPS-20K	31,300	PEG 200	30	225~235
BPS-20K	33,200	PEG 200	20	235~245
BPS-20K	39,000	PEG 200	20	235~245
BPS-20K	39,000	PEG 200	30	225~235

[a] BPS-20K molecular weight determined by SEC using NMP with 0.05 M LiBr at 50 °C

[a] BPS-20K ($\bar{M}_w$ = 31,300 g/mol) Solution cast film

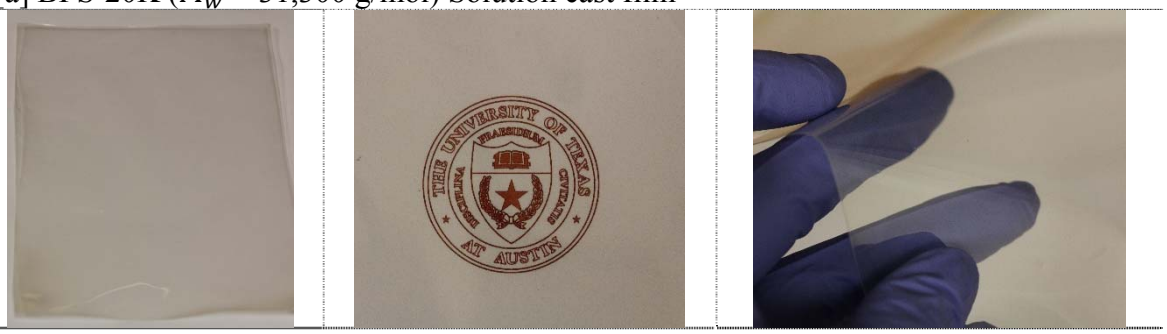

[b] BPS-20K ($\bar{M}_w$ = 31,300 g/mol)/PEG 200 20 wt% Extruded film

[c] BPS-20K ($\bar{M}_w$ = 31,300 g/mol)/PEG 300 20 wt% Extruded film

[d] BPS-20K ($\bar{M}_w$ = 31,300 g/mol)/PEG 400 20 wt% Extruded film

[e] BPS-20K ($\overline{M}_w$ = 31,300 g/mol)/PEG 600 20 wt% Extruded film

[f] BPS-20K ($\overline{M}_w$ = 31,300 g/mol)/PEG 200 30 wt% Extruded film

Figure 7.2 Pictures of [a] solution cast film and [b]~[f] extruded films of BPS-20K ($\overline{M}_w$ = 31,300 g/mol)/PEG blends. [a] The control film is a solution cast film of BPS-20K polymer. [b]~[f] Extruded films were prepared using different compositions (see Table 7.3).

[a] BPS-20K($\bar{M}_w$ = 33,200 g/mol) Solution cast film

[b] BPS-20K($\bar{M}_w$ = 33,200 g/mol)/PEG 200 20 wt% Extruded film

Figure 7.3 Pictures of [a] solution cast film and [b] extruded film of BPS-20K ($\bar{M}_w$ = 33,200 g/mol)/PEG 200 20 wt% blend. [a] The control film is a solution cast film of BPS-20K polymer. [b] Extruded film is BPS-20K/PEG 200 20 wt% blend (see Table 7.3).

[a] BPS-20K ($\bar{M}_w$ = 39,000 g/mol) Solution cast film

[b] BPS-20K ($\bar{M}_w$ = 39,000 g/mol)/PEG 200 20 wt% Extruded film

[c] BPS-20K($\bar{M}_w$ = 39,000 g/mol)/PEG 200 30 wt% Extruded film

Figure 7.4 Pictures of [a] solution cast films and [b, c] extruded films of BPS-20K ($\bar{M}_w$ = 39,000 g/mol)/PEG blends. [a] The control film is a solution cast film of BPS-20K polymer. [b]~[f] Extruded films are BPS-20K/PEG 200 20~30 wt% blends (see Table 7.3).

Whitening effect on stretching

Compared to the transparent BPS-20K solution cast films (Figures 7.2a, 7.3a, and 7.4a) of 30~40 μm thickness, some of the extruded films (see BPS-20K/PEG 200 20 wt% in Figures 7.2b, 7.3b, and 7.4b) are foggy and somewhat opaque when stretched to similar thicknesses. When no drawing force is applied to the film, the films of all compositions are transparent and very thick (~several hundred microns). However, as soon as a certain drawing force is applied to the film, the whitening effect occurs, and the films become rather opaque.

The opaqueness of thin film can result from several causes, such as crystallization (PEG materials are semicrystalline) of components, phase separation, surface roughness and stress-whitening involving void formation.

To confirm the origin of this whitening effect, DSC was run using the transparent and opaque parts of the same BPS-20K/PEG 200 20 wt% films as shown in Figure 7.5. As previously reported [1, 4], BPS and PEG materials are miscible, and thus a single T_g, regardless of optical characteristics, was observed in both thermograms. These T_g values are identical in each films (i.e., transparent and opaque films) and are in a similar range to the calculated T_g values using the Fox equation. No crystallization or melting peaks are found in the thermograms. Further studies as SAXS (small angle x-ray scattering) were conducted and crystallization was not found as well.

Also, surface roughness could be a factor to explain the opaqueness of these extruded films, because the opaqueness lessened when the films were immerged in water or mineral oil.

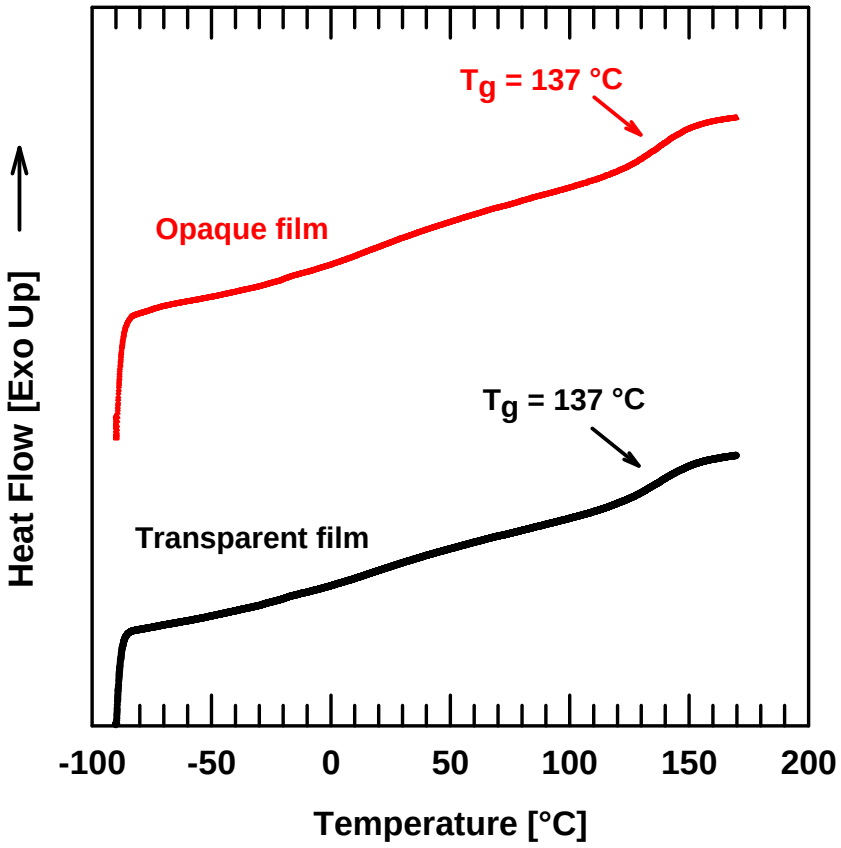

Figure 7.5 Final scan DSC thermograms of the opaque and transparent parts of BPS-20K/PEG 200 20 wt% extruded films. The thermograms have been displaced vertically for clarity. The arrows denote the location of the glass transition temperature (T_g). The samples were run using a heating rate of 20 °C/min under nitrogen purge. The T_g was recorded as the midpoint of the heat capacity step change.

Finally, stress whitening by void or craze formation could be an explanation for the opaqueness of the extruded films. When an axial drawing force is applied, some thermoplastics generate micro-voids in the films [12]. If the voids or clusters of voids have dimension, similar or larger than the wavelength of visible light (i.e., 380~750 nm), the films can appear white or opaque due to light scattering. Also, in some cases, this void formation does not significantly affect the mechanical properties of the films [12].

To explore whether this whitening effect was due to micro-voids formation during the stretching, the density and gas (N_2 and He) permeability values of BPS-20K/PEG 200 20 wt% films were measured and summarized in Table 7.4. The density was measured using mineral oil, as is often used for porous materials. To aid the density measurements, the gas permeation tests (constant-volume variable-pressure method) were conducted to check for the presence of any porosity [10]. Nitrogen (N_2) and helium (He) were selected since they represent a low permeability gas (i.e., large kinetic diameter, 3.64 Å), and He represents a high permeability gas (i.e., small kinetic diameter, 2.6 Å), respectively [13]. The measurements were performed at five different pressures (2 atm, 6 atm, 10 atm, 14 atm, and 18 atm) at 35 °C as shown in Figure 7.6, and the permeability values at 10 atm at 35 °C are reported in Table 7.4. The permeability values calculated from individual gas permeation tests at different pressures (2~18 atm) correspond to each other (see Figure 7.6). If there were any micro-voids having dimensions of 380~750 nm as mentioned above, the gas permeability could not be measured consistently.

When the PEG was completely extracted from the extruded films by soaking in deionized (DI) water at 75 °C for 2 days (^{1}H NMR analysis was conducted to confirm the remaining PEG wt% in the film, and the remaining PEG wt% was less than 0.5 wt%) (details in Chapter 8), the extruded/extracted film has similar gas permeability values as that of dense, solution cast films, and thus, selectivity values, P_{He}/P_{N_2}, are in a similar range as that of control BPS-20K films. Moreover, their density values are within similar ranges, indicating no presence of micro-voids (see Table 7.4).

Also, the molecular weight range of BPS-20K polymers in this study does not affect the density and gas permeability values as shown in Table 7.4. As the molecular weight of BPS-20K polymers increases from 31,300 g/mol to 39,000 g/mol, the density and gas permeability values are still in similar ranges.

Therefore, the whitening effect is not likely due to micro-voids, crystallization or phase separation. In this study, attempts were made to reduce the whitening effect of the extruded films by adjusting processing parameters such as increasing the processing temperatures at a fixed composition (i.e., PEG 20 wt%), etc. However, even at the highest processing temperature below the thermal degradation limits as reported previously [1], the whitening effect was unavoidable.

Further investigation is needed to identify the root cause of the whitening effect.

Table 7.4 Density and gas (N_2 and He) permeability of BPS-20K films prepared by solution casting method and extrusion. The control film is the solution cast, BPS-20K film. The BPS-20K/PEG 200 20 wt% films were prepared by extrusion: the first one is extruded film itself and another is the one in which PEG 200 was completely extracted by soaking in the deionized (DI) water at 75 °C for 2 days, and dried in the vacuum oven for 24 hours [c]. The data from polysulfone membranes are collected from literature [14-18] for comparison

Polymer	BPS-20K $\bar{M}_w$ [g/mol]	PEG M_n [g/mol]	PEG wt%	Type	Density [a] [g/cm3]	P_{He} [b] [Barrer]	P_{N_2} [b] [Barrer]	P_{He}/P_{N_2}
BPS-20K	31,300	-	-	Solution cast	1.376 ± 0.011	7.0 ± 0.5	0.087 ± 0.007	80
BPS-20K	39,000	-	-	Solution cast	1.353 ± 0.014	7.5 ± 0.2	0.079 ± 0.002	95
BPS-20K	31,300	PEG 200	20	Extrusion, PEG was extracted [c]	1.353 ± 0.003	7.0 ± 0.7	0.073 ± 0.007	96
Bisphenol A polysulfone		-	-	Solution cast	1.215 ± 0.017*	12.5 ± 0.5*	0.21 ± 0.01*	60
Radel A polysulfone		-	-	Solution cast	1.365**	9.7**	0.13**	75
Bisphenol A polysulfone		-	-	Extrusion	-	-	0.18***	-

[a] Measured using a Mettler Toledo density determination kit (Part# 238490, Switzerland) with mineral oil (d = 0.872 g/cm^3 at 23 °C, Cat# M8691, Sigma-Aldrich, St. Louis, MO, USA) at ambient temperature (22~23°C)

[b] Measured using a constant-volume variable-pressure method [10]. P_{He} and P_{N_2} values were determined at 35 °C and 10 atm. Permeability reported in Barrer, where 1 Barrer = $\frac{10^{-10} cc(STP) \cdot cm}{cm^2 \cdot s \cdot cmHg}$

* Data from Ref. [14-16]

** Data from Ref. [17]. P_{He} and P_{N_2} values were determined at 35 °C and 5 atm

*** Data from Ref. [18]. P_{N_2} values was read from Figure 6 at 35 °C and 10 atm in Ref. [18]

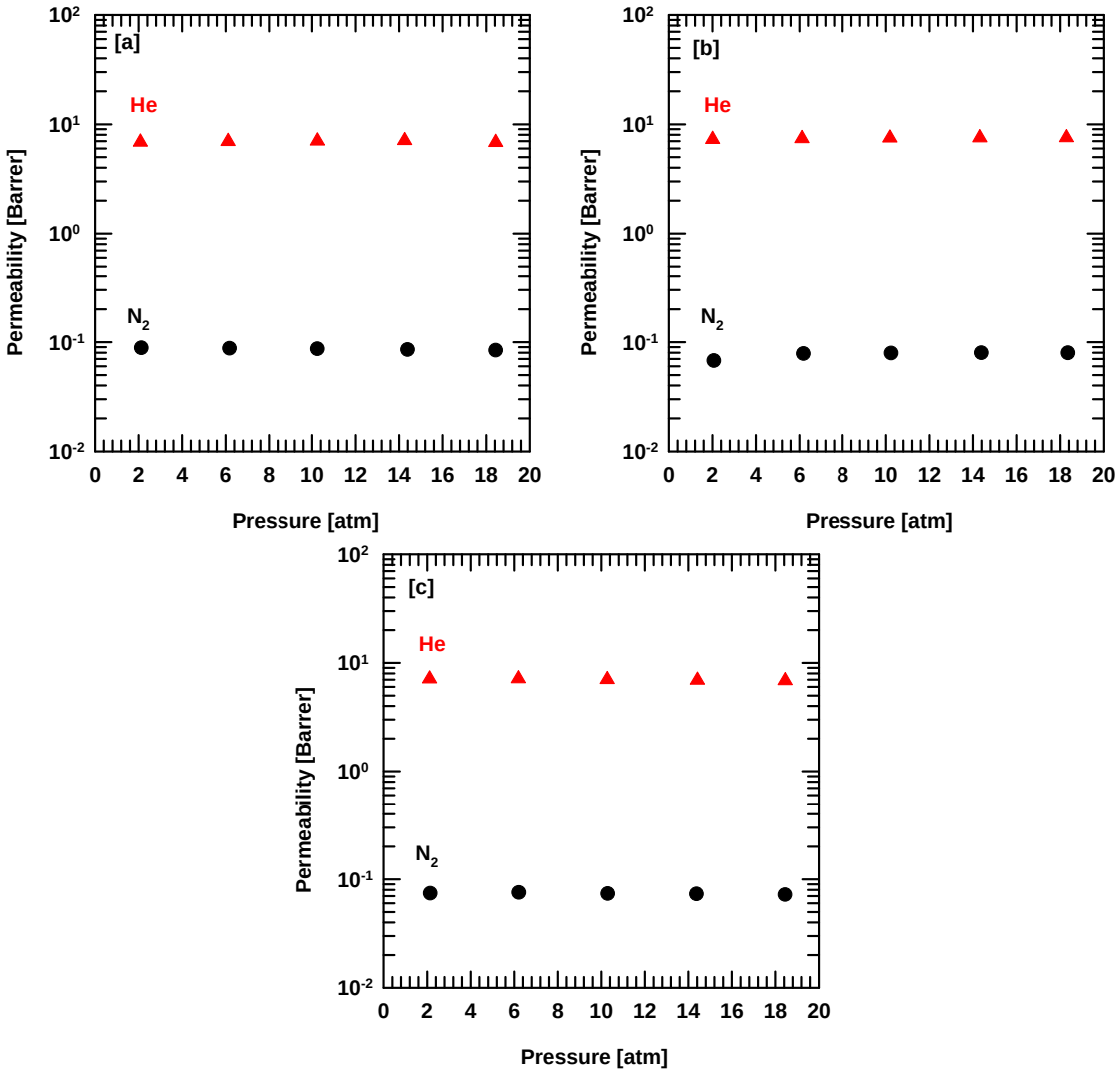

Figure 7.6 Nitrogen (N_2) and Helium (He) gas permeability [Barrer] as a function of pressure at 35 °C. [a] BPS-20K ($\bar{M}_w$ = 31,300 g/mol) solution cast film.[b] BPS-20K ($\bar{M}_w$ = 39,000 g/mol) solution cast film. [c] BPS-20K ($\bar{M}_w$ = 31,300 g/mol)/PEG 200 20 wt% extruded, PEG extracted film. PEG 200 20 wt% was completely extracted by soaking in the deionized (DI) water at 75 °C for 2 days, and dried in the vacuum oven for 24 hours. The remaining PEG wt% (< 0.5 wt%) was confirmed by ^{1}H NMR analysis. Data courtesy of Jae Sung Park.

7.3 CONCLUSIONS

In this chapter, various factors that influence film characteristics were identified and carefully adjusted to obtain reproducible films. These factors include the BPS-20K molecular weight, PEG molecular weight, PEG concentration, processing temperature, residence time in extruder, film drawing speed and winding torque of drums, etc. As a result, a uniform thickness and defect-free thin films were prepared and were used for further studies.

Some BPS-20K/PEG 20 wt% extruded films are foggy and rather opaque, and studies to identify the reason for this opaqueness were conducted. However, no evidence of crystallization, phase separation, or micro-voids was found, and further investigations are required for clear identification. Attempts to reduce this whitening effect for some extruded films were made by adjusting the processing conditions. However, even at the highest processing temperature below the thermal degradation limits, the whitening effect was unavoidable.

7.4 REFERENCES

[1] H. J. Oh, B. D. Freeman, J. E. McGrath, C. H. Lee, and D. R. Paul, "Thermal analysis of disulfonated poly(arylene ether sulfone) plasticized with poly(ethylene glycol) for membrane formation," *Polymer* vol. 55, no. 1, pp. 235-247, 2014.

[2] H. J. Oh, B. D. Freeman, J. E. McGrath, C. J. Ellison, S. Mecham, K.-S. Lee, and D. R. Paul, "Rheological studies of disulfonated poly(arylene ether sulfone) plasticized with poly(ethylene glycol) for membrane formation," *Polymer,* vol. 55, no. 6, pp. 1574-1582, 2014.

[3] http://www.xplore-together.com/products/micro-cast-film/fl35.

[4] C. H. Lee, D. VanHouten, O. Lane, J. E. McGrath, J. Hou, L. A. Madsen, J. Spano, S. Wi, J. Cook, W. Xie, H. J. Oh, G. M. Geise, and B. D. Freeman, "Disulfonated poly(arylene ether sulfone) random copolymer blends tuned for rapid water permeation via cation complexation with poly(ethylene glycol) oligomers," *Chemistry of Materials,* vol. 23, no. 4, pp. 1039-1049, 2011.

[5] W. Xie, J. Cook, H. B. Park, B. D. Freeman, C. H. Lee, and J. E. McGrath, "Fundamental salt and water transport properties in directly copolymerized disulfonated poly(arylene ether sulfone) random copolymer," *Polymer,* vol. 52, no. 9, pp. 2244-2254, 2011.

[6] W. Xie, H. B. Park, J. Cook, C. H. Lee, G. Byun, B. D. Freeman, and J. E. McGrath, "Advances in membrane materials: desalination membranes based on directly copolymerized disulfonated poly(arylene ether sulfone) random copolymers," *Water Sci Technol,* vol. 61, no. 3, pp. 619-24, 2010.

[7] H. B. Park, B. D. Freeman, Z.-B. Zhang, M. Sankir, and J. E. McGrath, "Highly chlorine-tolerant polymers for desalination," *Angewandte Chemie International Edition* vol. 47, no. 32, pp. 6019-6024, 2008.

[8] J. Bozzelli, "Eliminate bubbles, voids, sinks & blisters " *Plastics Industry Articles* http://articles.ides.com/processing/jb_sinks_bubbles.asp.

[9] J. G. Dorobny, *Handbook of thermoplastic elstomers*: Plastics Design Library, 2007.

[10] H. Czichos, T. Saito, and H. Smith, *Springer handbook of materials measurement methods*, p.^pp. 379-381: Springer.

[11] http://articles.ides.com/processing/jb_sinks_bubbles.asp.

[12] American Society of Metals, *Characterization and failure analysis of plastics*, p.^pp. 404-405: ASM International.

[13] S. Matteucci, Y. P. Yampolskii, and B. D. Freeman, "Transport of gases andvapors in glassy and rubbery polymers," *Materials science of membranes for gas and vapor separation*, Y. P. Yampolskii, I. Piannau and B. D. Freeman, eds., pp. 1-47: Wiley, 2006.

[14] J. S. Mchattie, W. J. Koros, and D. R. Paul, "Gas transport properties of polysulphones: 1. Role of symmetry of methyl group placement on bisphenol rings," *Polymer,* vol. 32, no. 5, pp. 840-850, 1991.

[15] Z. P. Smith, R. R. Tiwari, M. E. Dose, K. L. Gleason, T. M. Murphy, D. F. Sanders, G. Gunawan, L. M. Robeson, D. R. Paul, and B. D. Freeman, "Influence of diffusivity and sorption on helium and hydrogen separations in hydrocarbon, silicon, and fluorocarbon-based polymers," *Macromolecules,* vol. 47, no. 9, pp. 3170-3184, 2014.

[16] Z. P. Smith, R. R. Tiwari, T. M. Murphy, D. F. Sanders, K. L. Gleason, D. R. Paul, and B. D. Freeman, "Hydrogen sorption in polymers for membrane applications," *Polymer,* vol. 54, no. 12, pp. 3026-3037, 2013.

[17] K. Ghosal, R. T. Chern, and B. D. Freeman, "Gas permeability of radel a polysulfone," *Journal of Polymer Science Part B: Polymer Physics,* vol. 31, no. 7, pp. 891-893, 1993.

[18] A. J. Erb, and D. R. Paul, "Gas sorption and transport in polysulfone," *Journal of Membrane Science,* vol. 8, pp. 11-22, 1981.

Chapter 8: Kinetics of Poly(ethylene glycol) Extraction using Water from Plasticized Disulfonated Poly(arylene ether sulfone) Membranes Prepared by Melt Processing

8.1 INTRODUCTION

PEG must be extracted from extruded BPS-20K/PEG films before their use as a membrane [1]. Since PEG is highly water soluble, it can, in principle, be extracted in water after melt extrusion [2, 3]. For this reason, examination of the factors influencing diffusion of PEG from these films is essential to optimize this route to membrane preparation. The rate of PEG extraction is expected to be affected by molecular weight ($\bar{M}_n$) and concentration (wt%) of PEG in the extruded BPS-20K/PEG films, as well as the temperature. Such extraction studies are described here, and Fickian models were used to analyze the kinetics of PEG extraction.

8.2 MATERIALS AND EXPERIMENTAL

8.2.1 Materials

Polymer: 20 mol% disulfonated poly(arylene ether sulfone) (BPS-20K)

The 20 mol% disulfonated poly(arylene ether sulfone) random copolymer, BPS-20K, was used in this study (details in Chapter 3), and its properties are shown in Table 8.1.

Table 8.1 Characteristics of the polymer of this study

Material	$\bar{M}_w$[a] [g/mol]	IV[a] [ml/g]	T_g[b]* [°C]	Density[c]* [g/cm^3]
BPS-20K	31,300	41.1	256	1.376 ± 0.011

[a] Determined by SEC using NMP with 0.05 M LiBr at 50 °C. Specific refractive index increment (dn/dc) values were measured using an assumption of 100 % mass recovery. dn/dc values for BPS-20K polymers in this study are 0.17 [ml/g].

[b] Measured by DSC at 20 °C/min

[c] Measured using a Mettler Toledo density determination kit (Part# 238490, Switzerland) with *n*-heptane (Cat# 32287, Sigma-Aldrich, St. Louis, MO) at ambient temperature (20~22°C)
* Measurements were conducted using solution cast films. Transparent and uniform thickness films (30~40 μm) were formed by the solution casting method reported previously [4]

Plasticizer: Poly(ethylene glycol) 200 ~ 400 g/mol

Poly (ethylene glycol) (PEG) materials with molecular weight ($\bar{M}_n$) 200 g/mol, 300 g/mol and 400 g/mol were used as plasticizers (details in Chapter 3.2). The PEG concentration (wt%) in the extruded films was varied between 20 wt% and 30 wt% (see Table 8.2).

8.2.2 Experimental

Single layer, BPS-20K/PEG thin film preparation by extrusion

Single layer, thin films of BPS-20K/PEG were prepared using a 5 ml twin screw micro-compounder (DSM Xplore, the Netherlands) with an associated film die (heated film die, width of 65 mm, DSM Xplore, the Netherlands) and take-up system [5, 6] under an extra dry nitrogen atmosphere (99.9 %, Matheson Tri-Gas, Austin, TX) (details in Chapter 3.3).

A PEG concentration of 20 wt% is the minimum amount that is needed to prepare a uniform thickness and defect free membrane by extrusion. At this fixed PEG concentration of 20 wt%, extruded films prepared with PEG molecular weight ($\bar{M}_n$) of 600 g/mol exhibited many defects and voids, and, consequently, this composition (BPS-20K/PEG 600 20 wt%) was excluded for further study.

The sample composition and average film thicknesses for this study are summarized in Table 8.2. For each composition, 50 ~ 100 samples (typical dimension of a sample was 1 cm × 2 cm rectangular plane sheet with a uniform thickness) were prepared.

The thickness of each sample was measured in 8-13 positions and was averaged. For 20 wt% PEG containing samples (i.e., BPS-20K/PEG 20 wt%), the average thickness is in the range of 35 ~ 40 μm, and the variability in thickness in a single sample was of the order of 3.5 ~ 6 % with PEG molecular weight of 200 g/mol, 300 g/mol and 400 g/mol. This is comparable to the thickness variability (6 ~ 10 %) of solution cast membranes and commercial membranes reported previously [7, 8]. For 30 wt% PEG containing samples (i.e., BPS-20K/PEG 30 wt%), the average thickness was lower (~20 μm), although the film thickness was targeted to be in the range of 35 ~ 40 μm, and the variability of thickness was somewhat higher.

Table 8.2 Sample composition and film thickness of extruded BPS-20K/PEG films used in this study

Polymer	PEG M_n [g/mol]	PEG wt%	Film thickness [μm]
BPS-20K	PEG 200	20	35.7 ± 3.0
BPS-20K	PEG 300	20	35.1 ± 3.2
BPS-20K	PEG 400	20	38.9 ± 3.9
BPS-20K	PEG 200	30	21.7 ± 5.5

Extraction of PEG from extruded films

The kinetic desorption of PEG materials from the extruded BPS-20K/PEG films was conducted in ultra-pure deionized (DI) water (5-10 ppb TOC [9], from a Millipore Milli-Q system, Darmstadt, Germany) at different temperatures. Samples of known dimensions were soaked in DI water at three different temperatures (23 °C, 50 °C and 75 °C) for different times. The DI water was equilibrated in an iso-temp digital-control water bath (Model# 2340, Fisher Scientific, Waltham, MA) for at least 1 ~ 2 hours before experiments. The amount of water contacting the sample was much larger (500 ml per 20

~ 25 mg sample) than the extracted amount of PEG in the water, and the water was changed every 1-3 hours, so that the water activity was close to 1 throughout the experiments.

After soaking the sample in DI water for a known time (2 seconds ~ a week), the excess water on the sample surface was carefully removed using tissue paper, and the sample was dried at 25 °C in the vacuum overnight for ^{1}H NMR analysis. ^{1}H NMR data were recorded under the conditions reported in Chapter 3 (details in Chapter 3.7.2). The average PEG concentration (wt%) remaining in the sample at time t, $\langle C_t \rangle$, was calculated using the methods reported in Chapter 5 (details in Chapter 5.2.3.1.2).

8.3 RESULTS AND DISCUSSION

8.3.1 Fickian models

The extraction of PEG from the extruded films is somewhat different from the simple diffusion involved in the desorption of small molecules from a polymer films. First, while PEG molecules are released from the membrane into the water, water molecules are absorbed by the membrane. Thus, any diffusion coefficient obtained from analysis of the extraction process is an apparent value that reflects both exchange processes. Second, although the water contacting the samples was changed frequently, the slight buildup of PEG in the aqueous phase can, in principle, affect the results. However, a Fickian model provides a convenient framework for representing the extraction process.

Apparent diffusion coefficients for the extraction process were obtained by fitting the data to a simple, non-steady state, Fickian model [10]. Consider the PEG concentration (C) in a plane sheet membrane as shown in Figure 8.1: (1) X = 0 means the center of the membrane and L is the half thickness of the membrane, (2) at the region $-L < X < +L$, the initial concentration of PEG in the membrane (at t = 0) is uniform and is denoted as C_0,

and (3) the surface concentration of PEG in the membrane faces (at X = -L, +L) is assumed to be zero, i.e., $C_1 = 0$.

The PEG concentration, C, is a function of time, t, and location, X, i.e., C(t, X). The PEG concentration profile in the film changes with time as suggested in Figure 8.1. However, experimentally we can measure the average PEG concentration, $\langle C_t \rangle$, in the film as a function of time, t, by ^{1}H NMR analysis.

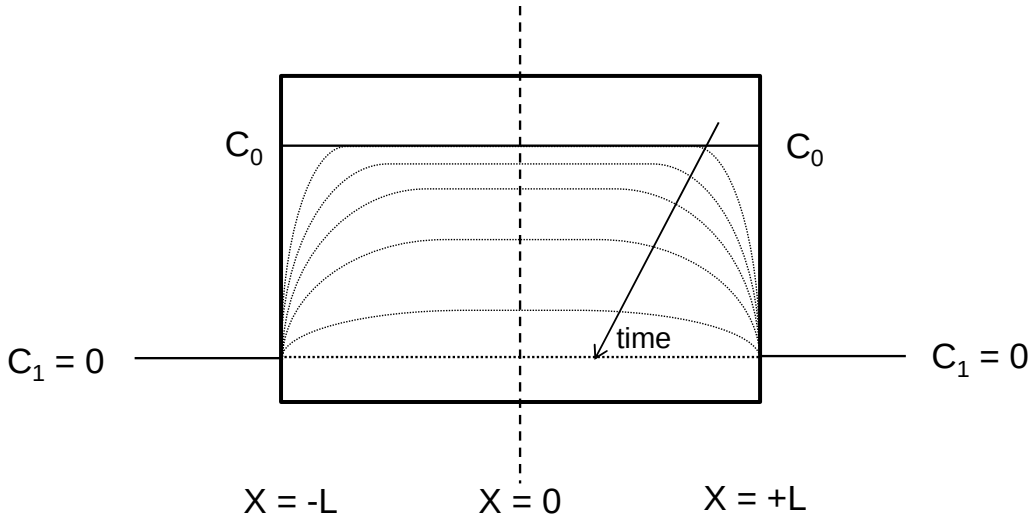

Figure 8.1 Schematic description of PEG concentration (C) in plane sheet membrane before extraction or at t = 0. X = 0 corresponds to the center of the membrane and L is the half of the membrane thickness. C_0 is the initial concentration of PEG in the membrane at t = 0. The surface concentration of PEG in the membrane (at X = +L, -L), C_1, is kept to be identical to the concentration of PEG in the water, i.e., $C_1 = 0$ [10]. Dashed lines briefly indicate the PEG concentration profile over time as the PEG extraction proceeds.

Thus, we will use the following solution of Fick's second law describing one-dimensional diffusion in plane sheet geometry [10]:

$$\frac{M_t}{M_\infty} = 1 - \sum_{n=0}^{\infty} \frac{8}{(2n+1)^2 \pi^2} \exp[-D(2n+1)^2 \pi^2 \frac{t}{L^2}] \qquad (8.1)$$

when M_t is the total amount of PEG extracted from the film at time, t, and M_∞ is the total amount of PEG extracted at infinite time and M_t/M_∞ can be related to $<C_t>$ and C_0, as follows:

$$\frac{M_t}{M_\infty} = 1 - \frac{<C_t>}{C_0} \tag{8.2}$$

At short times, when M_t/M_∞ is less than 0.6, the solution of Fick's law can be approximated [10, 11]:

$$\frac{M_t}{M_\infty} = \left(\frac{16D}{\pi L^2}\right)^{1/2} \cdot t^{1/2} \tag{8.3}$$

Therefore, the diffusion coefficient can be calculated the initial slope of M_t/M_∞ versus $t^{\frac{1}{2}}$ (i.e., early time approximation) as follows:

$$D = \frac{\pi L^2}{16}\left[\frac{d(M_t/M_\infty)}{dt^{1/2}}\right]^2 \tag{8.4}$$

8.3.2 Early time analysis of the data

The kinetics of PEG extraction from the extruded BPS-20K/PEG thin films at three different temperatures are illustrated in Figures 8.2, 8.3, 8.4, and 8.5 by plotting M_t/M_∞ versus $t^{\frac{1}{2}}$. The inset graphs show a magnified view of the first stage of desorption process (i.e., $M_t/M_\infty < 0.6$) for easier viewing, and R^2 values of each inset graph are presented in Table 8.3. The goodness-of-fit for linear regression, or R^2 values, are close to 1.0, indicating that all data points essentially conform to a straight line with little scatter [12]. The diffusion coefficients calculated in this way are summarized in Table 8.3.

As expected, the results in Figures 8.2, 8.3, 8.4, and 8.5 indicate that PEG extraction kinetics are faster at higher temperatures for every composition. For example, in the case of PEG 200 desorption from BPS-20K/PEG 200 20 wt% films (see Figure 8.2), the time required to reach $M_t/M_\infty = 0.6$ is 30 minutes at 25 °C, whereas it is only 100 seconds at 50 °C and 10 seconds at 75 °C. Interestingly, for PEG 200 extraction from BPS-20K/PEG

200 30 wt% films (see Figure 8.5), M_t/M_∞ values reach 0.8 within 5 seconds, and the data where $M_t/M_\infty < 0.6$ could not be obtained because of very fast extraction.

At a fixed temperature, the PEG desorption kinetics are more rapid for lower PEG molecular weights ($\bar{M}_n$) since shorter chain PEG molecules (i.e., smaller penetrants) have higher diffusion coefficients. Moreover, at a fixed PEG molecular weight of 200 g/mol, the PEG desorption kinetics are more rapid with increasing PEG concentration (wt%) between 20 wt% and 30 wt%. The samples containing more PEG wt% have a much lower glass transition temperature (T_g) (for example, the T_g of 20 wt% PEG containing samples is around 120-130°C, and the T_g of 30 wt% PEG containing samples is around 75-80 °C) as reported previously [6]. A polymer matrix with lower T_g is expected to display higher chain mobility, and thus it is likely to have a higher diffusion coefficient.

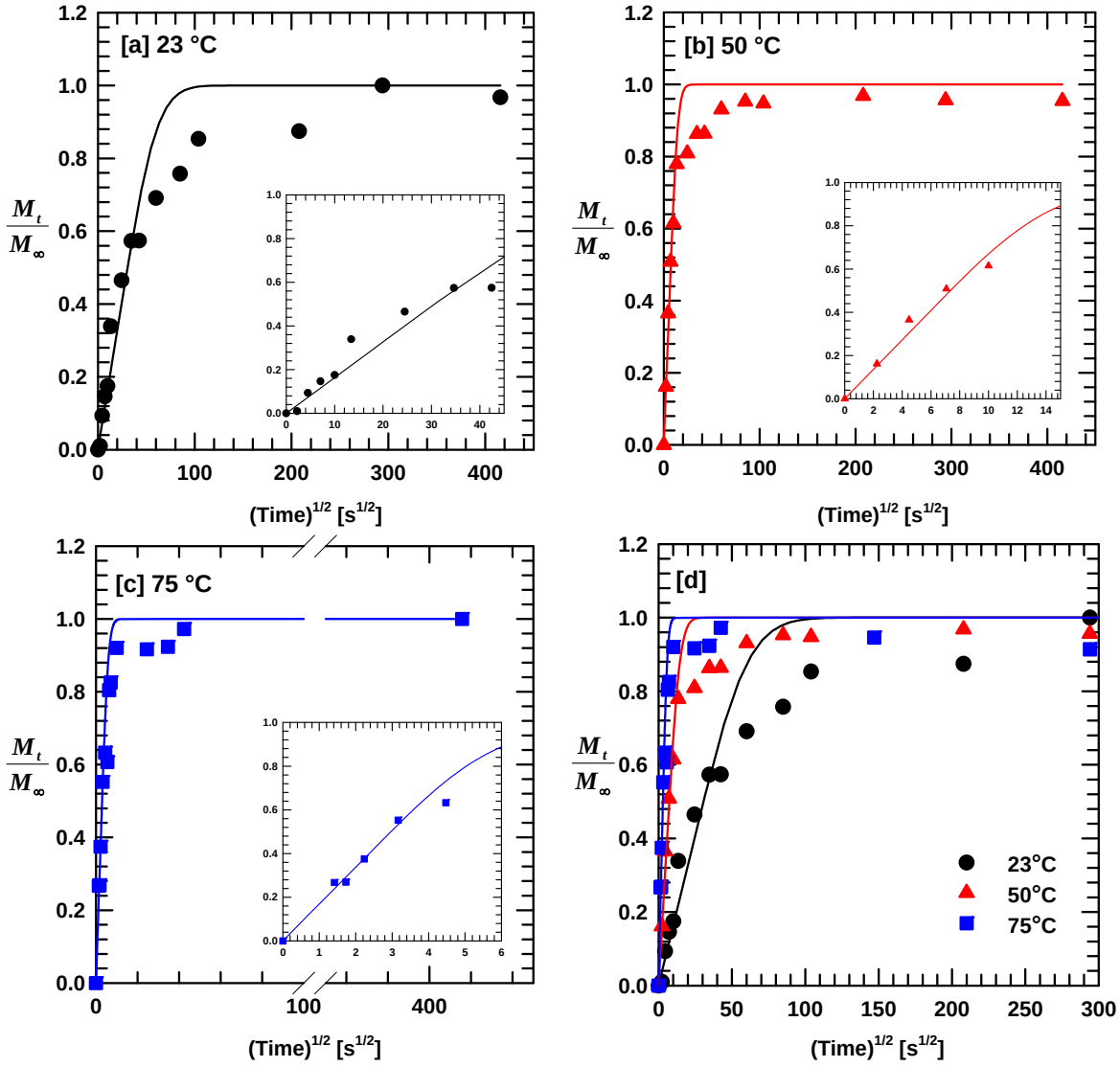

Figure 8.2 Extraction of PEG 200 from extruded BPS-20K/PEG 200 20 wt% films as a function of time at different temperatures: [a] 23 °C (●), [b] 50°C (▲) and [c] 75 °C (■), using the early time approximation Fickian model. [d] shows all extraction data of different temperatures for easier comparison. The inset graphs exhibit a magnified view near the origin ($M_t/M_\infty < 0.6$) where M_t/M_∞ is plotted versus $t^{1/2}$. R^2 values of each inset graph are presented in Table 8.3.

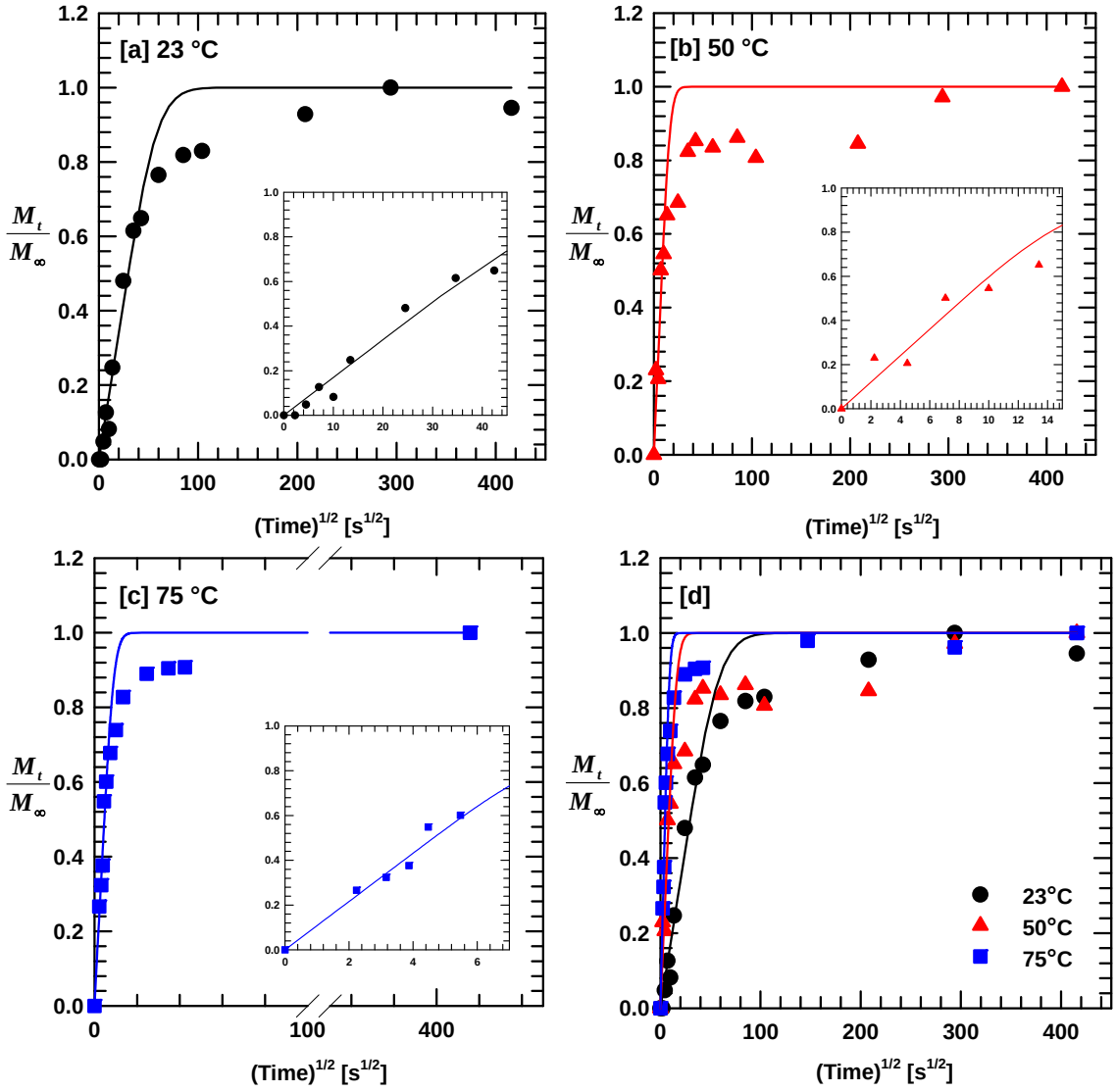

Figure 8.3 Extraction of PEG 300 from extruded BPS-20K/PEG 300 20 wt% films as a function of time at different temperatures: [a] 23 °C (●), [b] 50°C (▲) and [c] 75 °C (■), using the early time approximation Fickian model. [d] shows all extraction data of different temperatures for easier comparison. The inset graphs exhibit a magnified view near the origin ($M_t/M_\infty < 0.6$) where M_t/M_∞ is plotted versus $t^{1/2}$. R^2 values of each inset graph are presented in Table 8.3.

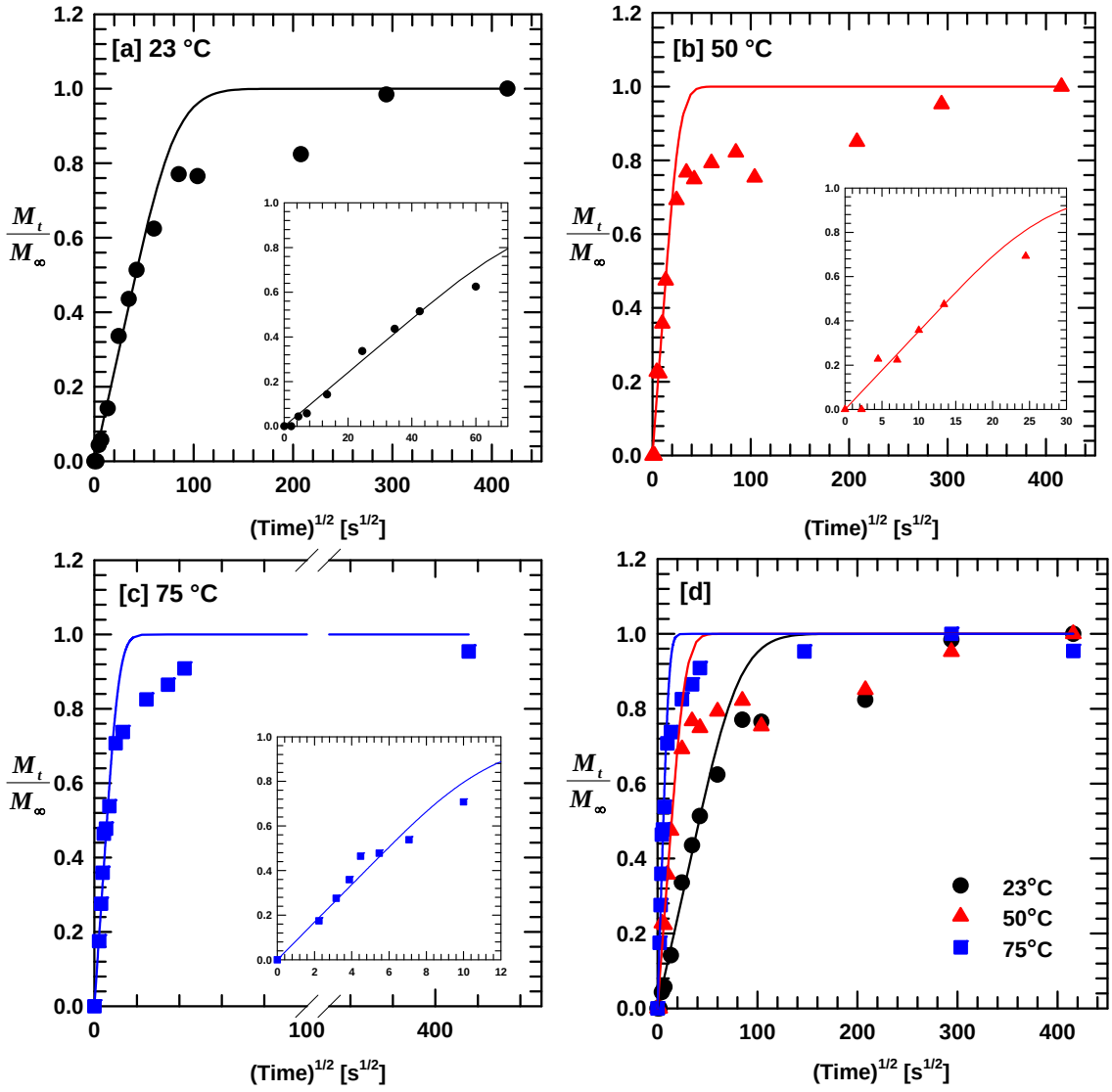

Figure 8.4 Extraction of PEG 400 from extruded BPS-20K/PEG 400 20 wt% films as a function of time at different temperatures: [a] 23 °C (●), [b] 50°C (▲) and [c] 75 °C (■), using the early time approximation Fickian model. [d] shows all extraction data of different temperatures for easier comparison. The inset graphs exhibit a magnified view near the origin ($M_t/M_\infty < 0.6$) where M_t/M_∞ is plotted versus $t^{1/2}$. R^2 values of each inset graph are presented in Table 8.3.

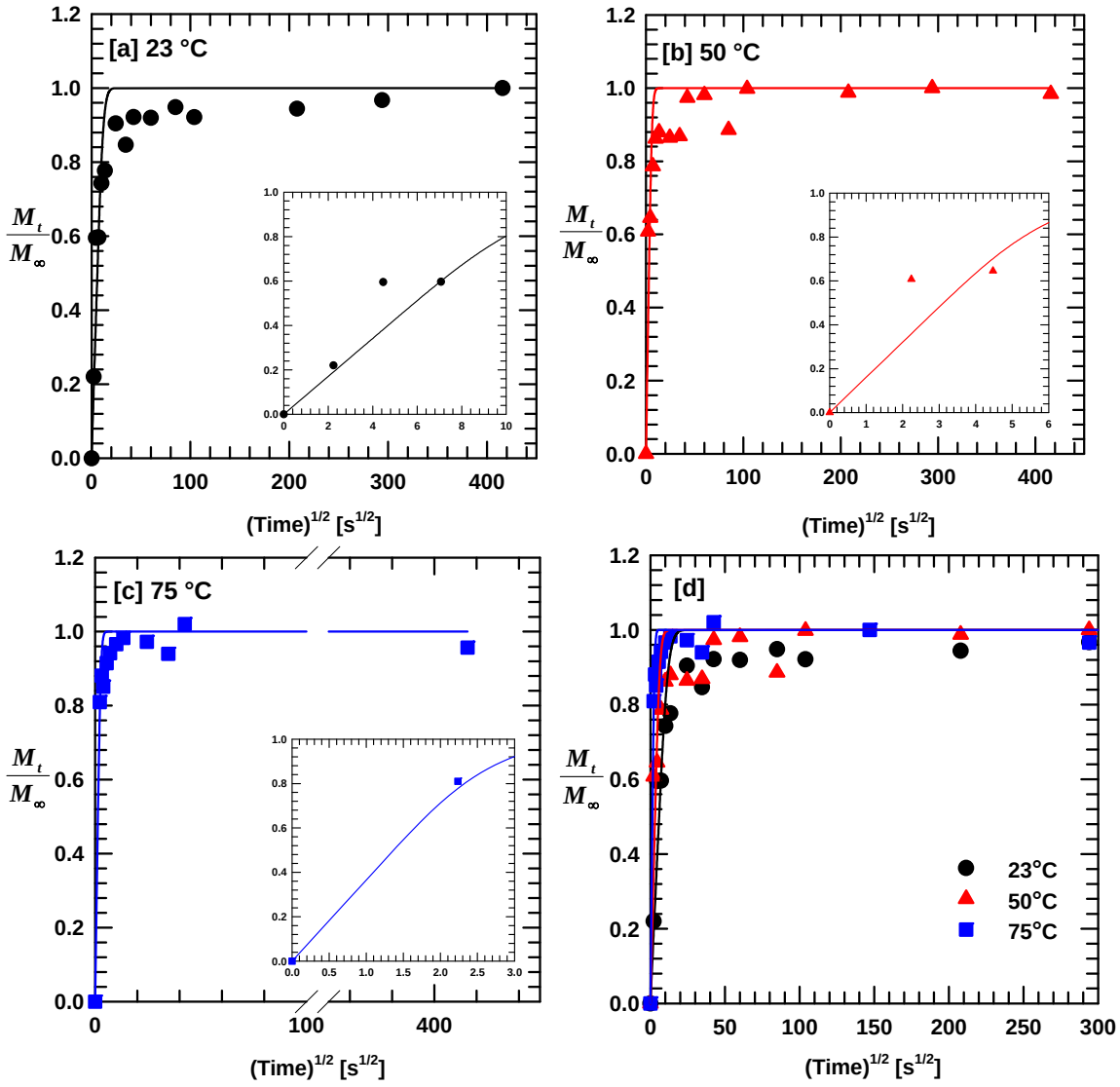

Figure 8.5 Extraction of PEG 200 from extruded BPS-20K/PEG 200 30 wt% films as a function of time at different temperatures: [a] 23 °C (●), [b] 50°C (▲) and [c] 75 °C (■), using the early time approximation Fickian model. [d] shows all extraction data of different temperatures for easier comparison. The inset graphs exhibit a magnified view near the origin ($M_t/M_\infty < 0.6$) where M_t/M_∞ is plotted versus $t^{1/2}$. R^2 values of each inset graph are presented in Table 8.3.

8.3.3 Analysis by complete solution of Fickian model

The early time approximation of Fickian model works well to estimate the diffusion coefficients of PEG molecules. In this section, the complete solution of Fickian model was employed to obtain diffusion coefficients for the extraction process and to compare them to those determined by the early time analysis.

Based upon the complete solution of Fickian model, the extraction data, M_t/M_∞, were plotted against log t, and compared to curves calculated by Equation (8.1) with diffusion coefficients in the range between 1.0×10^{-7} cm^2/s and 1.0×10^{-11} cm^2/s. To estimate the diffusion coefficients, the plots of M_t/M_∞ versus log t were shifted horizontally for superposition with the calculated curves, and, by using the shift factor, the diffusion coefficients reported in Table 8.3 were obtained.

As shown in Figure 8.6, early stage kinetic data fit well with the calculated curves, whereas the later stage kinetic data somewhat scatter. It is likely due to the fact that as the PEG extraction proceeds, the last remaining PEG molecules in the film are hard to diffuse into water, since the chemical potential gradient between the film and the surrounding water at the later stage is very small, so that there is not enough driving force for PEG extraction. Therefore, it is reasonable to use the early stage kinetic data for the estimation of diffusion coefficients and in this way, the diffusion coefficients estimated by the complete solution of Fickian model are comparable to those calculated by the early time approximation, indicating the analysis here are reasonably accurate.

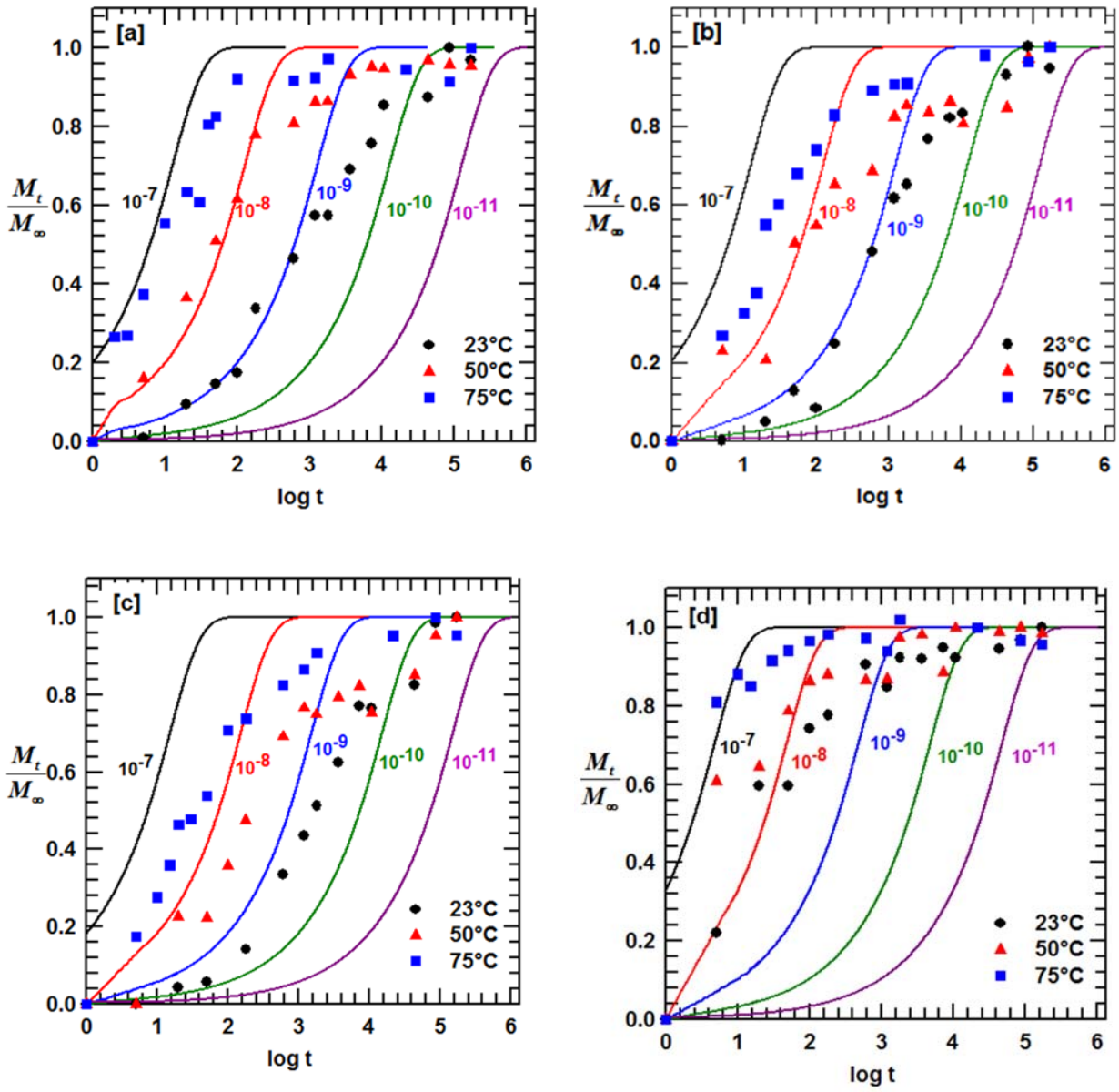

Figure 8.6 Extraction data of PEG materials from extruded BPS-20K/PEG films as a function of time at different temperatures: 23 °C (●), 50°C (▲), and 75 °C (■). [a] PEG 200 from extruded BPS-20K/PEG 200 20 wt% films. [b] PEG 300 from extruded BPS-20K/PEG 300 20 wt% films. [c] PEG 400 from extruded BPS-20K/PEG 400 20 wt% films. [d] PEG 200 from extruded BPS-20K/PEG 200 30 wt% films. Solid lines are the estimated M_t/M_∞ versus log t plots based on diffusion coefficients values between 1.0×10^{-7} cm^2/s and 1.0×10^{-11} cm^2/s using the complete Fickian model.

Table 8.3 Diffusion coefficients of PEG materials from extruded BPS-20K/PEG thin films. Diffusion coefficients are calculated by the early time approximation (Figures 8.2, 8.3, 8.4, and 8.5) and the complete solution of Fickian model (Figure 8.6). R^2 values were calculated from each inset graph in Figures 8.2, 8.3, 8.4, and 8.5

Polymer	PEG M_n [g/mol]	PEG wt%	Temp [°C]	Film thickness [μm]	R^2 [a]	D by early time approximation [cm^2/s]	D by complete solution [cm^2/s]
BPS-20K	PEG 200	20	23	35.34 ± 2.44	0.9554	6.54×10^{-10}	12.0×10^{-10}
BPS-20K	PEG 200	20	50	36.24 ± 2.99	0.9978	1.20×10^{-8}	1.00×10^{-8}
BPS-20K	PEG 200	20	75	35.46 ± 3.32	0.9901	7.02×10^{-8}	5.00×10^{-8}
BPS-20K	PEG 300	20	23	34.53 ± 3.40	0.9361	6.70×10^{-10}	7.00×10^{-10}
BPS-20K	PEG 300	20	50	35.44 ± 2.43	0.8926	8.88×10^{-9}	6.00×10^{-9}
BPS-20K	PEG 300	20	75	35.19 ± 3.53	0.9716	2.83×10^{-8}	3.80×10^{-8}
BPS-20K	PEG 400	20	23	39.36 ± 4.95	0.9422	4.43×10^{-10}	4.00×10^{-10}
BPS-20K	PEG 400	20	50	37.77 ± 2.78	0.9347	3.49×10^{-9}	3.50×10^{-9}
BPS-20K	PEG 400	20	75	39.65 ± 3.15	0.9442	2.19×10^{-8}	2.40×10^{-8}
BPS-20K	PEG 200	30	23	22.30 ± 6.34	0.9735	7.12×10^{-9}	9.00×10^{-9}
BPS-20K	PEG 200	30	50	21.05 ± 5.36	-*	2.24×10^{-8}	3.00×10^{-8}
BPS-20K	PEG 200	30	75	21.64 ± 4.36	-*	1.23×10^{-7}	1.00×10^{-7}

[a] R^2 is the goodness-of-fit for linear regression when $1-C_t/C_0$ is plotted against $t^{1/2}$ ($1-C_t/C_0 < 0.6$) in Figures 8.2, 8.3, 8.4, and 8.5. When R^2 is close to 1.0, all data points lie on a straight line with little scattering [12]

* Number of points is only two points because of fast diffusion

8.3.4 Influence of temperature on diffusivity

Diffusion coefficients can generally be related to an activation energy (ΔE_D) of diffusion by an Arrhenius expression as follows [13-15]:

$$D = D_0 \cdot \exp(\frac{\Delta E_D}{RT}) \tag{8.5}$$

where D is the diffusion coefficient, D_0 is the pre-exponential factor, R is gas constant (8.314 J/mol K), T is absolute temperature (K), and ΔE_D is the activation energy of diffusion (J/mol). This equation can be rewritten as:

$$\ln D = \ln D_0 - \frac{\Delta E_D}{RT} \tag{8.6}$$

When the diffusion coefficients calculated by the complete solution were plotted in this manner ($\ln D$ versus 1/T) as shown in Figure 8.7, this Arrhenius type model generates a reasonable fit for the diffusion coefficient values, and the model parameters are reported in Table 8.4.

Since the PEG molecular weights used in this study are in the similar range, their $\ln D$ versus 1/T curves lie close to each other, and the calculated ΔE_D values are in a similar range as well. Still, as PEG molecular weight increases at a fixed temperature and at a fixed PEG concentration, the diffusion coefficients of PEG decrease because of the effect of penetrant size on diffusion [16-18], and the ΔE_D values slightly increase.

The curve of BPS-20K/PEG 200 30 wt% films indicates that as PEG concentration (wt%) increases between 20 wt% and 30 wt%, at a fixed PEG molecular weight and at a fixed temperature, the diffusion coefficient values are higher and are less sensitive to temperature change. Thus, the ΔE_D value is lower, as explained.

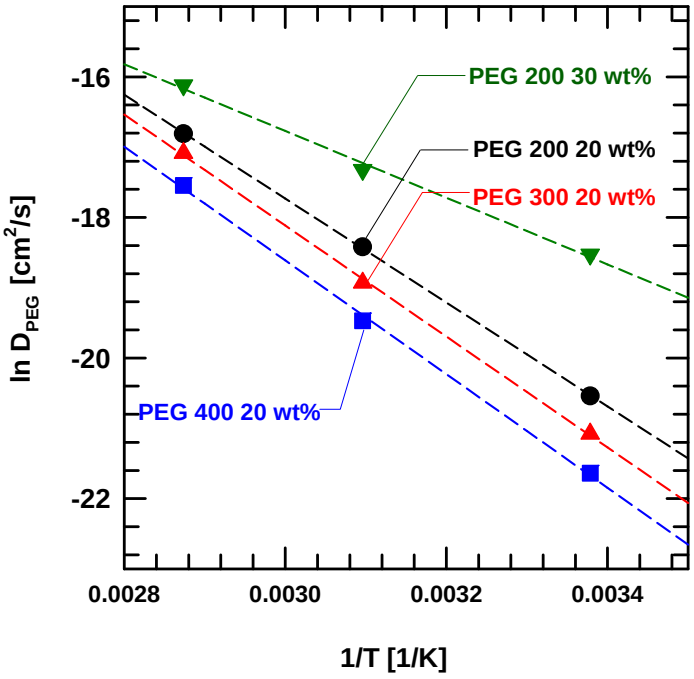

Figure 8.7 ln D_{PEG} versus 1/T of various extruded BPS-20K/PEG films. D_{PEG} values were determined from the complete solution of Fickian model.

Table 8.4 Parameters calculated from the Arrhenius type equation (8.6) from Figure 8.7

Polymer	PEG M_n [g/mol]	PEG wt%	ΔE_D [kJ/mol]	D_0 [cm^2/s]	$R^{2[a]}$
BPS-20K	PEG 200	20	61.4	85.4	0.9999
BPS-20K	PEG 300	20	65.7	265.2	0.9994
BPS-20K	PEG 400	20	67.3	287.6	0.9996
BPS-20K	PEG 200	30	39.5	0.1	0.9953

[a] R^2 is the goodness-of-fit for linear regression when ln D_{PEG} is plotted against 1/T in Figure 8.7. When R^2 is close to 1.0, all data points lie on a straight line with little scattering [12]

8.4 CONCLUSIONS

In this chapter, the effect of the PEG molecular weight ($\bar{M}_n$), PEG concentration (wt%) and temperature (°C) on the diffusion coefficient of PEG were studied to understand

the diffusion mechanism of PEG in extruded BPS-20K/PEG films. The early time approximation and complete solution of Fickian model were used to analyze the kinetic desorption of PEG materials from the extruded films and were found to fit well with the data. The diffusion coefficients of the PEG materials obtained from these analyses were well correlated with temperature and follow the Arrhenius equation.

Moreover, as expected, the PEG extraction kinetics are faster at higher temperatures, demonstrating that the diffusion coefficient of PEG materials is higher at higher temperatures. Also, at a fixed temperature, the PEG extraction kinetics are more rapid with decreasing PEG molecular weight ($\bar{M}_n$), and the ΔE_D values slightly decrease accordingly, since shorter chain PEG molecules (i.e., smaller penetrant size) have higher diffusion coefficients. Moreover, at the fixed PEG molecular weight ($\bar{M}_n$) of 200 g/mol, the PEG extraction kinetics were more rapid at higher PEG concentration (wt%) between 20 wt% and 30 wt%.

All PEG materials were successfully extracted from extruded BPS-20K/PEG thin films after melt extrusion. This information can be useful to optimize the extraction protocol of extruded membranes for desalination applications.

8.5 REFERENCES

[1] R. A. Register, and R. K. Prud'homme, "Melt rheology," *Ionomers*, M. R. Tant, K. A. Mauritz and G. L. Wilkes, eds., pp. 208-260: Blackie Academic & Professional, 1997.

[2] J.-Y. Sanchez, F. Chabert, C. Iojoiu, J. Salomon, N. E. Kissi, Y. Piffard, M. Marechal, H. Galiano, and R. Mercier, "Extrusion: an environmentally friendly process for PEMFC membrane elaboration," *Electrochimica Acta,* vol. 53, no. 4, pp. 1584-1594, 2007.

[3] Y. Molmeret, F. Chabert, N. E. Kissi, C. Iojoiu, R. Mercier, and J.-Y. Sanchez, "Toward extrusion of ionomers to process fuel cell membranes," *Polymers,* vol. 3, no. 3, pp. 1126-1150, 2011.

[4] W. Xie, J. Cook, H. B. Park, B. D. Freeman, C. H. Lee, and J. E. McGrath, "Fundamental salt and water transport properties in directly copolymerized disulfonated poly(arylene ether sulfone) random copolymer," *Polymer,* vol. 52, no. 9, pp. 2244-2254, 2011.

[5] H. J. Oh, B. D. Freeman, J. E. McGrath, C. J. Ellison, S. Mecham, K.-S. Lee, and D. R. Paul, "Rheological studies of disulfonated poly(arylene ether sulfone) plasticized with poly(ethylene glycol) for membrane formation," *Polymer,* vol. 55, no. 6, pp. 1574-1582, 2014.

[6] H. J. Oh, B. D. Freeman, J. E. McGrath, C. H. Lee, and D. R. Paul, "Thermal analysis of disulfonated poly(arylene ether sulfone) plasticized with poly(ethylene glycol) for membrane formation," *Polymer* vol. 55, no. 1, pp. 235-247, 2014.

[7] G. M. Geise, L. P. Palcon, B. D. Freeman, and D. R. Paul, "Sodium chloride sorption in sulfonated polymers for membrane applications," *Journal of Membrane Science,* vol. 423-424, pp. 195-208, 2012.

[8] G. M. Geise, "Water and salt transport structure/property relationships in polymer membranes for desalination power generation applications," Ph.D. Dissertation, Department of Chemical Engineering, The University of Texas at Austin, 2012.

[9] A. C. Sagle, E. M. Van Wagner, H. Ju, B. D. McCloskey, B. D. Freeman, and M. M. Sharma, "PEG-coated reverse osmosis membranes: desalination properties and fouling resistance," *Journal of Membrane Science,* vol. 340, no. 1-2, pp. 92-108, 2009.

[10] J. Crank, "4. Diffusion in a plane sheet," *The mathematics of diffusion*, pp. 44-68: Oxford Science Publications, 1956.

[11] H. S. Carslaw, and J. C. Jaeger, *Conduction of heat in solids*: Clarendon Press, 1986.

[12] R. B. D'Agostino, *Goodness-of-Fit-Techniques*: CRC Press, 1986.

[13] H. B. Park, and Y. M. Lee, "Polymeric membrane materials and potential use in gas separation " *Advanced Membrane technology and applications*, N. N. Li, A. G. Fane, W. S. Ho and T. Matsuura, eds., pp. 633-669, 2008.

[14] R. W. Baker, *Membrane technology and applications*, 3rd ed., West Sussex, United Kingdom: John Wiley and Sons Ltd, 2012.

[15] B. W. Rowe, L. M. Robeson, B. D. Freeman, and D. R. Paul, "Influence of temperature on the upper bound: theoretical considerations and comparison with experimental results," *Journal of Membrane Science,* vol. 360, pp. 58-69, 2010.

[16] H. Lin, and B. D. Freeman, “Gas permeation and diffusion in crosslinked poly(ethylene glycol diacrylate),” *Macromolecules,* vol. 38, pp. 8394-8407, 2005.

[17] S. Matteucci, Y. P. Yampolskii, and B. D. Freeman, "Transport of gases andvapors in glassy and rubbery polymers," *Materials science of membranes for gas and vapor separation*, Y. P. Yampolskii, I. Piannau and B. D. Freeman, eds., pp. 1-47: Wiley, 2006.

[18] R. W. Baker, and J. G. Wijmans, "Membrane separation of organic vapors from gas streams," *Polymeric gas separation membranes*, D. R. Paul and Y. P. Yampol'skii, eds., pp. 353-397, Boca Raton, FL.: CRC Press, 1994.

Chapter 9: Water and Salt Transport Properties of Disulfonated Poly(arylene ether sulfone) Membranes by Melt Extrusion: Effect of PEG Extraction using Water and Subsequent Drying Process

9.1 INTRODUCTION

In previous chapters, uniform thickness BPS/PEG membranes were prepared by melt extrusion, and the PEG plasticizer was removed from these films by water extraction. This chapter reports water and salt transport properties of BPS membranes prepared by extrusion and compares these to those of solution cast membranes to understand the effect of processing history on the transport properties of small molecules (i.e., water and salt) in BPS polymers. Water and salt transport properties include salt solubility (K_s), salt diffusivity (D_s), salt permeability (P_s), water uptake, water solubility (volume fraction of water in hydrated membranes, K_w), water diffusivity (D_w) and water permeability (P_w). The BPS membranes were prepared using various PEG $\overline{M}_n$ (200 ~ 400 g/mol) and concentration (20 ~30 wt%) [1, 2], and various PEG extraction methods (i.e., extraction temperature) were considered. This chapter investigates the influence of these different membrane preparation variables on the transport properties of BPS membranes.

9.2 RESULTS AND DISCUSSION

BPS-20K membranes were prepared by different preparation paths in terms of processing methods (i.e., solution casting vs. melt extrusion), PEG composition (molecular weight, $\overline{M}_n$: 200~400 g/mol and concentration 20~30 wt%) during melt extrusion, and PEG extraction temperatures (23 °C, 50 °C and 75 °C) after melt extrusion (see Table 9.1). To determine if there were any chemical and/or physical changes of BPS by these different preparation steps, some extruded films were dissolved in DMAc and solution cast again for further studies (marked as "Extrusion→Solution" in Table 9.1). The details of these studies will be explained later in this chapter. As shown in Table 9.1, densities and glass

transition temperatures (T_g) of BPS-20K membranes prepared by different routes are in a similar range, within the uncertainty of the measurements.

Table 9.1 Densities and glass transition temperatures of BPS-20K membranes prepared by different route

Processing method	Polymer	PEG $\bar{M}_n$ [g/mol]	PEG wt%	PEG extraction temp [°C]	PEG extraction time	Density [a] [g/cm^3]	T_g [b] [°C]
Solution*	BPS-20K	-	-	-	-	1.376 ± 0.011	256
Solution*	BPS-20K	-	-	50	1 hour	1.374 ± 0.001	256
Solution*	BPS-20K	-	-	75	1 hour	1.351 ± 0.001	251
Extrusion	BPS-20K	200	20	25	4 days	1.364 ± 0.017	256
Extrusion	BPS-20K	400	20	25	4 days	1.367 ± 0.002	256
Extrusion	BPS-20K	200	30	25	4 days	1.377 ± 0.007	254
Extrusion	BPS-20K	200	20	50	1 hour	1.363 ± 0.008	255
Extrusion	BPS-20K	200	20	75	1 hour	1.361 ± 0.006	255
Extrusion →Solution**	BPS-20K	200	20	75	2 days	-	256

*Transparent and uniform thickness films (20~40 μm) were formed by the solution casting method reported previously [3]

**"Extrusion→Solution" indicates that (1) the extruded BPS/PEG film was soaked in DI water at given temperature and time to remove most of PEG from the film, and then (2) dried at 110 °C in a vacuum oven for 24 hours to remove residual water from the film, and subsequently (3) dissolved in DMAc (10 wt% polymer solution), and solution cast on a glass plate, following the drying protocol reported previously [3]

[a] Measured using a Mettler Toledo density determination kit (Part# 238490, Switzerland) with *n*-heptane (Cat# 32287, Sigma-Aldrich, St. Louis, MO) at ambient temperature (20~22°C)

[b] Measured by DSC at 20 °C/min

9.2.1 Transport properties after PEG extraction using water

Water and salt transport properties of BPS membranes are summarized in Tables 9.2 and 9.3, respectively. These extruded/extracted BPS membranes were kept in DI water for at least one hour before testing. Changes in soaking time in DI water (i.e., one hour ~ 1 week) before testing at ambient temperature did not influence transport properties of these membranes. Similar observations were reported by Xie et al.[3].

Figure 9.1 shows water solubility (9.1a), water permeability (9.1b), and water diffusivity (9.1c) of BPS membranes prepared by different processing methods as a function of water uptake (g H_2O/100 g dry polymer). The motivation for plotting the data versus water uptake is from Yasuda, et al.'s work and previous studies from our research group, suggesting that membrane transport properties are governed by free volume [3-7]. In hydrated polymers, free volume is often proportional to sorbed water content (i.e., water uptake). When plotted in this manner, a strong correlation between water transport properties and water uptake can be found in Figure 9.1, as expected. Water solubility, permeability, and diffusivity increase as water uptake increases, and similar trends can be found with salt transport properties in Figure 9.2. Thus, this free volume-based theory can be used to correlate the diffusion of water and salt across the BPS membranes with water uptake [3, 6].

Table 9.2 Water permeabilities, water diffusivities and water solubilities of BPS-20K films prepared by different routes

Processing method	Polymer	PEG $\bar{M}_n$ [g/mol]	PEG wt%	PEG extraction temp [°C]	PEG extraction time	χ**	P_w^H [L µm/ (m^2 h bar)]	P_w^D [10^{-6} cm^2/s]	D_w [10^{-6} cm^2/s]	K_w
Solution*	BPS-20K	-	-	-	-	1.73	0.030 ± 0.003	0.115	1.15	0.10 ± 0.03
Solution*	BPS-20K	-	-	50	1 hour	1.50	0.049 ± 0.009	0.187	1.37	0.14 ± 0.01
Solution*	BPS-20K	-	-	75	1 hour	1.45	0.093 ± 0.007	0.355	2.28	0.15 ± 0.00
Extrusion	BPS-20K	200	20	25	3-4 days	1.41	0.263 ± 0.047	1.00	6.59	0.16 ± 0.02
Extrusion	BPS-20K	400	20	25	3-4 days	1.30	0.301 ± 0.015	1.15	6.20	0.19 ± 0.01
Extrusion	BPS-20K	200	30	25	3-4 days	1.09	1.73 ± 0.18	6.61	24.30	0.27 ± 0.01
Extrusion	BPS-20K	200	20	50	1 hour	1.30	0.528 ± 0.020	2.02	1.37	0.19 ± 0.01
Extrusion	BPS-20K	200	20	75	1 hour	1.18	1.135 ± 0.065	4.33	2.28	0.23 ± 0.02

*Transparent and uniform thickness films (20~40 µm) were formed by the solution casting method reported previously [3]

**χ was calculated using equation (2.19) (details in Chapter 2.3.1.2)

Table 9.3 Salt permeabilities, salt diffusivities and salt solubilities of BPS-20K films prepared by different routes

Processing method	Polymer	PEG $\bar{M}_n$ [g/mol]	PEG wt%	PEG extraction temp [°C]	PEG extraction time	P_s [10^{-9} cm^2/s]	D_s [10^{-7} cm^2/s]	K_s
Solution*	BPS-20K	-	-	-	-	0.058 ± 0.007	0.029 ± 0.006	0.020 ± 0.004
Solution*	BPS-20K	-	-	50	1 hour	0.12 ± 0.01	0.068 ± 0.004	0.018 ± 0.001
Solution*	BPS-20K	-	-	75	1 hour	0.42 ± 0.01	0.14 ± 0.02	0.031 ± 0.004
Extrusion	BPS-20K	200	20	25	3-4 days	2.47 ± 0.25	0.308 ± 0.029	0.08 ± 0.007
Extrusion	BPS-20K	400	20	25	3-4 days	4.03 ± 0.15	0.598 ± 0.071	0.068 ± 0.008
Extrusion	BPS-20K	200	30	25	3-4 days	55.40 ± 1.78	4.78 ± 0.21	0.116 ± 0.005
Extrusion	BPS-20K	200	20	50	1 hour	10.3 ± 0.84	1.16 ± 0.12	0.089 ± 0.010
Extrusion	BPS-20K	200	20	75	1 hour	26.0 ± 3.1	2.32 ± 0.04	0.112 ± 0.002
Extrusion →Solution**	BPS-20K	200	20	75	2 days	0.076 ± 0.020	0.059 ± 0.006	0.013 ± 0.001

*Transparent and uniform thickness films (20~40 μm) were formed by the solution casting method reported previously [3]

**"Extrusion→Solution" indicates that (1) the extruded BPS/PEG film was soaked in DI water at given temperature and time to remove most of PEG from the film, and then (2) dried at 110 °C in a vacuum oven for 24 hours to remove residual water from the film, and subsequently (3) dissolved in DMAc (10 wt% polymer solution), and solution cast on a glass plate, following the drying protocol reported previously [3]

** Relative variance of D_s was calculated by error analysis [8]

9.2.1.1 Effect of PEG molecular weight and concentration

Compared to the solution cast BPS-20K membrane, the extruded BPS-20K membranes prepared using various PEG $\bar{M}_n$ and concentrations and different PEG extraction temperatures (23 °C, 50 °C and 75 °C) exhibit significantly higher water uptake and, thus, higher water solubility as shown in Figure 9.1a. Water solubility is calculated using water uptake, membrane/water densities using equation (3.2) (details in Chapter 3.5.2), and, therefore is proportional to water uptake. Even extruded BPS membranes prepared using the lowest PEG concentration (20 wt%) and the lowest molecular weight (200 g/mol), and the lowest PEG extraction temperature (25 °C), have 60 % higher water solubility than a solution-processed sample. PEG concentration of 20 wt% is the minimum amount required for melt extrusion to produce uniform thickness membranes (details in Chapter 7).

At a fixed PEG concentration of 20 wt%, as PEG molecular weight increased from 200 g/mol to 400 g/mol, water solubility increased by almost 20 %. At a fixed PEG molecular weight of 200 g/mol, as PEG concentration increased from 20 wt% to 30 wt%, water solubility increased 1.7 times. Compared to the increase of water solubility as PEG molecular weight increases from 200 g/mol to 400 g/mol, the water solubility increase induced by increasing PEG concentration (i.e., from 20 wt% to 30 wt%) is larger.

9.2.1.2 Effect of PEG extraction temperature

As discussed in Chapter 8, the rate of PEG extraction from extruded BPS/PEG membranes is affected by temperature. PEG extraction kinetics are faster at higher temperatures and, therefore, only one hour of soaking time was required in water at high temperatures (i.e., 50 °C and 75 °C) to remove most of the PEG from BPS/PEG films.

As shown in Tables 9.2 and 9.3, using the BPS membranes prepared with the same PEG molecular weight (200 g/mol) and PEG concentration (20 wt%) (i.e., BPS-20K/PEG 200 g/mol 20 wt%), PEG was removed from the BPS/PEG films by soaking the films at different temperatures (23 °C, 50 °C and 75 °C). Soaking time was changed at different temperatures, and it was selected based on the minimum required time to remove most of PEG from the extruded films. The amount of PEG remaining in the sample after soaking is below the detection limit based on ^{1}H NMR analysis (details in Chapter 8).

Further soaking at ambient temperature (23 °C) does not change transport properties of BPS films, whereas prolonged soaking of samples at high temperatures can influence the transport properties significantly as reported previously [9-12]. Xie et al. observed that soaking BPS-32 membranes (K and H form) at 50 °C, 75 °C and in boiling water changed the transport properties substantially. For example, by soaking a BPS-32K film in boiling water for four hours, water permeability increased 2.3 times, salt permeability increased 8 times, and water uptake increased 1.5 times [12].

By immersing the same films at higher temperature, i.e., 75 °C, water uptake increase by 40 %. The thermal exposure also has a similar influence on water solubility of solution cast BPS-20K membranes used in this study. Solution cast films also show about 50 % higher water solubility by similar thermal exposure experiments.

In summary, extruded BPS-20K films show higher water uptake than those of solution cast membranes, and as PEG molecular weight and concentration used during extrusion increases and as PEG extraction temperature increases, water uptake (and water solubility) increases as shown in Figure 9.1a. As the water uptake increases, water permeability (Figure 9.1b) and water diffusivity (Figure 9.1c) increase. Therefore, consistent with Yasuda et al.'s findings regarding salt (NaCl) transport through hydrated

polymers [4], salt solubility and salt diffusivity increase as water uptake increase, as shown in Figure 9.2.

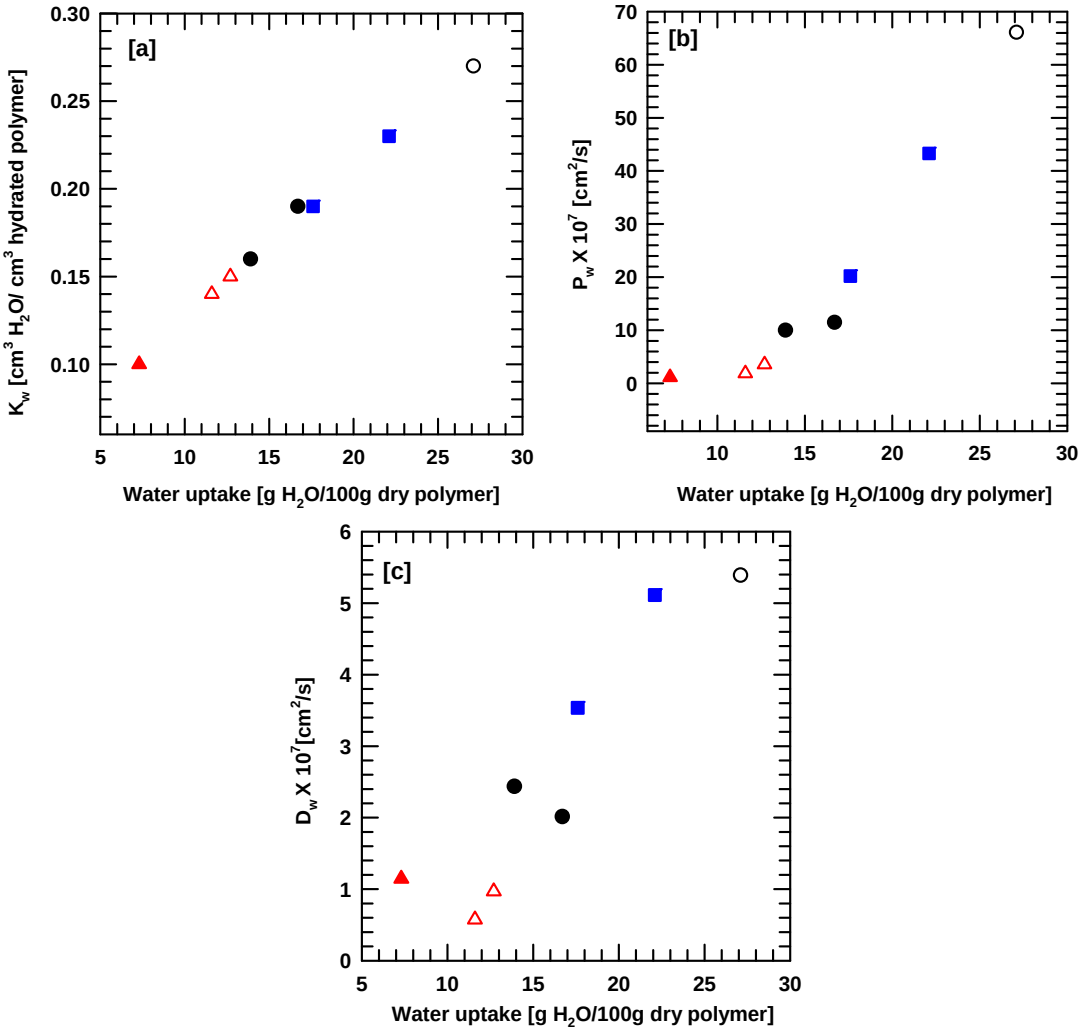

Figure 9.1 [a] water solubility (K_w, [cm^3 H_2O /cm^3 hydrated polymer]), [b] diffusive water permeability (P_w^D), and [c] water diffusivity (D_w) as a function of water uptake (g H_2O /100 g dry polymer). Symbols are (from left to right): 1) solution cast, control BPS-20K film (▲), 2, 3) solution cast BPS-20K film, soaked in 50 °C (left △) and 75 °C (right △) for 1 hour , 4, 5) extruded/extracted BPS-20K/PEG ($\bar{M}_n$: 200 (left ●), 400 g/mol (right ●)) 20 wt% films, soaked in 23 °C for 3-5 days , 6, 7) extruded/extracted BPS-20K/PEG 200 g/mol 20 wt%, soaked in 50 °C (left ■) and for 75 °C (right ■) for 1 hour , 8) extruded/extracted BPS-20K/PEG 200 g/mol 30 wt%, soaked in 23 °C for 3-5 days (○).

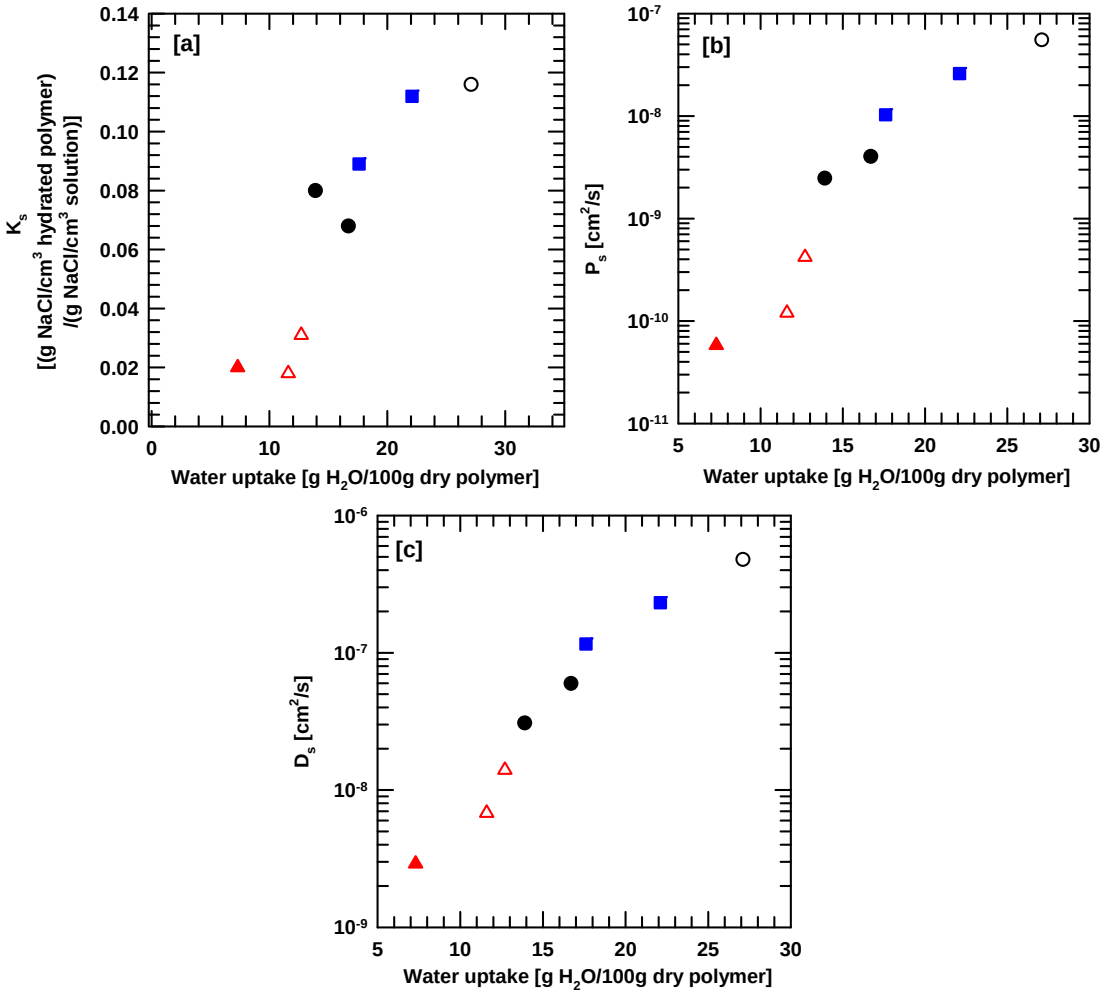

Figure 9.2 [a] salt solubility (K_s [(g NaCl/cm^3 hydrated polymer/(g NaCl /cm^3 solution)]), [b] salt permeability (P_s), and [c] salt diffusivity (D_s) as a function of water uptake (g of water/100 g of dried polymer. Symbols are (from left to right): 1) solution cast, control BPS-20K film (▲), 2, 3) solution cast BPS-20K film, soaked in 50 °C (left △) and 75 °C (right △) for 1 hour , 4, 5) extruded/extracted BPS-20K/PEG ($\bar{M}_n$: 200 (left ●), 400 g/mol (right ●)) 20 wt% films, soaked in 23 °C for 3-5 days , 6, 7) extruded/extracted BPS-20K/PEG 200 g/mol 20 wt%, soaked in 50 °C (left ■) and for 75 °C (right ■) for 1 hour , 8) extruded/extracted BPS-20K/PEG 200 g/mol 30 wt%, soaked in 23 °C for 3-5 days (○).

From free volume theory, the diffusivity, D, can be written in terms of free volume of polymer, v_f, as [4]:

$$D \propto \exp[-(\frac{v^*}{v_f})] \tag{9.1}$$

where v^* is the characteristic volume needed for the diffusion of a small penetrant molecule through a polymer. If the free volume of a membrane scales linearly with the volume fraction of diluent in the polymer, then diffusivity scales exponentially with changes in the volume fraction of diluent in the polymer. In hydrated polymers such as those in our study, the volume fraction of water in the hydrated polymer is expressed as water solubility, K_w.

Yasuda et al. proposed, based on the free volume theory, that the free volume of a hydrated polymer could be written as the summation of the free volume of the polymer and the free volume of water as [4]:

$$v_f = K_w \cdot v_{f,H_20} + (1\text{-}K_w) \cdot v_{f,polymer} \tag{9.2}$$

where v_{f,H_20} is the free volume of water, and $v_{f,polymer}$ is the free volume of dry polymer. Since the permeation of salt (NaCl) across a pure (i.e., dehydrated) polymer is likely to be negligible, most salt is likely to permeate through the hydrated regions of polymers and, thus, the available free volume for salt permeation is the free volume added by water. Thus, equation (9.2) becomes [4]:

$$v_f \cong K_w \cdot v_{f,H_20} \tag{9.3}$$

Therefore, the salt diffusivity, D_s, in hydrated polymers can be expressed as [4]:

$$\log D_s = \log D_0\text{-}B(\frac{1}{K_w}\text{-}1) \tag{9.4}$$

where D_0 is the salt (NaCl) diffusivity in pure water at 25 °C (i.e., 1.47×10^{-5} cm^2/s [3]), and B is a proportionality constant in terms of v^* and v_{f,H_20}. Based on this model, when the salt diffusivity is plotted as a function of $1/K_w$, a linear relationship is expected, starting at $1/K_w = 1$, i.e., the salt diffusivity in pure water.

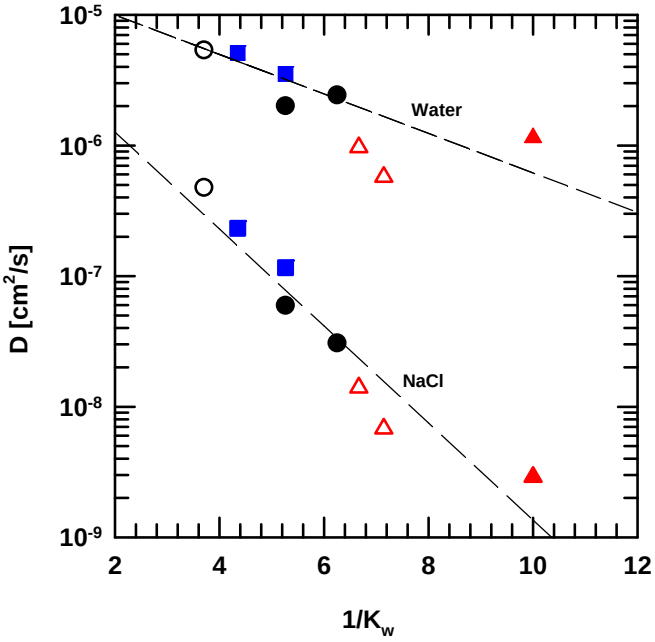

Figure 9.3 Water and salt diffusivity (D_w and D_s) versus $1/K_w$ of BPS-20K membranes prepared by different protocols. Dashed lines are the fit of Yasuda's model to the data. Symbols are (from right to left): 1) solution cast, control BPS-20K film (▲), 2, 3) solution cast BPS-20K film, soaked in 50 °C (right △) and 75 °C (left △) for 1 hour , 4, 5) extruded/extracted BPS-20K/PEG ($\bar{M}_n$: 200 (right ●), 400 g/mol (left ●)) 20 wt% films, soaked in 23 °C for 3-5 days , 6, 7) extruded/extracted BPS-20K/PEG 200 g/mol 20 wt%, soaked in 50 °C (right ■) and for 75 °C (left ■) for 1 hour , 8) extruded/extracted BPS-20K/PEG 200 g/mol 30 wt%, soaked in 23 °C for 3-5 days (○).

Figure 9.3 shows the water and salt diffusivity in this study plotted as a function of $1/K_w$. The dashed lines through the data are the fits of Yasuda's model. Both water and salt diffusivity scale exponentially with $1/K_w$, indicating that a reasonable empirical analysis can be done using Yasuda's model. Furthermore, the slope of the salt diffusivity versus $1/K_w$ is steeper than that of water diffusivity versus $1/K_w$. Since hydrated Na^+ and Cl^- ions are larger than a water molecule, larger penetrants exhibit a stronger dependence on free volume than smaller molecules. For instance, when water solubility increased 2.3 times in

this study (from the lowest to the highest value), the water diffusivity increased 14 times, but the salt diffusivity increased 165 times.

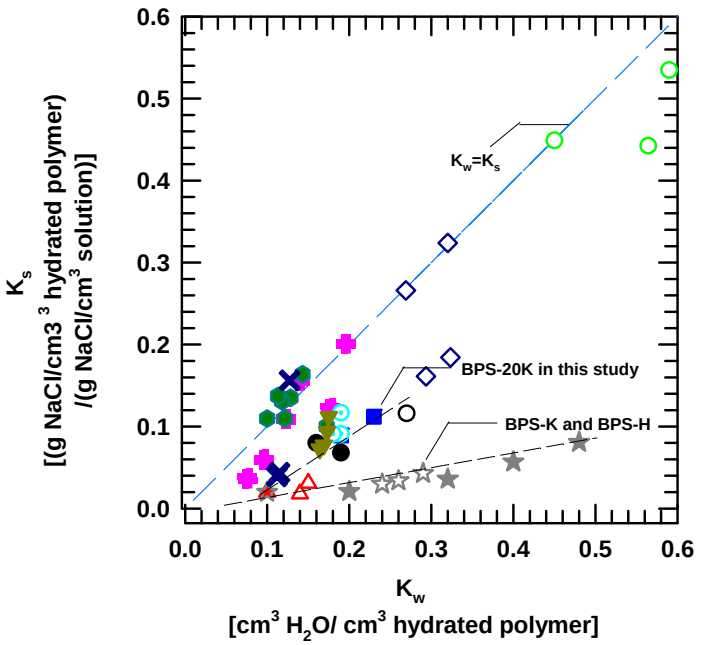

Figure 9.4 Effect of water solubility (K_w, [cm^3 H_2O /cm^3 hydrated polymer]) on salt solubility (K_s, [(g NaCl/cm^3 hydrated polymer/(g NaCl /cm^3 solution)]). Blue dashed line in the center represents a line where K_w=K_s. Symbols are: BPS-K films (☆) and BPS-H films (★) (sulfonation level is 20, 30, 35 and 40 mol%, from left to right) [3]. Hydroxypropylmethacrylate-glycerol methacrylate copolymers (HPMA-GMA, ○) [4], hydroxylethyl methacrylate (HEMA2, ◇) [4], methyl methacrylate-glycerol methacrylate copolymers (MMA-GMA, ✚) [6], hydroxylethyl methacrylate-methyl methacrylate copolymers (HEMA-MMA, ⊙) [4], cellulose acetate (CA, ✖) [4], hydroxypropyl methacrylate-methyl methacrylate copolymers (HPMA-MMA, ⬢) [4], hydroxypropyl methacrylate-glycidyl methacrylate copolymers (HPMA-GDMA, ▼) [4]

Figure 9.4 shows the salt solubility versus water solubility of BPS-20K films in this study and other data from previous studies for comparison [3, 4]. Salt solubility, K_s, is defined as the ratio of the salt (NaCl) concentration in the polymer, to the salt concentration

in the contiguous solution ([(g NaCl/cm^3 hydrated polymer)/(g NaCl /cm^3 solution)]) (details in Chapter 2.3.2). In hydrated polymers, the amount of salt sorbed in the polymer is likely to increase with increasing amount of sorbed water. However this result is not the case for all hydrated polymers. For example, some polymers such as Hydroxypropylmethacrylate-glycerol methacrylate copolymers (HPMA-GMA), and hydroxylethyl methacrylate (HEMA), etc. from Yasuda's work [4] show that salt solubility is almost identical to water solubility (i.e., $K_s = K_w$, blue dashed line in Figure 9.4) [4]. However, other polymers such as cellulose acetate (CA), and hydroxylethyl methacrylate-methyl methacrylate copolymers (HEMA-MMA), etc. [3, 4] show lower salt solubility compared to that of water solubility. Having lower salt solubility compared to water solubility indicates that polymers may prevent salt from being sorbed in the polymer matrix by interactions between salt ions, water, ionic groups in the polymer [3, 4].

Solution cast BPS-K and BPS-H polymers (sulfonation level is 20, 30, 35 and 40 mol%) from previous work [3, 13] exhibit significantly lower salt solubility values compared to their water solubility. On the other hand, the extruded/extracted BPS-20K films in this study exhibit higher salt solubility values than those of solution-processed BPS films, at a similar water solubility values. The reason for this trend is not explained yet, and further investigations are required and suggested in the recommendation section.

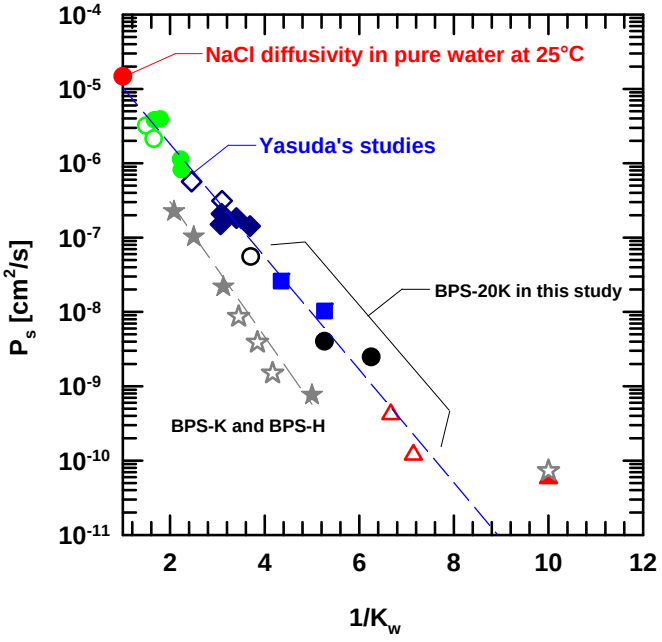

Figure 9.5 Salt permeability (P_s) versus $1/K_w$ at 25 °C. Symbols are (from right to left): 1) solution cast, control BPS-20K film (▲), 2, 3) solution cast BPS-20K film, soaked in 50 °C (right △) and 75 °C (left △) for 1 hour , 4, 5) extruded/extracted BPS-20K/PEG ($\bar{M}_n$: 200 (right ●), 400 g/mol (left ●)) 20 wt% films, soaked in 23 °C for 3-5 days , 6, 7) extruded/extracted BPS-20K/PEG 200 g/mol 20 wt%, soaked in 50 °C (right ■) and for 75 °C (left ■) for 1 hour , 8) extruded/extracted BPS-20K/PEG 200 g/mol 30 wt%, soaked in 23 °C for 3-5 days (○). Blue dashed line is the fitting line of data from Yasuda's work from Ref. [4] and the line was modified to go through the red point (●), where $1/K_w = 1$, denoting NaCl diffusivity in pure water at 25 °C. Grey dashed line is the trend line of BPS-H and BPS-K data [3]. Symbols are: BPS-K films (☆) and BPS-H films (★) (sulfonation level is 40, 35, 30 and 20 mol%, from left to right) [3]. Salt permeabilities of BPS polymers were determined by direct permeation tests. (Hydroxypropylmethacrylate-glycerol methacrylate copolymers (HPMA-GMA, ○), determined by direct permeation tests) [4], hydroxylethyl methacrylate (HEMA2, ◇, determined by direct permeation tests) [4], HPMA-GMA (●, determined by $P_s = D_s \cdot K_s$) [4], HEMA2 (◆, determined by $P_s = D_s \cdot K_s$) [4]

Figure 9.5 shows salt permeability as a function of $1/K_w$ of BPS-20K films in this study and other polymers from previous studies for comparison [3, 4, 13]. The grey dashed

line is the trend line of BPS-H and BPS-K data [3]. In highly hydrated polymers such as HPMA-GMA and HEMA from Yasuda's work [4], salt permeability increases as $1/K_w$ decreases, as indicated by the blue dashed line. The line was modified to go through the point where $1/K_w = 1$, which denotes the NaCl diffusivity in pure water at 25 °C [4]. For the highly hydrated, uncharged hydrogels from Yasuda's work, the major contribution of added free volume (i.e., sorbed water uptake) on salt permeability is from its effect on salt diffusivity. Similar to these highly hydrated polymers, the extruded/extracted BPS-20K films in this study follow the same trend line as that of Yasuda's studies, indicating that for these extruded/extracted BPS-20K films, the main contribution of increased free volume to the salt permeability is its influence on salt diffusivity as shown in Figure 9.4.

On the other hand, data from solution-processed BPS-H and BPS-K polymers are located below the trend line of Yasuda's work and also do not show a simple linear relationship between salt permeability and $1/K_w$. Xie et al. mentioned that this difference is because of low salt solubility of these polymers compared to highly hydrated polymers from Yasuda's studies [3] as shown in Figure 9.4. The reason that extruded/extracted BPS-20K membranes follow the same trend as highly hydrated, uncharged hydrogels from Yasuda's work is likely due to their higher salt solubility than that of solution-processed BPS polymers (see Figure 9.4).

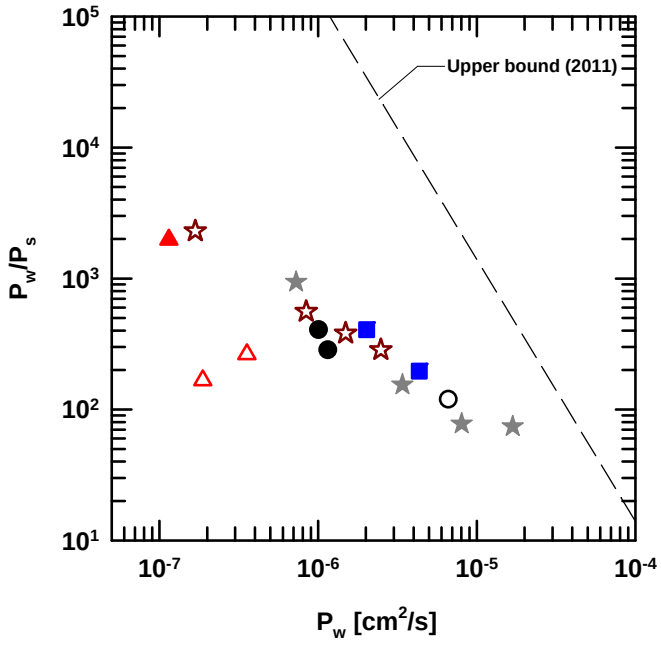

Figure 9.6 Water/salt permeability selectivity (P_w/P_s) versus P_w at 25 °C. Symbols are (from left to right): 1) solution cast, control BPS-20K film (▲), 2, 3) solution cast BPS-20K film, soaked in 50 °C (left △) and 75 °C (right △) for 1 hour , 4, 5) extruded/extracted BPS-20K/PEG ($\bar{M}_n$: 200 (left ●), 400 g/mol (right ●)) 20 wt% films, soaked in 23 °C for 3-5 days , 6, 7) extruded/extracted BPS-20K/PEG 200 g/mol 20 wt%, soaked in 50 °C (left ■) and for 75 °C (right ■) for 1 hour , 8) extruded/extracted BPS-20K/PEG 200 g/mol 30 wt%, soaked in 23 °C for 3-5 days (○). The dashed line represents the upper bound from Ref. [14]. Symbols are: BPS-K films (☆) and BPS-H films (★) (sulfonation level is 20, 30, 35 and 40 mol%, from left to right) [3]. For proper comparison, Pw were determined using equation (2.18), assuming $(1\text{-}K_W)^2(1\text{-}2\chi K_W) = 1$.

Figure 9.6 shows the water/salt permeability selectivity (P_w/P_s) versus water permeability (P_w) of BPS-20K membranes used in this study and solution processed BPS-H and BPS-K polymers for comparison [3]. There is a correlation between permeability and selectivity, which is called the permeability-selectivity trade-off relationship often used for gas separation membranes [3, 14, 15]. A polymer membrane which has higher permeability has a tendency to sacrifice selectivity. The dashed line is the so-called upper

bound of permeability selectivity versus water permeability, representing the currently available materials' best performance [14], and few materials have been reported to the right side of upper bound.

For the extruded/extracted BPS-20K films, as water permeability increased, permeability selectivity decreased parallel to the upper bound. This trend is similar to other solution processed BPS polymers. That is, as sulfonation level increased, water permeability increased, and permeability selectivity decreased [3, 13, 16]. However, the extruded/extracted BPS-20K films show higher permeability and lower selectivity than those of solution processed films. As PEG molecular weight and concentration increases and as PEG extraction temperature increases, permeability increased, and selectivity decreased. The extruded/extracted BPS-20K/PEG 20 wt% films show a similar range of permeability selectivity as those of solution processed BPS-30K and BPS-35K polymers, whereas the extruded/extracted BPS-20K PEG 200 g/mol 30 wt% films show a similar permeability selectivity range as that of solution processed BPS-35H polymer.

9.2.2 Origin of difference between solution cast and extruded films

Compared to solution cast BPS-20K films, extruded BPS-20K films prepared by different routes show different water and salt transport properties. To understand the origin of this difference, ^{1}H NMR analysis and FT-IR analysis were conducted with all samples, but no chemical structural change was detected.

To confirm if this difference is from a physical change of the polymer during the different preparation steps, one extruded/extracted sample (BPS-20K/PEG 200 g/mol, 20 wt%, PEG extracted at 25 °C for 3-4 days) was dried and dissolved in DMAc (10 wt% polymer solution) and solution cast on a glass plate, following the drying protocol reported previously [3]. The salt transport properties of this "extrusion → solution" sample in Table

9.3 are in a similar range as those of solution cast, control BPS-20K film, indicating that different processing histories change the polymer properties.

Interestingly, densities and T_gs of the extruded/extracted BPS-20K films are in a similar range, as reported in Table 9.1. Water and salt transport property measurements were conducted with hydrated polymers, so these samples were kept in DI water before use and have not been dried in a vacuum oven. On the other hand, samples for density and T_g measurements were carefully dried in a vacuum oven at high temperature (110 °C) for 48 hours to remove all excessive water from the sample before testing. Although these samples are prepared by same process in terms of PEG composition and PEG extraction methods, this additional drying process may generate a physical change in these films, so that the density and T_g values of dried samples are similar to those of solution cast films, whereas the water and salt transport properties of undried/hydrated samples are substantially different from those of solution processed samples.

To confirm this hypothesis, the extruded/extracted samples were dried at different temperatures and times, and their salt permeabilities were measured as shown in Figure 9.7. By merely drying the same sample for 2 days at ambient temperature, the salt permeability decreased 4 times. By drying at higher temperatures for longer time, the salt permeability decreased 10 times. Interestingly, the effect of drying on the extruded/extracted samples is irreversible. Thus, once the samples were dried, their salt permeability values did not recover to the original value. This result indicates the strong effect of processing history on BPS polymers.

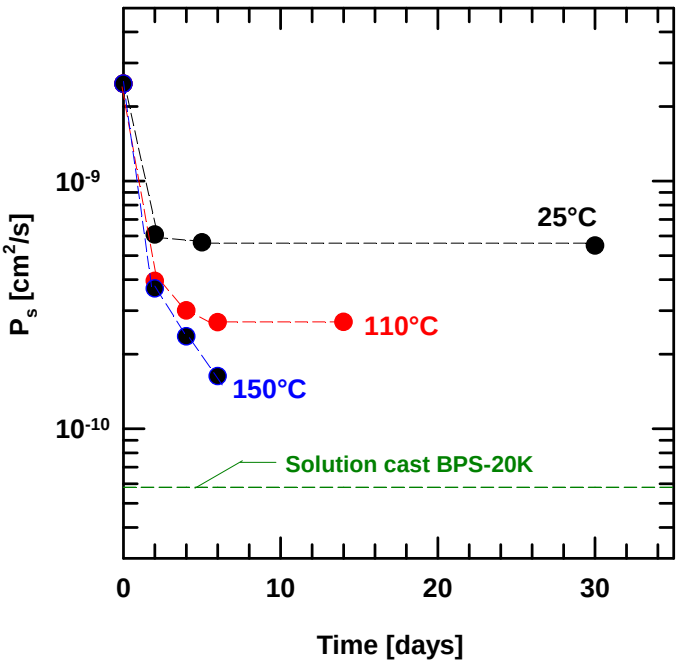

Figure 9.7 Salt permeability (P_s) of extruded/extracted BPS-20K membranes (prepared with PEG 200 g/mol, 20 wt%, and extraction was conducted at 23 °C in DI water for a week) dried at the various drying temperatures (25 °C, 110 °C, and 150°C) as a function of times. Green dashed line at the bottom is salt permeability of solution cast BPS-20K membranes.

However, even though a sample was dried at high temperatures for a long time to see if salt permeability recovers to that of solution processed BPS films, there was still a difference of 4× in salt permeability between the extruded/extracted/dried samples and solution processed samples, and further drying did not change the properties significantly. Thus, the effect of different processing methods (i.e., extrusion process) changes the physical structure (for example, generates additional free volume in the polymer matrix) of BPS polymers.

Similar observation have been reported previous by Xie [12] and Stevens, et al. [17]. Stevens and others reported that drying and annealing BPS-20K polymers (i.e., post thermal treatment after phase inversion) can significantly change the RO performance. For

example, overnight air drying reduces salt passage and water flux, because of dehydration of small pores and water-rich regions in hydrated polymers. Similarly, drying the extruded/extracted BPS-20K films at higher temperatures for longer time may lead to dehydration, resulting in less free volume and rearrangement of polymer chains.

PEG extraction from extruded BPS films generates additional free volume (i.e., higher water uptake), and this additional free volume is not likely to recover to the level of free volume as solution processed samples. Further investigations are required to identify the effect of processing history on the final properties.

9.3 CONCLUSIONS

BPS-20K membranes were prepared by different preparation paths in terms of processing methods (i.e., solution casting vs. melt extrusion), PEG composition (molecular weight, $\overline{M}_n$: 200~400 g/mol and concentration 20~30 wt%) during melt extrusion, and PEG extraction temperatures (23 °C, 50 °C and 75 °C) after melt extrusion to investigate the influence of these preparation variables on the transport properties of BPS membranes.

The extruded/extracted BPS-20K films show higher water uptake than those of solution cast membranes. As PEG molecular weight and concentration used during extrusion increases and as PEG extraction temperature increases, water uptake (and water solubility) increases. As water uptake increases, water and salt permeabilities and diffusivities increase, consistent with Yasuda et al.'s findings.

Compared to the increase of water and salt transport properties as PEG molecular weight increases from 200 g/mol to 400 g/mol, the water and salt transport property increases induced by increasing PEG concentration (i.e., from 20 wt% to 30 wt%) are larger. By immersing the same films at higher temperature, i.e., 75 °C, water uptake increase by 40 %.

Compared to solution cast BPS-20K films, extruded BPS-20K films prepared by different routes show different water and salt transport properties. To understand the origin of this difference, ^{1}H NMR analysis and FT-IR analysis were conducted but no chemical structural change was detected. The water and salt transport properties of a re-cast ("extrusion → solution") sample are in a similar range as those of solution processed sample, indicating that different processing history affects the transport properties.

Different processing methods have a significant effect on the structure of BPS polymers. PEG extraction from extruded BPS films generates additional free volume (i.e., higher water uptake), and this additional free volume is likely not to recover to the level of free volume of solution processed samples. Further investigation is required to identify the effect of processing history on the final properties.

9.4 REFERENCES

[1] H. J. Oh, B. D. Freeman, J. E. McGrath, C. J. Ellison, S. Mecham, K.-S. Lee, and D. R. Paul, "Rheological studies of disulfonated poly(arylene ether sulfone) plasticized with poly(ethylene glycol) for membrane formation," *Polymer,* vol. 55, no. 6, pp. 1574-1582, 2014.

[2] H. J. Oh, B. D. Freeman, J. E. McGrath, C. H. Lee, and D. R. Paul, "Thermal analysis of disulfonated poly(arylene ether sulfone) plasticized with poly(ethylene glycol) for membrane formation," *Polymer* vol. 55, no. 1, pp. 235-247, 2014.

[3] W. Xie, J. Cook, H. B. Park, B. D. Freeman, C. H. Lee, and J. E. McGrath, "Fundamental salt and water transport properties in directly copolymerized disulfonated poly(arylene ether sulfone) random copolymer," *Polymer,* vol. 52, no. 9, pp. 2244-2254, 2011.

[4] H. Yasuda, C. E. Lamaze, and L. D. Ikenberry, "Permeability of solutes through hydrated polymer membranes. Part I. Diffusion of sodium chloride," *Die Makromolekulare Chemie,* vol. 18, no. 1, pp. 19-35, 1968.

[5] H. Ju, A. C. Sagle, B. D. Freeman, J. I. Mardel, and A. J. Hill, "Characterization of sodium chloride and water transport in crosslinked poly(ethylene oxide) hydrogels," *Journal of Membrane Science,* vol. 358, no. 1-2, pp. 131-141, 2010.

[6] W. Xie, H. Ju, G. M. Geise, B. D. Freeman, J. I. Mardel, A. J. Hill, and J. E. McGrath, "Effect of free volume on water and salt transport properties in directly copolymerized disulfonated poly(arylene ether sulfone) random copolymers," *Macromolecules,* vol. 44, no. 11, pp. 4428-4438, 2011.

[7] G. M. Geise, C. L. Willis, C. M. Doherty, A. J. Hill, T. J. Bastow, J. Ford, K. I. Winey, B. D. Freeman, and D. R. Paul, "Characterization of Aluminum-Neutralized Sulfonated Styrenic Pentablock Copolymer Films," *Industrial & Engineering Chemistry Research* vol. 52, no. 3, pp. 1056-1068, 2013.

[8] P. R. Bevington, and D. K. Robinson, *Data reduction and error analysis for the physical sciences*, p.^pp. 43-44, 146-148, 194-217, McGraw Hill, 2003.

[9] C. E. Evans, R. D. Noble, S. Nazeri-Thompson, B. Nazeri, and C. A. Koval, "Role of conditioning on water uptake and hydraulic permeability of Nafion membranes," *Journal of Membrane Science,* vol. 279, pp. 521-528, 2006.

[10] N. P. Berezina, S. V. Timofeev, and N. A. Kononenko, "Effect of conditioning techniques of perfluorinated sulphocationic membranes on their hydrophylic and electrotransport properties," *Journal of Membrane Science,* vol. 209, pp. 509-518, 2002.

[11] J. E. Hensley, J. D. Way, S. F. Dec, and K. D. Abney, "The effects of thermal annealing on commercial Nafion membranes," *Journal of Membrane Science,* vol. 298, pp. 190-201, 2007.

[12] W. Xie, G. M. Geise, B. D. Freeman, C. H. Lee, and J. E. McGrath, "Influence of processing history on water and salt transport properties of disulfonated polysulfone random copolymers," *Polymer,* vol. 53, no. 7, pp. 1581-1592, 2012.

[13] W. Xie, J. Cook, H. B. Park, B. D. Freeman, C. H. Lee, and J. E. McGrath, "Advances in membrane materials: desalination membranes based on directly copolymerized disulfonated poly(arylene ether sulfone) random copolymers," *Water Science and Technology : a Journal of the International Association on Water Pollution Research,* vol. 61, no. 3, pp. 619-624, 2010.

[14] G. M. Geise, H. B. Park, A. C. Sagle, B. D. Freeman, and J. E. McGrath, "Water permeability and water/salt selectivity tradeoff in polymers for desalination," *Journal of Membrane Science,* vol. 369, pp. 130-138, 2011.

[15] G. M. Geise, H.-S. Lee, D. J. Miller, B. D. Freeman, J. E. McGrath, and D. R. Paul, "Water purification by membranes: the role of polymer science," *Journal of Polymer Science Part B: Polymer Physics,* vol. 48, no. 15, pp. 1685-1718, 2010.

[16] H. B. Park, B. D. Freeman, Z.-B. Zhang, M. Sankir, and J. E. McGrath, "Highly chlorine-tolerant polymers for desalination," *Angewandte Chemie International Edition* vol. 47, no. 32, pp. 6019-6024, 2008.

[17] D. M. Stevens, B. Mickols, and C. V. Funk, "Asymmetric reverse osmosis sulfonated poly(arylene ether sulfone) copolymer membranes," *Journal of Membrane Science,* vol. 452, pp. 193-202, 2014.

Chapter 10: Identification of Poly(ethylene glycol) Extraction Media other than Water

10.1 INTRODUCTION

In the previous chapter, we demonstrated that processing history has a great impact on water and salt transport properties of BPS polymers. Initially, only water was used to extract PEG from the extruded BPS/PEG films, since PEG is water soluble. Water is a swelling solvent for BPS films, since the BPS-20K used in this study has an average water uptake of 7-8 wt%. Also, as sulfonation level increases to 60 mol% (i.e., BPS-60K), water uptake increases to 67 wt% [1]. This swelling characteristic may influence free volume size and distribution throughout the extruded/extracted BPS films after PEG extraction. Therefore, in this chapter, to understand the effect of processing history clearly, we identified different PEG extraction mediums other than water for further studies.

10.2 RESULTS AND DISCUSSION

Several PEG extraction media other than water were identified: 1) a relatively non-swelling solvent (i.e., solvent uptake less than that of water), 2) a swelling solvent (i.e., solvent uptake similar to that of water), and 3) a highly swelling solvent (i.e., solvent uptake higher than that of water). PEG should be soluble in these solvents to allow PEG extraction after extrusion.

PEG is soluble in water, alcohols, chloroform, glycol ethers, aliphatic ketones, aliphatic hydrocarbons, esters, etc. [2, 3]. Sulfonated polysulfones are reported to be swollen by several solvents such as dioxane, methyl ethyl ketone, etc.[4]. Based on literature reviews, solvent sorption experiments were conducted using candidate extraction media, as shown in Table 10.1, to measure solvent mass uptake (wt%). The solvent mass uptake was converted to volume fraction of solvent in the swollen polymer by using the pure solvent and polymer densities (details in Chapter 3.5.2).

Solution cast BPS-20K films were prepared and cut into circular coupons with a diameter of 2.2 cm and thicknesses of 30-50 μm. These membrane coupons were dried at 110 °C for 2 days in a vacuum oven to remove residual water. The dried mass of each coupon was measured in an analytical balance before immersing in a solvent, and the wet mass was measured every 2-6 hours until a constant solvent mass uptake was reached. The total soaking time of a coupon in a solvent was 2-5 days, depending on the solvent. After a constant solvent mass uptake was obtained, the coupons were dried at 110 °C in a vacuum oven for 1-2 days to remove most of the residual solvent. FT-IR analysis and ^{1}H NMR analysis were conducted to verify that no chemical structure change occurred during the solvent soaking steps.

As shown in Table 10.1, some samples were deformed or dissolved during the solvent exposure experiments, and these solvents were removed from further studies. When BPS-20K membrane coupons were soaked in solvents such as acetone, which had a higher solvent uptake than water, the coupons were deformed and broken into pieces due to rapid swelling. Among the solvents which showed similar solvent volume fraction in swollen BPS-20K polymer, solvents which were less toxic and less costly were selected for further studies.

Table 10.1 Candidate solvents for PEG extraction

Solvent	Volume fraction of solvent in swollen BPS-20K polymer	Chemical structural change by FT-IR and ^{1}H NMR
Water	0.10 ± 0.03	No change
Methanol	0.11 ± 0.00	No change
Ethanol	0.13 ± 0.01	No change
Tetrahydrofuran (THF)	0.23 ± 0.01	*
Chloroform	0.24 ± 0.00	*
Isopropyl alcohol (IPA)	0.00 ± 0.00	No change
Acetone	0.27 ± 0.01	*
Acetonitrile	0.15 ± 0.01	No change
Benzene	0.22 ± 0.00	No change
Ethylene glycol (EG)	0.25 ± 0.02	Coupon
1,2, dichloroethane	0.16 ± 0.01	No change
1,2 dichlorobenzene	More than 0.24	**
Dioxane	More than 0.34	*
4/1 1,2-dichloroethane/IPA	0.19 ± 0.02	No change
Diethylene glycol dimethyl ether	Unable to measure	**
Ethyl acetate	0.28 ± 0.04	Not tested

*Coupon was deformed

** Equilibrium was not reached within 3 days

***Coupon dissolved

Based on the sorption experiments, three candidate solvents were selected as shown in Table 10.2, and their fundamental properties are summarized therein. Isopropyl alcohol (IPA) was chosen as a non-swelling solvent to BPS-20K (i.e., solvent uptake is lower than that of water), methanol exhibits similar solvent uptake than that of water, and finally ethanol exhibits higher uptake than that of water.

After soaking BPS-20K coupons in these solvents for 2-3 days, there was no structural change detected by FT-IR and ^{1}H NMR analyses. FT-IR spectra are shown in Figure 10.1, and ^{1}H NMR analyses are not shown here for brevity. Most of the selected solvents can be removed by drying at 110 °C in a vacuum oven for 24 hours, and this drying protocol was used in further studies.

Table 10.2 Three candidate solvents for PEG extraction

Classification	Solvent	Average volume fraction of solvent in swollen polymer	MW [a] [g/mol]	Density [a] [g/cm^3]	Boiling point[a] [°C]	Solubility parameter [MPa$^{1/2}$][b]
Water	Water	0.10	18	1	100	47.8
Lower than water	Isopropyl alcohol (IPA)	0.00	60	0.79	82	23.6
Similar to water	Methanol	0.11	32	0.79	65	29.6
Higher than water	Ethanol	0.13	46	0.79	78	26.5

[a] Data from Material Safety Data Sheet (MSDS) provided by manufacturers. Isopropyl alcohol (Cat# A416, certified ACS plus, Fisher Scientific, Waltham, MA) [5], methanol (Cat# A412, certified AVS, Fisher Scientific) [6], ethanol (Cat# 111000200, 200 proof anhydrous absolute PHARMCO-AAPER, Brookfield, CT) [7]

[b] Solubility parameter from Ref. [8]

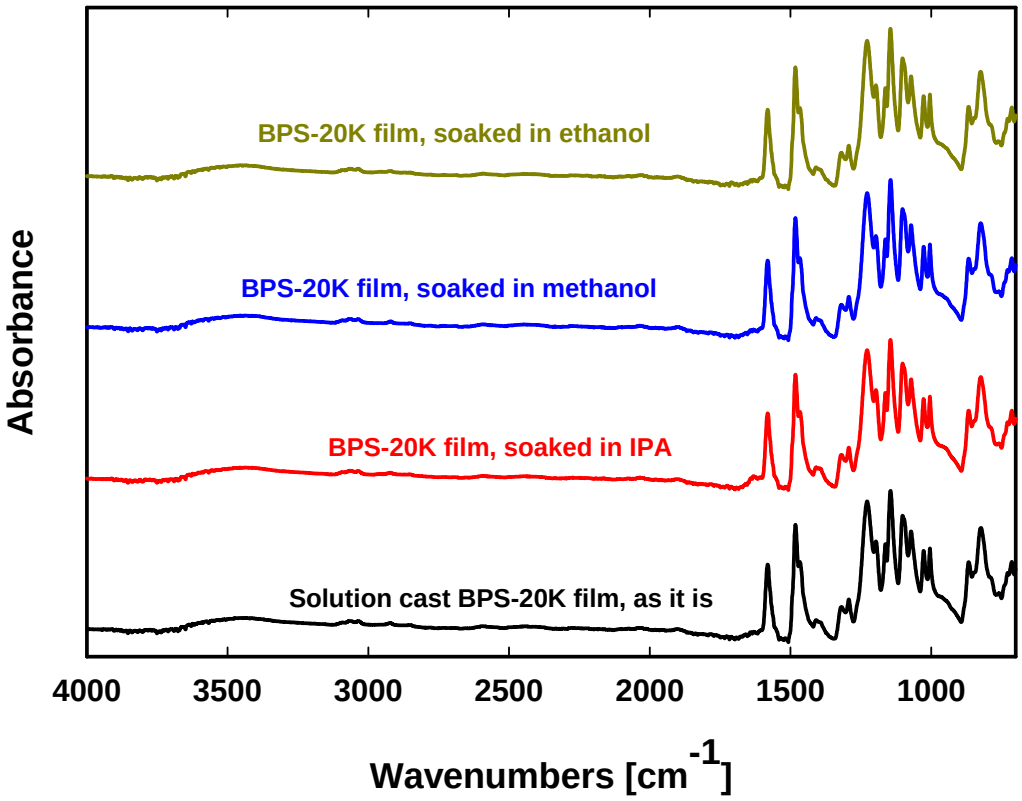

Figure 10.1 FT-IR (ATR mode) spectra of solution cast BPS-20K films after soaking in different solvents for 2-3 days and drying at 110 °C for 24 hours in a vacuum oven. FT-IR spectra are displaced vertically for easier viewing.

10.3 Conclusions

Three candidate solvents were selected to understand the effect of PEG extraction medium on the final properties of extruded BPS films. Isopropyl alcohol (IPA) was chosen as a non-swelling solvent for BPS-20K (i.e., solvent uptake is lower than that of water), methanol shows similar solvent uptake to that of water, and ethanol exhibits higher uptake than water. These solvents can be used for further studies to investigate the effect of processing history on the water and salt transport properties of extruded BPS films.

10.4 References

[1] F. Wang, M. Hickner, Y. S. Kim, T. A. Zawodzinski, and J. E. McGrath, “Direct polymerization of sulfonated poly(arylene ether sulfone) random(statistical)

copolymer: candidates for next proton exchange membranes," *Journal of Membrane Science,* vol. 197, no. 1-2, pp. 231-242, 2002.

[2] http://www.fao.org/ag/agn/jecfa-additives/specs/Monograph1/Additive-316.pdf.

[3] F. E. Bailey JR., and J. V. Koleske, *Poly(ethylene oxide)*, New York, U.S.A.: Academic Press, 1976.

[4] A. Noshay, and L. M. Robeson, "Sulfonated polysulfone," *Journal of Applied Polymer Science,* vol. 20, pp. 1885-1903, 1976.

[5] http://www.fishersci.com/ecomm/servlet/fsproductdetail_10652_679275__-1_0.

[6] http://www.fishersci.com/ecomm/servlet/fsproductdetail_10652_673173__-1_0.

[7] http://www.capitolscientific.com/Pharmco-Aaper-111000200CSPP-Ethyl-Alcohol-200-Proof-HPLC-Grade-Assay-99-98-24x1-Pint.

[8] C. M. Hansen, *Hansen Solubility Parameters: A User's Handbook*, 2nd ed.: CRC Press, 2007.

Chapter 11: Conclusions and Recommendations[7]

11.1 CONCLUSIONS

This dissertation discusses the formation and transport property characterization of sulfonated polysulfone desalination membranes by melt processing. One route to melt processing of high glass transition temperature polyelectrolytes, such as disulfonated poly(arylene ether sulfone) (BPS), involves mixing a plasticizer with the polymer.

Particularly, this study examines the feasibility of composite membranes that might be useful for desalination prepared via coextrusion of BPS with a suitable support layer material, polypropylene (PP).

11.1.1 Glass transition of BPS plasticized with PEG

Poly (ethylene glycol) (PEG) is used here to modify the glass transition temperature and rheology of BPS to enable coextrusion with PP. PEGs with molecular weights ranging from 200 to 600 g/mol were chosen since they can be conveniently removed by water extraction after membrane extrusion.

BPS and PEG are miscible, and the effect of PEG molecular weight and concentration on the T_g of BPS/PEG blends were investigated. As PEG molecular weight decreases and concentration increases, the blend T_g was depressed significantly.

---

7 Parts of this chapter have been adapted from the following articles with permission:
(1) H. J. Oh, B. D. Freeman, J. E. McGrath, C. H. Lee, and D. R. Paul, "Thermal analysis of disulfonated poly(arylene ether sulfone) plasticized with poly(ethylene glycol) for membrane formation," *Polymer* vol. 55, pp. 235-247, 2014.
(2) H. J. Oh, B. D. Freeman, J. E. McGrath, C. J. Ellison, S. Mecham, K.-S. Lee, and D. R. Paul, "Rheological studies of disulfonated poly(arylene ether sulfone) plasticized with poly(ethylene glycol) for membrane formation," *Polymer,* vol. 55, pp. 1574-1582, 2014.

11.1.2 Thermal stability of BPS/PEG during melt processing and identification of melt processing temperature

Based on the T_g values obtained in the blends and the rule of thumb that melt processing is performed 50~100 °C above the T_g, the potential highest melt processing temperature needed would be in the range of 230 °C, based upon the T_g of BPS-20K plasticized with 20 wt% of PEG 600. Therefore, it was essential to explore the thermal stability of these BPS-20K/PEG blend as well as the thermal stability and volatility of low molar mass PEG oligomers, which are related to extrusion of such blends.

Based on the PEG 200 characterization after isothermal holds at various temperatures and times, these PEGs were found to be thermally stable up to 220 °C for at least 10 minutes in air or 250 °C for at least 10 minutes in nitrogen. This information was used to extrude the BPS/PEG blend for membrane formation.

11.1.3 Rheological studies of BPS/PEG for membrane formation

It is important to control the BPS/PEG rheology within a specific range for coextrusion with PP to achieve uniform thickness and defect-free membranes [1]. The effects of various factors including PEG molecular weight, concentration, temperature, BPS molecular weight and BPS sulfonation level on the complex viscosity of blends are investigated. At a fixed PEG concentration, the blend viscosity decreases with decreasing PEG $\bar{M}_n$ since shorter chain PEG molecules themselves have a lower viscosity are more effective plasticizers than higher molecular weight PEG [2-4]. Also, at a fixed PEG molecular weight, as the PEG concentration increases, the blend viscosity decreases as expected when a polymer is diluted with a low molecular weight solvent or plasticizer [3]. At a fixed blend composition, the viscosity decreases with increasing temperature, decreasing BPS molecular weight and decreasing BPS sulfonation level as expected.

All of the viscosity data are consistent with a single master curve, and this master curve was established by Bueche and Harding [5, 6] for non-associating polymers such as PMMA and PS. Although sulfonated polysulfone contains ionic groups, this plasticized sulfonated polysulfone follows the same shear thinning behavior as non-associating polymers, suggesting that its flow is dominated by the relaxation of polymer entanglements rather than by ionic interactions. The weight average molecular weights obtained from analysis of the rheological data are comparable to the values measured by SEC. Using the rheological data, conditions were identified for coextrusion of BPS/PEG blends with PP.

11.1.4 Preparation of single layer, BPS/PEG thin film membranes by extrusion

The single layer, extruded membrane of BPS-20K/PEG blends were prepared using a twin screw micro-compounder and attached film die. Various factors that influence the film characteristics were identified and carefully adjusted to obtain reproducible films. These factors include the BPS-20K molecular weights, PEG molecular weight, PEG concentration, processing temperature, residence time in extruder, the film drawing speed and the winding torque of drums. As a result, the defect-free, thin films of uniform thickness in the range of 30~50 μm, as similar to those of solution cast BPS-20K films, were prepared.

Some of BPS-20K/PEG 20 wt% extruded films are foggy and rather opaque, and studies to identify the reason for opaqueness were conducted. However, no evidence of crystallization, phase separation, or micro-voids was found and further investigations such as SAXS are required for clear identification. This whitening effect of some extruded films has been tried to be reduced by adjusting the processing conditions. However, within the potential processing temperature range below the any thermal degradation limits as reported previously [2], the whitening effect was unavoidable.

11.1.5 Kinetics of PEG extraction from extruded BPS/PEG membranes

PEG must be extracted from extruded BPS-20K/PEG films before their use as a membrane [7]. Since PEG is highly water soluble, it can, in principle, be extracted in water after melt extrusion [8, 9]. For this reason, examination of the factors influencing diffusion of PEG from these films is essential to optimize this route to membrane preparation. The rate of PEG extraction is expected to be affected by molecular weight ($\overline{M}_n$) and concentration (wt%) of PEG in the extruded BPS-20K/PEG films, as well as the temperature. Such extraction studies are described here, and Fickian models were used to analyze the kinetics of PEG extraction.

The early time approximation and complete solution of Fickian model were used to analyze the kinetic desorption of PEG materials from the extruded films and were found to fit well with the data. The diffusion coefficients of the PEG materials obtained from these analyses were well correlated with temperature and follow the Arrhenius equation.

Moreover, as expected, the PEG extraction kinetics are faster at higher temperatures, demonstrating that the diffusion coefficient of PEG materials is higher at higher temperatures. Also, at a fixed temperature, the PEG extraction kinetics are more rapid with decreasing PEG molecular weight ($\overline{M}_n$), and the ΔE_D values slightly decrease accordingly, since shorter chain PEG molecules (i.e., smaller penetrant size) have higher diffusion coefficients. Moreover, at the fixed PEG molecular weight ($\overline{M}_n$) of 200 g/mol, the PEG extraction kinetics were more rapid at higher PEG concentration (wt%) between 20 wt% and 30 wt%.

All PEG materials were successfully extracted from extruded BPS-20K/PEG thin films after melt extrusion. This information can be useful to optimize the extraction protocol of extruded membranes for desalination applications.

11.1.6 Water and salt transport properties of extruded BPS membranes

BPS-20K membranes were prepared by different preparation paths in terms of processing methods (i.e., solution casting vs. melt extrusion), PEG composition (molecular weight, $\bar{M}_n$: 200~400 g/mol and concentration 20~30 wt%) during melt extrusion, and PEG extraction temperatures (23 °C, 50 °C and 75 °C) after melt extrusion to investigate the influence of these preparation variables on the transport properties of BPS membranes.

The extruded/extracted BPS-20K films show higher water uptake than those of solution cast membranes. As PEG molecular weight and concentration used during extrusion increases and as PEG extraction temperature increases, water uptake (and water solubility) increases. As water uptake increases, water and salt permeabilities and diffusivities increase, consistent with Yasuda et al.'s findings.

Compared to the increase of water and salt transport properties as PEG molecular weight increases from 200 g/mol to 400 g/mol, the water and salt transport property increases induced by increasing PEG concentration (i.e., from 20 wt% to 30 wt%) are larger. By immersing the same films at higher temperature, i.e., 75 °C, water uptake increase by 40 %.

Compared to solution cast BPS-20K films, extruded BPS-20K films prepared by different routes show different water and salt transport properties. To understand the origin of this difference, ^{1}H NMR analysis and FT-IR analysis were conducted but no chemical structural change was detected. The water and salt transport properties of a re-cast ("extrusion → solution") sample are in a similar range as those of solution processed sample, indicating that different processing history affects the transport properties.

Different processing methods have a significant effect on the structure of BPS polymers. PEG extraction from extruded BPS films generates additional free volume (i.e.,

higher water uptake), and this additional free volume is likely not to recover to the level of free volume of solution processed samples.

11.1.7 Identification of PEG extraction mediums other than water

Three candidate solvents were selected to understand the effect of PEG extraction medium on the final properties of extruded BPS films. Isopropyl alcohol (IPA) was chosen as a non-swelling solvent for BPS-20K (i.e., solvent uptake is lower than that of water), methanol shows similar solvent uptake to that of water, and ethanol exhibits higher uptake than water. These solvents can be used for further studies to investigate the effect of processing history on the water and salt transport properties of extruded BPS films.

11.2 RECOMMENDATIONS

11.2.1 Effects of PEG extraction media on the water and salt transport properties of extruded BPS films

As described in Chapter 10, other PEG extraction media other than water, such as IPA, ethanol, and/or methanol can be used for PEG extraction, and use of different PEG extraction media may change the microstructure of polymers, thus, leading to different water and salt transport properties.

11.2.2 Effects of other factors that influence the microstructure of BPS prepared by melt processing

11.2.2.1 Effect of BPS sulfonation level

In this study, we mainly have used 20 mol% disulfonated poly(arylene ether sulfone) random copolymers (i.e., BPS-20K) since it has a good balance of thermal stability and membrane performance [10-13]. The BPS with other sulfonation level (10-60 mol%) are also available [12], but the BPS with a sulfonation level range from 10 mol% to 35 mol% can be the materials of interest owing to their good transport properties: their

characteristics are reported in Table 11.1. The water and salt transport properties of BPS-10K have not been reported previously, and, thus, their characteristics were not included in Table 11.1. However, based on a general trend that as sulfonation level increases, water uptake and water and salt permeabilities increase, whereas NaCl rejection decreases, BPS-10K is expected to have lower water uptake and water and salt permeabilities and higher NaCl rejection.

Table 11.1 Characteristics of BPS polymer of different sulfonation level. All data are from Table 1 from Ref. [13]

Material	IEC [a] [meq/g]	Water uptake [%]	Water Permeability[b] [L μm m^{-2} h^{-1} bar^{-1}]	NaCl rejection[c] [%]	NaCl permeability[d] [10^{-8} cm^2/s]
BPS-20K	0.92	4.5	0.03	99.2	0.004
BPS-30K	1.34	9.1	0.17	96.2	0.3
BPS-35K	1.52	12.3	0.34	94.3	0.9

[a] Determined by ^{1}H NMR spectroscopy

[b] Measured by constant pressure trans-membrane crossflow filtration system at 25 °C. feed pressure was 27.6 bar

[c] Measured by constant pressure trans-membrane crossflow filtration system at 25 °C. feed pressure was 27.6 bar, feed concentration was 2,000 ppm, feed flow rate was 3.0 L/min, and Reynolds number, Re, was 3747)

[d] Measured by kinetic desorption experiments at 25 °C

The glass transition temperatures (T_g) of BPS decrease with decreasing sulfonation level [12], and, thus, BPS-10K is expected to show an easier melt processability. Also, the $T_{5\%}$ [°C], the 5 % weight loss temperature by TGA, is higher with decreasing sulfonation level [12], so BPS-10K is likely to have a stronger thermal stability during melt extrusion. Moreover, BPS-10K shows high NaCl rejection and low water permeability, and, thus, BPS-10K may be a good candidate for melt extrusion, since the addition of free volume by PEG extraction may help increase the water permeability.

BPS with higher sulfonation level has higher T_g, and lower $T_{5\%}$, indicating a difficult melt processability. However, BPS-32K was able to be melt extruded based on our preliminary experiments and might generate reproducible thin films by adjusting processing conditions. By using the BPS of different sulfonation level (10~35 mol%) and a similar molecular weight range, the effect of sulfonation level on the microstructure of extruded films can be investigated. The varied contents of ionic groups in the polymer matrix may generate different microstructures in the extruded films. This microstructural change can be correlated to the transport properties as well as thermal and mechanical properties of membranes.

11.2.2.2 Effect of different plasticizers

The PEG materials (molecular weight: 200~600 g/mol) have been mainly used to modify the glass transition temperature and viscosity of BPS in this study. As mentioned in the Chapter 2 (details in chapter 2.1.2.1), plasticizers of different polarity may exhibit different degrees of effects when plasticizing the polymer backbone and/or the ionic groups [14-17]. It has been suggested by Lundberg [14, 16] and others [14, 17, 18], the plasticizers with lower dielectric constant (i.e., more lipophilic or less polar), have a tendency to lower the polymer matrix T_g; however, the plasticizers with higher dielectric constant (i.e., less lipophilic or more polar) tend to interact with ionic groups. Therefore, different plasticizer type may generate different level of free volume or microstructural change when they are extracted after extrusion. This information can be correlated to the transport properties of BPS films after plasticizer extraction.

11.2.3 Coextrusion with PP

Effect of multi layering structure on water/salt transport properties

The multilayered membranes can be prepared using a microlayering coextrusion process at Case Western Reserve University. Figure 1.5 shows the multilayer coextrusion system for two components and the system consists of several extruders and multiplying dies, etc.[1, 19]. By using this system, multilayered membranes with at least two layers up to even thousands layers, where the thickness of each layer can be as thin as 100 nm, can be prepared. More details about the system are reported in previous literature [1, 19, 20]. Transport properties of multilayer structures can be different from those of single layer films, and the effect of confinement and others can be identified.

11.3 REFERENCES

[1] M. T. Ponting, A. Hiltner, and E. Baer, "Polymer nanostructures by forced assembly: process, structure, and properties," *Macromolecular Symposia,* vol. 294, no. 1, pp. 19-32, 2010.

[2] H. J. Oh, B. D. Freeman, J. E. McGrath, C. H. Lee, and D. R. Paul, "Thermal analysis of disulfonated poly(arylene ether sulfone) plasticized with poly(ethylene glycol) for membrane formation," *Polymer* vol. 55, no. 1, pp. 235-247, 2014.

[3] A. Eisenberg, and J. S. Kim, "Plasticization," *Introduction to ionomers*, pp. 244-256, Canada: John Wiley & Sons, Inc., 1998.

[4] A. J. Curtis, "Dielectric properties of polymeric systems," *Progress in dielectrics*, J. B. Birks and J. H. Schulman, eds., pp. 31-76, Hertfordshire, UK: Heywood & Company Ltd., 1960.

[5] D. R. Paul, "A study of spinnability in the wet-spinning of acrylic fibers," *Journal of Applied Polymer Science,* vol. 12, pp. 2273-2298, 1968.

[6] F. Bueche, and S. W. Harding, "A new absolute molecular weight method for linear polymers," *Journal of Polymer Science,* vol. 32, pp. 177-186, 1958.

[7] R. A. Register, and R. K. Prud'homme, "Melt rheology," *Ionomers*, M. R. Tant, K. A. Mauritz and G. L. Wilkes, eds., pp. 208-260: Blackie Academic & Professional, 1997.

[8] J.-Y. Sanchez, F. Chabert, C. Iojoiu, J. Salomon, N. E. Kissi, Y. Piffard, M. Marechal, H. Galiano, and R. Mercier, "Extrusion: an environmentally friendly process for PEMFC membrane elaboration," *Electrochimica Acta,* vol. 53, no. 4, pp. 1584-1594, 2007.

[9] Y. Molmeret, F. Chabert, N. E. Kissi, C. Iojoiu, R. Mercier, and J.-Y. Sanchez, "Toward extrusion of ionomers to process fuel cell membranes," *Polymers,* vol. 3, no. 3, pp. 1126-1150, 2011.

[10] W. Xie, J. Cook, H. B. Park, B. D. Freeman, C. H. Lee, and J. E. McGrath, "Advances in membrane materials: desalination membranes based on directly copolymerized disulfonated poly(arylene ether sulfone) random copolymers," *Water Science and Technology : a Journal of the International Association on Water Pollution Research,* vol. 61, no. 3, pp. 619-624, 2010.

[11] W. Xie, J. Cook, H. B. Park, B. D. Freeman, C. H. Lee, and J. E. McGrath, "Fundamental salt and water transport properties in directly copolymerized disulfonated poly(arylene ether sulfone) random copolymer," *Polymer,* vol. 52, no. 9, pp. 2244-2254, 2011.

[12] F. Wang, M. Hickner, Y. S. Kim, T. A. Zawodzinski, and J. E. McGrath, "Direct polymerization of sulfonated poly(arylene ether sulfone) random(statistical) copolymer: candidates for next proton exchange membranes," *Journal of Membrane Science,* vol. 197, no. 1-2, pp. 231-242, 2002.

[13] H. B. Park, B. D. Freeman, Z.-B. Zhang, M. Sankir, and J. E. McGrath, "Highly chlorine-tolerant polymers for desalination," *Angewandte Chemie International Edition* vol. 47, no. 32, pp. 6019-6024, 2008.

[14] A. Eisenberg, and J. S. Kim, "Introduction to ionomers," pp. 1-16, 30-31, 38-85, 114-117, 244-266: John Wiley & Sons, Inc., 1998.

[15] J. S. Kim, and A. Eisenberg, "Ion aggregation and its effect on ionomer properties," *Ionomers: characterization, theory and applications*, S. Schlick, ed., pp. 7-34: CRC Press, Inc., 1996.

[16] R. D. Lundberg, and H. S. Makowski, "The dual plasticization of sulfonated polystyrene ionomer," *Ions in Polymers*, A. Eisenberg, ed., pp. 67-76, Washington DC, USA: American Chemical Society, 1980.

[17] M. Drzewinski, and W. J. MacKnight, "Structure and properties of sulfonated polysulfone ionomers," *Journal of Applied Polymer Science,* vol. 30, no. 12, pp. 4753-4770, 1985.

[18] R. D. Lundberg, H. S. Makowski, and L. Westerman, *Ionic polymer plasticized with preferential plasticizers*, United States Patent No. 4 014 847, 1977.

[19] M. T. Ponting, "Gradient multilayered films & confined crystallization of polymer nanolayers by forced assembly coextrusion," Ph.D. Dissertation, Department of Macromolecular Science & Engineering, Case Western Reserve University, 2010.

[20] M. T. Ponting, Y. Lin, J. K. Keum, A. Hiltner, and E. Baer, "Effect of substrate on the isothermal crystallization kinetics of confined poly(ε–caprolactone) nanolayers," *Macromolecules,* vol. 43, no. 20, pp. 8619-8627, 2010.

Bibliography

"Archimedes' Principle, Http://Www.Britannica.Com/Ebchecked/Topic/32827/Archimedes-Principle".

Abdel-Jawad, M., S. Ebrahim, M. Al-Tabtabaei and S. Al-Shammari. "Advanced Technologies for Municipal Wastewater Purification: Technical and Economic Assessment." *Desalination* 124, no. 1-3 (1999): 251–261.

Al-Hadithi, T. S. R., H. A. Barnes and K. Walters. "The Relationship between the Linear (Oscillatory) and Nonlinear (Steady-State) Flow Properties of a Series of Polymer and Colloidal Systems." *Colloid and Polymer Science* 270, no. 1 (1992): 40-46.

Allen, G. , J. McAinsh and G. M. Jeffs. "Relaxation Phenomena in Some Aromatic Polymers: Effect of Water Content on the Low Temperature Relaxation." *Polymer* 12, no. 2 (1971): 85-100.

American Society of Metals. *Characterization and Failure Analysis of Plastics*: ASM International.

Bagrodia, S. and G. L. Wilkes. "Comments on the Effect of Cation, Type on Ionomer Properties." *Polymer Bulletin* 12, no. 5 (1984): 389-392.

Bailey Jr., F. E. and J. V. Koleske. *Poly(Ethylene Oxide)*. New York, U.S.A.: Academic Press, 1976.

Baker, R. W. "Vapor and Gas Separation by Membranes." In *Advanced Membrane Technology and Applications*, edited by N. N. Li, A. G. Fane, W. S. Ho and T. Matsuura, 562-563: John Wiley & Sons, Inc., 2008.

Baker, R. W. *Membrane Technology and Applications*. 3rd ed. West Sussex, United Kingdom: John Wiley and Sons Ltd, 2012.

Baker, R. W. and J. G. Wijmans. "Membrane Separation of Organic Vapors from Gas Streams." In *Polymeric Gas Separation Membranes*, edited by D. R. Paul and Y. P. Yampol'skii, 353-397. Boca Raton, FL.: CRC Press, 1994.

Barnes, H. A. and J. F. Hutton. "An Introduction to Rheology." 11-35: Wlsevier, 1989.

Bebin, P. and H. Galiano. "Processing of PEMFC Membranes by Extrusion: Part 1. Sulfonated Polysulfone in Acid Form." *Advances in Polymer Technology* 25, no. 2 (2006): 121-126.

Bebin, P. and H. Galiano. "Processing of Sulfonated Polysulfone for PEMFC Membrane Applications: Part 2. Polymer in Salt Form." *Advances in Polymer Technology* 25, no. 2 (2006): 127-133.

Berezina, N. P., S. V. Timofeev and N. A. Kononenko. "Effect of Conditioning Techniques of Perfluorinated Sulphocationic Membranes on Their Hydrophylic and Electrotransport Properties." *Journal of Membrane Science* 209, (2002): 509-518.

Bevington, P. R. and D. K. Robinson. *Data Reduction and Error Analysis for the Physical Sciences*, Edited by 3rd ed. McGraw Hill, 2003.

Bhargava, S. and S. L. Cooper. "Effect of Water on Viscosity and Shear-Thickening Behavior of Telechelic Ionomers in Nonpolar Solvents." *Macromolecules* 31, no. 2 (1998): 508–514.

Bigger, S. W., J. Scheirs Delatycki and N. C. Billingham. "Effect of Frequency, Molecular Weight and Thermal Oxidation on the Dynamic Mechanical Response of Poly(Ethylene Oxide)." *Polymer International* 26, no. 3 (1991): 181-186.

Bonotto, S. and E. F. Bonner. "Effect of Ion Valency on the Bulk Physical Properties of Salt of Ethylene-Acylyic Acid Copolymers." *Macromolecules* 1, (1968): 510-515.

Boris, D. C. and R. H. Bolby. "Rheology of Sulfonated Polystyrene Solutions." *Macromolecules* 31, (1998): 5746-5755.

Bozzelli, J. "Eliminate Bubbles, Voids, Sinks & Blisters " In *Plastics Industry Articles* http://articles.ides.com/processing/jb_sinks_bubbles.asp.

Brenner, D and A. A. Osward. "Effect of Counterion Structure on Ionomer Properties: Quaternary Phosphonium Counterions in Sulfonated Epdm." In *Ions in Polymers*, edited by A Eisenberg, 53-66. Washington DC, USA: American Chemical Society, 1980.

Broze, G., R. Jerome and P. Teyssie. "Halato-Telechelic Polymers. Vii. Viscoelastic Behavior of α,Ω-Divalent Cation Dicarboxylato Polybutadiene." *Journal of Polymer Science: Polymer Physics Edition* 21, (1983): 2205-2217.

Bueche, F. "Non-Newtonian Viscosity of Synthetic Rubber and Its Solutions." *Journal of Applied Physics* 30, no. 7 (1959): 1114.

Bueche, F. "Physical Properties of Polymer." 88-107. New York: Interscience Publishers, 1962.

Bueche, F. and S. W. Harding. "A New Absolute Molecular Weight Method for Linear Polymers." *Journal of Polymer Science* 32, (1958): 177-186.

Cabane, B. "Structure of Some Polymer-Detergent Aggregates in Water." *The Journal of Physical Chemistry* 81, no. 17 (1977): 1639-1645.

Canter, N. H. and D. J. Beckley. "Preferential Plasticization of Ionometric Compounds ". United States Patent No. 3 847 854, 1974.

Carslaw, H. S. and J. C. Jaeger. *Conduction of Heat in Solids*: Clarendon Press, 1986.

Ceccorulli, G., M. Pizzoli, M. Scandola, G. C. Alfonso and A. Turturro. "Dynamic Mechanical Relaxations of Poly(Vinylidene Fluoride)-Poly(Vinylpyrrolidone) Blends." *Polymer* 30, no. 7 (1989): 1251-1256.

Chen, L., C-y. Sheng, Y-x. Duan and J-m. Zhang. "Morphology, Microstructure and Properties of Peg-Plasticized Pvc." *Polymer-Plastic Technology and Engineering* 50, (2011): 412-417.

Connor, T. M., B. E. Read and G Williams. "The Dielectric, Dynamic Mechanical, and Nuclear Resonance Properties of Poly(Ethylene Oxide) as a Function of Molecular Weight." *Journal of Applied Chemistry* 14, no. 2 (1964): 74-80.

Cooper, W. "Copolymers of Butadiene and Unsaturated Acids: Crosslinking by Metal Oxides." *Journal of Polymer Science* 28, (1958): 195-206.

Cooper, W. "Ionic Interchange Reactions with Metal Salts of Copolymers from Butadiene and Unsaturated Acids." *Journal of Polymer Science* 28, no. 195 (1958): 628-629.

Cowie, J. M. G. and V. Arrighi. "Miscibility and Relaxation Processes in Blends." In *Polymer Blends and Alloys*, edited by G. O. Shonaike and G. P. Simon, 81-124. New York, USA: Marcel Dekker, Inc., 1999.

Cox, W. P. and E. H. Merz. "Correlation of Dynamic and Steady Flow Viscosities." *Journal of Polymer Science* 28, no. 119 (1958): 619-622.

Craig, D. Q. M. "A Review of Thermal Methods Used for the Analysis of the Crystal Form, Solution Thermodynamics and Glass Transition Behavior of Polyethylene Glycols." *Thermochimica Acta* 248, (1995): 189-203.

Crank, J. "4. Diffusion in a Plane Sheet." In *The Mathematics of Diffusion*, 44-68: Oxford Science Publications, 1956.

Curtis, A. J. "Dielectric Properties of Polymeric Systems." In *Progress in Dielectrics*, edited by J. B. Birks and J. H. Schulman, 2, 31-76. Hertfordshire, UK: Heywood & Company Ltd., 1960.

Czichos, H., T. Saito and H. Smith. *Springer Handbook of Materials Measurement Methods*: Springer.

D'Agostino, R. B. *Goodness-of-Fit-Techniques*: CRC Press, 1986.

Dealy, J. H. and K. F. Wissbrun. "Melt Rheology and Its Role in Plastic Processing: Theory and Applications." 74-80, 159-170: Van Nostrand Reinhold, 1990.

Dionisio, M., A. C. Fernandes, J. F. Mano, N. T. Correia and R. C. Sousa. "Relaxation Studies in Peo/Pmma Blends." *Macromolecules* 33, no. 3 (2000): 1002-1011.

Dorobny, J. G. *Handbook of Thermoplastic Elstomers*: Plastics Design Library, 2007.

Drzewinski, M and W. J. MacKnight. "Structure and Properties of Sulfonated Polysulfone Ionomers." *Journal of Applied Polymer Science* 30, no. 12 (1985): 4753-4770.

"Dsm Xplore Micro Film Device, Http://Www.Xplore-Together.Com/Microfilm-Device.Html".

Dutta, P., S. Sen, S. Mukherjee and K. Bhattacharyya. "Solvation Dynamics of Tns in Polymer (Peg)-Surfactant (Sds) Aggregate " *Chemical Physics Letters* 359, (2002): 15-21.

Duvdevani, I., R. D. Lundberg, C. Wood-Cordova and G. L. Wilkes. "Modification of Ionic Associations by Crystalline Polar Additives." In *Coulombic Interactions in Macromolecular System*, edited by A Eisenberg and F. E. Bailey, 184-200. Washington DC, USA: American Chemical Society, 1986.

Eisenberg, A and J. S. Kim. "Introduction to Ionomers." 1-16, 30-31, 38-85, 114-117, 244-266: John Wiley & Sons, Inc., 1998.

Erb, A. J. and D. R. Paul. "Gas Sorption and Transport in Polysulfone." *Journal of Membrane Science* 8, (1981): 11-22.

Erhadrdt, P. E., J. M. O'Reilly, W. E. Richards and M. W. Williams. "Viscoelastic Behavior of Styrene/N-Butylmethacrylate/Potassium Metharcylate Polymers." *Journal of Polymer Science Symposium* 45, no. 1 (1974): 139-151.

Evans, C. E., R. D. Noble, S. Nazeri-Thompson, B. Nazeri and C. A. Koval. "Role of Conditioning on Water Uptake and Hydraulic Permeability of Nafion Membranes." *Journal of Membrane Science* 279, (2006): 521-528.

Faucher, J. A., J. V. Koleske, E. R. Santee, J. J. Stratta and C. W. Wilson. "Glass Transitions of Ethylene Oxide Polymers." *Journal of Applied Physics* 37, no. 11 (1966): 3962-3964.

Ferry, J. D. "Viscoelastic Properties of Polymers." New York: Wiley, 1980.

Fitzgerald, J. J. and R. A. Weiss. "The Effects of Low Molar Mass Diluents on the Microstructure of Ionomers." *Journal of Polymer Science Part B: Polymer Physics* 28, no. 10 (1990): 1719-1736.

Flory, P. J. "Thermodynamics of High Polymer Solutions." *Journal of Chemical Physics* 10, (1942): 51-61.

Foreman, J., S.R. Sauerbrunn and C. L. Marcozzi. *Exploring the Sensitivity of Thermal Analysis Techniques to the Glass Transition*. TA Instruments Inc.

Fouissac, E. , M. Milas and M. Rinauldo. "Shear-Rate, Concentration, Molecular Weight and Temperature Viscosity Dependences of Hyaluronate, a Wormlike Polyelectrolyte." *Macromolecules* 26, no. 25 (1993): 6945-6951.

Fox, T. G. and P. J. Flory. "Second-Order Transition Temperatures and Related Properties of Polystyrene. I. Influence of Molecular Weight." *Journal of Applied Physics* 21, (1950): 581-591.

Fox, T. G. and S. Loshaek. "Influence of Molecular Weight and Degree of Crosslinking on the Specific Volume and Glass Temperature of Polymers." *Journal of Polymer Science* 15, no. 80 (1955): 371-390.

Gaikwad, A. N., E. R. Wood, T Ngai and T. P. Lodge. "Two Calorimetric Glass Transitions in Miscible Blends Containing Poly(Ethylene Oxide)." *Macromolecules* 41, no. 7 (2008): 2502-2508.

Geise, G. M. "Water and Salt Transport Structure/Property Relationship in Polymer Membranes for Desalination and Power Generation Applications." University of Texas at Austin 2012.

Geise, G. M., H-S Lee, D. J Miller, B. D. Freeman, J. E. McGrath and D. R. Paul. "Water Purification by Membranes: The Role of Polymer Science." *Journal of Polymer Science Part B: Polymer Physics* 48, no. 15 (2010): 1685-1718.

Geise, G. M., L. P. Palcon, B. D. Freeman and D. R. Paul. "Sodium Chloride Sorption in Sulfonated Polymers for Membrane Applications." *Journal of Membrane Science* 423-424, (2012): 195-208.

Geise, G. M., H. B. Park, A. C. Sagle, B. D. Freeman and J. E. McGrath. "Water Permeability and Water/Salt Selectivity Tradeoff in Polymers for Desalination." *Journal of Membrane Science* 369, (2011): 130-138.

Geise, G. M., C. L. Willis, C. M. Doherty, A. J. Hill, T. J. Bastow, J. Ford, K. I. Winey, B. D. Freeman and D. R. Paul. "Characterization of Aluminum-Neutralized Sulfonated Styrenic Pentablock Copolymer Films." *Industrial & Engineering Chemistry Research* 52, no. 3 (2013): 1056-1068.

Ghious, N. and M. T. Benaniba. "The Effect of Epoxidized Sunflower Oil on the Miscibility of Plasticizer Pvc/Nbr Blends." *International Journal of Polymeric Materials* 59, no. 7 (2010): 463-474.

Ghosal, K., R. T. Chern and B. D. Freeman. "Gas Permeability of Radel a Polysulfone." *Journal of Polymer Science Part B: Polymer Physics* 31, no. 7 (1993): 891-893.

Glastrup, J. "Degradation of Polyethylene Glycol. A Study of the Reaction Mechanism in a Model Molecule: Tetraethylene Glycol." *Polymer Degradation and Stability* 52, no. 3 (1996): 217-222.

Graessley, W. W. "Viscosity of Entangling Polydisperse Polymers." *The Journal of Chemical Physics* 47, no. 6 (1967): 1942.

Han, M. and B. Han. "The Solubilization of N-Pentane Gas in Sodium Dodecyl Sulfate-Polyethylene Glycol Solutions with and without Electrolyte." *Journal of Colloid and Interface Science* 267, (2003): 173-177.

Han, S. C. Kim and D. Kwon. "Thermal/Oxidative Degradation and Stabilization of Polyethylene Glycol." *Polymer* 38, no. 2 (1997): 317-323.

Hansen, C. M. *Hansen Solubility Parameters: A User's Handbook*. 2nd ed.: CRC Press, 2007.

Heinzer, M., M. Lee, R. Van Houten, O. Lane, J. E. McGrath and D. G. Baird. "Effects of Solvent-Casting Conditions on the Morphology and Properties of Highly Fluorinated Poly(Arylene Ethersulfone) Copolymer Films for Polymer Electrolyte Membranes." *Annual Technical Conference - Society of Plastics Engineers* 67, (2009): 606-610.

Hensley, J. E., J. D. Way, S. F. Dec and K. D. Abney. "The Effects of Thermal Annealing on Commercial Nafion Membranes." *Journal of Membrane Science* 298, (2007): 190-201.

Hiemenz, P. C. and T. P. Lodge. "Glass Transition." In *Polymer Chemistry*, 494: CPC Press, 2007.

Hird, B. and A Eisenberg. "Copolymers of Butadiene and Unsaturated Acids: Crosslinking by Metal Oxides." *Macromolecules* 25, (1992): 6466-6474.

Hofmann, G. H. "Polymer Blend Modification of Pvc." In *Polymer Blends and Mixtures*, edited by D. J. Walsh and J. S. Higgins, 117-148. the Netherlands: Martinus Nijhoff Publishers, 1985.

http://articles.ides.com/processing/jb_sinks_bubbles.asp.

http://www.capitolscientific.com/Pharmco-Aaper-111000200CSPP-Ethyl-Alcohol-200-Proof-HPLC-Grade-Assay-99-98-24x1-Pint.

http://www.fao.org/ag/agn/jecfa-additives/specs/Monograph1/Additive-316.pdf.

http://www.fishersci.com/ecomm/servlet/fsproductdetail_10652_673173__-1_0.

http://www.fishersci.com/ecomm/servlet/fsproductdetail_10652_679275__-1_0.

http://www.xplore-together.com/products/micro-cast-film/fl35.

Huang, H.-H. and E. M. Yorkgitis. "A Morphological Study on the Plasticization of Poly(Vinyl Chloride) by Diethylhexyl Succinate and Dibutyl Phthalate." *Journal of Macromolecular Science, Physics* B32, no. 2 (1993): 163-181.

Huggins, M. L. "Solutions of Long Chain Compounds." *Journal of Chemical Physics* 9, no. 5 (1941): 440.

Iwakura, K. and T. Fujimura. "Rheogoniometry of Molten Blends of Polystyrene and Styrenic Ionomers." *Journal of Applied Physics* 19, (1975): 1427-1437.

Jones, M. N. "The Interaction of Sodium Dodecyl Sulfate with Polyethylene Oxide." *Journal of Colloid and Interface Science* 23, (1967): 36-42.

Ju, H. "Water Transport Study in Crosslinked Poly(Ethylene Oxide) Hydrogels as Fouling-Resistant Membrane Coating Materials." the University of Texas at Austin, 2010.

Ju, H., A. C. Sagle, B. D. Freeman, J. I. Mardel and A. J. Hill. "Characterization of Sodium Chloride and Water Transport in Crosslinked Poly(Ethylene Oxide) Hydrogels." *Journal of Membrane Science* 358, no. 1-2 (2010): 131-141.

Kalika, D. S. "Viscoelastic Characterization of Polymer Blends." In *Polymer Blends: Volume 1: Formulation*, edited by D. R. Paul and C. B. Bucknall, 291-317. Canada: John Wiley & Sons, Inc., 2000.

Kariduraganavar, M. Y., R. K. Nagarale, A. A. Kittur and S. S. Kulkarni. "Ion-Exchange Membranes: Preparative Methods for Electrodialysis and Fuel Cell Applications." *Desalination* 197, no. 225-246 (2006).

Kim, J. S. and A Eisenberg. "Ion Aggregation and Its Effect on Ionomer Properties." In *Ionomers: Characterization, Theory and Applications*, edited by S. Schlick, 7-34: CRC Press, Inc., 1996.

Kim, J. S., R. J. Jackman and A Eisenberg. "Filler and Percolation Behavior of Ionic Aggregates in Styrene-Sodium Methacrylate Ionomers." *Macromolecules* 25, (1994): 6466-6474.

Kim, Y. S., L. Dong, M. A. Hickner, B.S. Pivovar and J. E. McGrath. "Processing Induced Morphological Development in Hydrated Sulfonated Poly(Arylene Ether Sulfone) Copolymer Membranes." *Polymer* 44, no. 19 (2003): 5729-5736.

Kim, Y. S., M. A. Hickner, L. Dong, B. S. Pivovar and J. E. McGrath. "Sulfonated Poly(Arylene Ether Sulfone) Copolymer Proton Exchange Membranes: Composition and Morphology Effects on the Methanol Permeability." *Journal of Membrane Science* 243, no. 1-2 (2004): 317-326.

Kim, Y. S., F. Wang, M. A. Hickner, B.S. Pivovar and J. E. McGrath. "Effect of Acidification Treatment and Morphological Stability of Sulfonated Poly(Arylene Ether Sulfone) Copolymer Proton-Exchange Membranes for Fuel-Cell Use above 100 °C." *Journal of Polymer Science Part B: Polymer Physics* 41, no. 22 (2003): 2816-2828.

Kitahara, Y., S. Takahashi and T. Fujii. "Thermal Analysis of Polyethylene Glycol: Evolved Gas Analysis with Ion Attachment Mass Spectrometry." *Chemosphere* 88, no. 5 (2012): 663-669.

Knop, K., R. Hoogenboom, D. Fischer and U. Schuber. "Poly(Ethylene Glycol) in Drug Delivery: Pros and Cons as Well as Potential Alternatives." *Angewandte Chemie International Edition* 49, no. 36 (2010): 6288-6308.

Kucera, J. "Understanding Ro Membrane Performance." *Chemical Engineering Progress* 104, no. 5 (2008): 30-34.

Laun, H. M. "Prediction of Elastic Strains of Polymer Melts in Shear and Elongation." *Journal of Rheology* 30, no. 3 (1986): 459-501.

Lee, C. H., D. VanHouten, O. Lane, J. E. McGrath, J. Hou, L. A. Madsen, J. Spano, S. Wi, J. Cook, W. Xie, H. J. Oh, G. M. Geise and B. D. Freeman. "Disulfonated Poly(Arylene Ether Sulfone) Random Copolymer Blends Tuned for Rapid Water Permeation Via Cation Complexation with Poly(Ethylene Glycol) Oligomers." *Chemistry of Materials* 23, no. 4 (2011): 1039-1049.

Li, L., G. Guo and Robert K. Prud'homme. "Shear Thickening Ionomers Prepared by Conjugate Addition Reaction." *ACS Polymer. Preprints* 47, no. 1 (2006): 271.

Li, Y., F. Wang, J. Yang, D. Liu, A. Roy, S. Case, J. Lesko and J. E. McGrath. "Synthesis and Characterization of Controlled Molecular Weight Disulfonated Poly(Arylene Ether Sulfone) Copolymers and Their Applications to Proton Exchange Membranes." *Polymer* 47, no. 11 (2006): 4210-4217.

Light, W. G., H. C. Chu and C. N. Tran. "Reverse Osmosis Tfc Magnum Elements for Chlorinated/Dechlorinated Feedwater Processing." *Desalination* 64, (1987): 411-421.

Lin, H. and B. D. Freeman. "Gas Permeation and Diffusion in Crosslinked Poly(Ethylene Glycol Diacrylate)." *Macromolecules* 38, (2005): 8394-8407.

Lin, H., T. Kai, B. D. Freeman, S. kalakkunnath and D. Kalika. "The Effect of Cross-Linking on Gas Permeability in Cross-Linked Poly(Ethylene Glycol Diacrylate)." *Macromolecules* 38, no. 20 (2005): 8381-8393.

Lodge, T. P. and P. C. Hiemenz. "Polymer Chemistry." 58-60, 481-485: CRC Press Taylor & Francis Group, 2007.

Lodge, T. P., E. R. Wood and J. C. Haley. "Two Calorimetric Glass Transitions Do Not Necessarily Indicate Immiscibility: The Case of Peo/Pmma." *Journal of Polymer Science Part B: Polymer Physics* 44, no. 4 (2005): 756-763.

Lu, X., W. P. Steckle and R. A. Weiss. "Ionic Aggregation in a Block Copolymer Ionomer." *Macromolecules* 26, no. 22 (1993): 5876-5884.

Lundberg, R. D. and H. S. Makowski. "The Dual Plasticization of Sulfonated Polystyrene Ionomer." In *Ions in Polymers*, edited by A Eisenberg, 187, 67-76. Washington DC, USA: American Chemical Society, 1980.

Lundberg, R. D., H. S. Makowski and L. Westerman. "Ionic Polymer Plasticized with Preferential Plasticizers." United States Patent No. 4 014 847, 1977.

Macosko, C. W. "Rheology: Priciples, Measurement and Application." 123-124, 141, 510-512: VCH Publishers. Inc., 1993.

Madaeni, S. S. and A. Rahimpour. "Effect of Type of Solvent and Non-Solvents on Morphology and Performance of Polysulfone and Polyethersulfone Ultrafiltration Membranes for Milk Concentration." *Polymers for Advanced Technologies* 16, no. 10 (2005).

Makowski, H. S., P. K. Agarwal, R. A. Weistt and R. D. Lundberg. "Ionic Domain Plasticizers. Tensile Enhancement of Zinc Sulfonate Epdm with Zinc Stearate." *Polymer Preprints (American Chemical Society, Division of Polymer Chemistry)* 20, no. 2 (1979): 281-286.

Makowski, H. S., D. Brenner and J. Bock. "Zinc Neutralized Sulfonated Elastomeric Polymer." United States Patent No. 4 137 203, 1979.

Makowski, H. S. and R. D. Lundberg. "Synthesis and Properties of Sulfonated Epdm." In *Ions in Polymers*, edited by A Eisenberg, 187, 3-19. Washington DC, USA: Americal Chemical Socienty 1980.

Malik, P., M. Castro and C Carrot. "Thermal Degradation During Melt Processing of Poly(Ethylene Oxide), Poly(Vinylidenefluoride-*Co*-Hexafluoropropylene) and Theri Blends in the Presence of Additives, for Conducting Applications." *Polymer Degradation and Stability* 91, no. 4 (2006): 634-640.

Matteucci, S., Y. P. Yampolskii and B. D. Freeman. "Transport of Gases Andvapors in Glassy and Rubbery Polymers." In *Materials Science of Membranes for Gas and Vapor Separation*, edited by Y. P. Yampolskii, I. Piannau and B. D. Freeman, 1-47: Wiley, 2006.

Maus, C., R. Fayt, R. Jerome and Ph. Teyssie. "Shear Thickening of Halato-Telechelic Polymers in Apolar Solvents." *Polymer* 36, no. 10 (1995): 2083–2088.

McCloskey, B. D. "Novel Surface Modifications and Materials for Fouling Resistant Water Purification Membranes." The University of Texas at Austin. 2009.

McGrum, N. G., B. E. Read and G Williams. "Anelastic and Dielectric Effects in Polymeric Solids." 308-312, 327-331,431-434,551-561. UK: John Wiley & Sons Ltd., 1947.

Mchattie, J. S., W. J. Koros and D. R. Paul. "Gas Transport Properties of Polysulphones: 1. Role of Symmetry of Methyl Group Placement on Bisphenol Rings." *Polymer* 32, no. 5 (1991): 840-850.

Milner, S. T. "Relating the Shear-Thinning Curve to the Molecular Weight Distribution in Linear Polymer Melts." *Journal of Rheology* 40, no. 2 (1996): 303-315.

Mkhatresh, O. A. and F. Heatley. "A 13C NMR Study of the Products and Mechanism of the Thermal Oxidative Degradation of Poly(Ethylene Glycol)." *Macromolecular Chemistry and Physics* 203, no. 16 (2002): 2273-2280.

Mkhatresh, O. A. and F. Heatley. "A Study of the Products and Mechanism of the Thermal Oxidative Degradation of Poly(Ethylene Oxide) Using ^{1}H and ^{13}C 1-D and 2-D NMR." *Polymer International* 53, no. 9 (2004): 1336-1342.

Molmeret, Y., F. Chabert, C. Iojoiu, N. E. Kissi and J.-Y. Sanchez. "Extruded Proton Exchange Membranes Based on Sulfonated Polyaromatic Polymers for Fuel Cell Application." In *The XV International Congress on Rheology: The Society of Rheology 80th Annual Meeting*, 1027. Monterey, CA: American Institute of Physics, 2008.

Molmeret, Y., F. Chabert, N. E. Kissi, C. Iojoiu, R. Mercier and J.-Y. Sanchez. "Toward Extrusion of Ionomers to Process Fuel Cell Membranes." *Polymers* 3, no. 3 (2011): 1126-1150.

Mortensen, M. N., H. Egssaard, S. Hvilsted, Y. Shashoua and J. Glastrup. "Tetraethylene Glycol Thermoxidation and the Influence of Certain Compounds Relevant to Conserved Archaeological Wood." *Journal of Archaeological Science* 39, (2012): 3341-3348.

Nakamura, K. "Dynamic Mechanical Properties of Plasticized Poly(Vinyl Chloride)." *Journal of Polymer Science: Polymer Physics Edition* 13, (1975): 137-149.

Nielsen, L. E., R. Buchdahl and R. Levreault. "Mechanical and Electrical Properties of Plasticized Vinyl Chloride Compositions." *Journal of Applied Physics* 21, no. 6 (1950): 607-615.

Noshay, A. and L. M. Robeson. "Sulfonated Polysulfone." *Journal of Applied Polymer Science* 20, (1976): 1885-1903.

Offord, G. T., S.R. Armstrong, B. D. Freeman, E. Baer, A. Hiltner and D. R. Paul. "Influence of Processing Strategies on Porosity and Permeability of B Nucleated Isotactic Polypropylene Stretched Films." *Polymer* 54, no. 11 (2013): 2796-2807.

Offord, G. T., S.R. Armstrong, B. D. Freeman, E. Baer, A. Hiltner, J. S. Swinnea and D. R. Paul. "Porosity Enhancement in B Nucleated Isotactic Polypropylene Stretched Films by Thermal Annealing." *Polymer* 54, no. 10 (2013): 2577-2589.

Oh, H. J., B. D. Freeman, J. E. McGrath, C. J. Ellison, S. Mecham, K-S Lee and D. R. Paul. "Rheological Studies of Disulfonated Poly(Arylene Ether Sulfone) Plasticized with Poly(Ethylene Glycol) for Membrane Formation." *Polymer* 55, no. 6 (2014): 1574-1582.

Oh, H. J., B. D. Freeman, J. E. McGrath, C. H. Lee and D. R. Paul. "Thermal Analysis of Disulfonated Poly(Arylene Ether Sulfone) Plasticized with Poly(Ethylene Glycol) for Membrane Formation." *Polymer* 55, no. 1 (2014): 235-247.

Oki, T. and S. Kanae. "Global Hydrological Cycles and World Water Resources." *Science* 313, no. 5790 (2006): 1068-1072.

Ordian, G. "Principles of Polymerization." 82: John Wiley and Sons, 2004.

Otocka, E. P., M. Y. Hellman and L. L. Blyler. "Terminal-Group Association in Carboxy- and Carboxylate-Terminated Polybutadiene." *Journal of Applied Physics* 40, (1969): 4421-4428.

Pankratz, T. "Membrane Desalination Opportunities, Technologies & Costs." In *The Osmosis Membrane Summit*. Amsterdam, 2008.

Park, H. B., B. D. Freeman, Z.-B. Zhang, M. Sankir and J. E. McGrath. "Highly Chlorine-Tolerant Polymers for Desalination." *Angewandte Chemie International Edition* 47, no. 32 (2008): 6019-6024.

Park, H. B. and Y. M. Lee. "Polymeric Membrane Materials and Potential Use in Gas Separation " In *Advanced Membrane Technology and Applications*, edited by N. N. Li, A. G. Fane, W. S. Ho and T. Matsuura, 633-669, 2008.

Paul, D. R. "A Study of Spinnability in the Wet-Spinning of Acrylic Fibers." *Journal of Applied Polymer Science* 12, (1968): 2273-2298.

Paul, D. R. "The Role of Membrane Pressure in Reverse Osmosis." *Journal of Applied Polymer Science* 16, (1972): 771-782.

Paul, D. R. "Relation between Hydraulic Permeability and Diffusion in Homogeneous Swollen Membranes." *Journal of Polymer Science: Polymer Physics Edition* 11, (1973): 289-296.

Paul, D. R. "Reformulation of the Solution-Diffusion Theory of Reverse Osmosis " *Journal of Membrane Science* 241, (2004): 371-386.

Paul, D. R., J. E. ST. Lawrence and J. H. Troell. "Flow Behavior of Concentrated Solutions of an Sbs Block Copolymer." *Polymer Engineering & Science* 10, no. 2 (1970): 70-78.

Pearson, R. G. "Hard and Soft Acids and Bases, Hsab, Part 1: Fundamental Principles." *Journal of Chemical Education* 45, no. 9 (1968): 581-587.

Pearson, R. G. "Hard and Soft Acids and Bases, Hsab. Part 2. Underlying Theories." *Journal of Chemical Education* 45, (1968): 643-648.

Petersen, R. J. "Composite Reverse Osmosis and Nanofiltration Membranes." *Journal of Membrane Science* 83, no. 1 (1993): 81-150.

Pieffer, D. G., R. D. Lundberg and I. Duvdevani. "Synthesis and Rheological Properties of Low Charge Density Polyampholytes in Nonaqueous Solvents." *Polymer* 27, no. 9 (1986): 1453-1362.

Pielichowski, K. and K. Flejtuch. "Differential Scanning Calorimetry Studies on Poly(Ethylene Glycol) with Different Molecular Weights for Thermal Energy Storage Materials." *Polymers for Advanced Technologies* 13, (2002): 690-696.

Pielichowski, K. and K. Flejtuch. "Non-Oxidative Thermal Degradation of Poly(Ethylene Oxide): Kinetic and Thermoanalytical Study." *Journal of Analytical and Applied Pyrolysis* 73, no. 1 (2005): 131-138.

Podzimek, S. "Light Scattering." In *Light Scattering, Size Exclusion Chromatography and Asymmetric Flow Field Flow Fractionation: Powerful Tools for the Characterization of Polymers, Proteins and Nanoparticles*, edited by S. Podzimek, 37-98: Wiley, 2011.

Ponting, M. T., A. Hiltner and E. Baer. "Polymer Nanostructures by Forced Assembly: Process, Structure, and Properties." *Macromolecular Symposia* 294, no. 1 (2010): 19-32.

Ponting, M. T., Y. Lin, J. K. Keum, A. Hiltner and E. Baer. "Effect of Substrate on the Isothermal Crystallization Kinetics of Confined Poly(E–Caprolactone) Nanolayers." *Macromolecules* 43, no. 20 (2010): 8619-8627.

Ponting, M. T. "Gradient Multilayered Films & Confined Crystallization of Polymer Nanolayers by Forced Assembly Coextrusion." Case Western Reserve University, 2010.

Read, B. E. "Mechanical Relaxation in Some Oxide Polymers." *Polymer* 3, (1962): 529-542.

Register, R. A. and R. K. Prud'homme. "Melt Rheology." In *Ionomers*, edited by M. R. Tant, K. A. Mauritz and G. L. Wilkes, 208-260: Blackie Academic & Professional, 1997.

Roovers, J., P. M. Toporowski and R. Ethier. "Viscoelastic Properties of Melts of 'Radel R' Polysulfone Fractions." *High Performance Polymers* 2, no. 3 (1990): 165-179.

Rowe, B. W., L. M. Robeson, B. D. Freeman and D. R. Paul. "Influence of Temperature on the Upper Bound: Theoretical Considerations and Comparison with Experimental Results." *Journal of Membrane Science* 360, (2010): 58-69.

Rundberg, R. D. and H. S. Makowski. "A Comparison of Sulfonate and Carboxylate Ionomers." In *Ions in Polymers*, edited by A Eisenberg, 187, 21-36. Washington DC, USA: American Chemical Society.

Sagle, A. C., E. M. Van Wagner, H. Ju, B. D. McCloskey, B. D. Freeman and M. M. Sharma. "Peg-Coated Reverse Osmosis Membranes: Desalination Properties and Fouling Resistance." *Journal of Membrane Science* 340, no. 1-2 (2009): 92-108.

Saho, L., R. A. Weiss and R. D. Lundberg. "Solution Behavior of Lightly Sulfonated Polystyrene Ionomer/Poly-Benzyl-L-Glutamate Complexes." *Journal of Polymer Science Part B: Polymer Physics* 33, no. 14 (1995): 2083-2092.

Sanchez, J.-Y., F. Chabert, C. Iojoiu, J Salomon, N. E. Kissi, Y. Piffard, M. Marechal, H. Galiano and R. Mercier. "Extrusion: An Environmentally Friendly Process for Pemfc Membrane Elaboration." *Electrochimica Acta* 53, no. 4 (2007): 1584-1594.

Sanchez, J.-Y., C. Iojoiu, R. Mercier, M. Marechal, N. E. Kissi, H. Galiano and F. Chabert. "Membrane Preparation Method Comprising the Extrusion of a Thermoplastic Polymer Bearing Alkaline Groupings." United States Patent No. 7,973,089 B2, 2011.

Sanchez, J.-Y., C. Iojoiu, Y. Piffard, N. E. Kissi and F. Chabert. "Extrusion of a Thermoplastic Polymer Bearing Acid Ionic Groupings." United States Patent No. 7956095 B2, 2011.

Scheris, J., S. W. Bigger and O. Delatycki. "Characterizing the Solid-State Thermal Oxidation of Poly(Ethylene Oxide) Powder." *Polymer* 32, no. 11 (1991): 2014-2019.

Schmeieder, K. and K. Wolf. "The Temperature and Frequency Dependence of the Mechanical Properties of Some High Polymers." *Kolloid-Zeitschrift* 127, (1952): 65-78.

Scott, K. "Water Desalination." In *Handbook of Industrial Membranes*, 489-517. Oxford: Elsevier, 2003.

Service, R. F. "Desalination Freshens Up." *Science* 313, (2006): 1088-1090.

Sigma-Aldrich, "Poly(Ethylene Glycol) 600 (Cat# 87333), Http://Www.Sigmaaldrich.Com/Catalog/Product/Sigma/87333?Lang=En&Region=Us".

Sigma-Aldrich, "Poly(Ethylene Glycol) Average Mn 300 (Cat# 202371), Http://Www.Sigmaaldrich.Com/Catalog/Product/Aldrich/202371?Lang=En&Region=Us".

Sigma-Aldrich, "Poly(Ethylene Glycol) Average Mn 400 (Cat# 202398), Http://Www.Sigmaaldrich.Com/Catalog/Product/Aldrich/202398?Lang=En&Region=Us".

Sigma-Aldrich, "Poly(Ethylene Glycol) Average Mol Wt 200 (Cat# P3015), Http://Www.Sigmaaldrich.Com/Catalog/Product/Sial/P3015?Lang=En&Region=Us".

Silverstein, R. M., F. X. Webster and D Kiemle. "Spectrometric Identification of Organic Compounds." 72-75: John Wiley & Sons Inc., 2005.

Smith, Z. P., Rajkiran R. Tiwari, M. E. Dose, K. L. Gleason, T. M. Murphy, D. F. Sanders, G. Gunawan, L. M. Robeson, D. R. Paul and B. D. Freeman. "Influence of Diffusivity and Sorption on Helium and Hydrogen Separations in Hydrocarbon, Silicon, and Fluorocarbon-Based Polymers." *Macromolecules* 47, no. 9 (2014): 3170-3184.

Smith, Z. P., Rajkiran R. Tiwari, T. M. Murphy, D. F. Sanders, K. L. Gleason, D. R. Paul and B. D. Freeman. "Hydrogen Sorption in Polymers for Membrane Applications." *Polymer* 54, no. 12 (2013): 3026-3037.

Stevens, D. M., B. Mickols and C. V. Funk. "Asymmetric Reverse Osmosis Sulfonated Poly(Arylene Ether Sulfone) Copolymer Membranes." *Journal of Membrane Science* 452, (2014): 193-202.

Tirrell, M. "Rheology of Polymeric Liquids." In *Rheology Principles, Measurements, and Applications*, edited by C. W. Macosko, 475-514: VCH Publishers, Inc., 1994.

UNEP. *Vital Water Graphics - an Overview of the State of the World's Fresh and Marine Waters, 2nd Edition*. Nairobi, Kenya: UNEP, 2008.

Utracki, L. A. "Polymer Alloys and Blends: Thermodynamics and Rheology." Hanser Publishers, 1989.

Wagner Jr., J. R. "Polymer Blend for Packaging Applications " In *Multilayer Flexible Packaging*, 158-159: Technology & Engineering, 2009.

Wang, F., M. Hickner, Y. S. Kim, T. A. Zawodzinski and J. E. McGrath. "Direct Polymerization of Sulfonated Poly(Arylene Ether Sulfone) Random(Statistical) Copolymer: Candidates for Next Proton Exchange Membranes." *Journal of Membrane Science* 197, no. 1-2 (2002): 231-242.

Webber, M. E. "Evergy Versus Water: Solving Both Crises Together." *Scientific American Special Edition Earth 3.0* 18, (2008): 34-41.

Weiss, R. A., J. J. Fitzgerald and D. Kim. "Viscoelastic Behavior of Lightly Sulfonated Polystyrene Ionomers." *Macromolecules* 24, no. 5 (1991): 1071-1076.

Weiss, R. A. and H. Zhao. "Rheological Behavior of Oligomeric Ionomers." *Journal of Rheology* 53, no. 1 (2009): 191-213.

Wijmans, J. G. and R. W. Baker. "The Solution-Diffusion Model: A Review." *Journal of Membrane Science* 107, (1995): 1-21.

Wiles, K. B., F. Wang and J. E. McGrath. "Directly Copolymerized Poly(Arylene Sulfide Sulfone) Disulfonated Copolymers for Pem-Based Fuel Cell Systems. I. Synthesis and Characterization." *Journal of Polymer Science Part A: Polymer Chemistry* 43, no. 14 (2005): 2964-2976.

Wilson, A. S. "Plasticizers: Principles and Practice." 9-18. Cambridge, UK: The Institute of Materials, 1995.

Witten, T. A. "Associating Polymers and Shear Thickening." *Journal de Physique* 49, no. 6 (1988): 1055-1063.

Witten, T. A. and M. H. Cohen. "Crosslinking in Shear-Thickening Ionomers." *Macromolecules* 18, no. 10 (1985): 1915-1918.

Wohlfarth, C. "Crc Handbook of Enthalpy Data of Polymer-Solvent Systems." Boca Raton, FL: Taylor & Francis Group, 2006.

Wool, R. P. "Polymer Interfaces: Structure and Strength." 102. Munich: Carl Hanser Verlag, 1995.

Wyatt, N. B., C. M. Gunther and M. W. Liberatore. "Increasing Viscosity in Entangled Polyelectrolyte Solutions by the Addition of Salt." *Polymer* 52, (2011): 2437-2444.

Xie, W. "Preparation and Characterization of Disulfonated Polysulfone Films and Polyamide Thin Film Composite Membranes for Desalination." The University of Texas at Austin. 2011

Xie, W., J. Cook, H. B. Park, B. D. Freeman, C. H. Lee and J. E. McGrath. "Advances in Membrane Materials: Desalination Membranes Based on Directly Copolymerized Disulfonated Poly(Arylene Ether Sulfone) Random Copolymers." *Water Science and Technology : a Journal of the International Association on Water Pollution Research* 61, no. 3 (2010): 619-624.

Xie, W., J. Cook, H. B. Park, B. D. Freeman, C. H. Lee and J. E. McGrath. "Fundamental Salt and Water Transport Properties in Directly Copolymerized Disulfonated Poly(Arylene Ether Sulfone) Random Copolymer." *Polymer* 52, no. 9 (2011): 2244-2254.

Xie, W., G. M. Geise, B. D. Freeman, H.-S. Lee, G. Byun and J. E. McGrath. "Polyamide Interfacial Composite Membranes Prepared from M-Phenylene Diamine, Trimesoyl Chloride and a New Disulfonated Diamine." *Journal of Membrane Science* 403-404, no. 1-2 (2012): 152-161.

Xie, W., G. M. Geise, B. D. Freeman, C. H. Lee and J. E. McGrath. "Influence of Processing History on Water and Salt Transport Properties of Disulfonated Polysulfone Random Copolymers." *Polymer* 53, no. 7 (2012): 1581-1592.

Xie, W., H. Ju, G. M. Geise, B. D. Freeman, J. I. Mardel, A. J. Hill and J. E. McGrath. "Effect of Free Volume on Water and Salt Transport Properties in Directly Copolymerized Disulfonated Poly(Arylene Ether Sulfone) Random Copolymers." *Macromolecules* 44, no. 11 (2011): 4428-4438.

Yang, L., F. Heatley, T. G. Blease and R. I. G. Thompson. "A Study of the Mechanism of the Oxidative Thermal Degradation of Poly(Ethylene Oxide) and Poly(Propylene Oxide) Using ^{1}h and ^{13}c-Nmr." *European Polymer Journal* 32, no. 5 (1996): 535-547.

Yasuda, H., C. E. Lamaze and L. D. Ikenberry. "Permeability of Solutes through Hydrated Polymer Membranes. Part I. Diffusion of Sodium Chloride." *Die Makromolekulare Chemie* 18, no. 1 (1968): 19-35.

Yasuda, H., C. E. Lamaze and A. Peterlin. "Diffusive and Hydraulic Permeabilities of Water in Water-Swollen Polymer Membranes." *Journal of Polymer Science Part A-2: Polymer Physics* 9, no. 6 (1971): 1117-1131.

Zdyrko, B., S. K. Varshney and I. Luzinov. "Effect of Molecular Weight on Synthesis and Surface Morphology of High-Density Poly(Ethylene Glycol) Grafted Layers." *Langmuir* 20, (2004): 6727-6735.

Vita

Hee Jeung Oh earned her Bachelor in Science in Biomolecular and Chemical Engineering at Korea Advanced Institute of Science and Technology (KAIST) in Daejeon, South Korea in 2008. She started her graduate studies in the department of Chemical Engineering in the University of Texas at Austin in 2008 under the guidance of Professors Donald R. Paul and Benny D. Freeman. She received a Master of Science and Engineering degree in Chemical Engineering in 2011 and completed her Ph.D. studies in May 2015.

Permanent email: hee@utexas.edu

This dissertation was typed by Hee Jeung Oh